2018

Morphological And Functional Characterization Of A Murine Garp2-Specific Knockout

Delores Stacks
University of Alabama at Birmingham

MORPHOLOGICAL AND FUNCTIONAL CHARACTERIZATION OF A MURINE GARP2-SPECIFIC KNOCKOUT

by

DELORES STACKS

TIMOTHY W. KRAFT, COMMITTEE CHAIR
STEVEN J. PITTLER, MENTOR
MARK O. BEVENSEE
CHRISTIANNE STRANG
KRISTINA M. VISSCHER

A DISSERTATION

Submitted to the graduate faculty of The University of Alabama at Birmingham,
in partial fulfillment of the requirements for the degree of
Doctor of Philosophy

BIRMINGHAM, ALABAMA

2018

MORPHOLOGICAL AND FUNCTIONAL CHARACTERIZATION OF A MURINE GARP2-SPECIFIC KNOCKOUT

DELORES STACKS

VISION SCIENCE GRADUATE PROGRAM

ABSTRACT

GARP2, found exclusively in retinal rod photoreceptors, has been proposed to function as a structural protein, a calcium binding protein, and a modulator of the phosphodiesterase regulating visual phototransduction cascade kinetics. GARP2 is a splice variant of the *Cngb1* gene which also encodes the β-subunit of the phototransduction cyclic nucleotide-gated cation channel and another glutamic acid-rich protein, GARP1. Mutations of the β-subunit and, recently discovered regions shared with the GARP encoding regions of *Cngb1*cause retinitis pigmentosa (RP), while overexpression of GARP2 in the absence of the β-subunit accelerates the observed *Cngb1*-mediated retinal degeneration in mouse β-subunit knockout disease models.

In this study, we have used a selective knockout of murine GARP2 (GARP2-KO) to assess functional and structural changes associated with its absence and to assess its role in the retina.

In the GARP2-KO mice, the morphology of the photoreceptors remained intact. However, regions of longer outer segments were sporadically observed that were misaligned relative to the retinal pigment epithelium. At one month, the GARP2-KO had normal electroretinogram responses under both light- and dark-adapted conditions. However, surprisingly, the GARP2-KO photoresponse was altered by three months of age showing both scotopic a- and b- wave reductions, reduced bipolar cell sensitivity to light, faster oscillatory potentials, and reduced scotopic critical flicker fusion responses.

To assess changes in gene expression triggered by the absence of GARP2, transcriptomes of GARP2-KO, *Cngb1*-X1, and WT mouse retinas were compared using RNAseq analysis. Ten commonly differentially expressed genes between the GARP2-KO and *Cngb1*-X1, both of which lack GARP2, were confirmed by RT-PCR that function in cell cycle regulation, maintenance of the connecting cilium, circadian rhythms, or retinoid signaling.

This work has shown that the length of the rod outer segment and the formation and transmission of electrical signals from the rod photoreceptor to the bipolar cell is somewhat dependent on the presence of GARP2. The GARP2-KO phenotype is a subtle, yet progressive, non-degenerative, functionally atypical model of vision.

KEYWORDS: *Cngb1*, GARP2, ERG, phototransduction, rod photoreceptor, RPE

ACKNOWLEDGMENTS

I would like to thank the University of Alabama at Birmingham School of Optometry, the Vision Science Graduate Program, and all the Vision Science faculty for accepting me into the Vision Science program and giving me the opportunity to do fantastic work with amazing people.

I would like to thank Dr. Marci DeRamus for performing ERG testing and teaching me Igor; Dr. David Crossman for his expertise and assistance with next-generation sequencing and pathway analysis; Dr. Carrie Huisingh and Dr. Gerald McGwin for their statistical analyses; Dr. Timothy Gawne for data processing advice; Dr. Christine Curcio for teaching me image analysis techniques; Dr. Jeff Messinger for histological processing of eyes, light microscopy and EM, and providing images for me to analyze; Dr. Alecia Gross, and Dr. Marina Gorbatyuk for helping me maintain sanity and focus; Dr. Thomas DeRamus for his Python coding abilities; Dr. Alex McKeown for Matlab coding; Alex Zotov for modifying LabView programs to suit my needs, assistance with Matlab coding, and writing Excel macros; Pravallika Kotla and Seth Fortmann for Western blots; and Dr. Timothy Kraft for allowing experiments to be performed on his instrumentation and assistance with ERG data analysis. I would also like to thank Dr. David Crossman, Dr. Michael Crowley, Dr. Malay Basu, and Mike Hanby for their assistance in designing and performing Next Generation Sequencing and helping me analyze those results.

Dr. Stefanie Varghese, Dr. Michael Twa, and Dr. Kelly Nichols, thank you for leading the VSGP, the other students and I appreciate your efforts.

Thank you to my committee members: Dr. Mark Bevensee, Dr. Christianne Strang, and Dr. Kristina Visscher; and my committee chair: Dr. Timothy Kraft. I would like to say a special thank you to my mentor, Dr. Steven Pittler, for taking me into his laboratory, paying extra for the experiments where I put the "re" in research and providing the space I needed to work, learn, and achieve. I will always be grateful. Thanks to each of you.

Molecular graphics and analyses were performed with the UCSF Chimera package. Chimera is developed by the Resource for Biocomputing, Visualization, and Informatics at the University of California, San Francisco (supported by NIGMS P41-GM103311). This work was supported by NIH grant EY018143 and an NEI Core grant for vision research, P30 EY03039 to SJP.

TABLE OF CONTENTS

LIST OF TABLES

LIST OF FIGURES

LIST OF ABBREVIATIONS

*	premature stop codon
11cRDH5	11-cis retinol dehydrogenase 5
A	adenine
AAV	adeno-associated virus
ABCA	ATP-binding cassette transporter
ABCR4	ATP-binding cassette, sub-family 4
ABI	Applied Biosystems Incorporated
Ac(λ)	collecting area of a rod photoreceptor
Ag	phototransduction gain
Ala	alanine
Arg	arginine
Asn	asparagine
atRDH8	all-trans retinol dehydrogenase 8
BB	basal body
BLAST	Basic Local Alignment Search Tool
bp	base pairs
C	cytosine
c.	cDNA transcript
Cacnaf1	Ca_v 1.4 L-type voltage-gated calcium channel α1 subunit

CC	connecting cilium
cDNA	complementary deoxyribonucleic acid
CFF	critical flicker fusion frequency
cGMP	cyclic guanosine monophosphate
Cit	Citron Rho-Interacting Serine/Threonine Kinase
CLZ	carboxy terminal leucine zipper
CNG	cyclic-nucleotide gated
CNGA1	rod photoreceptor cyclic-nucleotide gated channel α-subunit
CNGA2	olfactory cyclic-nucleotide gated channel α-subunit
CNGA3	cone photoreceptor cyclic-nucleotide gated channel α-subunit
CNGA4	olfactory cyclic-nucleotide gated channel α-subunit
Cngb1	cyclic-nucleotide gated channel β-subunit
Cngb1b	cyclic-nucleotide gated channel β-subunit (olfactory)
CRALBP	cellular retinaldehyde-binding protein 1
CRBP	cellular retinol-binding protein
Crebbp	cAMP response element binding (CREB) - binding protein
Cys	cysteine
d	diameter of photoreceptor outer segment
DC	direct current
DCS	domain conservation score
del	deletion mutation
delins	insertion deletion mutation
DNA	deoxyribonucleic acid

DRM	detergent resistant membrane
ELM	external limiting membrane
EM	electron microscopy
ERG	electroretinography
f	light funneling factor
FFT	Fast Fourier Transform
Foxo3	Forkhead box O3
fs	frameshift mutation
FWHM	full-width, half-maximum
$\Delta\Delta G$	transition free energy
G	guanine
GABA	gamma-aminobutryic acid
GAR1	GARP gene (now *Cngb1*)
Garem	growth factor receptor bound protein 2 (GRB2) associated, regulator of mitogen-activated protein kinase 1 (MAPK1)
GARP1	glutamic acid rich protein 1
GARP2	glutamic acid rich protein 2
GARP2-KO	glutamic acid rich protein 2 knockout mouse
GC	guanylate cyclase
GCAP	guanylate cyclase activating protein
GCL	ganglion cell layer
GDP	guanosine diphosphate
Gln	glutamine
GRB14	growth factor receptor bound protein 14

GTP	guanosine triphosphate
Gly	glycine
HCN1	hyperpolarization activated cyclic nucleotide gated channel 1
HDAC	histone deacetylase
hGARP	early name for GARP2
HMsERG	Handheld Multi-species Electroretinogram
hRCNC1	early name for CNG channel α-subunit
hRCNC2a	early name for possible CNG channel β-subunit
hRCNC2b	early name for possible CNG channel β-subunit
Hz	Hertz
IACUC	Institutional Animal Care and Use Committee
IFT	intraflagellar transport
iGluR	ionotropic glutamate receptors
ILM	internal limiting membrane
I^n	flash intensity in photons/μm^2
I_{50}	flash intensity that produces the half maximal response
Ile	isoleucine
INL	inner nuclear layer
ins	insertion mutation
IP	intraperitoneal
IPA	Ingenuity Pathway Analysis
IPL	inner plexiform layer
IRBP	interphotoreceptor retinoid binding protein

IS	inner segment
L	length of photoreceptor outer segment
l	flash illuminance
L-cone	long wavelength sensitive (red) cone photoreceptor
LED	light emitting diode
Leu	leucine
LRAT	lecithin retinol acyltransferase
Lys	lysine
M-cone	medium wavelength sensitive (green) cone photoreceptor
mGluR	metabotropic glutamate receptor
mm	millimeter
mm10	*mus musculus* genome assembly version 10
MMP	matrix metalloproteinase
mRNA	messenger ribonucleic acid
ms	millisecond
NCBI	National Center for Biotechnology Information
NCKX1	sodium/potassium/calcium exchanger 1
ND	neutral density
Nek5	NIMA (Never In Mitosis A) Related Kinase 5
NFL	nerve fiber layer
nGnG	non-GABAergic non-glycinergic
NGS	Next Generation Sequencing
NO	nitric oxide

Nrip1	nuclear receptor-interacting protein 1
OCT	optical coherence tomography
ONL	outer nuclear layer
OPL	outer plexiform layer
OPs	oscillatory potentials
p.	protein transcript
PARP	poly-ADP-ribose-polymerase
PCR	polymerase chain reaction
PDE6	phosphodiesterase 6
PDE6γ	phosphodiesterase 6 gamma subunit
Phe	phenylalanine
PE	phosphatidylethanolamine
PM	postnatal month
PONDR	predictors of natural disordered regions
PPDE	posterior probability of differential expression
Pro	proline
PTK	protein tyrosine kinase
PTP	protein tyrosine phosphatase
PVDF	polyvinylidene fluoride
qRT-PCR	quantitative-reverse transcription polymerase chain reaction
R	response to a flash of light
R*	number of activated rhodopsin molecules/photoisomerizations
R2	linear regression coefficient of determination

rd1	PDE6 β-subunit mutant mouse model of RP
RDS	retinal degeneration slow
Rec8	REC8 meiotic recombination protein
RGC	retinal ganglion cells
RGS9	regulator of G-protein signaling 9
R_{max}	maximum amplitude of photoresponse
ROS	rod outer segment
RP	retinitis pigmentosa
RP45	retinitis pigmentosa (*Cngb1* associated)
RPE	retinal pigment epithelium
RPE65	retinoid isomerohydrolase
RQ	relative quantitation
s	second
S-cone	small wavelength sensitive (blue) cone photoreceptor
SD-OCT	spectral domain - optical coherence tomography
SDS-PAGE	sodium dodecyl sulfate polyacrylamide gel
Ser	serine
SNR	signal-to-noise ratio
S_{pupil}	surface area of the pupil
S_{retina}	surface area of the retina
T	thymine
Tα	transducin α subunit
t_{delay}	delay for events of phototransduction

Trp	tryptophan
TTP	time-to-peak
Tyr	tyrosine
UAB	University of Alabama at Birmingham
UCSC	University of California, Santa Cruz
Val	valine
Vmn2r29	vomeronasal 2 receptor 29
WT	wildtype
Cngb1-X1	*Cngb1* mutant mouse exon 1 and 2 deleted (No β-subunit, No GARPs)
Cngb1-X26	*Cngb1* mutant mouse exon 26 deleted (No β-subunit)
ZFN	zinc finger nuclease
Zmynd10	zinc finger MYND-type containing 10
γ	quantum efficiency of phototransduction
$\Delta D(\lambda)$	axial density of rhodopsin at a specific wavelength
ΔT	flash duration
μm	micron
μV	microvolt
π	pi
$\tau(\lambda)$	light transmission through ocular media
Φ	number of photoisomerizations

INTRODUCTION

Glutamic acid-rich protein 2, GARP2, is an abundantly expressed protein, with expression levels nearing those of the phototransduction cascade phosphodiesterase and is found exclusively in the rod photoreceptor. To elucidate the *in vivo* role of GARP2 we studied the effects of its selective ablation in a murine knockout model (GARP2-KO).

The literature review includes a brief description of the eye, retina, retinal cell types, and biochemical processes within the retina which allow photons of light to be detected and transduced into an electrical signal. GARP2 is rod photoreceptor-specific so relevant rod morphology and physiology will be presented in greater detail than the other cell types. *Cngb1,* the gene encoding GARP2, also encodes two other proteins, GARP1 and the β-subunit of the rod cyclic nucleotide-gated cation channel, CNGB1a, that is essential for phototransduction. Therefore, these proteins and the *Cngb1* gene will be thoroughly reviewed. The clinical significance of this work, the specific form of retinitis pigmentosa caused by mutations within *Cngb1,* will be discussed after discussion of the functions of the proteins encoded by this gene. The introduction concludes with the research goals and hypotheses. Next, the methodology used to test our morphological, functional, and genetic hypotheses will be presented, followed by our findings in the results section. Finally, the meaning and relevance of the results, limitations of this study, and ideas for future directions will be discussed.

Eye and Retinal Anatomy

The first recorded anatomical description of ocular tissue was in 200 AD by Aelius Galen of Pergamon (reviewed in Bieganowski, 2005). Galen accurately described the cornea, sclera, lens capsule, retina, aqueous and vitreous humors, and extraocular musculature, although he had no concept of the physiology of the tissue. Modeling Galen's style, what follows is a brief description of the eye and retinal anatomy.

Starting from the exterior anterior eye, the cornea is the clear protective tissue covering the iris whose highly pigmented epithelial cells determine eye color. Between the iris and the cornea is the anterior segment filled with aqueous humor. The cornea connects to the sclera, or the white of the eye, at the limbus. The sclera covers the posterior of the eye and thins at the lamina cribrosa, where the optic nerve fibers exit the eye. The colored part of the eye, the iris, is muscular and has both sympathetic and parasympathetic innervation for pupil dilation and constriction, respectively. The lens capsule is posterior to the iris and is connected to ciliary muscles permitting shape changes required for lens accommodation, or the ability to focus on objects in near or far space. The posterior segment of the eye from the posterior lens capsule to the inner surface of the retina is filled with a thick jelly-like substance called the vitreous humor. The inner, posterior surface of the eye is lined with a thin tissue comprised of specialized layers of cells, known as the neural retina.

A labeled histological section of the retina (Figure 1) shows the vertical alignment of the cell types within the retinal layers. Starting with the layer immediately apposed to

the vitreous humor and moving proximal to distal, the layers are: the inner limiting membrane (ILM), nerve fiber layer (NFL), ganglion cell layer (GCL), inner plexiform layer (IPL), inner nuclear layer (INL), outer plexiform layer (OPL), outer nuclear layer (ONL), external limiting membrane (ELM), rod/cone inner segments (IS) and outer segments (ROS), and the retinal pigment epithelium (RPE). Posterior to the RPE is the retinal blood supply, the choroid plexus, which branches from the ophthalmic artery, the first branch of the internal carotid (Hayreh, 1962) and the outmost layer of the eye, the sclera.

The end-feet of Müller cells form tight junctions across the surface of the retina comprising the ILM, which separates the neural retina from the vitreous humor. The NFL is composed of axons from the GCL which form the optic nerve and terminate in the visual cortex of the brain. The GCL is composed of the retinal ganglion cells. The IPL is a synaptic region where bipolar cells and amacrine cells synapse with the retinal ganglion cells. The INL houses the cell bodies of the bipolar cells, amacrine cells, Müller cells, and horizontal cells. The OPL is the synaptic region between the photoreceptors, bipolar cells, and horizontal cells. The ONL contains columns of tightly packed photoreceptor nuclei. The ELM delimits the inner segment and outer segment regions of the photoreceptor, a boundary layer made up of tight junctions between photoreceptor inner segments and Müller cells. The outer segment (ROS) is the site of phototransduction, the primary signaling event in this layer of the photoreceptor cells. The monolayer of epithelial cells, the retinal pigment epithelium (RPE), forms the blood/retina barrier, generates the pigment melanin, and supports photoreceptor function in several different ways.

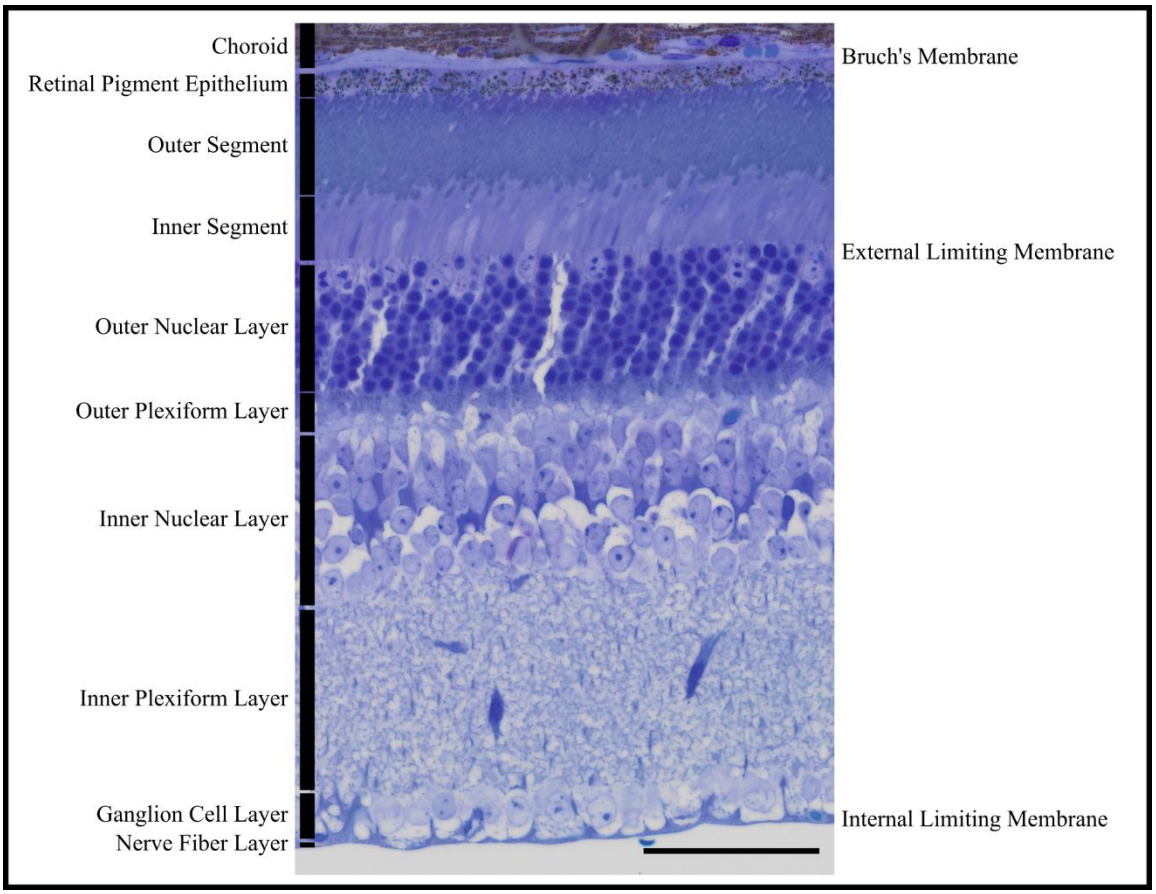

Figure 1: Layers of the retina. From outer retina to the inner retina, top to bottom. Choroid provides the blood supply. Bruch's membrane separates the choroid from the retinal pigment epithelium (RPE). The outer segment (ROS), inner segment (RIS), outer nuclear layer (ONL), and outer plexiform layer (OPL) together contain complete rod and cone photoreceptors; the ROS contains the phototransductive elements, the RIS handles energy and protein production, and the ONL houses stacked layers of photoreceptor nuclei. The OPL is where the photoreceptors, bipolar cells, and horizontal cells form synaptic connections. The cell bodies of the bipolar cells, horizontal cells, and amacrine cells are found in the inner nuclear layer (INL). The inner plexiform layer (IPL) is comprised of synapses between bipolar cells, ganglion cells, and amacrine cells. The ganglion cell layer (GCL) houses the cell bodies of the retinal ganglion cells. The nerve fiber layer (NFL) is composed of ganglion cell axons, which merge into the optic nerve and extend to the brain. Scale bar = 50 μm.

Retinal Pigment Epithelium (RPE)

The outermost retinal layer is a monolayer of epithelial cells, the retinal pigment epithelium (RPE). The underlying choroidal blood supply via the basement membrane of the RPE is a source of retinal oxygen, nutrients, and metabolic waste removal (Adler & Southwick, 1992; Keeling, Lotery, Tumbarello, & Ratnayaka, 2018). The tight junctions between RPE cells at the basement membrane form an extension of the blood-brain barrier providing retinal immune privilege (Grisanti, Ishioka, Kosiewicz, & Jiang, 1997). The RPE provides modified hemoglobin, called neuroglobin to facilitate oxygen exchange through the retinal layers without compromising optical clarity (Schmidt et al., 2003). Ionic regulation of the intra-photoreceptor space, also known as the sub-retinal space, is also partially maintained by the RPE (Oakley, 1977). The microvillus processes on the apical surface of the RPE engulf the end-tips of the outer segments of rods and cones, mediating endophagocytosis in a circadian-regulated pattern with peak phagocytosis of rods occurring before dawn (Bridges, Hollyfield, Besharse, & Rayborn, 1976; Feeney, 1973; Johnson, 1975; Lo & Bernstein, 1981; Marshall, 1971; R H Steinberg, 1974). The phagosomes are apparent inside the RPE for about two hours before complete digestion and reuse of precursor components (Kevany & Palczewski, 2010). In humans and other primates, the drusen containing waste from phagolysosomes are deposited under the basement membrane leading to basal laminar deposits, the buildup of which can cause age-related macular degeneration and geographic atrophy (Cohen, 1971; De Schweinitz, 1892; Gass, 1972; Sanders, Gay, & Newman, 1971). The RPE contains melanosomes that generate the pigment melanin, which absorb stray photons of light, decreas-

ing retinal photo-oxidative stress (Burke et al., 2011). Many of the steps of the visual cycle that replaces the chromophore used in rod phototransduction (11-cis-retinal) occur in the RPE (Kiser, Golczak, & Palczewski, 2014).

Müller Cells

Müller cells are the primary glial cells of the retina. The cell bodies are found in the INL, and the cells span vertically, reaching almost every retinal layer, from the ILM to the RPE. The junctions of Müller cell end feet at the ILM separate the retina from the vitreous humor. The ELM, found between the photoreceptor ROS and RIS, is not an actual membrane, but a morphologically distinct line formed by a layer of tight junctions between the Müller glia and photoreceptors. Also, processes from Müller cells wrap around the small and large retinal blood vessels and capillaries to reinforce the immune privilege of the retina and to maintain the blood-brain barrier (Kumar, Pandey, Miller, Singh, & Kanwar, 2013). Homeostasis of the retina is, in part, maintained by the Müller glia through its redistribution of potassium ions (Eberhardt, Amann, Feuchtinger, Hauck, & Deeg, 2011), recycling of surplus neurotransmitters, such as GABA and glutamate (Bringmann et al., 2009; White & Neal, 1976), and control of pH within the intraphotoreceptor space (Sarthy & Lam, 1978). The RPE participates in the visual cycle supplying chromophore for rods and cones; the Müller glia is a separate additional pathway for cone chromophore regeneration (J.-S. Wang & Kefalov, 2009).

Photoreceptors

Photoreceptors are non-motile primary cilia. On a basic level, rod photoreceptors are required for scotopic (dim light) vision (Figure 2), and cone photoreceptors are required for photopic (bright light) vision. Cones are classified by the range of light wavelengths its cone opsin responds to best, which varies by species. In humans, L-cones, with red opsin, peak around 560 nm; M-cones, with green opsin, peak around 530 nm; and S-cones, with blue opsin, peak around 420 nm (Baylor, Nunn, & Schnapf, 1984; Shlaer, Smith, & Chase, 1941; J.-S. Wang & Kefalov, 2009). Rod photoreceptors express rhodopsin which exhibits a greater gain, or rate of activation, than the color vision opsins found in cone photoreceptors (Alpern, Pugh, & Jr, 1974), thus facilitating vision in dim light. In humans, there are about 100 – 120 million rod photoreceptors and around 6 – 7 million cone photoreceptors with the majority of cones found in the macular region, which is the region of highest visual acuity. Rods are found more peripherally with a peak in density forming a ring around the fovea (Curcio, Sloan, Kalina, & Hendrickson, 1990). Structurally, human cones are 40 – 50 microns long, 0.5 – 4 microns in diameter, and have a broader outer segment base that tapers to a cone-like peak. The fovea is the area with the highest density of cone photoreceptors, and the foveal cones are smaller in diameter than cones located in the peripheral retina. Rods are around 100 microns long, 2 microns in diameter, with uniformly straight rod-like outer segments. In the mouse retina, no fovea or macular region exists, the rod photoreceptors are around 26 microns long and 1.3 microns in diameter (Carter-Dawson & Lavail, 1979). The spectral sensitivity of the mouse is different from humans because mice lack long-wavelength red opsins and their S-cones are sensitive to wavelengths in the ultraviolet spectrum (Haverkamp et al., 2005).

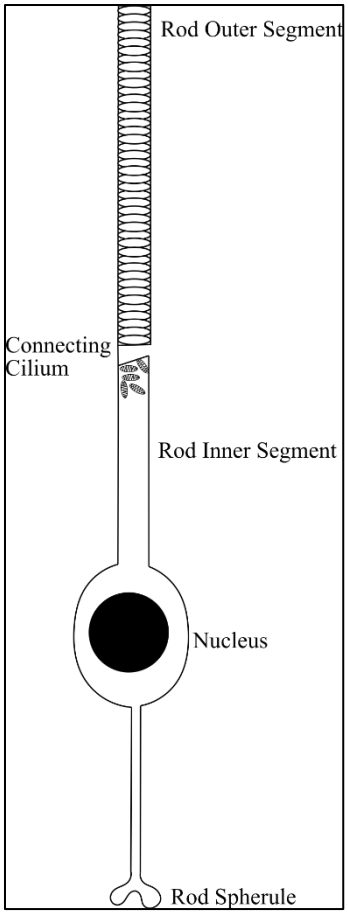

Figure 2: The rod photoreceptor. The rod outer segment, which is surrounded by microvillus processes of the RPE is composed of stacks of membranous disks that house phototransductive proteins. The inner segment is the site of protein synthesis and energy production. The connecting cilium uses intraflagellar transport to move proteins and molecules between the inner and outer segments and provides a diffusion barrier between the two regions. The nuclei of the photoreceptors stack in vertical columns within the ONL. The rod synapses with the downstream bipolar cells and horizontal cells at the rod spherule.

Outer Segment. The rod outer segment (ROS) is composed of layers of membranous discs surrounded by the plasma membrane and is divided into separate functional areas, the morphogenic region where nascent ROS discs are formed and the phototransductive region where the phototransduction cascade occurs (Goldberg, Moritz, & Williams,

2016). The upper end of the rod photoreceptor phototransductive region is in contact with the apical surface of the RPE and is surrounded by its microvillus processes in a region referred to simply as the retina/RPE interface or in the context of noninvasive imaging as the RPE/ROS interdigitation zone (Turgut, 2017).

Two proposed mechanisms of disc morphogenesis are 1) fusion of vesicles transported from the inner segment through the connecting cilium (Chuang, Zhao, & Sung, 2007), and 2) evagination of the photoreceptor plasma membrane (Roy H. Steinberg, Fisher, & Anderson, 1980). Although the complete mechanism is not understood, the evagination model has proven to be the most accurate by tannic acid staining, which stains plasma membranes in a non-penetrative manner showing that the most recently formed five to seven discs are exterior to the plasma membrane of the rest of the photoreceptor (J. D. Ding, Salinas, & Arshavsky, 2015).

Connecting Cilium. Connecting the outer and inner segments is the connecting cilium (Figure 3). The four components of the connecting cilium are the axoneme, found in the outer segment; the transition zone, which represents the actual connecting cilium; the basal body; rootlet; and periciliary ridge. The axoneme is composed of a 9 + 0 arrangement of microtubules, the same arrangement as every other non-motile primary cilium, examples being kidney cells and cells of the dendritic olfactory knob (Pazour & Witman, 2003). The transition zone and ciliary necklace, a series of Y-linked proteins, serve as a diffusion barrier between the inner and outer segments of the photoreceptor (Reiter, Blacque, & Leroux, 2012). The Henneguy-Lenhossek theory proclaims basal bodies to be

analogous to mitotic centrioles (Henneguy, 1898; Lenhossek, 1898). The centrioles are declared basal bodies once they dock on the surface of the cell membrane (Dawe, Farr, & Gull, 2007). The exact mechanism of primary ciliary centriole migration and docking are not understood (Dawe et al., 2007). The rootlet maintains ciliary stability but is not required for ciliary morphogenesis (J. Yang et al., 2005). The periciliary ridge is a feature first found in frog eyes but not seen in mammals (Peters, Palade, Schneider, & Papermaster, 1983), but the presence of the Usher proteins delimits a periciliary region despite the missing histological landmark (Maerker et al., 2008).

The functional role of the connecting cilium is intraflagellar transport (IFT). Dynein and kinesin motors on the axoneme provide retrograde and anterograde transport between the inner and outer segments (Goldstein & Yang, 2000). This activity is responsible for light and dark translocation of arrestin (and some other proteins) from the inner segment to the outer segment (Nair et al., 2005; Pearring, Salinas, Baker, & Arshavsky, 2013) and the transport of newly formed phototransduction molecules to the morphogenic region of the outer segment (Young, 1968).

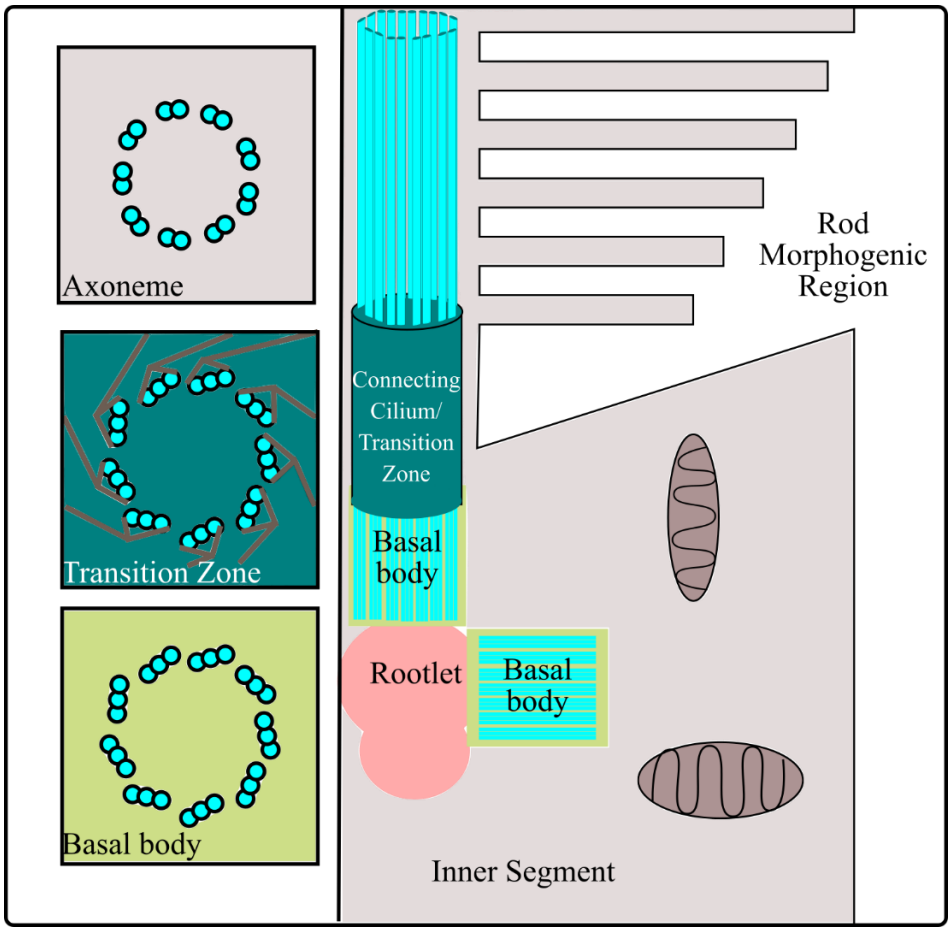

Figure 3: Connecting cilium of the rod photoreceptor. The photoreceptor axoneme is a 9+0 arrangement of microtubules traversing the edge of the outer segment; arising from the centrosome derived rootlet that extends all the way to the synaptic region of the rod and the basal body in the ellipsoid region of the inner segment. Trafficking of proteins and soluble materials through the connecting cilium is dependent on kinesin and dynein motors for anterograde and retrograde transport, respectively. The Y-linkers found within the connecting cilium transition zone are thought to provide a diffusion barrier for insoluble and large materials, separating the inner and outer segments. Adapted from "Three-Dimensional Architecture of the Rod Sensory Cilium and Its Disruption in Retinal Neurodegeneration" by J. C. Gilliam, J. T. Chang, I. M. Sandoval, Y. Zhang, T. Li, S. J. Pittler, W. Chiu, and T. G. Wensel, 2012, Cell, 151, p. 1031. Copyright 2012 by Elsevier. Adapted with permission.

Inner Segment and Nucleus. The ellipsoid region of the inner segments of both rods and cones house many long, thin mitochondria which form a distinctive auto-reflective band when viewed with optical coherence tomography (OCT) (Liu, Li, Liu, Xu, & Wang, 2016). The inner segment is the location for protein synthesis and all typical housekeeping events that occur in nearly all cells (Pearring et al., 2013). Ion channels are present in the inner segment to offset the ionic changes that occur during phototransduction, including the sodium-calcium potassium exchanger type 1, NCKX1, hyperpolarization-activated cation channels, and calcium-activated chloride channels (Barnes, 1994). The inner segment is largely responsible for maintenance of the rod photoreceptor dark current as it contains NA^+/K^+-ATPases. Potassium efflux from the inner segment perpetuates signal transmission from the outer segment to the rod synapse after closure of the CNG channels due to the events of phototransduction (Hagins, Penn, & Yoshikami, 1970; Penn & Hagins, 1969).

Within the outer nuclear layer, below the inner segment, photoreceptor cell bodies become very thin, enlarging only to engulf the nucleus. This unique shape allows the nuclei of the photoreceptors to align in vertical columns allowing maximal photoreceptor ROS density within the retinal mosaic for acute vision and light detection. Within mouse rod photoreceptor nuclei, euchromatin, the chromosomal material containing genes, is found peripheral to the heterochromatin, creating an interesting histological pattern that is dense in the center and clear towards the periphery, which is the opposite of what is typically seen in diurnal animal retinas (Solovei et al., 2009).

Rod Spherule. The synapse of the rod photoreceptor is referred to as a rod spherule, and that of the cone photoreceptor is referred to as a cone pedicle, both of which are found in the OPL (Figure 4). The spherule of the rod is connected to the cell body by a 0.5 μm diameter nerve fiber (De Robertis & Franchi, 1956). Each evaginated ribbon synapse in the rod spherule has attached vesicles containing the excitatory neurotransmitter, glutamate, which is released by rods constantly under a dark-adapted, depolarized state (Copenhagen & Jahr, 1989; Ehinger, Ottersen, Storm-Mathisen, & Dowling, 1988; Marc & Lam, 1981). The size of synaptic vesicles within the rod spherule can be modulated by experimentally extended periods of dark adaptation, with maximum vesicle size achieved after 24 hours of darkness, followed by vesicular shrinking after 48 hours of continuous darkness that persists through at least nine days (De Robertis & Franchi, 1956). L-type calcium channels provide the requisite calcium for vesicle filling, docking, and neurotransmitter release, however, experiments show endoplasmic reticulum stores may be involved in the maintenance of presynaptic calcium concentrations, especially in the dark (Križaj, 2012). Each rod spherule typically has one invaginating ribbon synapse filled by two horizontal cells, and two bipolar cells (S. Li et al., 2016). Müller cell processes are found within the OPL just outside of the synaptic region of the spherule. Gap junctions are found in the rod spherule connecting it to surrounding rod spherules and cone pedicles allowing communication of rod signals through cone pathways in a direct manner (Raviola & Gilula, 1973).

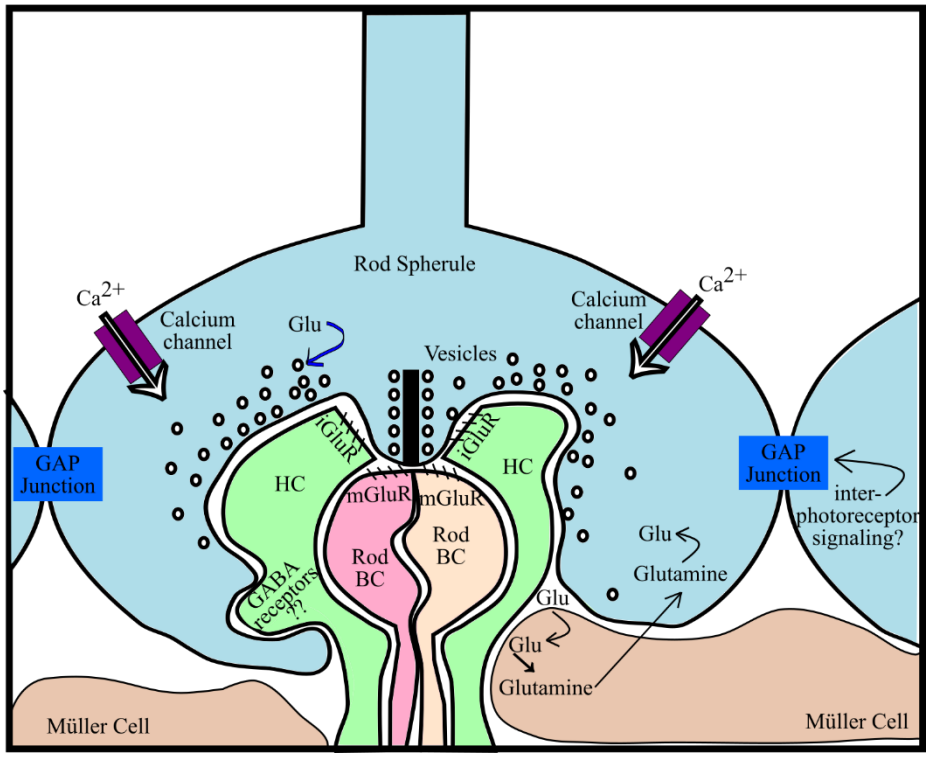

Figure 4: The rod spherule. The evaginated ribbon synapse of the dark-adapted rod photoreceptor releases vesicles of glutamate directly onto two rod bipolar cells (BC) and two horizontal cells (HC) to activate metabotropic glutamate receptors (mGluR) and ionotropic glutamate receptors (iGluR), found on BCs and HCs, respectively. Surplus glutamate is recovered post-synaptically by processes of the Müller cells outside of the synaptic region. The Müller cells convert glutamate into the synaptically inactive molecule, glutamine, and release it near the spherule for reabsorption. The rod converts glutamine into glutamate and packages it into vesicles for synaptic release. The docking and release of synaptic vesicles is a calcium-dependent process, and to meet the demand, the spherule has calcium channels. Gap junctions between rod spherules to each other and cone pedicles are thought to facilitate interphotoreceptor signaling or provide the rod photoreceptor access to the cone bipolar cell pathway. Adapted from "Circuitry for Rod Signals Through the Retina" by H. Kolb, 2011, Webvision. Moran Eye Center, http://webvision.med.utah.edu/book/part-iii-retinal-circuits/circuitry-for-rod-cells-through-the-retina/. Copyright 2011 by Helga Kolb. Adapted with permission.

Bipolar Cells

Bipolar cells send the signal generated in the photoreceptors and modulated by the horizontal cells inward to retinal ganglion cells and amacrine cells. There are around ten distinct types of bipolar cells, distinguished by their anatomy and pharmacology, whether they directly synapse with either rods or cones and what type of glutamate receptor (GluR) they express, metabotropic (mGluR) or ionotropic (iGluR). mGluRs transduce signal via a cGMP and G-protein mediated cascade similar to phototransduction in rods, which causes ion channels to close and depolarize (Nawy & Jahr, 1991; Shiells & Falk, 1990). iGluRs have an intrinsic ion channel that opens when activated by synaptic glutamate (Yamashita & Wässle, 1991). iGluRs are further characterized by the agonist they respond to and are either N-methyl-D-aspartate (NMDA) receptors, c-amino-3-hydroxy5-methyl-4-isoxazolepropionate (AMPA) receptors or kainate (KA) receptors (Asztély & Gustafsson, 1996).

Cone bipolar cells are considered ON bipolar if they depolarize in response to a light stimulus, expressing mGluRs in the OPL, or OFF bipolar if they hyperpolarize and express iGluRs. Rod bipolar cells are depolarizing and express mGluRs (Hughes, 1997; Puller, Ivanova, Euler, Haverkamp, & Schubert, 2013). It has been shown mouse and rat rod photoreceptors can directly activate cone OFF bipolar cells through activation of their AMPA iGluRs (Hack, Peichl, & Brandstätter, 1999). Rod bipolar cells do not directly synapse with ganglion cells in the IPL, but instead send signals to ganglion cells via A_{II} amacrine cells instead (Raviola & Dacheux, 1987). The b-wave of the scotopic electroretinogram (ERG) reflects the ionic electrical activity of rod bipolar cell stimulation (Hack et al., 1999).

Horizontal Cells

Horizontal cells are retinal interneurons with cell bodies in the INL and synapses found in the OPL. Each rod spherule ribbon synapse contacts two horizontal cells. Horizontal cells remain depolarized in the dark and hyperpolarize in response to the decrease of glutamate in the light, creating negative feedback circuits to surrounding photoreceptors (Weiler & Kewitz, 1993). γ-aminobutyric acid (GABA) is an inhibitory neurotransmitter found throughout the nervous system. Depolarized horizontal cells release GABA at surrounding cone synapses which opens cone chloride channels to inhibit light-evoked responses by changing synaptic voltage (Wu, 1992).

Amacrine Cells

Amacrine cells are inhibitory interneurons that modulate signal transmission between bipolar cells and retinal ganglion cells. Morphologically, amacrine cells are classified by the width of their dendritic arbors, which indicates the size of their receptive fields, stratification within the IPL, which determines if they process signals from ON or OFF bipolar cell pathways; and by the neurotransmitter they release, gamma-aminobutyric acid (GABA), glycine, or neither (nGnG) (Vaney, 1990). As previously mentioned the rod bipolar cells synapse to amacrine cells in the IPL to transmit a signal to the retinal ganglion cells without making direct connections (Raviola & Dacheux, 1987).

Oscillatory potentials, which are the oscillating wavelets found on the rising b-wave, are thought to arise from synaptic activity within the IPL of either the bipolar cells to amacrine cells, amacrine cells to ganglion cells, or activation of ganglion cells

(Heynen, Wachtmeister, & van Norren, 1985). Although the exact origin of OPs isn't defined, the recording is widely used clinically as OPs tend to be one of the first waveforms affected in some visually impairing diseases such as diabetic retinopathy, hypertension, and Parkinson's disease (Barber, 2003; Batcha et al., 2012; Hassan-Karimi et al., 2012; Kupersmith, Shakin, Siegel, & Lieberman, 1982; Macdonald, Naash, & Ayyagari, 2011; Mactier, Bradnam, & Hamilton, 2013; Marmor et al., 1988; Mcculloch, Marmor, Brigell, & Bach, 2015; Speros & Price, 1981; Sullivan et al., 1995; Wachtmeister, 1998).

Ganglion Cells

Retinal ganglion cells are classified based on the size of their receptive fields, and where they terminate within the brain. The following is a description of human/primate retinal ganglion cell types. Parvocellular midget retinal ganglion cells are the most abundant, receiving signals from very few photoreceptors per cell, and are sensitive to changes in color versus changes in contrast (Dacey & Petersen, 1992). Magnocellular parasol retinal ganglion cells are large, less abundant, are sensitive to changes in low contrast stimuli, not color and receive input from many rods and cones per cell (Solomon, Lee, & Sun, 2006). Koniocellular bistratified retinal ganglion cells are as abundant as parasol cells, receive input from rods and cones, are sensitive to mid-contrast stimuli and may be involved in color vision (Szmajda, Grünert, & Martin, 2008). Magnocellular, parvocellular, and koniocellular ganglion cells terminate in the lateral geniculate nucleus which projects to the visual cortex (Yücel, Zhang, Weinreb, Kaufman, & Gupta, 2003). Intrinsically photosensitive retinal ganglion cells contain the photopigment melanopsin

and are involved in circadian entrainment when they terminate in the suprachiasmatic nucleus or control the pupillary light reflex if termination is in the Edinger-Westphal nucleus (S. K. Chen, Badea, & Hattar, 2011).

Phototransduction Cascade – Activation

The process of vision is dependent upon a series of chemical reactions that start with the smallest particle of light, a photon. The chromophore 11-cis retinal photoisomerizes into all-trans-retinal (Wald, 1968). All-trans-retinal does not fit into the binding site of 11-cis-retinal, so rhodopsin changes configuration into the unstable metarhodopsin II, which eventually splits into opsin and all-trans-retinal during photoresponse recovery (Wald, 1968). Activated rhodopsin activates the G-protein coupled receptor, transducin (Surya, Foster, & Knox, 1995), leading to the displacement of guanine diphosphate (GDP) from transducin's α-subunit (Tα), which is replaced with guanine triphosphate (GTP) (Wessling-Resnick & Johnson, 1987). Each molecule of activated rhodopsin activates ~4,000 transducin molecules in the isolated bovine retina at 37°C (Kahlert & Hofmann, 1991). According to the Pugh lab, the rate of this reaction is around 7,000 Tα-GTP complexes per second per activated molecule of rhodopsin (Lamb & Pugh Jr., 1992). Tα-GTP activates the rod photoreceptor phosphodiesterase, PDE6, causing a drop in cyclic-guanosine monophosphate (cGMP) (Deterre et al., 1986). The rate of PDE6 activation is calculated to be the same as the rate of transducin activation (Lamb & Pugh Jr., 1992). The decrease in intracellular cGMP concentration causes the molecules of cGMP that were bound the cyclic-nucleotide gated cation channel (CNG channel) to release, and the

channel closes (Matthews, 1987). The closure of this cation channel hyperpolarizes the photoreceptor. Fusion of glutamate-containing vesicles for release at the synapse is drastically reduced as is the release of glutamate, which is the signal to hyperpolarize rod bipolar cells and horizontal cells (Massey, 1990). A summary of these events can be seen in Figure 5.

Phototransduction Cascade – Inactivation

As the constitutively active sodium calcium potassium exchanger (NCKX1) continues to work, extruding one calcium and one potassium ion for four sodium ions, and the CNG channels are closed from phototransduction, calcium levels within the rod drop (Reiländer et al., 1992). Fusion of glutamate-containing vesicles for release at the synapse is drastically reduced as is the release of glutamate, which is the signal to hyperpolarize rod bipolar cells and horizontal cells (Massey, 1990). A summary of these events can be seen in Figure 4. When calcium levels are low, recoverin, a calcium binding protein, dissociates from rhodopsin kinase allowing it to phosphorylate metarhodopsin II (Klenchin, Calvert, & Bownds, 1995). Arrestin then attaches to the phosphorylated metarhodopsin molecule completely inactivating it (Gurevich & Benovic, 1993). Regulator of G-protein signaling (RGS9) is a GTPase activating protein that causes intrinsic

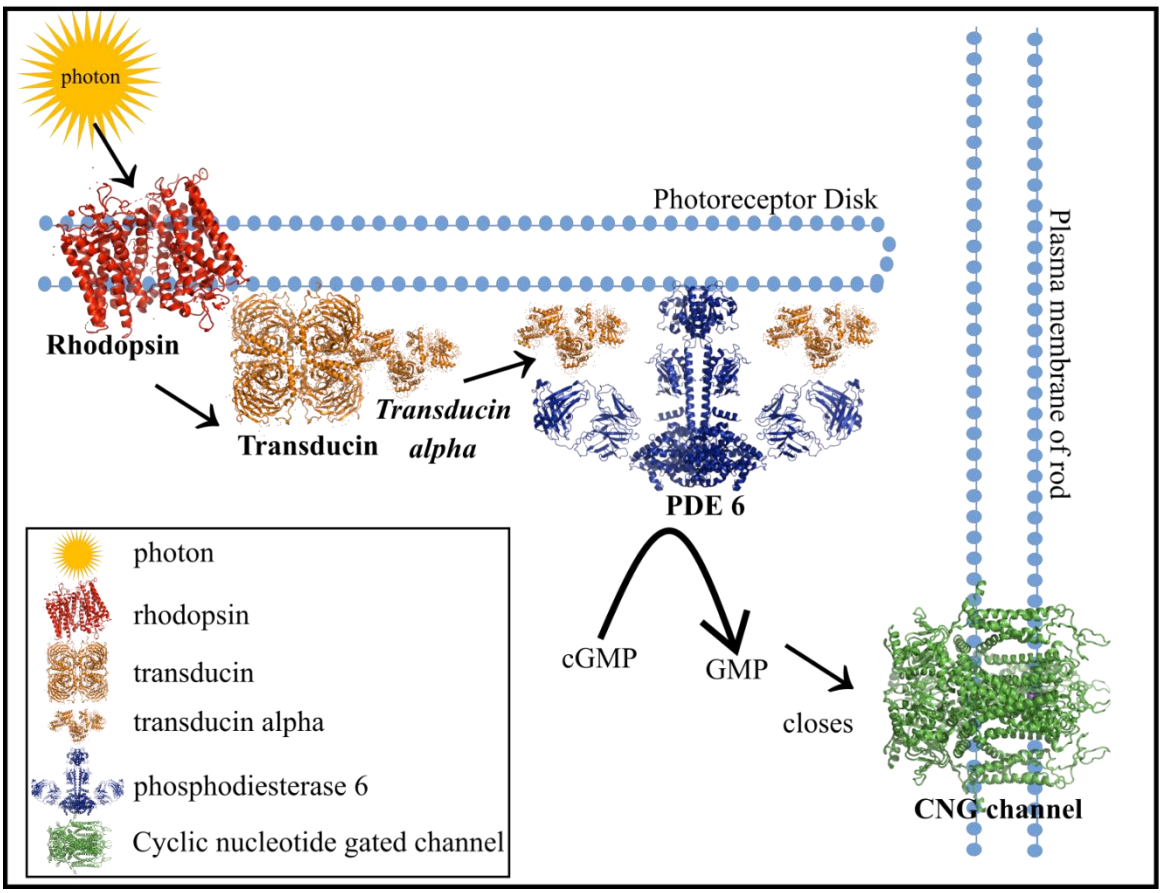

Figure 5: Phototransduction activation. A photon of light changes rhodopsin structure by photoisomerizing 11-cis-retinal to all-trans-retinal. This activates transducin, releasing its α-subunit, which displaces the inhibitory γ-subunits of PDE6. The resulting hydrolysis of cGMP decreases intracellular concentration, and the CNG channel closes causing photo-receptor hyperpolarization. [Crystal structures from protein database files. Rhodopsin - (Palczewski et al., 2000); Transducin βγ - (Sondek, Bohm, Lambright, Hamm, & Sigler, 1996); Transducin α - (Noel, Hamm, & Sigler, 1993); PDE6 - (Guo & Ruoho, 2011); CNG channel: (Gushchin, Gordeliy, & Grudinin, 2012)]

GTPase activity to cleave the Tα-GTP generating Tα-GDP (C. K. Chen et al., 2000). Due to a conformational change, Tα-GDP loses its affinity for PDE6 and dissociates, allowing the inhibitory subunit of the PDE6, PDE6γ, to reattach (Mou & Cote, 2001). While the CNG channel was closed, the intracellular levels of calcium dropped, activating the calcium level sensing molecule, guanylate cyclase activating protein (GCAP) (Gorczyca, Gray-Keller, Detwiler, & Palczewski, 1994). GCAP then activates guanylate cyclase (GC) which restores the dark-adapted levels of cGMP, promoting CNG channel opening (Goraczniak, Duda, Sitaramayya, & Sharma, 1994). When the CNG channels open, intracellular calcium levels return to normal and GCAP inactivates, causing GC to return to basal levels of activity, vesicle fusion can resume, and glutamate release is restored. The cell depolarizes, and the photoreceptor returns to the dark-adapted state. A schematic of photoreceptor inactivation is shown in Figure 6.

Visual Cycle

A schematic of the visual cycle can be seen in Figure 7. After phototransduction, the chromophore may still be bound to rhodopsin, which is a molecule of retinylidene, and together known as all-trans retinylidene. The Schiff base of all-trans retinylidene is N-retinylidene-phosphatidylethanolamine (N-retinylidene-PE), which is the preferred substrate for the transporter protein, ATP-binding cassette (ABCR4). ABCR removes the isomerized chromophore from the disk membrane into the lumen of the photoreceptor. After a reduction reaction catalyzed by all-trans-retinol dehydrogenase (RDH8), N-retinylidene-PE and all-trans-retinal are transformed into all-trans retinol, which exits the

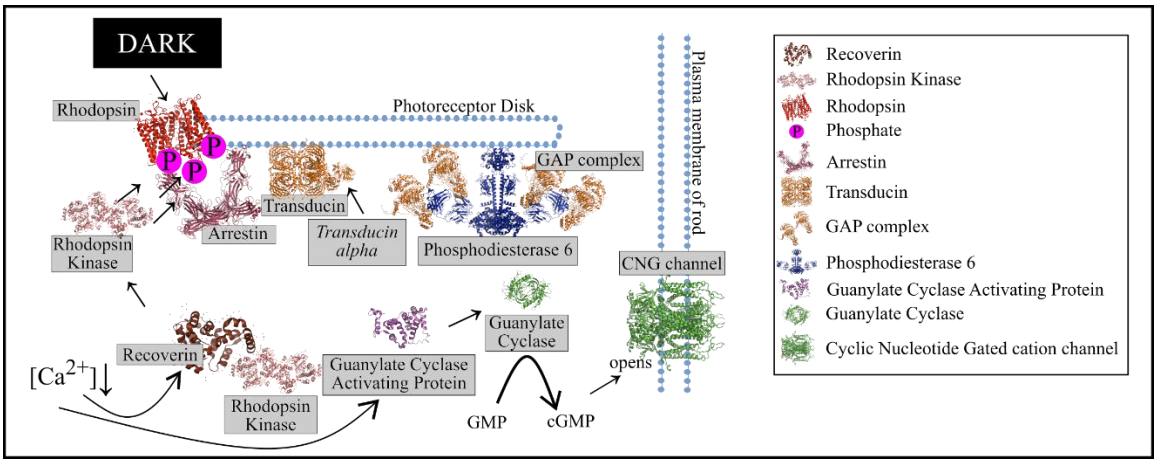

Figure 6: Phototransduction inactivation. In the dark calcium levels are low and causes the activation of recoverin and guanylate cyclase activating protein. Active recoverin releases from rhodopsin kinase, which then phosphorylates rhodopsin for binding with arrestin. Transducin-α is displaced from PDE6 by the GAP complex which replaces the inhibitory γ-subunits on PDE6. Guanylate cyclase activating protein activates guanylate cyclase causing intracellular cGMP levels to increase allowing the CNG channels to reopen and the photoreceptor transiently depolarizes, returning to the dark state. Crystal structures of proteins from PDB files. [Arrestin - (Zhan, Gimenez, Gurevich, & Spiller, 2011); Recoverin - (Flaherty, Zozulya, Stryer, & McKay, 1993); Rhodopsin kinase - (Ames, Levay, Wingard, Lusin, & Slepak, 2006) Guanylate cyclase activating protein - (Ames, Dizhoor, Ikura, Palczewski, & Stryer, 1999); Guanylate cyclase - (Winger, Derbyshire, Lamers, Marletta, & Kuriyan, 2008); GAP complex - (Slep et al., 2001)]

outer segment into the sub-retinal space where it is attached to the interphotoreceptor matrix binding protein (IRPB) that transports it to the RPE. In the RPE, cellular retinol binding protein (CRBP) carries all-trans retinol to the smooth endoplasmic reticulum-bound enzymes, lecithin-retinol transferase (LRAT), retinoid isomerohydrolase (RPE65), and 11-cis retinol dehydrogenase (RDH5). LRAT converts 11-trans retinol into an all-trans-retinyl ester. RPE65 converts all-trans-retinyl ester into 11-cis retinol. RDH5 converts 11-cis retinol into11-cis retinal which is loaded onto the cellular retinaldehyde-binding protein, CRALBP (Y. Xue et al., 2015). IRBP receives 11-cis retinal from CRALBP and delivers from the subretinal space into the photoreceptor (Kiser, Golczak, Maeda, & Palczewski, 2013).

CNGB1 and GARPs – The History

The "Other" GARPs

Before GARPs were discovered in the retina, glutamic acid-rich proteins were found in the porcine brain with a molecular weight of 56 – 58 kDa (Ishioka, Isobe, Okuyama, Numata, & Wada, 1980). Preliminary analysis of the amino acid sequence indicated that the protein functioned as a calcium-binding protein due to its acidity and negative charge (Ishioka et al., 1980). Interestingly, when assessing the molecular weight using sodium dodecyl sulfate-polyacrylamide gel electrophoresis (SDS-PAGE), the motility of this glutamic acid-rich protein depended on the presence or absence of SDS buffer, appearing larger when SDS was present (Ishioka et al., 1980). Micro glutamic acid-rich proteins (micro-GARPs) were then discovered and isolated from the human brain (Nomata, Watanabe, & Wada, 1983) and the bovine brain (T. Isobe, Ishioka, Kadoya, &

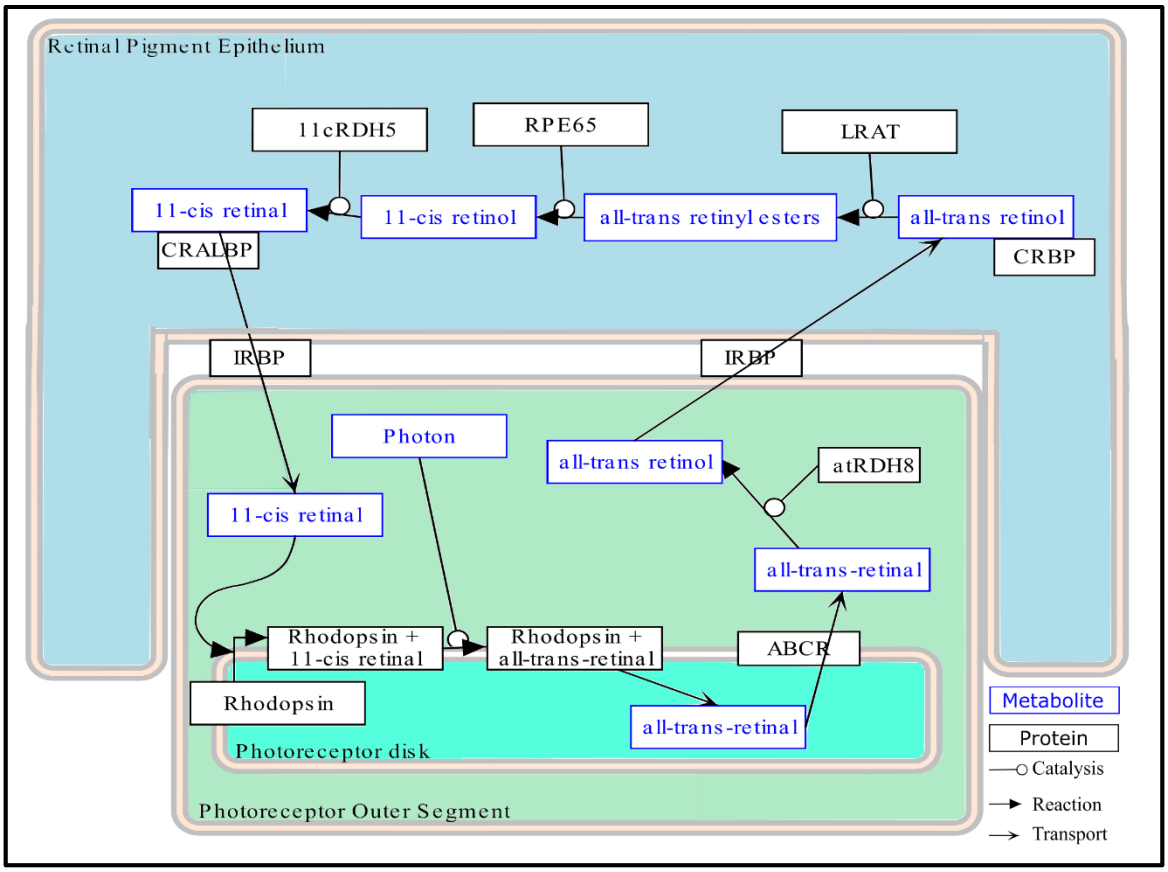

Figure 7: The visual cycle. Steps of the visual cycle occur in the photoreceptor outer segments and within the RPE. The cycle begins and ends with the molecule of chromophore, 11-cis-retinal, bound to rhodopsin. Abbreviations: ABCR – ATP Binding Cassette, Subfamily A member 4; atRDH8 – all-trans-retinol dehydrogenase; IRBP – interphotoreceptor retinoid-binding protein; LRAT – lecithin retinol acyltransferase; RPE65 – retinoid isomerohydrolase; 11cRDH5 – 11-cis retinol dehydrogenase; CRALBP – cellular retinal binding protein. Adapted from "The Visual Cycle: Generation of 11-cis-retinal for Photoreceptors" by H. Kolb, 2011, American Society for Photobiology, http://www.photobiology.info. Copyright 2009 by American Society for Photobiology. Adapted with permission.

Okuyama, 1982). The bovine micro-GARPs were ~10 kDa and composed of approximately 50% glutamic acid residues (T. Isobe et al., 1982). The amino terminus of the bovine and porcine brain glutamic acid-rich proteins was identical (T. Isobe et al., 1982). The protein sequence of the micro-GARPs was homologous to the C-terminus of the neurofilament 68-kDa protein (Toshiaki Isobe & Okuyama, 1985). Later, it was determined the glutamic acid-rich proteins isolated from the porcine, bovine, and human brains, along with a few other acidic neural proteins, were proteolytic degradation products of the 68-kDa neurofilament protein (Weber & Geisler, 1983).

Discovery of the Rod Photoreceptor CNG Channel and GARPs

Initially, the rod CNG channel was reported to be homomeric, composed of 63 kDa subunits (Cook, Hanke, & Kaupp, 1987; Kaupp et al., 1989), which we now know as CNGA1, or the α-subunit. A second protein of 240 kDa was also identified, but as it eluted separately it was considered a protein uninvolved with channel formation or activity (Cook et al., 1987), and this is now known to be the β-subunit.

When the homomeric CNGA1 channel was first isolated, cloned and heterologously expressed, properties were similar to, but not exactly matching, isolated patch clamp recordings of native rod photoreceptor plasma membrane tissue (Cook et al., 1987; Kaupp et al., 1989). These channels were opened/activated by cGMP, but lacked the previously reported L-cis-diltiazem blockade observed in native rod photoreceptor plasma membrane and isolated disks (K.-W. Koch, Cook, & Kaupp, 1987; Stern, Kaupp, & Macleish, 1986).

CNGA1 was once referred to as human rod cyclic nucleotide channel subunit 1, hRCNC1. CNGB1 was called hRCNC2 (T. Y. Chen et al., 1993). Two variants of the β-subunit were found, a 623 aa protein localized to the ROS and OPL, named hRCNC2b, and a 909 aa OPL exclusive transcript, hRCNC2a (T. Y. Chen et al., 1993). Focus was placed on the ROS version – the protein without the elongated N'-terminus, hRCNC2b. Electrophysiological studies (patch clamp) of recombinant mutant channels found the heteromeric channel, composed of CNGA1 and CNGB1 was substantially inhibited by L-cis-diltiazem, while the homomeric CNGA1 channel was 100 times less inhibited by L-cis-diltiazem. Expression of only CNGB1 formed no channels (T. Y. Chen et al., 1993). It is observed that when native rod CNG channels are isolated and separated by SDS-PAGE, that 63 kDa and 240 kDa bands are presented. The 240kDa protein is suspected to be a complex containing hRCNC2b, and to be the β-subunit to the already characterized 63kDa α-subunit (T. Y. Chen et al., 1994).

Another investigator also eluted the 240 kDa protein with the 63 kDa CNG channel protein along with another protein, spectrin, which is a structural constituent of many plasma membranes (Molday, Cook, Kaupp, & Molday, 1990).

The first GARP protein was found in the bovine retina by cDNA cloning. The coding region of the transcript is1770 bp encoding a 590 aa protein predicted to have a molecular weight of 65 kDa. A glutamic acid-rich domain (68 Glu of 109 aa) was found toward the N-terminus of the predicted protein (Sugimoto, Yatsunami, Tsujimoto, Khorana, & Ichikawa, 1991). This protein was reported to have very high homology to the neurofilamentous glutamic acid-rich proteins found in the bovine brain (Sugimoto et al., 1991).

The GAR1 gene (now known to be the CNGB1 gene) was found to span 11 kb, 12 exons, 11 introns, ORF = 697 bp, 299 aa and was localized to human chromosome 16q13 using fluorescence in situ hybridization. The protein consists of 14% proline, 14% glutamate and has nine potential phosphorylation sites. GAR1 represents a subset of the entire *Cngb1* locus, encoding only the GARP region of the *Cngb1* channel β-subunit, and GARP1 and GARP2. (M D Ardell et al., 1995). The composition of this murine protein was similar to the bovine GARP protein isolated by Sugimoto that co-purified with PDE6 (M D Ardell et al., 1995; Sugimoto et al., 1991). The 240 kDa protein is the complete β-subunit (Körschen et al., 1995). The actual bovine cDNA for the β-subunit codes for a 1394 amino acid protein with a predicted molecular weight of 155 kDa; amino acids 1-571 represent the GARP region and 572-1394 the β-subunit of the CNG channel region (Körschen et al., 1995). Northern blotting of retinal mRNA showed three transcripts when using a cDNA probe specific for the GARP part 7.4 kb, 4.2 kb, and 1.6 kb (Körschen et al., 1995). Western blotting using antibodies against the glutamic acid-rich region detects the β-subunit and a doublet of two other proteins (Körschen et al., 1995). C-terminal Immunohistochemistry with a C-terminal antibody localized the β-subunit mainly in the ROS, but also weakly in the OPL and NFL (Körschen et al., 1995).

The *Cngb1* locus maps to human chromosome 16q13 (Michelle D. Ardell et al., 1996). The size of the β-subunit is now reported as 1251 aa with a molecular weight of 140 kDa, and the γ-subunit, now called, hGARP2 has a molecular weight of 32kDa but runs on a gel at 67 kDa (Michelle D. Ardell et al., 1996). A novel 10 kb transcript encoding an unknown 70 kDa protein is also reported (Michelle D. Ardell et al., 1996), but has

not been further characterized. Terminology was updated for the GARP proteins as truncated GARP, the 299 amino acid product thought to be the γ-subunit, and full-length GARP, the 590 amino acid glutamic acid-rich protein isolated from the bovine retina, by the first group to successfully clone cDNAs encoding all three proteins (Colville & Molday, 1996).

Characterization of the CNG Channel

Cngb1, the gene. Cngb1, formerly known as GAR1, was analyzed for donor and acceptor splice sites across its 33 exons spread over 100 kb on human chromosome 16q13 possibly encoding 4 or more protein transcripts based on the possible alternative splicing scenarios (M D Ardell, Bedsole, Schoborg, & Pittler, 2000). mRNA probes used to perform in situ hybridization of RP genes found mRNA for CNGB1 in the photoreceptor, INL, and GCL (Trifunović et al., 2008).

CNG channel stoichiometry. The first studies of the rod CNG channel predicted the channel to be composed of two alpha and two beta subunits (He, Ruiz, & Karpen, 2000; Shammat & Gordon, 1999). However, the stoichiometry of the CNG channel has now been shown to be three CNGA1: one CNGB1 by heterologous expression of mutant fluorescent channel subunits in *Xenopus laevis* oocytes and measuring fluorescence resonance energy transfer (FRET) between donor and acceptor fluorophores attached to the proteins (Zheng, Trudeau, & Zagotta, 2002). The carboxy-terminal leucine zipper (CLZ)

domain of the CNGA1 channel, found just beneath the CNBD, mediates a 3:1 stoichiometry based on cross-linking experiments (Zhong, Molday, Molday, & Yau, 2002). When the CLZ is deleted, the CNG channel can have more than one β-subunit and is therefore vital to CNG channel 3:1 stoichiometry (Shuart, Haitin, Camp, Black, & Zagotta, 2011). Cross-linking and examination of the molecular weights of the rod CNG channel confers a three alpha to one beta conformation (Weitz, Ficek, Kremmer, Bauer, & Kaupp, 2002).

CNG channel subunit interactions. A region of the N-terminus of the β-subunit (amino acids 677 to 701) was found to interact with a region on the C-terminus of the α-subunit (amino acids 609-693) of the CNG channel (Trudeau & Zagotta, 2002a). If the C-terminal region of the α-subunit was deleted, the channels were not expressed on the surface of the membrane, which causes an RP phenotype (Trudeau & Zagotta, 2002a). If the N-terminal region on the β-subunit was deleted, then the channel lost its sensitivity to calcium/calmodulin inhibition (Trudeau & Zagotta, 2002b). So, both subunits need to be present in a complex to properly localize to the ROS and to bind calcium/calmodulin. Calcium/calmodulin inhibits the rod CNG channel by disrupting inter-subunit interaction (Trudeau & Zagotta, 2002b). The same mechanism of inhibition through inter-subunit disruption by calcium-calmodulin is active in the olfactory system, but the residues are not the same, as the C-terminus of CNGA1 binds to the N-terminus of CNGB1, while the N-terminus of CNGA4 binds to the C-terminus of CNGB1b (Trudeau & Zagotta, 2003). Ion permeability of the heterooligomeric channel shows ammonium is more permeable than lithium which is more permeable than sodium and potassium which have similar

permeabilities and are more permeable than rubidium which is more permeable than cesium (Körschen et al., 1995)

Localization. Photoreceptor CNG channels, both rod, and cone varieties, localize to cholesterol and sphingolipid detergent-resistant membrane (DRM) domains on the plasma membrane of the OS and in cultured, transfected HEK293 cells (X. Q. Ding, Fitzgerald, Matveev, McClellan, & Elliott, 2008). Guanylate cyclase, CNG channels, and PDE6 were found to localize to the disk rims and incisures of ROS in the phototransductive region, separated from the morphogenic region by a diffusion barrier (Nemet, Tian, & Imanishi, 2014). Peripherin/rds and NCKX1 interact with the β-subunit, possibly to anchor the exchanger and facilitate disc to plasma membrane stability (Poetsch, Molday, & Molday, 2001). Peripherin-2 was found to couple rhodopsin to CNGB1 at the disk rims to make phototransductive microdomains (Becirovic et al., 2014). The RP causing mutation p.G266D on peripherin disrupts its connection with rhodopsin (Becirovic et al., 2014). The cytoskeleton protein, 4.1G, co-immunoprecipitated with CNG channels not associated with peripherin-2, binding to the channel using 4.1G's FERM (4.1, ezrin, radixin, moesin domain) and CTD (C-terminal domain) regions (Cheng & Molday, 2013). As mentioned previously, the CNG channel co-precipitates with the structural protein spectrin (Molday et al., 1990), which is required for CNG channel and NCKX1 expression within the rod inner segment (Kizhatil, Sandhu, Peachey, & Bennett, 2008).

Matrix metalloproteinases (MMPs). MMP-9 and MMP-2 were applied to heterologously expressed CNG channels and patch clamp technology was used to assess the effect on CNG channel responses (P. C. Meighan, Meighan, Rich, Brown, & Varnum, 2012). MMP9 increased the affinity for and efficacy of cGMP in rod heterotetrameric CNG channels (P. C. Meighan et al., 2012). Looking at the opening transition free energy, ΔΔG is ¾ reduced in heteromeric channels versus homomeric under MMP9 application meaning the β-subunit is not affected by MMP9, or is not affected in a manner that alters channel gating (P. C. Meighan et al., 2012). Glycosylation inside the pore region of the α-subunit in cones, CNGA3, inhibits MMP mediated ligand sensitivity and channel conductance changes, but not when rod CNGA1 subunits are glycosylated (S. E. Meighan, Meighan, Rich, Brown, & Varnum, 2013).

Ankyrin G. Ankyrin G coimmunoprecipitates with the β-subunit of rods and deletion of ankyrin G reduced CNG channel expression (Kizhatil, Baker, Arshavsky, & Bennett, 2009). Mutagenesis experiments of the β-subunit with the RP variant that truncates the C terminal 28 amino acids (Kondo et al., 2004) showed no binding of ankyrin-G and were mislocalized to the perinuclear region of the rod and not the ROS (Kizhatil et al., 2009). When ankyrin G site is deleted in bovine models, CNGB1 is appropriately trafficked, and the N-terminal VXPX sequence suggested to be critical for trafficking, is only observed in rodent CNGB1, indicating that it is not likely a critical factor in CNGB1 trafficking across species. Deletion of the GARP region of CNGB1 in rods, however, does prevent trafficking to the OS and CNGB1 is found in the IS and calyceal processes.

Calcium/calmodulin. Experiments creating mutations of β-subunit C-terminal and N-terminal sequences found that ablation of the calcium/calmodulin binding sites did not prevent its inhibitory effect on the channel (Grunwald, Yu, Yu, & Yau, 1998). Y498 on CNGA1 and Y1097 on CNGB1 are tyrosine phosphorylation sites possibly regulating calcium/calmodulin binding and inhibition (Molokanova, Krajewski, Satpaev, Luetje, & Kramer, 2003). The phosphorylation is mediated by PTK and PTP protein tyrosine kinases and phosphatases activated by insulin-like growth factor 1 (Molokanova et al., 2003). Phosphorylation of CNGA1, not CNGB1, inhibits calcium/calmodulin binding based on electrophysiological testing of mutants where the proposed phosphorylated tyrosine is replaced with phenylalanine and heterologously expressed in *Xenopus laevis* oocytes (Krajewski, Luetje, & Kramer, 2003). The rate-limiting step of CNG channel inhibition is the binding of calcium/calmodulin (Trudeau & Zagotta, 2004). The effect on light adaptation in mice of CNG channel inhibition by calcium/calmodulin was tested by deleting the binding site from mice (J. Chen et al., 2010). Deletion of the calcium/calmodulin binding site on CNGB1 does not affect light adaptation in the manner it was postulated. However, it does change the response waveform leading to new speculation that calcium regulates the rate of decay of PDE6 (J. Chen et al., 2010). The calcium/calmodulin binding domain of the β-subunit found at N-terminal amino acids A162-D264 was found to be of the LQ type, indicating that calcium/calmodulin only binds under low calcium concentrations (Ungerer et al., 2011).

Inhibitory interactions. CNG channels were found to be inhibited by all-trans-retinal, the isomerized chromophore from the phototransduction cascade, by closing channels and decreasing channel affinity to cGMP (McCabe et al., 2004). Growth factor receptor-bound protein 14 (GRB14) binds to the C-terminus of CNGA1 and reduces cGMP binding, and causes channel closure (Gupta, Rajala, Daly, & Rajala, 2010). Dequalinium, an organic divalent cation, blocks CNGA1 homomeric channels, and in a voltage-dependent manner, native CNGA1/CNGB1 heteromeric channels (T. Rosenbaum, Islas, Carlson, & Gordon, 2003). Dopamine signaling inhibition reduces retinal cGMP in the *rd1* mouse via an unknown mechanism, but not by changing CNG channel expression (Ju Zhang, Richmond, & Ogilvie, 2014).

Characterization of the GARPs

GARP proteins are determined to be intrinsically disordered using the software predictors of natural disordered regions (PONDR® www.pondr.com) with 89% of GARP1 and 80% of GARP2 showing intrinsic disorder (Batra-Safferling et al., 2006). Affinity column chromatography results showed that GARPs might bind to PDE6, guanylate cyclase, and ABCR (Körschen et al., 1999). Körschen also reported GARP2 inhibits active PDE6, possibly to prevent unnecessary cGMP turnover during light saturation, i.e., daytime since cone photoreceptors do not express GARPs (Körschen et al., 1999). Isotonic washes of homogenized purified ROS left PDE6 and GARP2, hypotonic washes removed PDE6 & GARP2, anion exchange chromatography led to coelution of PDE6 and GARP2, gel filtration chromatography did not separate PDE6 and GARP2.

Sulfolink beads with PDE6 specific antibody always pulled down GARP2, unless PDE6 was absent (Pentia, Hosier, & Cote, 2006). Pentia also reported GARP2 inhibited spontaneous, non-transducin mediated activation of PDE6, with no effect on PDE6 already activated by transducin (Pentia et al., 2006). Crosslink and pulldown of proteins using antibodies specific for GARP1, GARP2, and the GARP region of CNGB1 would immunoprecipitate peripherin/*rds*, and vice versa hence the hypothesis the GARPs are essential to rod photoreceptor structure (Poetsch et al., 2001), (see Figure 8).

In a cryo-EM study of the connecting cilium structure in models of retinal degeneration, a mouse model lacking all three *Cngb1* gene products was studied and invalidated the peripherin/rds to GARP2 interdisc spacing structural hypothesis. The spacing of the discs, 32 nm, is divisible by the 8 nm tubulin dimer repeat of the axoneme and was normal in these mice, thus GARP2 is not required for disc/disc interaction (Gilliam et al., 2012).

Using confocal microscopy and fluorescent tags on GARP2, the β-subunit, and *rds*/peripherin, CNGB1 binds to *rds*/peripherin in both the inner segment and outer segment, and GARP2 binds to *rds*/peripherin at the disk morphogenic region of the ROS and only in the OS (Ritter et al., 2011). CNGB1 fluorescence was also observed in the OPL. Fluorescence of CNGB1 was only observed when the fluorophore was attached to the N-terminus and not the C-terminus (Ritter et al., 2011). A minor interaction between CNGB1 and rhodopsin was also observed but thought to be random noise (Ritter et al., 2011).

A mouse model overexpressing GARP2 (GARP2-Ox) exhibited a 20% shorter ROS, no change in photoreceptor sensitivity to light, a two-fold increase in phototransduction

gain, and ~70% longer flash recovery time (Sarfare et al., 2014). The GARP2-Ox line was crossed to a knockout of retinal degeneration slow (RDS) (Chakraborty, Conley, DeRamus, Pittler, & Naash, 2015). The RDS/ GARP2-Ox phenotype included: malformed ROS disc rims; "leaky" GARP2 expression in cones; accelerated retinal degeneration; aberrant GARP2 localization throughout the IS, ONL, and OPL although heterozygous RDS and GARP2-Ox trafficked properly to the OS; but there was a functional decrease in scotopic ERG a- and b- wave with deterioration of cone function (Chakraborty et al., 2015). Using a mouse model of RP, which lacks all three CNGB1 proteins (*Cngb1*-X1) (Youwen Zhang et al., 2009), as a background for individual expression of wildtype levels of GARP1 and GARP2, normal levels of GARP2 accelerated the degeneration over the previously observed and recorded levels (Deramus et al., 2017).

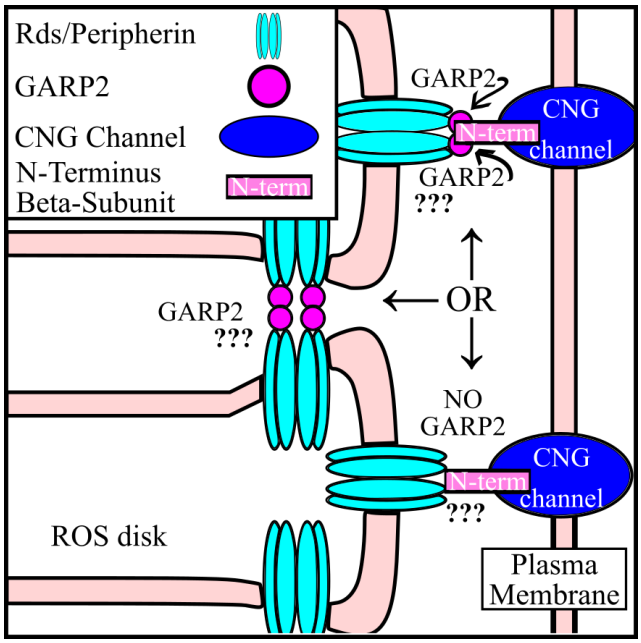

Figure 8: GARP2 localization for ROS disk rim stability. GARP2 is proposed to connect *rds*/peripherin found in rod disk rims to the plasma membrane-bound CNG channel β-subunit. Also, GARP2 was proposed to bind molecules of *rds*/peripherin vertically between disk membranes facilitating rod photoreceptor interdisc structural stability. Adapted from "Glutamic Acid-rich Proteins of Rod Photoreceptors Are Natively Unfolded" by R. Batra-Safferling, K. Abarca-Heidemann, H. G. Körschen, C. Tziatzios, M. Stoldt, I. Budyak, D. Willbold, H. Schwalbe, J. Klein-Seetharaman, and U. B. Kaupp, 2004, Journal of Biological Chemistry, 281, p.1458, Copyright 2006 by The American Society for Biochemistry and Molecular Biology, Inc. Adapted with permission.

Retinitis Pigmentosa and the CNG Channel

Retinitis Pigmentosa (RP) is a collection of hereditary blinding diseases caused by mutations in any one of over 200 genes (Daiger, Rossiter, Greenberg, Christoffels, & Hide, 1998). Each type of RP is classified and numbered by the gene containing the causative mutation. Most of the mutations causing RP are in genes encoding phototransduction, metabolic, or ciliary proteins. Typical RP affects rod photoreceptors first, meaning

the patient loses the ability to see under scotopic and dim illumination conditions, clinically referred to as nyctalopia. Often, peripheral cone photoreceptors malfunction and die concurrently with or very soon after rod photoreceptor cells, causing the patient to additionally lose photopic peripheral vision. Finally, in more severe forms of the disease, central cones begin to die, leading to loss of acute vision and complete blindness can occur. Our protein of interest, GARP2, is a rod photoreceptor-specific splice variant of *Cngb1,* a gene known to cause RP (OMIM #613767) when any one of several mutations occur. A summary of the known *Cngb1* mutations is listed in Table 1 with GARP2 exon mutations in boldface type.

Table 1: *Cngb1* mutations causing retinitis pigmentosa. The mutations in bold affect GARP2 encoding exons.

Mutation	Effect of mutation	Citation
p.Gly993Val	Human RP Terminates C-terminus (Kondo et al., 2004)	(Bareil et al., 2001)
c.3444+1G>A	Last 28 amino acids truncated so no ankyrin G binding (Kizhatil et al., 2009) Skips exon deletes 170 aa replaces with 68 wrong amino acids (Becirovic et al., 2010)	(Kondo et al., 2004)
c.2957A>T p.Asn986Ile	Missense mutation	(Simpson, Clark, Alexander, Silvestri, & Willoughby, 2011)
c.412+1G>A c.2284C>T p.Arg762Cys	Splice site mutation Missense mutation	(Azam et al., 2011)
c.2387delA2389_2390insAGCTAC	Canine RP (progressive retinal atrophy) frameshift and premature stop codon	(P. A. Winkler et al., 2013)
c.2685delA2687_2688insTAGCTA	Canine RP Indel	(Ahonen, Arumilli, & Lohi, 2013)
p.Cys632* c.1896C>A p.Gly1050fs c.3150delG	Patient heterozygous for premature stop codon mutation and frameshift mutation.	(Nishiguchi et al., 2013)
c.1589C> G; p.Pro530Arg	Missense mutation	(Fu et al., 2013)
p.Arg762Cys	Exon 23 Missense mutation	(Bocquet et al., 2013)
p.Arg86Gln	Exon 4 West African polymorphism (non-disease-causing)	(Gibriel et al., 2013)
p.Arg765Cys	Missense mutation	(Schorderet, Bernasconi, Tiab, Favez, & Escher, 2014)
p.Tyr787* c.2361C>A p.Phe963Sfs*4 c.[2888_2889delTT]	Heterozygous for two mutations.	(Xu et al., 2014)
c.2493-2A>G	Frameshift in Exon 26 leading to a premature stop codon and a truncated β-subunit of 831 aa instead of 1251 aa.	(Maria et al., 2015)

c.413-1G>A	**Frameshift at Exon 7 and premature stop codon**	**(Saqib et al., 2015)**
c.2493-2_2495delinsGGC p.Ser831fs	Frameshift and premature stop codon	(Maranhao et al., 2015)
p.Leu849fs	Macular cystoid spaces	(Lingao et al., 2016)
p.Lys175fs	**Macular cystoid spaces**	**(Lingao et al., 2016)**
c.939G>A; p.Trp313*	Exon 13 premature stop codon	(Fradin et al., 2016)
c.2293C > T p.Arg765Cys	Exon 26 missense	(Habibi et al., 2016)
c.2957A>T p.Asn986Ile	Exon 29 Missense mutation	(Hull et al., 2017)
c.262C>T p.[Gln88*]	Exon 3 Nonsense mutation	(Hull et al., 2017)
c.664C>T p.[Gln222*]	Exon 10 Nonsense mutation	(Hull et al., 2017)
c.952C>T p.[Gln318*]	Exon 13 Nonsense mutation	(Hull et al., 2017)
c.2185C>T p.[Arg729*]	Exon 22 Nonsense mutation	(Hull et al., 2017)
c.3142_3143insGTGG p.[Ala1048fs*13]	Exon 31 Frameshift mutation	(Hull et al., 2017)
c.2544dupG p.[Leu849Alafs*3]	Exon 26 Frameshift mutation	(Hull et al., 2017)
c.761+2T>A	Intron 10 – affects splice donor site	(Hull et al., 2017)
p.Trp639* c.1917G>A p.Tyr787* c.2361C>A	Exon 20 and Exon 24 heterozygous RP patient	(Banerjee, Yao, Zhang, Niu, & Chen, 2017)
c.3150delG p.Phe1051Leufs*12	Frameshift and nonsense	(Petersen-Jones et al., 2018)
c.2284C>T p.Arg762Cys	Missense	(Petersen-Jones et al., 2018)
c.2508C>A p.Tyr836*	Nonsense	(Petersen-Jones et al., 2018)
c,1122-9G>A p.?	Unknown protein effect	(Petersen-Jones et al., 2018)
c.2218-2A>G p.?	Unknown protein effect	(Petersen-Jones et al., 2018)
c.2544_2545insC p.Leu849Profs*3	Frameshift and premature stop codon	(Petersen-Jones et al., 2018)
c.522_523insC p.Lys175Glnfs*4	**Frameshift and premature stop codon**	**(Petersen-Jones et al., 2018)**
c.1896C>A p;Cys632*	Nonsense	(Petersen-Jones et al., 2018)

Cngb1-KO Mouse Models

Cngb1-X26: No β-subunit, retains GARPs. Exon 26 of the *Cngb1* gene encoding the pore and S6 segments of the β-subunit was ablated in the *Cngb1*-X26 mouse line, removing all isoforms of CNGB1 from all tissues in the mouse, including olfactory tissue, while retaining GARP1 and GARP2 (Huttl et al., 2005). Homomeric CNGA1 channels were weakly observed in the ROS, although the mRNA levels were equal to WT (Huttl et al., 2005). The rods were lost entirely by six months, and no photoreceptors remained at 11

months. Structurally, the disks of the ROS were not different from WT meaning the β-subunit is not necessary for structural integrity (Huttl et al., 2005). Optokinetic measurements of the *Cngb1*-X26 mouse showed a decline in visual acuity (Schmucker, Seeliger, Humphries, Biel, & Schaeffel, 2005). The olfactory function of the *Cngb1*-X26 was diminished, as tested with electro-olfactogram, due to CNGB1 ablation (Michalakis et al., 2006). Olfactory protein trafficking was altered with CNGA2/CNGA4 channels trapped in the olfactory knobs instead of the typical location, the olfactory cilia (Michalakis et al., 2006). This means that CNGB1 also is required in the olfactory system for proper function and protein localization (Michalakis et al., 2006).

The unfolded protein response (UPR) mechanism was examined in the *Cngb1*-X26 mouse and found not to be activated in the *Cngb1*-X26, invalidating the equivalent light hypothesis of retinal degeneration (Lisman & Fain, 1995), as the absence of CNG channels is equivalent to constant channel closure which happens in light conditions (T. Wang & Chen, 2014). Examination of the retinal degeneration mechanism of the *Cngb1*-X26 shows that non-apoptotic mechanisms cause the degeneration in this model. There were increased cGMP and PAR accumulation, (histone deacetylase) HDAC activity, PARP (Poly-ADP-ribose-polymerase) activity and calpain that were not active in WT non-RP control mouse retinas (Arango-Gonzalez et al., 2014). Flow cytometry, immunohistochemistry, and gene expression analysis of *Cngb1*-X26 shows microglial activation before photoreceptor degeneration (Blank et al., 2018).

A cross between the *rd1* mouse and the *Cngb1*-X26 mutant mouse delayed the degeneration of the *rd1* RP phenotype (Paquet-Durand et al., 2011). The *rd1* mouse had peak cell death at p13, *Cngb1*-X26 at p24 and the cross at p18 (Paquet-Durand et al.,

2011). The rescue is proposed to be from the lack of calcium entry into the ROS due to the lack of CNG channels (Paquet-Durand et al., 2011). A mouse RP model deleted for cone CNGA3 and rod CNGB1 (the *Cngb1*-X26 mouse) was found to have gene expression changes indicating synaptogenesis, and morphological examination shows new neurites growing in the ONL from the bipolar cells and horizontal cells (Michalakis et al., 2013). A murine double KO of *Cngb1*-X26 and hyperpolarization-activated cyclic nucleotide-gated channel 1 (HCN1) degenerated more quickly with more calpain activity than *Cngb1*-X26 alone (Schön et al., 2015). The synaptic Ca_v 1.4 L-type voltage-gated calcium channel α1-subunit encoded by *Cacna1f* was added to the double knockout to make this triple knockout: *Cngb1*-X26/HCN1$^{-/-}$/*Cacna1f*$^{-/-}$, which degenerated slower than the double-KO but faster than *Cngb1*-X26 alone. HCN1$^{-/-}$ crossed to the CNGA3$^{-/-}$ mouse also exhibited accelerated degeneration (Schön et al., 2015). The *rd1* mouse model was crossed with the Ca_v1.4 L-Type calcium α1-subunit knockout, *Cacna1f*$^{-/-}$, and a decrease in calpain activity was noted, and the degeneration was slowed, but not permanently (Schön, Paquet-Durand, & Michalakis, 2016).

AAV mediated replacement of the CNGB1b subunit into rod photoreceptors using sub-retinal injections in 2-week-old *Cngb1*-X26 knockout mouse pups successfully delayed retinal degeneration and promoted normal retinal function (S. Koch et al., 2012; Michalakis et al., 2014).

Cngb1-X1*, No β-subunit, no GARPs.* Deletion of exon 1 of *Cngb1* in a mouse model (*Cngb1*-X1) removed the β-subunit and both GARPs (Youwen Zhang et al., 2009). Structurally, disk morphogenesis is altered in the *Cngb1*-X1 knockout mouse, and functionally, sensitivity to light is reduced in *Cngb1*-X1 mice (Youwen Zhang et al., 2009). Examination of cone function of the *Cngb1*-X1 mouse through advanced age shows the cones survive several months after the loss of all detectable ERG function of rod photoreceptors at about 12-14 months (Youwen Zhang et al., 2012). The primary indicator of cone function is a stable critical flicker fusion frequency (CFF) despite a critically reduced/absent b-wave of the scotopic ERG (Youwen Zhang et al., 2012). *Cngb1*-X1 was used to study mechanisms of different models of retinal degeneration by cryo-EM with a specialized focus on the connecting cilium and basal body (Gilliam et al., 2012). The connections of the *Cngb1*-X1 knockout to the CC and BB were normal as was the intradiscal spacing, but the ROS discs were overgrown, protruding toward and even through the plasma membrane (Gilliam et al., 2012). This is inconsistent with the hypothesis that GARPs regulate intradiscal spacing and integrity, but indicates that microtubules from the CC may regulate spacing, as the disks were spaced by 32 nm, a multiple of the 8 nm tubulin repeat distance within the microtubule (Gilliam et al., 2012). The *Cngb1*-X1 was used as the background genotype to assess the effects of GARP1 and GARP2 expression in the absence of the β-subunit. It was discovered that GARP2 expressed at WT levels accelerates the rate of degeneration of *Cngb1*-X1 mutant both morphologically and functionally. Interestingly, expression of GARP1 with GARP2 slowed the degeneration of *Cngb1*-X1 (Deramus et al., 2017).

To understand the proposed interactions between *rds*/peripherin, rhodopsin, and the CNG channel, crosses of the knockouts were made and tested in heterozygous and homozygous knockout combinations (Chakraborty, Conley, Pittler, & Naash, 2016). Rhodopsin and *Cngb1*-X1 degenerated no faster than *Cngb1*-X1 alone (Chakraborty et al., 2016). The crosses between *rds* mice and rhodopsin knockout mice with the *Cngb1*-X1 mouse had accelerated degeneration affecting both rod and cone function, with the RDS genotype having the most severe disease phenotype (Chakraborty et al., 2016).

Research Goal

Some of the questions being addressed are: Why is there so much GARP2? What is its function? Why is it only found in rod photoreceptors? Going into this project, there was very little known about the role of GARP2 in the regulation of the structure and function of the rod photoreceptor. This project was initiated at the time when the GARP2-Ox mice were also being studied in the lab, and only some basic information about GARP was known such as the relative abundance, the primary sequence, and the severe phenotype observed when expression of the β-subunit and GARPs are genetically ablated.

Ablating GARP2 selectively and specifically, while retaining β-subunit expression, was hypothesized to be an effective way to determine how GARP2 contributes to rod photoreceptor structure and function. So, the three questions we sought to answer through the characterization of the GARP2-KO were as follows. Did the morphology of the rod photoreceptors and the retina change, and if so how? Did visual function change,

and if so, how? Moreover, finally, did ablating GARP2 change the global gene expression pattern, and if so, how?

We hypothesized that ablation of GARP2 would affect the morphology of the rod outer segments, the gain of phototransduction and possibly other physiologic measures, and aspects of the global gene expression pattern of the retina. Our hypotheses are based on morphological and functional changes observed in the GARP2-Ox model and *in vitro* assays involving GARP2. The aim of this study is to systematically assess any changes occurring in the GARP2-KO retina utilizing spectral domain optical coherence tomography (SD-OCT), light and electron microscopy (EM), ERG, analysis of next-generation sequencing (NGS) of the retinal transcriptome, and structural modeling of GARP1 and GARP2 using computational modeling software.

MATERIALS AND METHODS

Animal Care

Homozygous GARP2-KO and WT mouse lines were housed and cared for by the Animal Resources Program at UAB in accordance with UAB IACUC guidelines and the ARVO statement on the use of laboratory animals. Each line was bred through at least five generations before use in these experiments. Mice were housed in 12/12-hour light/dark cyclic lighting, in standard rodent cages, on a standard chow diet.

Zinc Finger Nuclease (ZFN)-Mediated Knockout of GARP2

We worked with Sigma Chemical Company to utilize their CompoZR^{TM} ZFN technology to identify the best deletion site near the targeted GARP2-specific exon 12a at the *Cngb1* locus 5'-TGG ACA AGC ATT GTC nnn nnn ACT GGG GTT GTA **GGA TG**G A-3' with the lower case representing the requisite 4-7 bp space between zinc finger targets to allow proper folding for FokI restriction enzyme cleavage, and the restriction site is shown in bold. Nucleotide BLAST from NCBI (S F Altschul et al., 1997; Stephen F. Altschul, Gish, Miller, Myers, & Lipman, 1990; Boratyn et al., 2012; Camacho et al., 2009; Madden, Tatusov, & Zhang, 1996; Morgulis et al., 2008; States & Gish, 1994; J Zhang & Madden, 1997; Z. Zhang, Schwartz, Wagner, & Miller, 2000) was used to ensure ZFN specificity to exon 12a. The UAB Transgenic Facility injected

mRNA encoding the ZFN into the male pronucleus of fertilized eggs. When the pups were genotyped, we identified one founder mouse with different deletions on each allele. Sanger sequencing was performed using the primers: Sense – 5'-GGG GTG GTG GTG AAT GTC CTT-3' and Antisense – 5'-CTT TAC AAA GAC TAC TCT GGG GTT GAG C-3'. Each allele was separable and germ-line transmissible. The allele with the longer deletion was bred to homozygosity and used for this study.

PCR Confirmation of GARP2-KO and Genotyping

Genotyping was performed on DNA extracted from mouse tail tissue, using a previously described extraction method (Z. Wang & Storm, 2006). PCR was performed using Epicentre FailSafe PCR premix and primers flanking the region outside of exon 12a, which was the ZFN target region. Sense – 5'-GGG GTG GTG GTG AAT GTC CTT-3' and Antisense – 5'-CTT TAC AAA GAC TAC TCT GGG GTT GAG C-3'. The PTC-200 thermal cycler (MJ Research-GMI, Ramsey, MN, US) was set to the following parameters: 1 cycle at 94°C for 5 minutes to denature the DNA; 33 cycles of: 94°C for 45 seconds, 61°C for 45 seconds, and 72°C for 105 seconds; 1 cycle of 72°C for 7 minutes; and a post-run hold temperature of 4°C until removal from the instrument. The WT animal has a band of 2.15 kb while the GARP2-KO has a band of 1.34 kb.

Western Blot

Protein lysates were prepared from whole retinas of age-matched WT and GARP2-KO mice using 10mM Tris-HCl and 0.1% Triton-X 100. Protein was quantified using the Bio-Rad Protein Assay (Bio-Rad Cat# 500-0006). 30 μg of each lysate was then separated on a 10% Mini-protean TGX gel and transferred onto a PVDF membrane using the Trans-Blot Turbo transfer system (Bio-Rad.) The membrane was incubated with affinity-purified rabbit polyclonal antibodies against CNGB1 N-terminus [Reference], and β-actin (1:1000 Sigma-Aldrich Cat# A2228) primary antibodies overnight at 4°C, then incubated with corresponding fluorescent secondary antibodies (Li-Cor Cat# 827-11081, 827-08364) for 1 hr at room temperature, and imaged using the LI-COR Odyssey Quantitative Fluorescence Imaging System.

Light and Transmission Electron Microscopy

Mouse eyes were enucleated following euthanasia with 5% isoflurane and cervical dislocation. The eyes were oriented by superior temporal corneal cauterization. The whole eye was incubated at room temperature for 1 hour in 2% paraformaldehyde, and 2.5% glutaraldehyde in 0.1 M sodium cacodylate buffer for fixation. The eyecup after removal of the lens and anterior segment was secondarily fixed in 1% osmium tetroxide and 0.125% potassium ferrocyanide in 0.1 M sodium cacodylate buffer for 2 hours in the dark followed by dehydration in a graded series of alcohol. The eyes cups were then transitioned to propylene oxide and embedded in Embed 812 resin. Light microscopy sections were cut at 0.8 μm thickness, stained with 0.1% Toluidine blue. Images were

collected with an Olympus VS-120 microscope (BX61VS platform) running VS-ASW-2.9 software. Ultrathin sections (80–90 nm) were mounted on copper grids and visualized with a JEOL 1200 electron microscope equipped with a 4-megapixel digital camera (AMT Gatan, Inc; Pleasanton, CA; ES1000-785). Measurements of outer segment length and width, disk rim spacing, and phagosome counting were performed in ImageJ (NIH, Bethesda, MD) (Abràmoff, Magalhães, & Ram, 2004; Schneider, Rasband, & Eliceiri, 2012). All reagents used for processing and staining tissue for imaging were acquired from Electron Microscopy Services.

Electroretinography (ERG)

Recording Parameters

An HMsERG unit (Ocuscience, Rolla, MO, US) was used to assess changes in retinal function over a time course of 1, 3, 6, and 10 months of age. A custom-designed ERG rig (Laboratory of Dr. Timothy W. Kraft, the University of Alabama at Birmingham) with options to regulate shutter speed and the ability to record under DC conditions was used for further ERG testing of critical flicker fusion frequency (CFF), Lamb Pugh phototransduction gain model analysis of the a-wave, dose-response sensitivity curves, and c-wave recordings (Clark & Kraft, 2012; DeRamus & Kraft, 2018).

The light stimulus of the HMsERG was a ganzfeld dome with 8 LEDs which were digitally programmed to provide the desired flash intensity by modulating the stimulus duration. The recording electrode of the HMsERG was a thin silver wire placed directly on the cornea from canthus to canthus and held in place with a clear 3 mm contact lens,

and a ground needle electrode was placed in the skin of the cheek parallel to the mandible. Isoflurane anesthesia (1.5% isoflurane, 100% oxygen) delivered by an EZ-Anesthesia instrument (Euthanex Corp, Palmer, PA, US) was used during the HMsERG procedure. Mouse body heat was maintained at 37°C with a digital heating pad controlled by a rectally inserted thermometer. Data acquisition software was preinstalled on the instrument and accessible via personal computer through ERGVIEW software (version 4.400AV).

The custom ERG rig provided the 505 nm light stimuli through a fiber optic, 100 W, tungsten-halogen light source fitted with calibrated neutral density filters to one eye while the ground electrode was placed on the contralateral eye. General anesthesia for ERG testing on the custom rig was by IP injection of ketamine and xylazine, 90.9 mg/kg and 9 mg/kg body weight, respectively. The body temperature of the mouse was maintained by a reusable, microwave-warmed heating pad. A custom LabView virtual instrument handled data acquisition and storage.

Scotopic recordings were performed on animals that were dark-adapted overnight. Topical ophthalmic application of 0.5% proparacaine, 2.5% phenylephrine hydrochloride, and 1% tropicamide (Bausch & Lomb; Rochester, NY, US) caused local anesthesia and mydriasis of the eye, respectively. Electrical contact between the cornea and the recording electrodes for both setups was maintained by applying 2.5% hypromellose ophthalmic solution (AKORN, Lake Forest, IL, US) on the cornea before electrode/contact lens or fiber optic electrode placement.

Scotopic testing on the HMsERG instrument used pre-programmed protocols Scotopic I, with a 3.333 ND filter placed over the ganzfeld dome, and Scotopic II without

a filter. The scotopic flash intensities ranged from -5 to 1 log units, or 0.03 – 25,000 mcd*s/m^2.

ERG testing on the custom rig was performed as previously described (Clark & Kraft, 2012). The scotopic flash intensities ranged from 0.04 to 6.18 log photons per µm incident to the cornea. Photopic ERG consisted of a 3-minute light adaptation after performing all dark-adapted tests, with a 6.18 log photon/µm flash stimulus under continued background illumination. For CFF testing an LED source was programmed to increase sinusoidal flicker linearly from 0.1 to 55 Hz for photopic and 0.1 to 30 Hz for scotopic testing conditions (DeRamus & Kraft, 2018). DC recording conditions were used to measure c-wave, with six light intensities increasing from 0.6 to 6.2 log photons/μm^2, the stimulus duration was 5 s, and the recording time was 9 seconds.

Data were imported into Igor Pro (Version 6.37, Wavemetrics Inc.) for measurement of a- and b- wave amplitudes and time to peak, areas under the curve for c-waves, amplitude and timing of oscillatory potentials, and curve fitting for sensitivity and phototransduction gain. The response waveforms were baseline corrected, and the midpoints of the flashes were set to time equals zero seconds. For HMsERG recordings, a manufacturer provided plot of flash intensity versus flash duration was digitized using Plot Digitizer written by Joseph A. Huwaldt (http://plotdigitizer.sourceforge.net/) and interpolated in Igor Pro to calculate photons per flash.

Sensitivity Analysis

For each animal, flash intensity versus a-wave response and flash intensity versus b-wave response was plotted and fit to a modified Michaelis-Menten dose-response equation (Baylor, Hodgkin, & Lamb, 1974; R. A. Bush & Sieving, 1994; Fain & Dowling, 1973; Fulton & Rushton, 1978; Massof et al., 1984; Normann & Perlman, 1979; Peachey, Alexander, & Fishman, 1989):

$$R = R_{max} \times \frac{I^n}{I^n + I_{50}^n} + base$$

where R is the response amplitude (of either the a-wave or b-wave) at a specific flash intensity, R_{max} is the maximum amplitude of the response for the specific animal, I^n is the flash intensity in photons/μm^2, I_{50} is the flash intensity that produces half of the maximum response.

Another metric of sensitivity is the b-wave response in μV per photoisomerization (Φ) at the b-wave threshold which is determined by the dimmest scotopic stimulus that consistently elicits a b-wave signal twice as large as the background noise for all animals.

Phototransduction Gain

The Lamb Pugh model of phototransduction was used to curve fit the leading edge of the a-wave to determine gain (Baylor et al., 1984; Breton, Schueller, Lamb, & Pugh, 1994; Hood & Birch, 1993; Lamb & Pugh, 1992; Pugh & Lamb, 1993):

$$f(t) = \{1 - \exp\left[-0.5 \times \Phi \times A_g \times \left(t - t_{delay}\right)^2\right]\} \times R_{max}$$

Φ is the number of photoisomerizations per rod per flash (see above for calculation), t_{delay} is the brief delay for the events of the phototransduction cascade to begin, and A_g is the mathematically derived rate of phototransduction that focuses on PDE6 activation and CNG channel closure which combined cause the photoreceptor hyperpolarization during phototransduction that is recorded as the a-wave.

This equation was used to calculate the number of activated rhodopsin molecules or photoisomerizations (Φ) per flash (Lyubarsky, Daniele, & Pugh, 2004):

$$\Phi = \pi \times l \times \Delta T \times 1500 \times \tau(\lambda) \times \frac{S_{pupil}}{S_{retina}} \times A_c(\lambda)$$

where Φ is the number of photoisomerizations, l is the flash luminance, ΔT is the flash duration taken as 2 ms, $\tau(\lambda)$ is the light transmission through the ocular media at a specific wavelength taken as 0.7 (Mathew Alpern, Fulton, & Baker, 1987), S_{pupil} is the surface area of the pupil taken as 3.2 mm^2 (Lyubarsky et al., 2004), S_{retina} is the surface area of the retina taken as 17.8 mm^2, and $A_c(\lambda)$ is the collection area of the photoreceptor which was calculated for each group separately since the lengths of the ROS were not the same, using this equation (Baylor et al., 1984):

$$A_c(\lambda) = f \times \frac{\pi \times d^2}{4} \times [1 - 10^{-\Delta D(\lambda) \times L}] \times \gamma$$

where f is a dimensionless factor that accounts for light funneling taken as 1.3 (Baylor et al., 1984), d is the diameter of the rod measured as 1.25 μm, $\Delta D(\lambda)$ is the axial density of

rhodopsin at a specific wavelength of 0.019 o.d./μm (Mathew Alpern et al., 1987), *L* is the length of the photoreceptor outer segment taken as 25.08 for WT and 28.47 for GARP2-KO (measured experimentally), and γ represents the quantum efficiency of phototransduction taken as 2/3 (Lyubarsky et al., 2004).

The family of flash responses used for gain curve fitting was elicited by five flash intensities between 2.97 and 4.17 log photons per micron incident to the cornea. Flash intensities greater than 5 log photons elicit cone responses, so they were excluded from fitting. Before ensemble fitting, to remove background noise from the traces, we applied a 200 Hz Gaussian filter, which preserves the amplitude and timing characteristics of the curve. The portion of the a-wave responses that were fit was limited between 5 ms after the flash to 80% of the a-wave amplitude to avoid contamination by the b-wave.

Critical Flicker Fusion Frequency (CFF)

An average of six single sweep flicker traces and an average of six baseline traces (no stimulus) for each animal under light- and dark-adapted conditions were used for CFF analysis. Fast Fourier Transform (FFT) with magnitude squared output was performed on the flicker and baseline traces and plotted to visually assess the quality of the flicker recording which appeared as a separation of the flicker trace from the background trace at low frequency and then merged into the background trace as the frequency increased. If no separation between flicker FFT and background FFT traces was observed, the traces were excluded from analysis. Otherwise, the difference between the flicker FFT and background FFT traces was calculated, plotted, and linearly fit between 4.44 –

21.8 Hz for dark-adapted CFF and 7.33 – 23.1 Hz for light-adapted CFF. The coefficients from the linear fit equation were used to solve for the CFF value at the 6.18 log unit response which was pre-determined by repeated testing on WT control mice, to match a 3 μV criterion response (DeRamus & Kraft, 2018).

Oscillatory Potentials (OP)

Scotopic and photopic oscillatory potentials were digitally isolated from the dark-adapted and light-adapted 6.18 log photon/μm flash responses using a 65 Hz highpass and 300 Hz lowpass 5th order Butterworth filter (LabView, National Instruments). After baseline correction, the area under the absolute value of the recording for the 150 ms epoch before the flash was subtracted from the absolute value of the first 150 ms after the flash to remove noise. OP recordings were excluded from analysis if the signal area was less than twice the noise area. The amplitude and timing of each of the first five peaks were recorded. Occasionally a 6th OP peak was observed. However, it was excluded from this analysis.

Measurement of C-waves

The c-waves were normalized to the amplitude of the b-wave and baseline corrected before measurement of the area under the curve from a midpoint in the ascending c-wave to a point just prior to termination of the stimulus. The time to peak and non-normalized c-wave amplitudes were also measured.

Optical Coherence Tomography (OCT)

In vivo retinal morphology was assessed using spectral domain OCT (840 nm; Envisu Class-R; transverse resolution = 2.5 μm; axial resolution = 1.6 μm) obtained with Bioptigen InVivoVueTM 1.4 software, and measured with Bioptigen Diver 2.4 software (Bioptigen, Inc, Morrisville, NC). Animals were anesthetized with ketamine/xylazine (Bioniche Teoranta; Inverin, Co. Galway, Ireland) at 100 mg/kg and 10 mg/kg body weight, respectively. Mydriasis and local anesthesia were accomplished using 1% tropicamide (Bausch & Lomb; Rochester, NY) and 0.5% proparacaine (Falcon Pharmaceuticals; Fort Worth, TX), respectively. Artificial tears (Systane Ultra; Alcon OTC; Houston, TX) and ophthalmic saline were frequently applied to prevent dryness and maintain corneal clarity. A 1.4 mm rectangular volume scan, which was centered on the optic nerve head, was used to measure retinal layer thicknesses. The OCT data acquisition settings for the measurement scan were: 1000 A-scans/B-scan x 100 B-scans/volume x 1 frame/B-scan.

Next Generation Sequencing

Retinas and RPE were collected from five mice at 1 month of age for mRNA extraction between 11 AM & 1 PM for four genotypes: GARP2-KO, WT, and two other *Cngb1* knockout models of retinitis pigmentosa, *Cngb1*-X1 and *Cngb1*-X26, which are a deletion of the rod photoreceptor β-subunit and GARPs, and a deletion of only the β-subunit, respectively. mRNA was extracted using the RNAqueous-4-PCR kit (Ambion) using the protocol provided by the manufacturer. The samples for each genotype were

pooled, 10 retinas per genotype, and sequenced by the UAB Heflin Center for Genomic Sciences – Genomics Core Lab on the Illumina NexSeq 500 sequencing platform, using standard reagents and conditions. The quality of the Next Generation Sequencing (NGS) reads were ascertained using FastQC (Andrews, 2010). NGS reads were aligned to UCSC mm10 mouse genome using STARaligner (version 2.5.1) (Dobin et al., 2013). EBSeq in RSEM (version 1.2.28) from the BioConductor package in R (Leng et al., 2013, 2015; B. Li & Dewey, 2011) was used to compare each mutant to WT to determine significant changes in gene expression which is defined by EBSeq as a gene with a posterior probability of differential expression (PPDE) > 95%. A GeneVenn diagram (Pirooznia, Nagarajan, & Deng, 2007) of the genes for each mutant with a PPDE > 95% was made to determine which genes could be related to the loss of GARP2. The comparison of interest was between GARP2-KO and *Cngb1*-X1, as their commonly differentially expressed genes may reflect their common lack of GARP2 and those common genes were selected for Ingenuity Pathway Analysis (IPA) (QIAGEN Inc., https://www.qiagenbioinformatics.com/products/ingenuitypathway-analysis) (Krämer, Green, Pollard, Tugendreich, & Tugendreich, 2014). The genes belonging to the top five most likely affected gene networks were selected for expression verification using qRT-PCR.

qRT-PCR Expression Verification

Taqman 96-Well Custom Array 10 µL plates were ordered containing primers targeting the selected gene targets. RPE and retinas of 3-month old GARP2-KO and WT mice were collected between 11 AM & 1 PM, which is the same as the NGS samples, to

avoid circadian rhythm induced changes in gene expression (n=3 mice, 6 eyes per genotype). RNAqueous-4PCR kit (Ambion, Thermo Fisher, USA) using the protocol provided by the manufacturer was utilized to isolate mRNA from the tissue. The High Capacity cDNA Reverse Transcription kit with RNase Inhibitor (Applied Biosystems, Thermo Fisher, USA) was used following manufacturer provided protocols for the reverse transcription reaction of mRNA into cDNA on the ABI QuantStudio 3 thermocycler (Applied Biosystems, Thermo Fisher, USA). The quality of the cDNA was tested by performing a PCR using primers specific to mouse β-actin, which is a ubiquitously expressed protein in the retina. The cDNA was loaded into the TaqMan plates, using TaqMan master mix and QuantStudio 3 platform performed thermocycling and data collection procedures. Data analysis was performed on the web-based Relative Quantification (RQ) application, found on the Thermo Fisher Cloud website (https://apps.thermofisher.com/apps).

Computational Structural and Functional Modeling of GARPs

Iterative Threading ASSEmbly Refinement (I-TASSER) Protein Structure and Function Prediction software was used to ideate the differences between GARP1 and GARP2. Murine GARP1 and GARP2 amino acid sequences in FASTA format were submitted to the I-TASSER server (https://zhanglab.ccmb.med.umich.edu/I-TASSER/). The authors have published the structure/function prediction algorithm (Roy, Kucukural, & Zhang, 2010; Jianyi Yang et al., 2015; Yang Zhang, 2008), but briefly, the protein database was searched for template proteins that have regions of similar amino acid se-

quences, and if no matches are found, simulation decoys are created, and their low-energy states predict the structure. To predict protein function, the server matches the structural models to enzyme commission (EC), gene ontology (GO), and ligand binding site databases. Each structural prediction is given an accuracy score, and the functional prediction accuracy is based on the accuracy assigned to the structural model. PDB model files were processed into the images shown here using Chimera (Pettersen et al., 2004)

Murine GARP2 protein sequence:

MLGWVQRVLPQPPGTPQKTVETAGPQPETESKPEANPQPEPEPQQEPEPEPEPEPE
PEPEPEPEPEPEPEPEPEPEPVPEEAPPEVQALPPEEPMEGEGEAEAGPSLQETQVADP
AQPTSQAQVAVAKVNRPSSWMLSWFWRGMQKVVPQPVCSNGGQNLAAGERD
PDQGGAQIPEPCGTGDPGSAEASGTQDTEPSLWLLRWLEQNLEKVLPQPPPPSLA
WKVEPEAAVLDPDPPGTPMQMEPTESPSQPNPGPLEPEEEPAAEPQPGFQSSSLPP
PGDPVRLIEWLLHRLEMALPQPVLHGKAAEQEPGCPGMCDVQTRATAAGGL

Murine GARP1 protein sequence:

MLGWVQRVLPQPPGTPQKTVETAGPQPETESKPEANPQPEPEPQQEPEPEPEPEPE
PEPEPEPEPEPEPEPEPEPEPVPEEAPPEVQALPPEEPMEGEGEAEAGPSLQETQVADP
AQPTSQAQVAVAKVNRPSSWMLSWFWRGMQKVVPQPVCSNGGQNLAAGERD
PDQGGAQIPEPCGTGDPGSAEASGTQDTEPSLWLLRWLEQNLEKVLPQPPPPSLA
WKVEPEAAVLDPDPPGTPMQMEPTESPSQPNPGPLEPEEEPAAEPQPGFQSSSLPP

PGDPVRLIEWLLHRLEMALPQPVLHGKAAEQEPGCPGMCDVQTISILPVEQVEHD
LVLEEVDSCWEDAQQEDGASPQETEVAPAHEEESEAIVEIPRELTKIQEEREDEQE
EDEEEKEEEKKKGEEEKEKEEEEKEKEKEKEEEKEEEEKEEEEEEEKEEEEEEKEE
EEKEEEEKEEEEEEEEEEEEPIVLLDSCLVVQADVDECQLERTPSELASIQELPEEK
EEKEEEKEEEKEEEEEKKEEEVEKKEEGEATNSTVSRITPLPATSGTQYHG

Statistical Analyses

The statistical data analysis for this paper was generated using SAS software, Version 9.3 of the SAS System for 64-bit Windows. Copyright © 2002 – 2010. SAS Institute Inc. SAS and all other SAS Institute Inc. product or service names are registered trademarks or trademarks of SAS Institute Inc., Cary, NC, USA. Wilcoxon rank-sum statistical tests were performed to compare ERG gain, time delays, Michaelis-Menten sensitivity, CFF, OP area, c-wave area and OCT retinal layer thickness measurement comparisons. Model 3 generalized estimating equations were used to compare ERG a-waves, b-waves and respective peak times. Unpaired, two-tailed, student t-tests were performed in Excel 2016 for phagosome counting, ROS length measurement, disk rim to disk rim spacing, and disk rim to plasma membrane spacing measurement comparisons.

RESULTS

Generation of the GARP2-KO Mouse

Exon 12a of *Cngb1*, which encodes the last eight amino acids of GARP2 that are unique, was targeted for deletion to remove the potential for GARP2 expression. Zinc finger nuclease (ZFN) gene-editing technology was used to create this knockout as it creates targeted double-strand breaks in genomic DNA using the FokI endonuclease, based on the alignment and subsequent folding of the two zinc fingers designed to recognize and bind to a specific 15 – 20 bp target per finger and those targets separated by 4 – 7 bp (see Figure 9). Knockout by ZFN is a consequence of the endogenous cellular DNA double-strand break repair mechanism of non-homologous end joining, which most often leads to deletions or insertions at the targeted double-strand break on one or both alleles. From 11 founder mice, one founder was identified (Z5 in Figure 10A) that had different deletions on each allele. One allele carried a complete deletion of exon12a (811 bp deletion), and the other allele had a deletion of the splice acceptor site and most of the 3' untranslated region (503 bp deletion). These alleles were separately bred to homozygosity, and the allele with a complete deletion of the GARP2-specific exon 12a was used exclusively in this study (Figure 10A inset). The knockout was confirmed by Sanger DNA-sequencing and PCR genotyping using oligonucleotide primers specific to regions outside of the ZFN target site. The WT DNA PCR amplicon is 2.15 kb, and the knockout amplicon is 1.33 kb (Figure 10A).

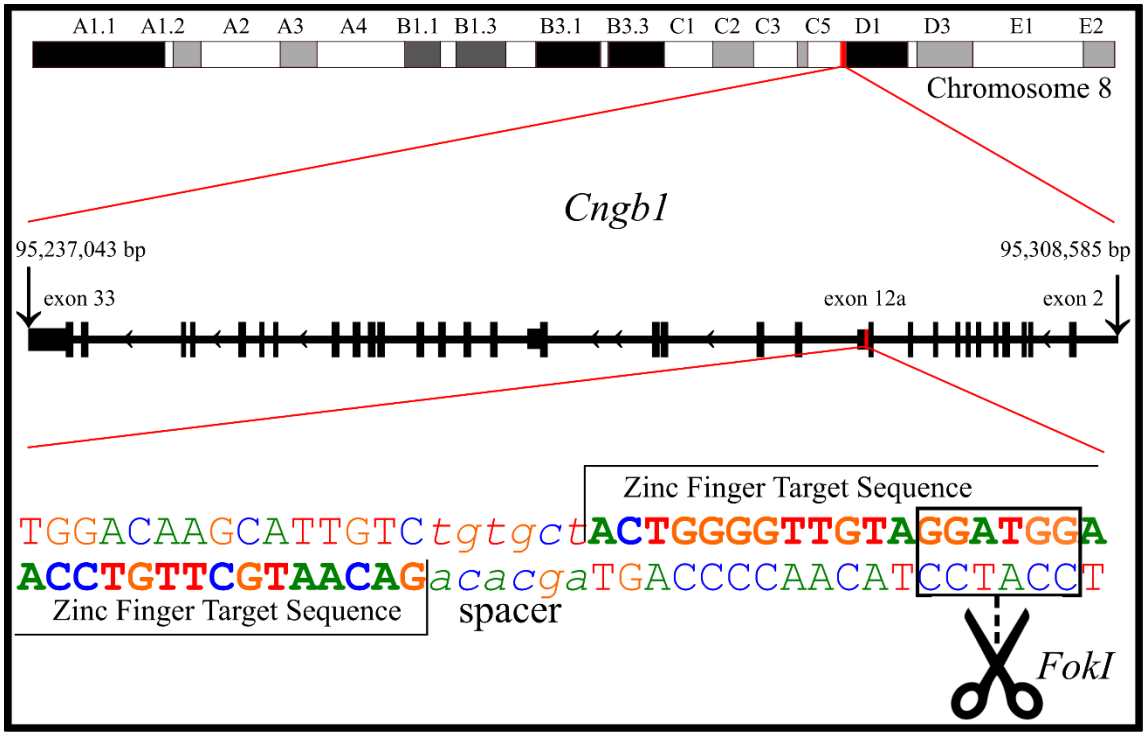

Figure 9: Schematic of the ZFN target site for knockout. *Cngb1* is located on murine chromosome 8 and is composed of 33 exons. The full 33 exon transcript encodes the β-subunit of the CNG channel vital to the phototransduction cascade. Through alternative splicing events at exons 17 and 12a, GARP1 and GARP2 are generated, respectively. A zinc finger nuclease created to bind specifically to a sequence near the GARP2 specific exon 12a was used to make a double strand break, which when repaired by non-homologous end joining can lead to a targeted deletion.

Confirmation of GARP2 Ablation

Western blot analysis confirmed that protein expression of GARP2 was ablated in our ZFN-mediated knockout mouse in contrast to the WT mouse that has a distinct band at 62 kDa when immunoblotted with an anti-GARP2 antibody (Figure10B). The high number of negatively charged glutamic acid residues causes the 31.9 kDa GARP2 protein to appear larger on a Western blot, which has been previously documented (Batra-Safferling et al., 2006).

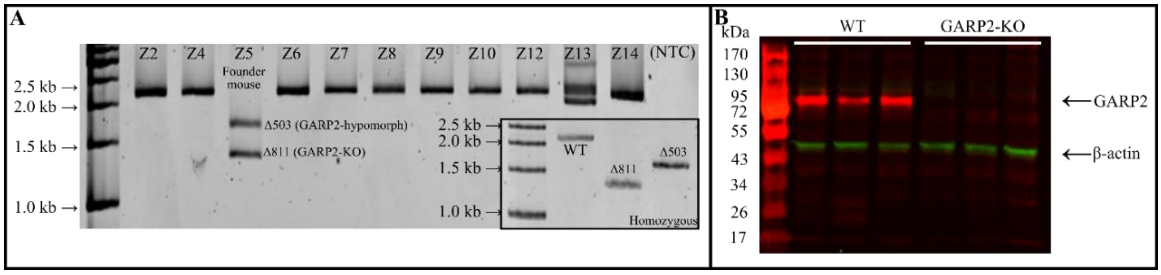

Figure 10: Confirmation of GARP2-KO. A) Genotyping PCR was performed with mouse tail DNA isolated from 11 potential founders. Two deletions of differing size are apparent in the in Z5: Δ503 bp is missing the 3' untranslated region and splice acceptor site, and Δ811 bp is missing all of GARP2 specific exon 12a. Each deletion was separately bred to homozygosity as confirmed by PCR (inset). The Δ503 deletion was a hypomorphic allele of GARP2 (not shown) that was not further studied. The longer Δ811 deletion is a complete knockout of GARP2 and the focus of this study. B) To confirm that the protein expression of GARP2 was ablated, we performed Western blotting of retinal homogenates from three WT and three GARP2-KO mice using a GARP2 specific antibody.

Anatomical Anomalies of the GARP2-KO ROS

The overall thicknesses of the GARP2-KO retinal layers are no different through the age of 10 months as observed by OCT (Figure 11). However, histologic analysis of retinal tissue sections revealed regions of elongated ROS across the GARP2-KO retina. Comparing the means of the measurements, the GARP2-KO has an increased ROS length of about 1 μm or 3.75% panretinally (WT = 26.43 ± 2.88 μm, n = 239; GARP2-KO = 27.39 ± 3.84 μm, n = 99; *p-value = 0.03**). A histogram of ROS length in 2-micron increments plotted against the normalized frequency of occurrence for each genotype shows a noticeably biphasic distribution in the GARP2-KO (Figure 12). A curve fit of the WT histogram was a normal Gaussian-like monophasic distribution with a peak at 27.5 ± 0.08 μm (Full Width at Half Maximum (FWHM): 3.7 ± 0.13, Area = 1.99, Height: 0.29 ± 0.008). The peak height the curve represents the median height measured and is not a representation of the mean of the WT population. A multipeak Gaussian fit of the GARP2-KO histogram found two distribution peaks at 26.8 ± 0.78 μm and 34.0 ± 2.6 μm (Peak 1: FWHM 7.2 ± 1.4, Area: 1.7 ± 0.5, Height: 0.22 ± 0.03; Peak 2: FWHM: 7.0 ± 4.1, Area: 0.51 ± 0.4, Height: 0.07 ± 0.03; Total fit area: 2.18 ± 0.63). For all future calculations requiring ROS length, we used the mean length. Measured width of the ROS disks was unchanged (WT = 1.25 ± 0.13 μm, n = 100; GARP2-KO = 1.25 ± 0.18, n = 100; *p-value = 0.95*, unpaired, two-tailed, student's t-test).

In the more elongated regions of the GARP2-KO retina, the end tips of the ROS lie parallel to the microvillus processes of the RPE, instead of assuming their normal interdigitated position (Figure 13). To determine if the regions of misalignment within the interdigitation zone interrupted daily phagocytosis of the ROS end tips by the RPE, we

counted phagosomes from eyes of three-month-old mice harvested one hour after "lights on" in the animal facility, which correlates to one hour after dawn (Figure 14). No difference was found in the number of phagosomes counted in the GARP2-KO RPE versus WT RPE per 100 µm (WT = 2.80 ± 1.57, distance = 11,779 µm; GARP2-KO = 2.33 ± 0.58 distance = 16,936 µm, *p-value* = 0.24).

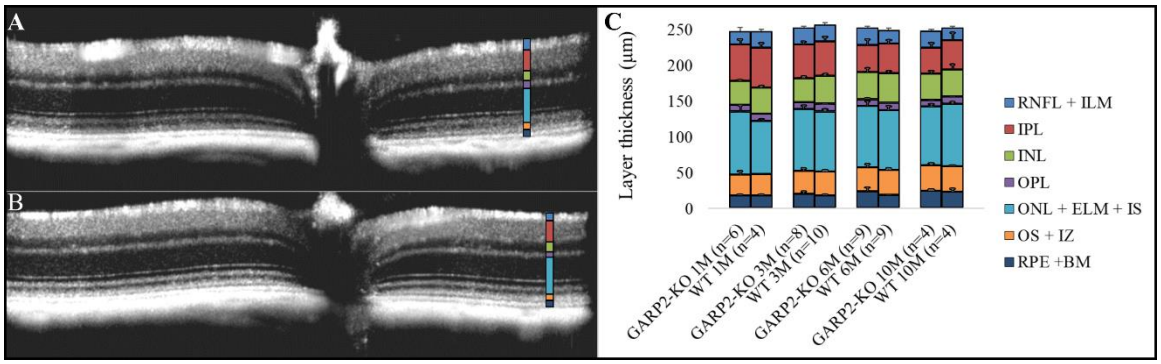

Figure 11: *In vivo* imaging of GARP2-KO and WT retinas with optical coherence tomography. Retinal OCT images were acquired at 1, 3, 6, and 10-month timepoints to include assessment of any age-related structural perturbations. Shown in A) and B) are representative OCT images of three-month-old GARP2-KO and WT retinas, respectively. C) Measurements of the retinal layers (Error bars = SD). On the right side of the OCT images, the overlying colored bar corresponds to the retinal layers as determined by the Diver 2.0 software program used for the analysis, in the same order and colors as the bar chart. No significant differences between retinal layer thicknesses were detected. Abbreviations: RNFL – Retinal Nerve Fiber Layer; IPL – Inner Plexiform Layer; OPL – Outer Plexiform Layer; ONL+IS – Outer Nuclear Layer and Inner Segment; OS – Outer Segment; RPE – Retinal Pigment Epithelium. (1-month: WT n = 4, GARP2-KO n = 6; 3-month WT n = 10, GARP2-KO n = 8; 6m WT n = 9, GARP2-KO n =9; 10-month WT n = 4, GARP2-KO n = 7).

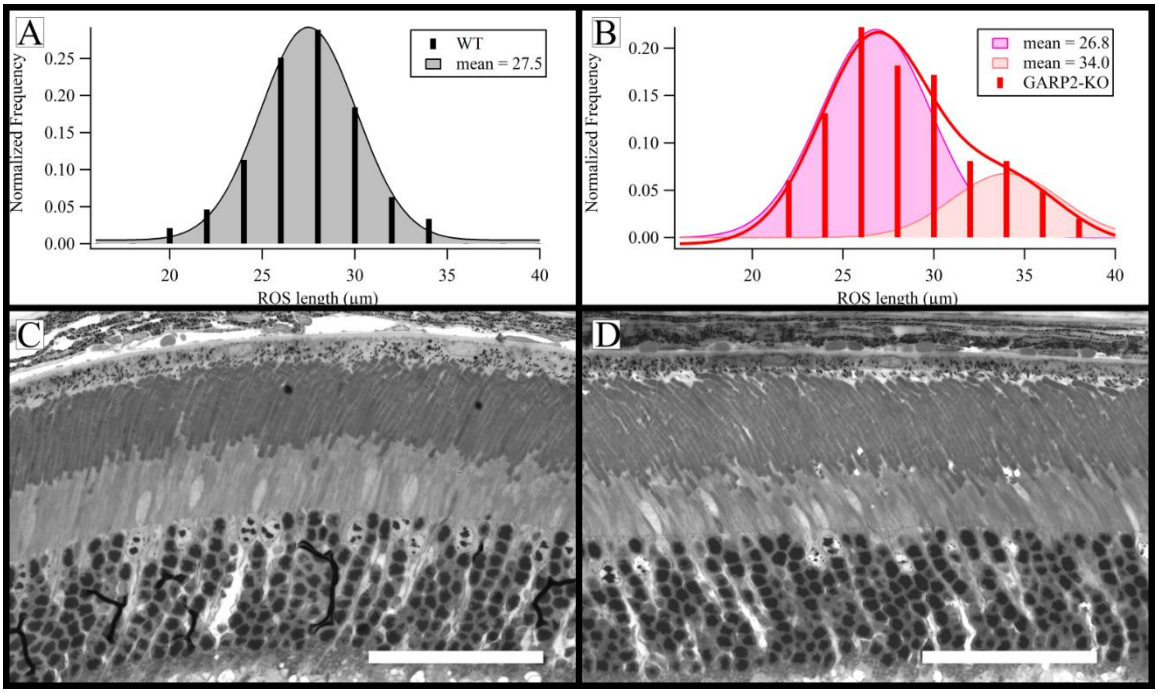

Figure 12: Rod outer segment lengths vary across the GARP2-KO retina. A) Histogram of WT ROS length by the frequency of occurrence normalized by the percent of total ROS lengths counted, fit by a Gaussian distribution. B) A multipeak Gaussian curve fit of the GARP2-KO distribution of lengths reveals a biphasic distribution of elongated ROS. C) and D) are toluidine blue stained sections of WT and GARP2-KO retina, respectively. Original magnification 1000x. Scale bars = 50 µm.

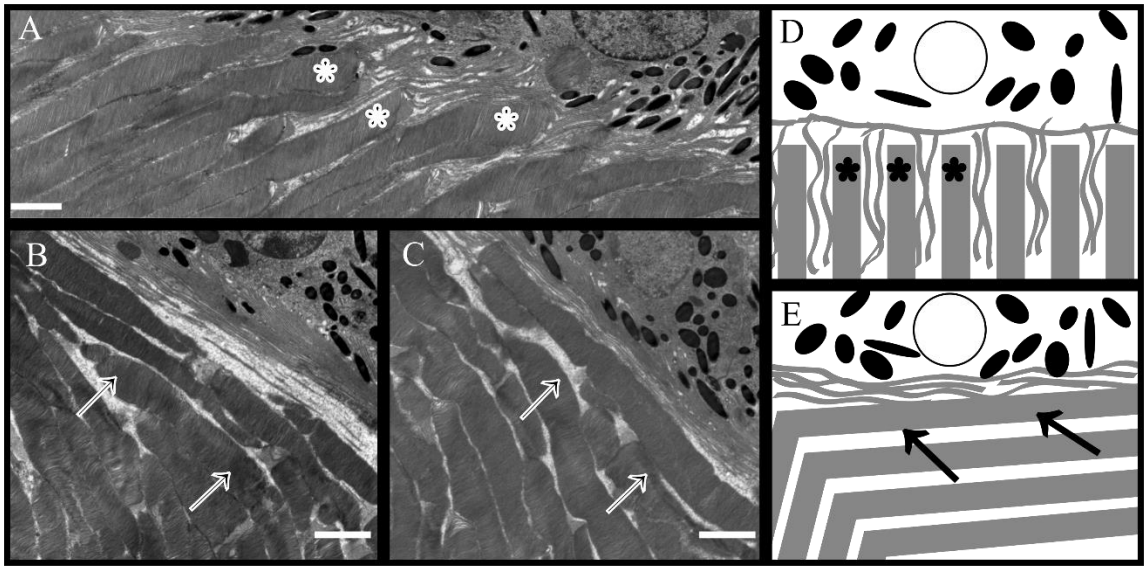

Figure 13: Regional ROS/RPE interdigitation zone misalignment in GARP2-KO. A) In this WT retina, the end tips of the ROS are normally interdigitated with the microvillus processes of the RPE. Asterisks denote three of several ROS end tips in the image with microvillus processes in proper alignment. B) and C) The GARP2-KO retinas exhibit regional misalignment of the interdigitation zone, with longer ROS lying parallel to the microvillus processes, indicated by arrows. D) A cartoon of normal RPE/ROS interdigitation versus E) the abnormal regions of interdigitation seen in the GARP2-KO that corresponds with the micrographs in A-C. Scale bars = 2 μm.

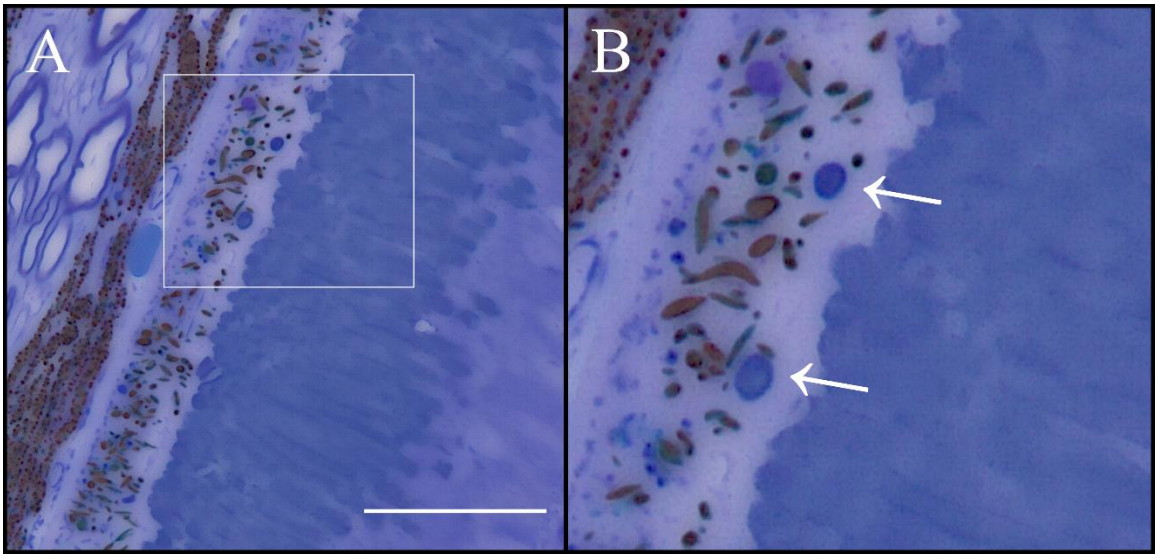

Figure 14: Phagosome counting selection criteria. A) GARP2-KO retinal section stained with Toluidine blue and imaged at 100x magnification. Three selection criteria were used for phagosome recognition and inclusion: 1) Staining at the same intensity and color as the ROS. 2) Relatively circular morphology to avoid inclusion of melanosomes or mitochondria. 3) Localization to the apical 1/3 of the RPE cell, to avoid inclusion of organelles. B) An enlargement of the area enclosed by the box in panel A, which shows two phagosomes indicated by the arrows. Scale bar = 25 μm.

Scotopic ERG Reductions in GARP2-KO

To determine if the GARP2-KO exhibited a change in rod photoreceptor function with age, we compared the electrical activities of WT and GARP2-KO animals at 1, 3, 6, and 10 months of age. At 1-month no change in a-wave or b-wave amplitude or corresponding peak times was observed. A reduction of a-wave and b-wave amplitudes was first observed at 3-months and persisted through the last recorded age of 10-months. At 3-months the maximum photoreceptor a-wave responses were 33% lower in the GARP2-KO, while the maximum b-wave responses arising from the downstream bipolar cells were decreased by 47%. Figure 15A shows a family of averaged ERG traces for the GARP2-KO animals in comparison to the WT animals across a range of stimulus intensities, ending with the brightest saturating flash stimuli in dark-adapted animals. In Figure 16, b-waves are plotted with respect to their corresponding a-waves in panels A – C for 1-month, 3-month, and 10-month ages, respectively. The coefficients from a linear least squares regression fit of the data in those plots indicate three characteristics of the relationship between the a-waves and b-waves. The R^2 values are all greater than 0.75 showing the dependency of the b-wave amplitude upon the amplitude of the a-wave which has been previously described (Perlman, 1983). The y-intercepts of the regression fits are lower in the GARP2-KO animals at all ages, even at one month when the difference between the groups is not statistically significant, meaning that the ratio of b-wave to a-wave amplitude is continuously decreased. The slopes of the linear fits change through the progression of time 6% larger in the GARP2-KO at one month, 2% larger at three months, and 15% lower at ten months, meaning the b-wave is getting smaller with respect to a-wave as the animal ages.

Decline in A- to B-wave Ratios with Age

Another way to examine the relationship between a-wave and b-wave responses is to look at the ratio of expected b-wave to actual b-wave versus a-wave amplitude (Figure 16 D-F). Expected b-waves were interpolated from the WT linear regression fits. The actual (experimentally recorded) b-waves were divided by the expected b-wave depending on the a-wave amplitude. In Figure 16D, the a-wave to b-wave ratios overlap at 1-month, and the groups begin to separate at 3-months (Figure 16E), and the trend persists through 10-months. The b-wave ratio method developed by Ido Perlman (Perlman, 1983) used normal and abnormal human ERG samples to determine the normal b-wave ratio range of 0.8 to 1.2, or that the actual b-wave should fall within a 20% range of expected b-wave. The human range is delineated on the plot and appears to fit the WT mouse data well across all ages. The GARP2-KO ratios fall within the normal range at one-month (Figure 16D) when no difference is observed between responses, but by three months most of the ratio points are well below the expected range (Figure 16E), and the trend continues through 10-months (Figure 16F).

Bipolar Cell Response is Less Sensitive to Light

Michaelis-Menten dose-response analysis (Baylor, Lamb, & Yau, 1979b) of the a-wave shows no change in the intensity of light required to elicit the half-maximal response (I_{50}) (Figure 15B). However, the b-wave I_{50} is shifted to the right, indicating more light is necessary to elicit the maximal b-wave response (Figure 15C). (See Table 1 for a

summary of responses and associated p-values). As another metric of sensitivity, we calculated the amount of electrical response in μV per photoisomerization (R*) at the b-wave threshold, or the dimmest scotopic stimulus producing a reliable b-wave response (signal to noise ratio > 2.0), for both GARP2-KO and WT (at a flash intensity of 1.13 photons/μm^2 incident to the cornea). The GARP2-KO b-wave threshold value was 61% lower than WT (See Table 2).

No Change in Phototransduction Gain

The amplification constant, or phototransduction gain, in the Lamb-Pugh phototransduction model represents the activation of PDE6, rate of channel closure, and photoreceptor hyperpolarization based on the leading edge of the a-wave (Lamb & Pugh, 1992). A phototransduction gain was observed in the GARP2-Ox model (Sarfare et al., 2014), therefore, gain change could also be likely in the GARP2-KO. The leading edges of the family of a-waves were individually, and as a group, ensemble fit to the Lamb-Pugh model of phototransduction gain (see Methods) with no significant differences observed between the gain or time delay of the GARP2-KO when compared to WT (Figure 17).

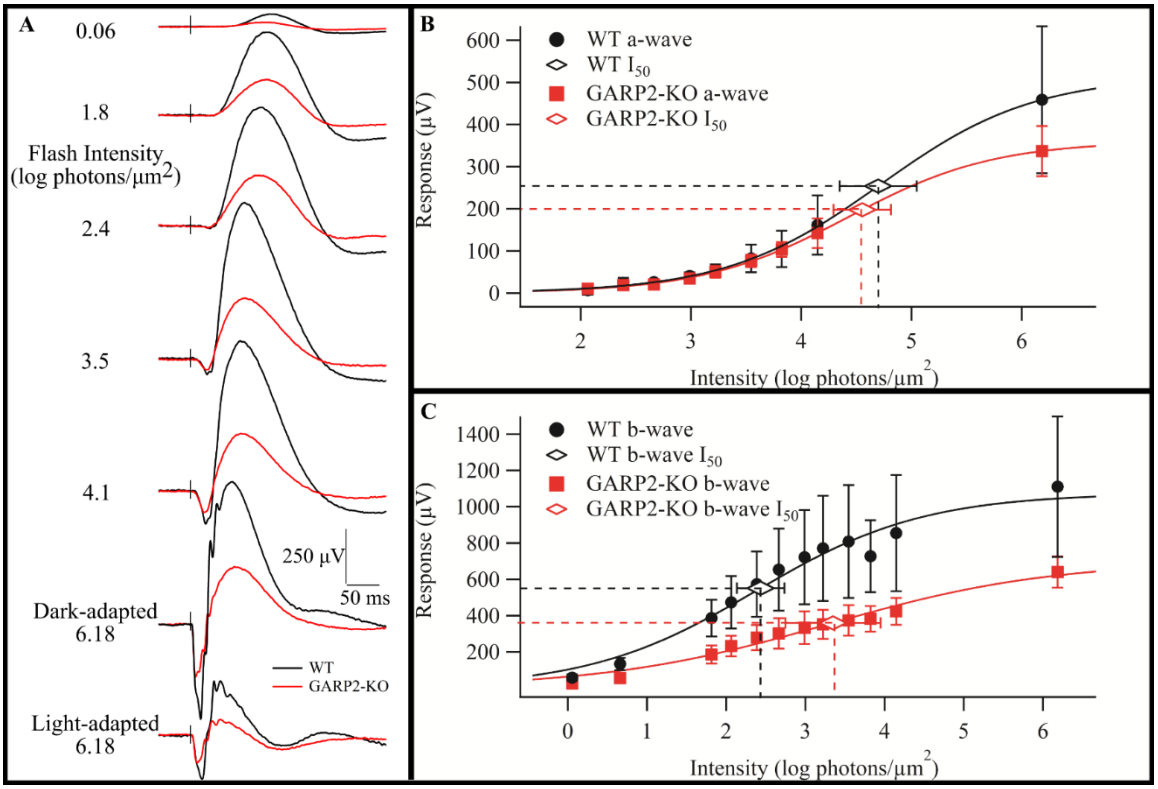

Figure 15: GARP2-KO has reduced a- and b-wave amplitudes and reduced sensitivity. A) Average ERG traces of WT and GARP2-KO for increasing scotopic flash intensities and a photopic saturating camera flash (top to bottom). Scotopic dose-response curves for B) average a-wave responses and C) average b-wave responses with I_{50} is indicated by a diamond-shaped marker. The I_{50} for the a-wave is not different between groups. The b-wave I_{50} is shifted to the right in the GARP2-KO, requiring a higher intensity stimulus to achieve its half-maximal response. (a-wave p-value = 0.03*; b-wave p-value = 0.001*). (I_{50}: WT: 2.44 ± 0.34, n=6; GARP2-KO: 3.35 ± 0.66, n = 6; p-value = 0.02*). Error bars represent SD.

Table 2: Comparison of observed morphological and functional features of the GARP2-KO versus WT.

Parameter	WT	GARP2-KO	*p-value*
ROS length (μm) (3-month)	26.43 ± 2.88 (239)	27.39 ± 3.84 (99)	*0.01**
ROS width (μm) (3-month)	1.25 ± 0.13 (100)	1.25 ± 0.18 (100)	*0.95*
R_{max} a-wave (μV) (3-month)	460 ± 150 (8)	306 ± 70 (9)	*<0.05**
a-wave ttp (ms) (3-month)	14.3 ± 2.4 (8)	11.1 ± 5.7 (9)	*0.56*
I_{50} a-wave (log photons/μm) (3-month)	4.70 ± 0.35 (6)	4.55 ± 0.26 (7)	*0.37*
R_{max} b-wave (μV) (3-month)	1108 ± 333 (8)	589 ± 103 (9)	*0.001**
b-wave ttp (ms) (3-month)	60.8 ± 7.3 (8)	66.3 ± 16.9 (9)	*0.47*
I_{50} b-wave (log photons/μm) (3-month)	2.44 ± 0.34 (8)	3.35 ± 0.66 (9)	*<0.05**
b-wave threshold (μV/R*) (3-month)	370 ± 89 (8)	143 ± 62 (9)	*<0.001**
Phototransduction Gain (/s^2) (3-month)	8.77 ± 1.54 (8)	9.32 ± 2.82 (9)	*0.63*
T_{delay} (ms) (3-month)	5.83 ± 0.91 (8)	5.63 ± 1.91 (9)	*0.79*
Dark Adapted OP area (1-month) [α]	2.91 ± 0.76 (7)	3.51 ± 0.68 (7)	*0.14*
Dark Adapted OP area (3-month) [α]	2.93 ± 0.52 (5)	2.01 ± 0.61 (9)	*<0.05**
Dark Adapted OP (3-month)			
• Area (μV*ms)	2.98 ± 1.22 (6)	1.66 ± 0.4 (7)	*<0.05**
• Sum Amplitude (μV)	843 ± 325 (6)	606 ± 126 (8)	*0.12*
• Sum ttp (ms)	138 ± 5.2 (6)	123 ± 5.3 (8)	*<0.001**
Light Adapted OP (3-month)			
• Area (μV*ms)	1.91 ± 0.34 (6)	0.92 ± 0.2 (6)	*0.11*
• Sum Amplitude (μV)	327 ± 70 (6)	261 ± 38 (7)	*0.06*
• Sum ttp (ms)	164 ± 5.0 (6)	151 ± 7.5 (7)	*<0.01**
Dark-adapted CFF (Hz) (3-month)	21.4 ± 1.9 (7)	17.6 ± 2.0 (5)	*<0.01**
Light-adapted CFF (Hz) (3-month)	36.7 ± 3.4 (6)	36.5 ± 9.94 (6)	*0.96*

[α] OPs isolated from Ocuscience HMsERG instrument recordings

*Indicates statistical significance

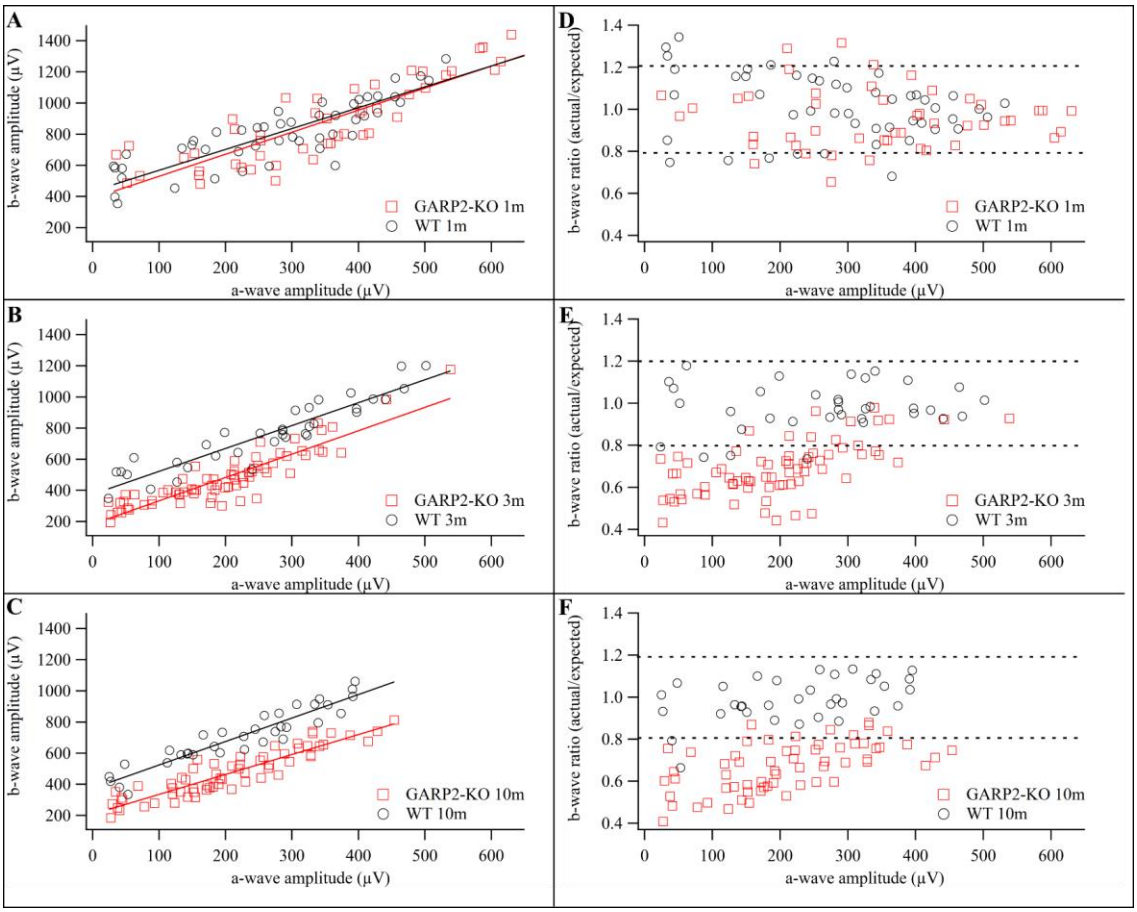

Figure 16: GARP2-KO has lower than predicted b-wave amplitudes for the observed a-wave. A) – C) plot of GARP2-KO and WT b-wave amplitudes with respect to a-wave amplitude for 1, 3, and 10 months of age, respectively. Coefficients of the linear regression of each group are represented as follows: Age: Genotype (n) – Slope ± 1SD, y-intercept ± 1SD, R^2. 1-month: WT – 1.34 ± 0.11, 435 ± 36, 0.75; GARP2-KO – 1.42 ± 0.12, 389 ± 46, 0.74. 3-month: WT – 1.47 ± 0.10, 376 ± 30, 0.86; GARP2-KO – 1.50 ± 0.10; 0.81. 10-month: WT – 1.51 ± 0.10; 374 ± 25, 0.88; GARP2-KO – 1.28 ± 0.07, 208 ± 17, 0.84. D) – F) b-wave ratio (actual b-wave: expected b-wave) with respect to a-wave amplitude is shown. The expected b-waves were interpolated from the shown linear fits of the WT animals at each time point, panels A-C. The previous assessment of human subjects using this method found that normal human b-wave ratios fall between 0.8 and 1.2. D) At one-month WT and GARP2-KO points overlap and are mostly within the previously reported range (indicated by dashed lines). E) By the three-month time point, there is a distinct separation between WT and GARP2-KO, with WT falling inside the normal range and GARP2-KO mostly below normal. F) At 10-months the decrease is still observed.

Oscillatory Potentials Peak Faster in the GARP2-KO

Oscillatory potentials (OPs) arise from the inner retinal amacrine and horizontal cells and are superimposed on the rising b-wave. Using a 5th order Butterworth filter with a passband of 65-300 Hz we isolated OPs from the dark-adapted and light-adapted 6.18 log photons per μm^2 incident to the cornea stimulated response (Figure 18). We utilized a novel approach to examine the OP response amplitude and peak times simultaneously by measuring the area under the absolute value of the OP trace, producing a time-integrated response, with the units of μV*s. The signal was compared to the noise by subtracting the area under the baseline (150 ms before the flash) from the OP area, which is the absolute value of the curve from 0.0 to 150 ms. If the signal to noise ratio was not ≥ 2, the recording was considered poor quality and was excluded from analysis. The area under the absolute value of the isolated OP peaks is significantly reduced under dark-adapted conditions compared to WT (WT = 2.98 ± 1.2 μV*s (n = 6), GARP2-KO = 1.66 ± 0.4 μV*s (n = 7), *p-value* < *0.05**). The area under the OP peaks isolated from light-adapted conditions is not different between the GARP2-KO and WT (WT = 1.91 ± 0.3 μV*s (n = 6), GARP2-KO = 0.92 ± 0.2 μV*s (n = 6), *p-value* > *0.1 N.S.*).

The amplitude and times-to-peak were measured and summed for each flash condition for the first five OP peaks. The summed response amplitudes of the OPs are not different in the GARP2-KO (Table 3). However, interestingly, the summed ttps are significantly faster in the GARP2-KO under both light-adapted and dark-adapted conditions (Table 3). A complete overview of all ERG results can be found in Table 2.

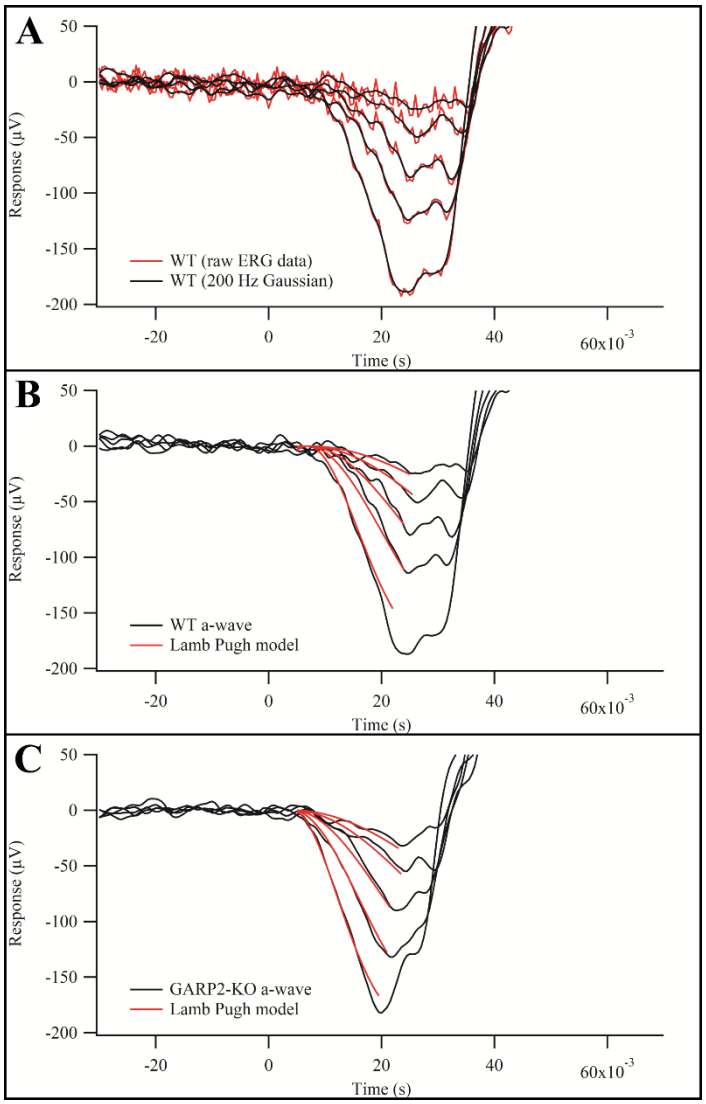

Figure 17: Lamb-Pugh a-wave model of phototransduction gain. The leading edge of the a-wave was ensemble fit to the Lamb-Pugh model of phototransduction gain to assess changes in the kinetics of the photoresponse. A) 200 Hz Gaussian filters were employed before fitting to remove noise but preserve peak timing, amplitude, and shape, as seen here. B) and C) are examples of curve fits for a family of a-wave responses of one WT animal and one GARP2-KO animal, respectively. No change in gain or T_{delay}, which accounts for the activation steps of phototransduction, were observed. (Gain: WT: 8.77 ± 1.54; GARP2-KO: 9.32 ± 2.82; p-value: 0.63) (T_{delay}: WT: 5.84 ± 0.91; GARP2-KO: 5.63 ± 1.91; p-value: 0.79).

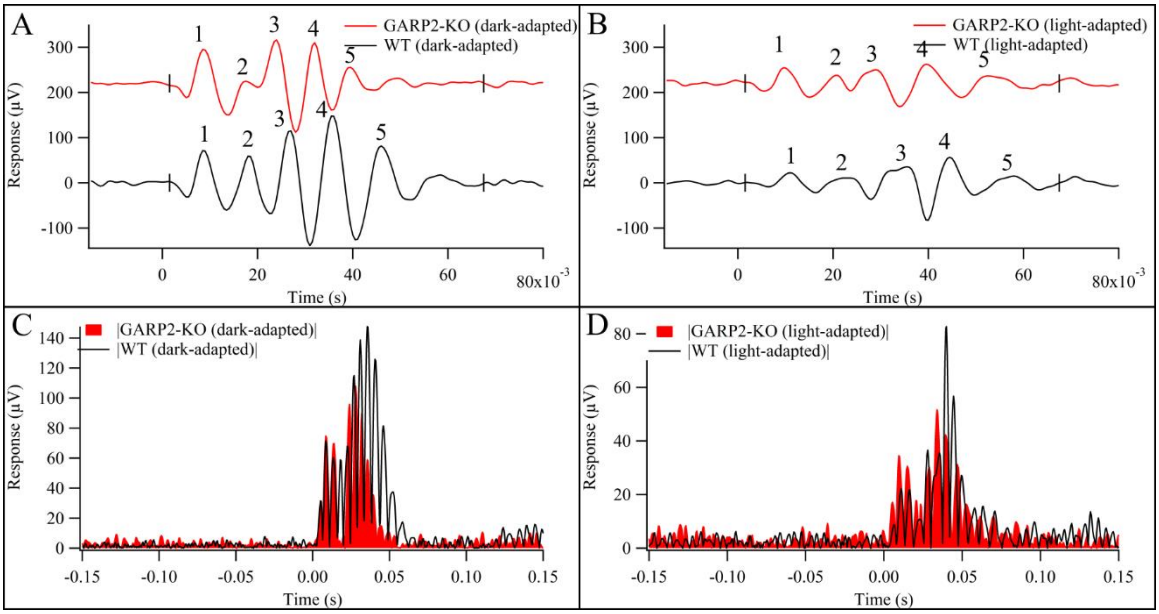

Figure 18: Oscillatory potentials of GARP2-KO. A) Dark-adapted and B) Light-adapted OPs isolated from flashes with the intensity of 6.18 log photons per μm^2 incident to the cornea for each condition. Peaks labeled 1-5 were measured for amplitude and timing and the results summarized in Table 2. If a sixth OP peak was observed, it was not included in the sum amplitude or time calculations. C) and D) are the absolute values of the recordings shown in A) and B) respectively. Background noise was the area under the curve measured from 150 ms before the flash to time 0. The time-integrated response is the area measured from 0 to 150 ms which is from the midpoint of the flash until a point well after the last observed OP peak, to ensure inclusion of any late occurring OPs.

Table 3: Individual scotopic oscillatory potential peak amplitudes and timing of GARP2-KO vs. WT at three months of age.

OP Peak	**GARP2-KO**	**WT**	***p-value***
	OP peak amplitude (μV)		
1	111.5 ± 32.7	95.7 ± 40.9	*0.45*
2	86.2 ± 27.8	104.8 ± 52.5	*0.45*
3	104.4 ± 21.7	160.7 ± 67.2	*0.07*
4	199 ± 47.4	256.4 ± 111.3	*0.26*
5	105.7 ± 14.3	225.7 ± 78.9	*<0.01**
Sum	843 ± 325	606 ± 126	*0.12*
	OP time-to-peak (ms)		
1	8.8 ± 0.3	8.7 ± 1.5	*0.92*
2	17.5 ± 0.7	18.9 ± 0.6	*<0.01**
3	24.3 ± 1	26.7 ± 1.8	*<0.05**
4	32.3 ± 1.4	36.8 ± 1.2	*<0.001**
5	40.1 ± 2.1	47.1 ± 1.7	*<0.001**
Sum	138 ± 5.2	123 ± 5.3	*<0.001**
	Area under the absolute value of scotopic OP (μV*s)		
	2.98 ± 1.2 (6)	1.66 ± 0.4 (7)	*<0.05**

C-Waves Not Changed in GARP2-KO

To assess one aspect of RPE function which is performed in concert with the Müller cells, the flux of potassium ions through the retina after a prolonged light stimulus, we measured the time-integrated c-wave response. After normalization of the c-wave to b-wave amplitude, the area under the curve was measured from the rising phase of the c-wave until the point immediately prior to stimulus cessation. No difference was found between the GARP2-KO and WT measured areas (Table 2).

Scotopic CFF is Decreased in the GARP2-KO

The bipolar cell ON- and OFF- pathways are responsible for the temporal resolution of the visual system. Since the b-wave, which arises in the bipolar cells, was reduced in the GARP2-KO we assessed the health of the temporal signaling pathways by measuring the critical flicker fusion frequency (CFF). Scotopic CFF in the GARP2-KO mouse was 18% smaller than WT. Photopic CFF was no different. See Table 2 for light- and dark-adapted CFF values.

Ten Differentially Expressed Genes Confirmed

Our laboratory maintains mouse lines with various deletions in the *Cngb1* gene, the GARP2-KO, created for this study, which is a deletion of GARP2, *Cngb1*-X1 which is a deletion of the β-subunit of the CNG channel and both GARP1 and GARP2, and *Cngb1*-X26 which is a deletion of the β-subunit of the CNG channel with normal expression of the GARP proteins.

Quality control performed in FastQC (Andrews, 2010) provided the number of sequence reads per sample, the average length of each sequence, the number of sequences flagged as poor quality, GC content, and Phred score, which is a prediction of base calling accuracy in sequencing where a score of 30 indicates a 1 in 1000 probability of being incorrectly identified and a score of 40 is a 1 in 10,000 chance (Bokulich et al., 2013). The number of sequence reads detected for each sample is as follows: WT produced ~32 million sequence reads, GARP2-KO produced ~35 million sequence reads, *Cngb1*-X1 produced ~34 million sequence reads, and *Cngb1*-X26 produced ~45 million sequence reads. The average length of each sequence was consistently 51 bp for all samples. No sequences were flagged as poor quality. The GARP2-KO and *Cngb1*-X26 samples had a GC content of 50%, while the WT and *Cngb1*-X1 animals had a GC content of 51%. The Phred scores for each sample was 38, meaning over 99.9% accuracy was predicted. Transcriptome analysis by next-generation sequencing (NGS) of mRNA extracted from one-month-old GARP2-KO, *Cngb1*-X1, *Cngb1*-X26, and WT retinas revealed differentially expressed genes in each mutant in comparison to WT with the cut-off criteria being a posterior probability of differential expression (PPDE) ≥ 95%. In Figure 19, the identified significantly differentially expressed genes compared to WT are represented in a Venn diagram with overlapping areas showing genes that are in common between groups based on expression of GARP1, GARP2, and the β-subunit. Fold change values for each section of the Venn diagram can be found in Appendix H. Since GARP2-KO and *Cngb1*-X1 are both null for GARP2, we attributed their commonly differentially expressed genes to be a possible direct effect of the missing protein of interest, GARP2, and those genes are represented in the Venn Diagram as the region of overlap between

GARP2-KO and *Cngb1*-X1 and were used for analysis by Ingenuity Pathway Analysis (IPA) software (Krämer et al., 2014). Table 4 shows the top five affected gene networks based on IPA network score and their associated differentially expressed genes, which were the targets for qRT-PCR validation. To verify IPA network analysis and NGS fold-change results qRT-PCR was performed using mRNA extracted from 3-month old GARP2-KO and WT mice, which is a time point coinciding with the observed functional changes, with single target primers specific to the selected network genes (Appendix G). Using cutoff criteria of p-value ≤ 0.05 and fold change ≥ 1, six genes were significantly down-regulated: *Zymnd10*, *Foxo3*, *Nrip1*, *Crebbp*, *Garem*, and *Cit*, and four genes were significantly up-regulated: *Myb*, *Vmn2r29*, *Nek5*, and *Rec8*. The qRT-PCR fold change results for these genes can be found in Table 5 along with the NGS fold change results.

GARP1 and GARP2 are Predicted Single-Domain Proteins

To ideate the physical differences between the structures of GARP1 and GARP2 we utilized I-TASSER computational structure prediction software. I-TASSER requires singular domain protein segments for accurate analysis. ThreaDom was utilized to ensure GARP1 and GARP2 met the single protein domain criteria (Z. Xue, Xu, Wang, & Zhang, 2013), which is found in the ITASSER suite. Figure 20 shows the Domain Conservation Scores (DCS) for all amino acids composing GARP1 (Figure 20A) and GARP2 (Figure 20B). A sharp DCS cutoff within the protein to a value around zero would indicate a change in domain. The plot of DCS shows that every amino acid is ranked with a DCS value around 1 meaning only one domain is present.

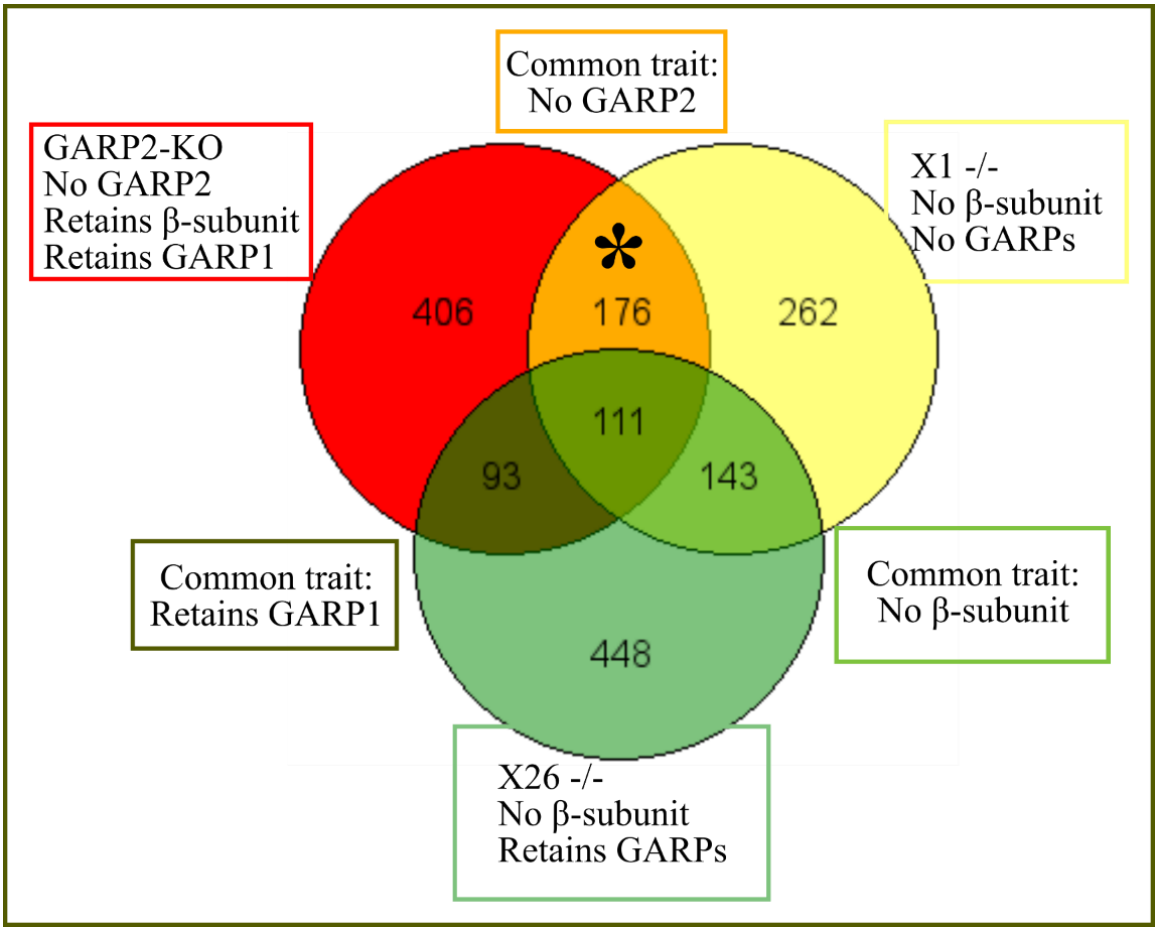

Figure 19: GeneVenn diagram of differentially expressed genes by genotype via Next Generation Sequencing**.** Transcriptome sequencing of three *Cngb1* mutants was compared to determine which differentially expressed genes were due to ablation of specific proteins. Here we focus on the group of genes in common between the GARP2-KO and *Cngb1*-X1 mice as they are both missing GARP2, indicated in the figure by an asterisk (*****).

Table 4: Genes chosen for expression verification by qRT-PCR. Ingenuity Pathway Analysis of the top five affected networks with associated commonly differentially expressed genes between two different GARP2-null mutants versus WT.

Developmental disorder, ophthalmic disease, organismal injury and abnormalities (IPA network score 48)							
Adnp	*Apod*	*Arid5b*	*Cnp*	*Crebbp*	*Crybb2*	*Crygb*	*Crygc*
Crygd	*Cryge*	*Crygf*	*Garem1*	*Grifin*	*Hba1/2*	*Hfe2*	*Igfals*
Klfs	*Myb*	*Nebl*	*Nr2c2*	*Nr3c2*	*Nrip1*	*Olig2*	*Pcdh17*
Slurp1	*Spen*						
Nervous system development and function, cancer, neurological disease (IPA network score 40)							
Arhgap5	*Birc7*	*Cacna1e*	*Chat*	*Foxo3*	*Gal3st1*	*Glg1*	*Hivep3*
Itgb8	*Klf9*	*Klk6*	*Lrch3*	*Map3k13*	*Mbp*	*Mobp*	*Mog*
Pde3a	*Peg3*	*Rims1*	*Stx1b*	*Syngap1*	*Tnks*		
Skeletal and muscular disorders, neurological disease, immunological disease (IPA network score 26)							
Bcas1	*Cdkl5*	*Ces1*	*Chrm2*	*Cit*	*Gabbr2*	*Gpr17*	*Irs2*
Lyst	*Mag*	*Necab1*	*Ntsr2*	*Slc2a4*	*Slc36a4*	*Vmn2r32*	*Wasf3*
Cancer, organismal injury and abnormalities, hematological disease (IPA network score 24)							
Ago2	*C11orf98*	*Ccnt1*	*Cldn11*	*Hspb1*	*Ikzf4*	*Isg15*	*Myl2*
Pcdhac2	*Ptch1*	*Tenm4*	*Tmem160*	*Trip11*	*Trpm6*	*Zmynd10*	
Cellular movement, cell morphology, nervous system development and function (IPA network score 24)							
C18orf25	*C18orf54*	*Ccdc186*	*Cntn5*	*Fa2h*	*Gjc2*	*Hapln2*	*Hcn4*
Hist1h2bk	*Mag*	*Mog*	*Nkx6-2*	*Opalin*	*Tmem888*	*Wwc2*	

Table 5: Confirmed differentially expressed genes from GARP2-KO retinal mRNA. The fold changes of each of the differentially expressed genes versus WT expression level is listed below for the initial (1-month timepoint) NGS assay and confirmatory (3-month timepoint) qRT-PCR.

Gene Symbol	**Gene Name**	**NGS fold change 1M**	**qRT-PCR fold change 3M**
Rec8	REC8 meiotic recombination protein	-16.4	71.4 *(<0.01*)*
Nek5	NIMA (Never In Mitosis A) – related expressed kinase 5	-22.4	4.97 *(<0.01*)*
Vmn2r29	Vomeronasal 2 receptor 29	-6.04	2.56 *(<0.05*)*
Myb	Myeloblastosis oncogene	-2.94	1.52 *(<0.05*)*
Nrip1	Nuclear receptor interacting protein 1	-5.05	-1.27 *(<0.001*)*
Foxo3	Forkhead box, O3	-3.58	-1.28 *(<0.05*)*
Garem	GRB2 associated regulator of MAPK1	-2.77	-1.29 *(<0.05*)*
Crebbp	CREB binding protein	-2.75	-1.43 *(<0.05*)*
Cit	Citron rho-interacting serine/threonine kinase	-4.95	-1.57 *(<0.05*)*
Zmynd10	Zinc finger, MYND domain containing 10	+5.16	-5.24 *(<0.001*)*

Predicted Structures of GARP1 And GARP2

The I-TASSER platform first utilizes a local meta-threading-server (LOMETS) (S. Wu & Zhang, 2007) to find similar protein templates based on primary amino acid sequence within the protein database (PDB). I-TASSER (Roy et al., 2010; Jianyi Yang et al., 2015; Yang Zhang, 2008) and then performs structure assembly to either join matching PDB templates or to iteratively model sequences with no matching PDB templates. The lowest energy model is then used in COACH to find ligand binding sites and associated ligands, enzyme commission (EC), and gene ontology (GO) functional annotations (S. Wu & Zhang, 2007; Jianyi Yang, Roy, & Zhang, 2013).

Although both proteins are intrinsically disordered, meaning a stable backbone structure does not exist and therefore complicated to characterize, the modeling algorithm looks for the lowest energy configurations, which is biologically the preferred conformation for any protein. If the protein passes, even momentarily, through the predicted configuration, the proposed ligand binding and predicted functions are possible. Each model iteration is given a c-score or confidence score that falls between -5 and 2, with a larger value indicating higher confidence in the predicted structure. The predicted model with the highest c-score is given a TM-score, and root mean square difference (RMSD) calculation. The TM-score is a measure of similarity between the model and template protein from the protein database and is insensitive to the length of the proteins. TM-score is given on a scale of 0 to 1 where 1 indicates a perfect match, a TM-score higher than 0.5 indicates the proteins have similar folding patterns, and a TM-score of 0.17 is an unrelated protein. The RMSD calculation is given in Å, as it is the difference between the average distance of all the amino acid residues comprising the predicted

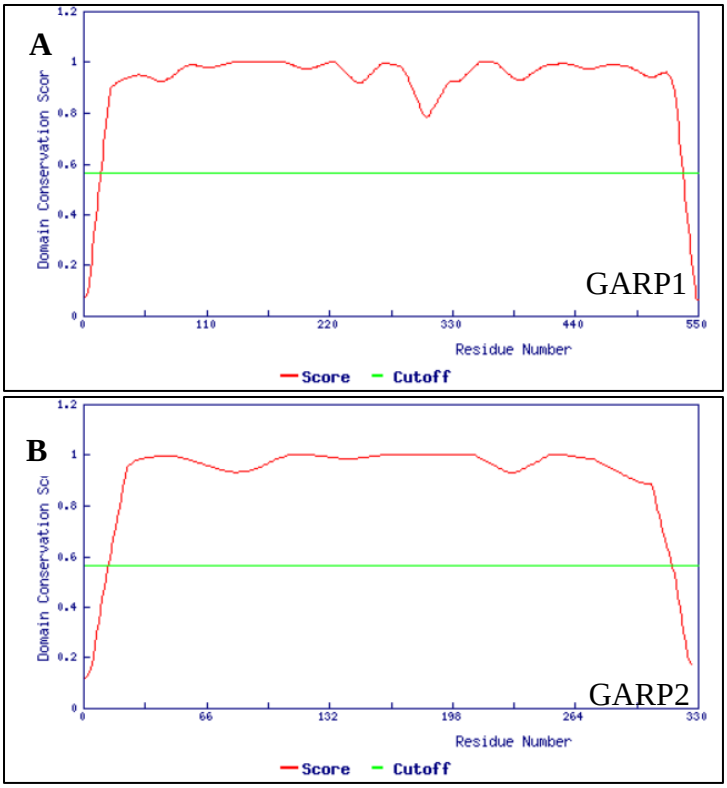

Figure 20: ThreaDom output indicating singular protein domains in GARP1 and GARP2. Multiple threading alignments of the given amino acid sequence to templates within the protein database give domain matches for continuous and discontinuous protein domains calculating a domain conservation score (DCS) for each amino acid. These are plotted above, A) GARP1 and B) GARP2. All amino acids for both GARP1 and GARP2 have domain conservation scores near 1 indicating continuity and the presence of only one domain.

model versus all the amino acids comprising the database protein. TM-score was designed as an alternative comparison metric to offset the effect protein length has on the RMSD (Wu & Zhang, 2007).

For every predicted model of GARP1 and GARP2, the c-score values are very low, verifying the intrinsic disorder of each protein. In Figure 21 the top predicted model for each protein (GARP1 Figure 21A; GARP2 Figure 21B) is shown with a graph of the normalized b-factor. The b-factor is a measure of the thermal stability of the α-carbon for each amino acid residue in the protein (Jianyi Yang, Wang, & Zhang, 2016). B-factors are used to predict areas of protein folding and ligand binding pockets (Sheriff, Hendrickson, Stenkamp, Sieker, & Jensen, 1985), as well as areas of intrinsic disorder (Radivojac et al., 2004). Table 6 shows the top ten predicted ligands, the BioLiP abbreviation, binding site residues, and c-scores for GARP1 and GARP2.

We used the ConCavity software feature in I-TASSER (Capra, Laskowski, Thornton, Singh, & Funkhouser, 2009) to find the predicted active amino acid residues for each of the top predicted models for GARP1 and GARP2. The active amino acid residues predict functional regions or putative ligand binding sites of the protein. These results are listed and ranked in the COACH results of Table 5. No ligands were provided by the ConCavity suite as it assesses the amino acid structure without aligning to known PDB templates with a pocket finding algorithm, then computational mapping allows the prediction of valid binding residues.

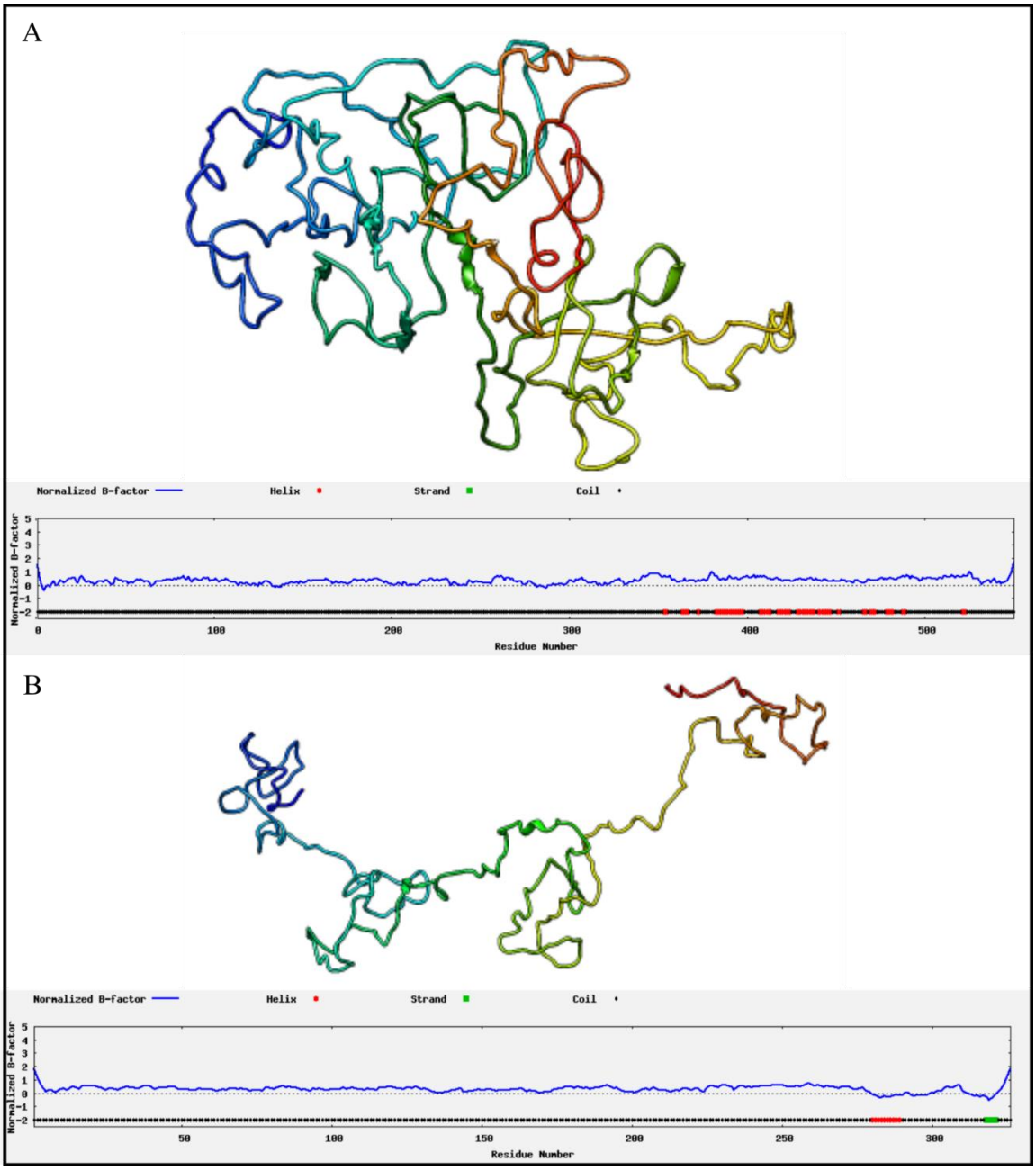

Figure 21: Top computationally predicted model structures. A) GARP1 and B) GARP2. Underneath each model is a graph of the normalized b-factors for each amino acid residue which is a measure of thermal stability. Negative b-factors indicate protein stability while positive b-factors indicate more flexibility. For both GARP1 and GARP2, although the proteins are intrinsically disordered, it appears they are even more flexible at their C- and N- termini. Model fit information: A) GARP1: c-score = -2.36; TM-score = 0.44 ± 0.14; RMSD = 13.3 ± 4.1 Å B) GARP2: c-score = -2.54; TM-score = 0.42 ± 0.14; RMSD = 12.4 ± 4.3 Å.

Table 6: COACH predicted ligands and binding residues for GARP1 and GARP2. The c-scores are calculated in part by the structural stability of the proteins, which we have already discussed is low for these intrinsically disordered proteins. With a c-score of 0.02, there are 12 residues predicted to bind calcium, which has already been determined experimentally to be true.

GARP1			
Rank	Ligand	Binding Residues	c-score
1	CH1 – 3'-Deoxycytidine 5'-triphosphate	310, 311, 317, 319, 320, 321	0.05
2	VDY – 25-Hydroxyvitamin D3	2, 5, 9	0.05
3	CLA – Chlorophyll A	105, 134, 138	0.03
4	MG – Magnesium	428, 431	0.03
5	GLC – alpha-D-glucose	316, 457, 461	0.02
6	MG – Magnesium	392, 397	0.02
7	ConCavity ligand binding sites	216, 237, 239	0.02
8	ConCavity ligand binding sites	188, 189, 190, 246	0.02
9	PEPTIDE	540, 541	0.02
10	ZN – Zinc	363, 365	0.02

GARP2			
Rank	Ligand	Binding Residues	c-score
1	ATP – Adenosine triphosphate	190, 191, 224, 228	0.05
2	ZN – Zinc	58, 62	0.05
3	XYS – Xylopranose	316, 318	0.03
4	0KY – 3-[(2R)-2-ethoxypropyl]-2-thioxo-1,2,3,9-tetrahydro-6H-purin-6-one	54, 55	0.02
5	**CA – Calcium**	162, 164, 166, 168, 169	0.02
6	**CA – Calcium**	65, 68, 70, 71, 72, 78, 79	0.02
7	MG – Magnesium	96, 136	0.02
8	ConCavity ligand binding sites	79, 82, 88, 89, 95, 96, 99, 102, 104, 105, 125, 127, 129, 131, 133, 134, 142	0.02
9	Nuc.Acid	124, 126	0.02
10	TPP – Thiamine diphosphate	183, 185, 214, 218	0.02

DISCUSSION

In this study, we have successfully generated a selective knockout of GARP2 in the mouse retina. Based on the finding that knockout of the β-subunit and GARPs lead to retinal degeneration (*Cngb1*-X1; Zhang et al. 2009) and knockout of only the β-subunit without effecting GARP expression (*Cngb1*-X26; Huttl et al., 2005), leads to a retinal degeneration with features that are distinct from the *Cngb1*-X1, we hypothesized that selective GARP2 knockout would alter structure and function of the rod photoreceptor. Indeed, structural and functional deviations from WT were observed in the GARP2-KO. However the robustness of the phenotype is subtler than expected.

Structural Changes

Some of the rod outer segments in the GARP2-KO retina are longer than WT (Figure 12). These changes are not always observed, and the regions that they appear are not constricted to any quadrant or discernable location (i.e., more central or peripheral, near the optic nerve, near the ora serrata, etc.) In the GARP2-Ox model, ROS lengths were reported to be uniformly 20% shorter than WT (Sarfare et al., 2014), so underexpression (or no expression as in the GARP2-KO) might reasonably be expected to produce an overgrowth of ROS. The high variability we observed in length was surprising. One possibility to explain the variability and sporadic nature of the phenomenon is that

the effect itself is transient, and then could, in fact, be occurring panretinally. Thus, at any given time, as captured by a histology timepoint, the effect may or not be observed depending on the frequency of occurrence and the time needed for resolution. *In vivo* and *ex vivo* observations of the GARP2-KO mouse morphology are seemingly contradictory, as regions of the ROS appear longer than WT when viewed histologically, but not different from WT when imaged by OCT. The SD-OCT manufacturer (Bioptigen) specifications list the axial resolution of the instrument as 2.5 μm. The longer ROS regions are folded and lie parallel to the RPE at the interdigitation zone, possibly masking the length, below the instrument's axial resolution threshold. Alternatively, it could be more due to the sporadic nature of the elongations, which is consistent with the fact that the change was not observed in all histologic sections.

We also considered that the folding of the ROS end tips parallel to the RPE observed in the overgrowth regions could interfere with circadian regulated phagocytosis of the ROS, leading to longer ROS lengths, but phagosome counts were unchanged between GARP2-KO and WT groups.

In the *Cngb1-X1* knockout of the β-subunit and GARPs, cryo-EM measurements of intradiscal spacing were not different from WT at 32 nm corresponding to every fourth 8 nm tubulin repeat on the ciliary axoneme (Gilliam et al., 2012), indicating that GARP2 is not involved in maintaining disk spacing, and thus may not bind to the *rds*/peripherin complex. Recently, it was proposed that *rds*/peripherin links rhodopsin to the CNG channel, establishing a complex of phototransduction initiator (rhodopsin) and ultimate effector (the CNG channel) facilitating the sensitivity needed for single photon responses (Becirovic et al., 2014). GARP2 may support this linkage as the proteins do interact *in*

vitro (Körschen et al., 1999; Pentia et al., 2006), but since the overall structure of the discs remains intact in *Cngb1-X1* mouse, the possibility that GARP2 regulates disc structural integrity is ruled out.

Functional Changes

Functionally, by ERG analyses, the GARP2-KO mouse was not different from WT at one month (Figure 16, Panels A and D). By three months, however, the GARP2-KO mouse exhibited significant deficits in nine of twenty functional properties analyzed from the ERG data (Table 2). Since GARP2 is solely expressed in rod photoreceptors, it is not surprising that eight of the nine functional changes occurred in rod signaling pathways. Scotopic a- and b- wave amplitudes were reduced by 33% and 47%, respectively, with no significant amplitude reduction observed in photopic recordings (Figure 15A, Table 2).

Modified Michaelis-Menten dose-response analysis of the GARP2-KO a-wave versus intensity indicated that although the response amplitude is decreased, the intensity of light required to elicit the half-maximal response is the same for both GARP2-KO and WT mice (Figure 15B, Table 2), which means the sensitivity of the GARP2-KO photoreceptors to light is the same as WT photoreceptors. The amount of light required to elicit the half maximal b-wave response in the GARP2-KO was 37% higher than WT, indicating a reduction in bipolar cell sensitivity. (Figure 15C, Table 2). The observed reduction in sensitivity was verified by comparing the b-wave response amplitude at threshold

(Saszik, Robson, & Frishman, 2002), which is at a flash intensity below 5 - 10 photoisomerizations per rod where the intensity to response plot is linear and the signal-to-noise ratio was greater than 2 (Baylor, Lamb, & Yau, 1979a, 1979c; Field & Rieke, 2002). The b-wave threshold response of the GARP2-KO was 61% lower than the WT threshold response.

The GARP2-KO b-wave amplitudes are reduced beyond the predicted reduction based on lower a-wave amplitudes alone by 3 months of age (Figure 16). This enhanced b-wave reduction indicates an insufficiency in signal transduction from the rod photoreceptors to the bipolar cells at the photoreceptor synapse, not just a "small signal in, small signal out" scenario. Since GARP2 is not found in WT bipolar cells, the observed effect is predicted to be a defect in the primary activity of the rod spherule, the synaptic release of glutamate, which is a calcium-dependent event.

In vitro analysis of GARP2 shows that the protein is a low-affinity, high-capacity calcium-binding protein (Haber-Pohlmeier et al., 2007). Although the majority of GARP2 is localized to the ROS, proteins with immunoreactivity to N-terminal CNGB1 antibodies also localize to the synaptic region in the OPL, (T. Y. Chen et al., 1993, 1994; Körschen et al., 1995, Sarfare et al., 2014), placing GARP2 in the proper position to affect synaptic function or calcium-dependent processes, which could be altered in the GARP2-KO. Synaptic vesicle docking which leads to glutamate release is a calcium-dependent process (Vaithianathan & Matthews, 2014). The influx of calcium into the spherule occurs through voltage-gated calcium channels that remain open when the rod is depolarized, i.e., in the dark (Copenhagen & Jahr, 1989). Calcium is extruded from the synaptic terminal

primarily by the Na^+ K^+ ATPase (Morgans, El Far, Berntson, Wässle, & Taylor, 1998). The signal to the bipolar cells of a light stimulus detected by the rod is a graded decrease in glutamate release (Morgans, 2000). The active zone of the rod spherule releases around 40 vesicles of glutamate per second in the dark which prevents depolarization of the downstream bipolar cells (Rao, Buchsbaum, & Sterling, 1994). Vesicle fusion to the plasma membrane requires cooperative binding of 4 calcium ions, and an intracellular calcium concentration of at least 10 μM (Heidelberger, Heinemann, Neher, & Matthews, 1994). I-TASSER software predicts 12 putative calcium-binding residues within GARP2 (Table 6). If GARP2 normally binds calcium in the synapse, the absence of GARP2 would lead to an increase in intracellular synaptic free calcium. Increased calcium may increase the rate of vesicular docking and subsequent neurotransmitter release. Mammalian rod bipolar cells are ON-type, meaning they depolarize in response to decreased glutamatergic input, such as when the graded decrease in glutamate occurs due to the events of phototransduction (Dacheux & Raviola, 1986). The proposed increase in synaptic glutamate release, attributed to higher calcium levels due to the ablation of GARP2, would prevent full ON-bipolar cell depolarization and decrease the amplitude of the b-wave.

The synaptic transmission from the rod photoreceptors to rod bipolar cell pathways is measured not only through the b-wave of scotopic flash ERGs, but temporally through the scotopic CFF (Kalloniatis & Luu, 2007), which was reduced by 18% in the GARP2-KO. Although there is a photoreceptor component to CFF responses, selective

pharmacological blockade of the bipolar cells and inner retinal cells revealed the sizeable contribution of the bipolar cells to the CFF recording (Ronald A. Bush & Sieving, 1996).

The gain of phototransduction of the GARP2-Ox mouse was increased, leading to the prediction that in the GARP2-KO, an opposite effect of a decreased gain would be observed. Contrary to this prediction, no change in gain, compared to WT, was found. The gain of phototransduction, as calculated from the Lamb-Pugh equation, is a metric of the amplification of transduction within a rod representing the product of the rate of PDE activation per activated rhodopsin model, the rate of cGMP hydrolysis, and the Hill coefficient, which is a measure of cooperative ligand binding (Breton et al., 1994). The increase in phototransduction gain of the GARP2-Ox mouse (Sarfare et al., 2014) likely reflects a change in PDE6 activation; either more PDE6 catalytic subunits were being activated, or an increase in PDE6 activity was occurring, which may not be possible as PDE6 approaches the theoretical limit of perfect enzyme catalysis (Cote, 2004). The GARP2-Ox results are consistent with previously performed crosslinking and immunoprecipitation experiments linking GARP2 to the inhibitory gamma subunit of PDE6 (PDE6-γ) (Körschen et al., 1999; Pentia et al., 2006).

Pentia et al. showed that PDE6-γ, the inhibitory subunit of PDE6, was prevented from spontaneously dissociating from PDE6 in the presence of GARP2. This was suggested to participate in the reduction of noise associated with non-transducin- α mediated activity, that may help to facilitate the single photon response of rods (Pentia et al., 2006). In a mouse overexpression model of PDE6-γ, the gain of phototransduction was decreased, indicating cytosolic PDE6-γ subunits could bind and inhibit the catalytic α- and β- subunits of the PDE6 holoenzyme (Tsang, 2006). Two threonine residues on

PDE6-γ were replaced with alanine residues in a transgenic mouse model to preserve PDE6-γ structure but prevent threonine kinase phosphorylation. In that study, the ttp was increased, and peak amplitudes were reduced, indicating that phosphorylation events regulate the rate of the photoresponse (Tsang et al., 2007). GARP2 is negatively charged, as are the phosphoryl groups added by threonine kinases (Matte, Tari, & Delbaere, 1998). Considering the association of PDE6-γ and GARP2, and the concept of charge repulsion, perhaps the photoresponse-altering threonine kinase activity upon PDE6-γ is accelerated in the absence of GARP2? Based on the gain of phototransduction in the GARP2-KO mouse, this is not what is occurring, since gain is a direct reflection of PDE6 activity, which did not differ from WT, indicating the observed functional reductions of the GARP2-KO mouse are not occurring in the phototransduction cascade.

The GARP2-KO and WT c-waves are not different from each other. We report the amplitude and timing of c-waves as a metric of RPE health. The c-waves were recorded with 0.01 Hz AC filtering applied at the time of collection instead of a DC filter. The error was identified when updating the recording setup, and the waveform of the c-wave from the new setup was noticed to be different. FFT of the c-waves collected by the old setup versus new revealed the 0.01 Hz AC filtering artifact. Its application decreased the overall trans-corneal signal recorded from the RPE and Müller cells that contribute to generating the c-wave. The actual c-wave, however, was recorded for both groups, albeit at a reduced level due to the AC filter, meaning the groups are comparable and no difference exists.

Gene Expression Changes

Gene expression changes reported here are from within the subset of commonly differentially expressed genes between the *Cngb1*-X1 and GARP2-KO. We chose to focus on this comparison of genotypes because both lines lack GARP2 and their commonly differentially expressed genes versus WT may best represent a direct effect of GARP2 ablation. The ten genes identified as differentially expressed (Table 5) provide insight into some seemingly unrelated phenomena that are discussed in the following paragraphs.

As noted above, the function of the RPE as measured through the ERG c-wave was unchanged. However, gene expression suggests that RPE function may not be normal. *Foxo3*, a transcription factor that regulates autophagic processes (Israeli, 2013; van der Vos et al., 2012; Zhao et al., 2007) was downregulated in the GARP2-KO. *Foxo3* also regulates circadian rhythms via controlling *Clock* expression (Chaves et al., 2014), and phagocytosis of the ROS end tips is a circadian event (Bosch, Horwitz, & Bok, 1993). *Nrip1*, a retinoic acid receptor interacting protein was downregulated, which is a transcription factor that binds to retinoic acid receptors to activate transcription of genes with retinoic acid response elements promoters (Y. Chen, Kerimo, Khan, & Wei, 2002). As many steps of the visual cycle, a retinoid-dependent process, happen in the RPE it is possible the change in *Nrip1* expression also occurred in the RPE. The RPE was collected in addition to the neural retina for gene expression analysis, as morphological changes indicated a possible RPE dysfunction.

Although GARP2 has been shown to coimmunoprecipitate with *rds*/peripherin, the interaction may have less to do with maintaining ROS disc structure, but rather more

to do with support of the ciliary axoneme. *Zymnd10*, which is vital to the dynein arm assembly of the axoneme of primary cilia (Moore et al., 2013), and the dynein arm is responsible for the retrograde movement of material from the ROS to the cell body (Goldstein & Yang, 2000). This transcript, *Zymnd10*, was downregulated in the confirmatory qRT-PCR performed after RNA-seq analysis. Furthermore, *Cit*, a serine-threonine kinase, vital to cytokinesis (Yamashiro et al., 2003), an active process within the connecting cilium (J. L. Rosenbaum & Witman, 2002) was also downregulated. *Nek5* and *Rec8* that function to regulate centrosome integrity for ciliary growth by interacting with γ-tubulin (Prosser & Fry, 2015), to stabilize the centrosome for axoneme growth (Nigg & Stearns, 2011), respectively, were both upregulated. The molecular changes indicated in the connecting cilium could contribute to the explanation for the changes in ROS length in GARP2-KO and GARP2-Ox retinas. Immunofluorescent interaction imaging shows peripherin/*rds* binds to CNGB1 in the inner segment of the rod and to GARP2 in the outer segment(Ritter et al., 2011). The mechanism behind the differential binding of GARP2 and CNGB1 to peripherin/*rds* may explain the altered expression pattern of axonemal genes.

One of the genes confirmed to be downregulated in the GARP2-KO is a transcription factor that regulates expression of rod-specific versus cone-specific genes, *Crebbp* (Hennig, Peng, & Chen, 2013), along with upregulation of a protein known to interact with *Crebbp*, *Myb* (Morris, Forbes-Osborne, Pillai, & Fadool, 2011). *Garem*, a protein believed to interact with proteins containing high levels of proline was downregulated (Taniguchi et al., 2013). Bovine GARP2 is composed of 14% proline (Sugimoto et al.,

1991), a composition that is closely maintained in mammalian GARPs. *Vmn2r29* a protein with an intrinsically disordered N-terminus similar to CNGB1, normally expressed in olfactory tissue as part of a G-protein signaling cascade, but also in the retina for an undetermined purpose, was upregulated (Lioubinski et al., 2006; H. Yang, Shi, Zhang, & Zhang, 2005). This change could be an internal compensatory mechanism for GARP2 ablation. Oxidative stress processes involve three of the ten confirmed differentially expressed gene products: up-regulated was *Nek5* (Melo Hanchuk, Papa, La Guardia, Vercesi, & Kobarg, 2015); down-regulated were *Garem* (Taniguchi et al., 2013) and *Foxo3* (Brunet, 2004).

Computational Ligand-Binding Analysis

Some of the ligands predicted to bind GARP2 also are predicted to bind to GARP1 despite major differences in the structural predictions (Table 6). This idea is, however, consistent with both GARPs sharing 291 amino acids of primary structure. The shared ligands, zinc and magnesium, are divalent cations which can bind to either of these negatively charged glutamic acid-rich proteins. GARP2 has 12 putative calcium-binding residues, which is the only experimentally verified ligand thus far (Haber-Pohlmeier et al., 2007).

Dietarily induced magnesium-deficiency in rats caused necrosis of the RPE, and the ROS exhibited a curved morphology, purportedly to evade the necrotic RPE cells (Gong, Amemiya, & Takaya, 2001). The GARP2-KO photoreceptors in the elongated regions bend at the RPE/ROS interdigitation zone. Intracellular calcium concentrations

were much higher in the magnesium-deficient rats (Gong et al., 2001). The observed increase in calcium concentration is due to underactivity of the plasma membrane-bound, magnesium-dependent sodium-potassium ATPase (Na^+/K^+-ATPase) (B. S. Winkler & Riley, 1977). When intracellular retention of sodium occurs, mitochondrial sodium-calcium exchangers are activated, increasing cytosolic calcium concentration (Agarwal, Iezhitsa, & Agarwal, 2014). Most of the energy expended by rod photoreceptors is used for maintenance of the depolarizing dark current, a process dependent upon the activity of the Na^+/K^+-ATPase (Okawa, Sampath, Laughlin, & Fain, 2008).

GARP1 and GARP2 are also predicted to bind to similar ligands with different molecular compositions. GARP1 is predicted to bind cytidine triphosphate (CTP), while GARP2 is predicted to bind ATP; both ligands are high energy molecules, but CTP is used more as a co-factor in enzymatic reactions versus providing energy like ATP (Lieberman, 1956). Both proteins are predicted to bind distinct types of sugar, GARP1 to glucopyranose and GARP2 to xylopyranose. GARP1 is predicted to bind to vitamin D which is necessary for calcium regulation and nutrient absorption (Kulie, Groff, Redmer, Hounshell, & Schrager, 2009), while GARP2 is predicted to bind to vitamin B1, a cofactor in mitochondrial reactions (Kulie et al., 2009). GARP1 is proposed to bind chlorophyll A, a molecule similar in structure to hemoglobin centered around magnesium instead of heme (Hendry & Jones, 1980). Although many of the ligands predicted to bind the GARPs have similar structures and functions, the predicted binding sites are dissimilar, GARP1 ligands are predicted to bind in regions of the protein not shared with GARP2.

Future Directions

Isolated tissue and single cell ERG experiments should be performed on the GARP2-KO retina to assess the kinetics of other phases of the photoreceptor response, especially shutoff of the photoresponse, by pharmacological blockade of downstream signaling cascades arising from the bipolar cells, horizontal cells, amacrine cells, and retinal ganglion cells. The shutoff of the photoresponse in the GARP2-Ox mouse model was 69% slower than WT. Without pharmacological blockade of the retinal cells downstream of the photoreceptors, the shut-off of the GARP2-KO cannot be measured.

Experiments have not been performed to analyze the synaptic glutamate outflow or calcium localization in the GARP2-KO retina, so further testing is required to substantiate any claim of GARP2 activity in the spherule or if the role of calcium buffering by GARP2 is causing the observed functional deficits in the knockout.

Next-generation sequencing of the GARP2-KO in triplicate or more, instead of the ten retinas from each genotype pooled sample approach utilized here, may decrease the number of identified differentially expressed gene targets and could increase confidence in those genes identified. Our NGS experiment was performed on one-month-old mice after morphological changes have occurred, but the physiological changes in the GARP2-KO become apparent at the three-month time point, which is when we performed confirmation qRT-PCR. Next-generation sequencing of these mice at both time points, early and late, would reveal if the morphological and the physiological phenotypes are due to the same mechanisms as assessed by the gene profile. The transcriptome of the GARP2-Ox mouse was not included in our previous comparisons, but opposite expression patterns could reveal pathways involving GARP2.

Mutant animals expressing the recently discovered RP-causing frameshift and premature stop codon mutations within the GARP2 exons of *Cngb1* would be clinically beneficial to determining the patient phenotype and disease progression. Since all the known mutations involve frameshifts, CNGB1 is truncated very early and likely not expressed. GARP2 expression in RP models *Cngb1*-X1 and *rd1* accelerates the progression of the disease (Chakraborty et al., 2015; Deramus et al., 2017). If a mutant form of GARP2 is expressed in the patients with frameshift mutations in the GARP2 region, it is important to consider the potential for the mutant GARP2 to be driving accelerated retinal degeneration as observed in the animal models. The first step in these studies will be to determine in animal models if appreciable levels of truncated GARP2 is being made and distributed to the outer segment or synapse.

Since GARP2 is intrinsically disordered, it does not exist alone in a single conformation. Determining the *in vivo* structure might be achieved if GARP2 were bound to another protein during crystallization, but intrinsically disordered proteins may still adopt different conformations even when bound to an identical partner (Uversky, 2010). The best determination of the protein structure of GARP2 is dependent on what is known about the constituent amino acids, the primary sequence of those amino acids, and the way they interact in proteins with known secondary and tertiary structures, which is the prediction generated by I-TASSER. Calcium was one of the predicted ligands for GARP2 (Table 6), and GARP2 has been experimentally proven to be a high capacity calcium-binding protein (Haber-Pohlmeier et al., 2007). Interaction assays between each of the proposed ligands with either or both GARPs could provide clues to the functional phenotype observed.

In summary, we showed that the GARP2-KO mouse retina is functionally the same as WT at one-month of age, but by three months, reductions in ERG a-wave, b-wave, and scotopic CFF become apparent and persist through ten months of age. Morphologically, observed at the age of 18 days, there is a distinct regional lengthening of the ROS in the GARP2-KO retina with the RPE/ROS interdigitation zone disruption in those elongated regions. The morphological and functional changes consistent with altered gene expression emphasize the importance of GARP2 within the rod photoreceptor for structural integrity and signal transduction.

REFERENCES

Abràmoff, M. D., Magalhães, P. J., & Ram, S. J. (2004). Image Processing with ImageJ Second Edition. *Biophotonics International*, *11*(7), 36–42. https://doi.org/10.1017/CBO9781107415324.004

Adler, A. J., & Southwick, R. E. (1992). Distribution of glucose and lactate in the interphotoreceptor matrix. *Ophthalmic Research*, *24*(4), 243–252. https://doi.org/10.1159/000267174

Agarwal, R., Iezhitsa, L., & Agarwal, P. (2014). Pathogenetic role of magnesium deficiency in ophthalmic diseases. *BioMetals*, *27*(1), 5–18. https://doi.org/10.1007/s10534-013-9684-5

Ahonen, S. J., Arumilli, M., & Lohi, H. (2013). A CNGB1 Frameshift Mutation in Papillon and Phalène Dogs with Progressive Retinal Atrophy. *PLoS ONE*, *8*(8), e72122. https://doi.org/10.1371/journal.pone.0072122

Alpern, M., Fulton, A. B., & Baker, B. N. (1987). "Self-screening" of rhodopsin in rod outer segments. *Vision Research*, *27*(9), 1459–1470. https://doi.org/10.1016/0042-6989(87)90155-6

Alpern, M., Pugh, E. N., & Jr. (1974). The density and photosensitivity of human rhodopsin in the living retina. *The Journal of Physiology*, *237*(2), 341–370.

Altschul, S. F., Gish, W., Miller, W., Myers, E. W., & Lipman, D. J. (1990). Basic local alignment search tool. *Journal of Molecular Biology*, *215*(3), 403–410. https://doi.org/10.1016/S0022-2836(05)80360-2

Altschul, S. F., Madden, T. L., Schäffer, A. A., Zhang, J., Zhang, Z., Miller, W., & Lipman, D. J. (1997). Gapped BLAST and PSI-BLAST: a new generation of protein database search programs. *Nucleic Acids Research*, *25*(17), 3389–3402.

Ames, J. B., Dizhoor, A. M., Ikura, M., Palczewski, K., & Stryer, L. (1999). Three-dimensional structure of guanylyl cyclase activating protein-2, a calcium-sensitive modulator of photoreceptor guanylyl cyclases. *Journal of Biological Chemistry*, *274*(27), 19329–19337. https://doi.org/10.1074/jbc.274.27.19329

Ames, J. B., Levay, K., Wingard, J. N., Lusin, J. D., & Slepak, V. Z. (2006). Structural basis for calcium-induced inhibition of rhodopsin kinase by recoverin. *Journal of Biological Chemistry*, *281*(48), 37237–37245. https://doi.org/10.1074/jbc.M606913200

Andrews, S. (2010). FastQC: a quality control tool for high throughput sequence data. Retrieved July 25, 2018, from http://www.bioinformatics.babraham.ac.uk/projects/fastqc

Arango-Gonzalez, B., Trifunović, D., Sahaboglu, A., Kranz, K., Michalakis, S., Farinelli, P., … Paquet-Durand, F. (2014). Identification of a common non-apoptotic cell death mechanism in hereditary retinal degeneration. *PLoS ONE*, *9*(11), e112142. https://doi.org/10.1371/journal.pone.0112142

Ardell, M. D., Aragon, I., Oliveira, L., Porche, G. E., Burke, E., & Pittler, S. J. (1996). The beta-subunit of human rod photoreceptor cGMP-gated cation channel is generated from a complex transcription unit. *FEBS Letters*, *389*(2), 213–218. https://doi.org/10.1016/0014-5793(96)00588-1

Ardell, M. D., Bedsole, D. L., Schoborg, R. V, & Pittler, S. J. (2000). Genomic organization of the human rod photoreceptor cGMP-gated cation channel beta-subunit gene. *Gene*, *245*(2), 311–318.

Ardell, M. D., Makhija, A. K., Oliveira, L., Miniou, P., Viegas-Péquignot, E., & Pittler, S. J. (1995). cDNA, gene structure, and chromosomal localization of human GAR1 (CNCG3L), a homolog of the third subunit of bovine photoreceptor cGMP-gated channel. *Genomics*, *28*(1), 32–38. https://doi.org/S0888-7543(85)71102-0 [pii]\r10.1006/geno.1995.1102

Asztély, F., & Gustafsson, B. (1996). Ionotropic glutamate receptors. *Molecular Neurobiology*, *12*(1), 1–11. https://doi.org/10.1007/BF02740744

Azam, M., Collin, R. W. J., Malik, A., Khan, M. I., Shah, S. T. A., Shah, A. A., … Hollander, A. I. den. (2011). Identification of Novel Mutations in Pakistani Families With Autosomal Recessive Retinitis Pigmentosa. *Archives of Ophthalmology*, *129*(10), 1377. https://doi.org/10.1001/archophthalmol.2011.290

Banerjee, S., Yao, J., Zhang, X., Niu, J., & Chen, Z. (2017). Next generation sequencing identified novel heterozygous nonsense mutation in CNGB1 gene associated with retinitis pigmentosa in a Chinese patient. *Oncotarget*, *8*(51), 88345–88350. https://doi.org/10.18632/oncotarget.21728

Barber, A. J. (2003). A new view of diabetic retinopathy: a neurodegenerative disease of the eye. *Progress in Neuro-Psychopharmacology and Biological Psychiatry*, *27*(2), 283–290. https://doi.org/10.1016/S0278-5846(03)00023-X

Bareil, C., Hamel, C. P., Delague, V., Arnaud, B., Demaille, J., & Claustres, M. (2001). Segregation of a mutation in CNGB1 encoding the beta-subunit of the rod cGMP-gated channel in a family with autosomal recessive retinitis pigmentosa. *Human Genetics*, *108*(4), 328–334. https://doi.org/10.1007/s004390100496

Barnes, S. (1994). After transduction: Response shaping and control of transmission by ion channels of the photoreceptor inner segment. *Neuroscience*. https://doi.org/10.1016/0306-4522(94)90072-8

Batcha, A. H., Greferath, U., Jobling, A. I., Vessey, K. A., Ward, M. M., Nithianantharajah, J., … Fletcher, E. L. (2012). Retinal dysfunction, photoreceptor protein dysregulation and neuronal remodelling in the R6/1 mouse model of Huntington's disease. *Neurobiology of Disease*, *45*(3), 887–896. https://doi.org/10.1016/j.nbd.2011.12.004

Batra-Safferling, R., Abarca-Heidemann, K., Körschen, H. G., Tziatzios, C., Stoldt, M., Budyak, I., … Kaupp, U. B. (2006). Glutamic acid-rich proteins of rod photoreceptors are natively unfolded. *Journal of Biological Chemistry*, *281*(3), 1449–1460. https://doi.org/10.1074/jbc.M505012200

Baylor, D. A., Hodgkin, A. L., & Lamb, T. D. (1974). The electrical response of turtle cones to flashes and steps of light. *The Journal of Physiology*, *242*(3), 685–727. https://doi.org/10.1113/jphysiol.1974.sp010731

Baylor, D. A., Lamb, T. D., & Yau, K. W. (1979a). Responses of retinal rods to single photons. *The Journal of Physiology*, *288*, 613–634.

Baylor, D. A., Lamb, T. D., & Yau, K. W. (1979b). The membrane current of single rod outer segments. *The Journal of Physiology*, *288*(4), 589–611. https://doi.org/10.1016/0042-6989(79)90077-4

Baylor, D. A., Lamb, T. D., & Yau, K. W. (1979c). The membrane current of single rod outer segments. *The Journal of Physiology*, *288*, 589–611.

Baylor, D. A., Nunn, B. J., & Schnapf, J. L. (1984). The photocurrent, noise and spectral sensitivity of rods of the monkey macaca fascicularis. *J. Physiol.*, *357*, 575–607. https://doi.org/10.1113/jphysiol.1984.sp015518

Becirovic, E., Nakova, K., Hammelmann, V., Hennel, R., Biel, M., Michalakis, S., & Toland, A. E. (2010). The Retinitis Pigmentosa Mutation c.3444+1G.A in CNGB1 Results in Skipping of Exon 32. *PLoS ONE*, *5*(1). https://doi.org/10.1371/journal.pone.0008969

Becirovic, E., Nguyen, O. N. P., Paparizos, C., Butz, E. S., Stern-Schneider, G., Wolfrum, U., … Biel, M. (2014). Peripherin-2 couples rhodopsin to the CNG channel in outer segments of rod photoreceptors. *Human Molecular Genetics*, *23*(22), 5989–5997. https://doi.org/10.1093/hmg/ddu323

Bieganowski, L. (2005). [Galen from Pergamon (130-200)--views in ophthalmology. Part II--anatomic description of the eye]. *Klinika Oczna*, *107*(1–3), 173–176.

Blank, T., Goldmann, T., Koch, M., Amann, L., Schön, C., Bonin, M., … Michalakis, S. (2018). Early microglia activation precedes photoreceptor degeneration in a mouse model of CNGB1-linked retinitis pigmentosa. *Frontiers in Immunology*, *8*(JAN), 1930. https://doi.org/10.3389/fimmu.2017.01930

Bocquet, B., Marzouka, N. al D., Hebrard, M., Manes, G., Sénéchal, A., Meunier, I., & Hamel, C. P. (2013). Homozygosity mapping in autosomal recessive retinitis pigmentosa families detects novel mutations. *Molecular Vision*, *19*(July), 2487–2500.

Bokulich, N. A., Subramanian, S., Faith, J. J., Gevers, D., Gordon, J. I., Knight, R., … Caporaso, J. G. (2013). Quality-filtering vastly improves diversity estimates from Illumina amplicon sequencing. *Nature Methods*, *10*(1), 57–59. https://doi.org/10.1038/nmeth.2276

Boratyn, G. M., Schäffer, A. A., Agarwala, R., Altschul, S. F., Lipman, D. J., & Madden, T. L. (2012). Domain enhanced lookup time accelerated BLAST. *Biology Direct*, *7*(1), 12. https://doi.org/10.1186/1745-6150-7-12

Bosch, E., Horwitz, J., & Bok, D. (1993). Phagocytosis of outer segments by retinal pigment epithelium: phagosome-lysosome interaction. *Journal of Histochemistry & Cytochemistry*, *41*(2), 253–263. https://doi.org/10.1177/41.2.8419462

Breton, M. E., Schueller, A. W., Lamb, T. D., & Pugh, E. N. (1994). Analysis of ERG a-wave amplification and kinetics in terms of the G- protein cascade of phototransduction. *Investigative Ophthalmology and Visual Science*, *35*(1), 295–309.

Bridges, C. D., Hollyfield, J. G., Besharse, J. C., & Rayborn, M. E. (1976). Visual pigment loss after light-induced shedding of rod outer segments. *Experimental Eye Research*, *23*(6), 637–641.

Bringmann, A., Pannicke, T., Biedermann, B., Francke, M., Iandiev, I., Grosche, J., … Reichenbach, A. (2009). Role of retinal glial cells in neurotransmitter uptake and metabolism. *Neurochemistry International*, *54*(3–4), 143–160.

https://doi.org/10.1016/J.NEUINT.2008.10.014
Brunet, A. (2004). Stress-Dependent Regulation of FOXO Transcription Factors by the SIRT1 Deacetylase. *Science*, *303*(5666), 2011–2015. https://doi.org/10.1126/science.1094637
Burke, J. M., Kaczara, P., Skumatz, C. M. B., Zareba, M., Raciti, M. W., & Sarna, T. (2011). Dynamic analyses reveal cytoprotection by RPE melanosomes against non-photic stress. *Molecular Vision*, *17*(November), 2864–2877.
Bush, R. A., & Sieving, P. A. (1994). A proximal retinal component in the primate photopic ERG a-wave. *Investigative Ophthalmology and Visual Science*, *35*(2), 635–645.
Bush, R. A., & Sieving, P. A. (1996). Inner retinal contributions to the primate photopic fast flicker electroretinogram. *Journal of the Optical Society of America A*, *13*(3), 557. https://doi.org/10.1364/JOSAA.13.000557
Camacho, C., Coulouris, G., Avagyan, V., Ma, N., Papadopoulos, J., Bealer, K., & Madden, T. L. (2009). BLAST+: architecture and applications. *BMC Bioinformatics*, *10*(1), 421. https://doi.org/10.1186/1471-2105-10-421
Capra, J. A., Laskowski, R. A., Thornton, J. M., Singh, M., & Funkhouser, T. A. (2009). Predicting protein ligand binding sites by combining evolutionary sequence conservation and 3D structure. *PLoS Computational Biology*, *5*(12), e1000585. https://doi.org/10.1371/journal.pcbi.1000585
Carter-Dawson, L. D., & Lavail, M. M. (1979). Rods and cones in the mouse retina. I. Structural analysis using light and electron microscopy. *Journal of Comparative Neurology*. https://doi.org/10.1002/cne.901880204
Chakraborty, D., Conley, S. M., DeRamus, M. L., Pittler, S. J., & Naash, M. I. (2015). Varying the GARP2-to-RDS ratio leads to defects in rim formation and rod and cone function. *Investigative Ophthalmology and Visual Science*, *56*(13), 8187–8198. https://doi.org/10.1167/iovs.15-17785
Chakraborty, D., Conley, S. M., Pittler, S. J., & Naash, M. I. (2016). Role of RDS and rhodopsin in Cngb1-related retinal degeneration. *Investigative Ophthalmology and Visual Science*, *57*(3), 787–797. https://doi.org/10.1167/iovs.15-18516
Chaves, I., Van Der Horst, G. T. J., Schellevis, R., Nijman, R. M., Koerkamp, M. G., Holstege, F. C. P., … Hoekman, M. F. M. (2014). Insulin-FOXO3 signaling modulates circadian rhythms via regulation of clock transcription. *Current Biology*, *24*(11), 1248–1255. https://doi.org/10.1016/j.cub.2014.04.018
Chen, C. K., Burns, M. E., He, W., Wensel, T. G., Baylor, D. A., & Simon, M. I. (2000). Slowed recovery of rod photoresponse in mice lacking the GTPase accelerating protein RGS9-1. *Nature*, *403*(6769), 557–560. https://doi.org/10.1038/35000601
Chen, J., Woodruff, M. L., Wang, T., Concepcion, F. a, Tranchina, D., & Fain, G. L. (2010). Channel modulation and the mechanism of light adaptation in mouse rods. *The Journal of Neuroscience : The Official Journal of the Society for Neuroscience*, *30*(48), 16232–16240. https://doi.org/10.1523/JNEUROSCI.2868-10.2010
Chen, S. K., Badea, T. C., & Hattar, S. (2011). Photoentrainment and pupillary light reflex are mediated by distinct populations of ipRGCs. *Nature*, *476*(7358), 92–96. https://doi.org/10.1038/nature10206
Chen, T. Y., Illing, M., Molday, L. L., Hsu, Y. T., Yau, K. W., & Molday, R. S. (1994). Subunit 2 (or beta) of retinal rod cGMP-gated cation channel is a component of the

240-kDa channel-associated protein and mediates Ca(2+)-calmodulin modulation. *Proceedings of the National Academy of Sciences of the United States of America*, *91*(24), 11757–11761. https://doi.org/10.1073/pnas.91.24.11757

Chen, T. Y., Peng, Y. W., Dhallan, R. S., Ahamed, B., Reed, R. R., & Yau, K. W. (1993). A new subunit of the cyclic nucleotide-gated cation channel in retinal rods. *Nature*, *362*(6422), 764–767. https://doi.org/10.1038/362764a0

Chen, Y., Kerimo, A., Khan, S., & Wei, L.-N. (2002). Real-Time Analysis of Molecular Interaction of Retinoid Receptors and Receptor-Interacting Protein 140 (RIP140). *Molecular Endocrinology*, *16*(11), 2528–2537. https://doi.org/10.1210/me.2002-0124

Cheng, C. L., & Molday, R. S. (2013). Interaction of 4.1G and cGMP-gated channels in rod photoreceptor outer segments. *Journal of Cell Science*, *126*(Pt 24), 5725–5734. https://doi.org/10.1242/jcs.137679

Chuang, J. Z., Zhao, Y., & Sung, C. H. (2007). SARA-Regulated Vesicular Targeting Underlies Formation of the Light-Sensing Organelle in Mammalian Rods. *Cell*, *130*(3), 535–547. https://doi.org/10.1016/j.cell.2007.06.030

Clark, M. E., & Kraft, T. W. (2012). Measuring rodent electroretinograms to assess retinal function. *Methods in Molecular Biology (Clifton, N.J.)*, *884*, 265–276. https://doi.org/10.1007/978-1-61779-848-1_19

Cohen, D. N. (1971). Drusen of the optic disc and the development of field defects. *Archives of Ophthalmology (Chicago, Ill. : 1960)*, *85*(2), 224–226.

Colville, C. A., & Molday, R. S. (1996). Primary structure and expression of the human beta-subunit and related proteins of the rod photoreceptor cGMP-gated channel. *Journal of Biological Chemistry*, *271*(51), 32968–32974. https://doi.org/10.1074/jbc.271.51.32968

Cook, N. J., Hanke, W., & Kaupp, U. B. (1987). Identification, purification, and functional reconstitution of the cyclic GMP-dependent channel from rod photoreceptors. *Proceedings of the National Academy of Sciences of the United States of America*, *84*(2), 585–589. https://doi.org/10.1073/pnas.84.2.585

Copenhagen, D. R., & Jahr, C. E. (1989). Release of endogenous excitatory amino acids from turtle photoreceptors. *Nature*, *341*(6242), 536–539. https://doi.org/10.1038/341536a0

Cote, R. H. (2004). Characteristics of Photoreceptor PDE (PDE6): similarities and differences to PDE5. *International Journal of Impotence Research*, *16*, S28–S33. https://doi.org/10.1038/sj.ijir.3901212

Curcio, C. A., Sloan, K. R., Kalina, R. E., & Hendrickson, A. E. (1990). Human photoreceptor topography. *Journal of Comparative Neurology*, *292*(4), 497–523. https://doi.org/10.1002/cne.902920402

Dacey, D. M., & Petersen, M. R. (1992). Dendritic field size and morphology of midget and parasol ganglion cells of the human retina. *Proceedings of the National Academy of Sciences of the United States of America*, *89*(20), 9666–9670. https://doi.org/10.1073/pnas.89.20.9666

Dacheux, R. F., & Raviola, E. (1986). The Rod Pathway in the Rabbit Retina: A Depolarizing Bipolar and Amacrine Cell. *The Journal of Neurosci Ence*, *6*(2), 331–345.

Daiger, S., Rossiter, B., Greenberg, J., Christoffels, A., & Hide, W. (1998). Data services

and software for identifying genes and mutations causing retinal degeneration. *Investigative Ophthalmology and Visual Science*, *39*, S295.

Dawe, H. R., Farr, H., & Gull, K. (2007). Centriole/basal body morphogenesis and migration during ciliogenesis in animal cells. *Journal of Cell Science*, *120*(1), 7–15. https://doi.org/10.1242/jcs.03305

De Robertis, E., & Franchi, C. M. (1956). Electron microscope observations on the submicroscopic organization of the retinal rods. *The Journal of Biophysical and Biochemical Cytology*, *2*(3), 319–330. https://doi.org/10.1083/jcb.2.3.307

De Schweinitz, G. E. (1892). Hyaline bodies (Drusen) in the nerve-head. *Transactions of the American Ophthalmological Society*, *6*, 349–359.

DeRamus, M. L., & Kraft, T. W. (2018). Optimizing ERG Measures of Scotopic and Photopic Critical Flicker Frequency. *Ash J., Anderson R., LaVail M., Bowes Rickman C., Hollyfield J., Grimm C. (Eds) Retinal Degenerative Diseases. Advances in Experimental Medicine and Biology*, *1074*, 145–150. https://doi.org/10.1007/978-3-319-75402-4_18

Deramus, M. L., Stacks, D. A., Zhang, Y., Huisingh, C. E., McGwin, G., & Pittler, S. J. (2017). GARP2 accelerates retinal degeneration in rod cGMP-gated cation channel β-subunit knockout mice. *Scientific Reports*, *7*. https://doi.org/10.1038/srep42545

Deterre, P., Bigay, J., Robert, M., Pfister, C., K??hn, H., & Chabre, M. (1986). Activation of retinal rod cyclic GMP-phosphodiesterase by transducin: Characterization of the complex formed by phosphodiesterase inhibitor and transducin alpha-subunit. *Proteins: Structure, Function, and Bioinformatics*, *1*(2), 188–193. https://doi.org/10.1002/prot.340010210

Ding, J. D., Salinas, R. Y., & Arshavsky, V. Y. (2015). Discs of mammalian rod photoreceptors form through the membrane evagination mechanism. *Journal of Cell Biology*, *211*(3), 495–502. https://doi.org/10.1083/jcb.201508093

Ding, X. Q., Fitzgerald, J. B., Matveev, A. V., McClellan, M. E., & Elliott, M. H. (2008). Functional activity of photoreceptor cyclic nucleotide-gated channels is dependent on the integrity of cholesterol- and sphingolipid-enriched membrane domains. *Biochemistry*, *47*(12), 3677–3687. https://doi.org/10.1021/bi7019645

Dobin, A., Davis, C. A., Schlesinger, F., Drenkow, J., Zaleski, C., Jha, S., … Gingeras, T. R. (2013). STAR: Ultrafast universal RNA-seq aligner. *Bioinformatics*, *29*(1), 15–21. https://doi.org/10.1093/bioinformatics/bts635

Eberhardt, C., Amann, B., Feuchtinger, A., Hauck, S. M., & Deeg, C. A. (2011). Differential expression of inwardly rectifying K+ channels and aquaporins 4 and 5 in autoimmune uveitis indicates misbalance in M??ller glial cell-dependent ion and water homeostasis. *Glia*, *59*(5), 697–707. https://doi.org/10.1002/glia.21139

Ehinger, B., Ottersen, O. P., Storm-Mathisen, J., & Dowling, J. E. (1988). Bipolar cells in the turtle retina are strongly immunoreactive for glutamate. *Proceedings of the National Academy of Sciences of the United States of America*, *85*(21), 8321–8325. https://doi.org/10.1073/pnas.85.21.8321

Fain, G. L., & Dowling, J. E. (1973). Intracellular Recordings from Single Rods and Cones in the Mudpuppy Retina. *Science*, *180*(4091), 1178–1181. https://doi.org/10.1126/science.176.4040.1240

Feeney, L. (1973). The phagolysosomal system of the pigment epithelium. A key to retinal disease. *Investigative Ophthalmology*, *12*(9), 635–638.

Field, G. D., & Rieke, F. (2002). Nonlinear Signal Transfer from Mouse Rods to Bipolar Cells and Implications for Visual Sensitivity. *Neuron*, *34*(5), 773–785. https://doi.org/10.1016/S0896-6273(02)00700-6

Flaherty, K. M., Zozulya, S., Stryer, L., & McKay, D. B. (1993). Three-dimensional structure of recoverin, a calcium sensor in vision. *Cell*, *75*(4), 709–716. https://doi.org/10.1016/0092-8674(93)90491-8

Fradin, M., Colin, E., Hannouche-Bared, D., Audo, I., Sahel, J. A., Biskup, S., … Bonneau, D. (2016). Run of homozygosity analysis reveals a novel nonsense variant of the CNGB1 gene involved in retinitis pigmentosa 45. *Ophthalmic Genetics*, *37*(3), 357–359. https://doi.org/10.3109/13816810.2015.1087578

Fu, Q., Wang, F., Wang, H., Xu, F., Zaneveld, J. E., Ren, H., … Sui, R. (2013). Next-generation sequencing-based molecular diagnosis of a Chinese patient cohort with autosomal recessive retinitis pigmentosa. *Investigative Ophthalmology & Visual Science*, *54*(6), 4158–4166. https://doi.org/10.1167/iovs.13-11672

Fulton, A. B., & Rushton, W. A. H. (1978). Rod ERG of the mudpuppy: Effect of dim red backgrounds. *Vision Research*, *18*(7), 785–792. https://doi.org/10.1016/0042-6989(78)90118-9

Gass, J. D. (1972). Drusen and disciform macular detachment and degeneration. *Transactions of the American Ophthalmological Society*, *70*, 409–436.

Gibriel, A. A. Y., Tate, R. J., Yu, Y., Rawson-Lax, E., Hammer, H. M., Tettey, J. N. A., … Converse, C. A. (2013). The p.Arg86Gln change in GARP2 (glutamic acid-rich protein-2) is a common West African-related polymorphism. *Gene*, *515*(1), 155–158. https://doi.org/10.1016/j.gene.2012.11.005

Gilliam, J. C., Chang, J. T., Sandoval, I. M., Zhang, Y., Li, T., Pittler, S. J., … Wensel, T. G. (2012). Three-dimensional architecture of the rod sensory cilium and its disruption in retinal neurodegeneration. *Cell*, *151*(5), 1029–1041. https://doi.org/10.1016/j.cell.2012.10.038

Goldberg, A. F. X., Moritz, O. L., & Williams, D. S. (2016). Molecular basis for photoreceptor outer segment architecture. *Progress in Retinal and Eye Research*, *55*, 52–81. https://doi.org/10.1016/j.preteyeres.2016.05.003

Goldstein, L. S. B., & Yang, Z. (2000). Microtubule-Based Transport Systems in Neurons: The Roles of Kinesins and Dyneins. *Annual Review of Neuroscience*, *23*(1), 39–71. https://doi.org/10.1146/annurev.neuro.23.1.39

Gong, H., Amemiya, T., & Takaya, D. K. (2001). Retinal Changes in Magnesium-deficient Rats. https://doi.org/10.1006/exer.2000.0928

Goraczniak, R. M., Duda, T., Sitaramayya, a, & Sharma, R. K. (1994). Structural and functional characterization of the rod outer segment membrane guanylate cyclase. *The Biochemical Journal*, *302 (Pt 2*(2), 455–461. https://doi.org/10.1042/bj3020455

Gorczyca, W. A., Gray-Keller, M. P., Detwiler, P. B., & Palczewski, K. (1994). Purification and physiological evaluation of a guanylate cyclase activating protein from retinal rods. *Proceedings of the National Academy of Sciences of the United States of America*, *91*(9), 4014–4018. https://doi.org/10.1073/pnas.91.9.4014

Grisanti, S., Ishioka, M., Kosiewicz, M., & Jiang, L. Q. (1997). Immunity and Immune Privilege Elicited by Cultured Retinal Pigment Epithelial Cell Transplants. *Investigative Ophthalmology & Visual Science*, *38*(8), 1619–1626.

Grunwald, M. E., Yu, W. P., Yu, H. H., & Yau, K. W. (1998). Identification of a domain

on the β-subunit of the rod cGMP-gated cation channel that mediates inhibition by calcium-calmodulin. *Journal of Biological Chemistry*, *273*(15), 9148–9157. https://doi.org/10.1074/jbc.273.15.9148

Guo, L. W., & Ruoho, A. E. (2011). N-terminal half of the cGMP phosphodiesterase γ-subunit contributes to stabilization of the GTPase-accelerating protein complex. *Journal of Biological Chemistry*, *286*(17), 15260–15267. https://doi.org/10.1074/jbc.M110.210567

Gupta, V. K., Rajala, A., Daly, R. J., & Rajala, R. V. S. (2010). Growth factor receptor-bound protein 14: a new modulator of photoreceptor-specific cyclic-nucleotide-gated channel. *EMBO Reports*, *11*(11), 861–867. https://doi.org/10.1038/embor.2010.142

Gurevich, V. V, & Benovic, J. L. (1993). Visual arrestin interaction with rhodopsin. Sequential multisite binding ensures strict selectivity toward light-activated phosphorylated rhodopsin. *Journal of Biological Chemistry*, *268*, 11628–11638.

Gushchin, I. Y., Gordeliy, V. I., & Grudinin, S. (2012). A novel dimerization interface of cyclic nucleotide binding domain, which is disrupted in presence of cAMP: Implications for CNG channels gating. *Journal of Molecular Modeling*, *18*(9), 4053–4060. https://doi.org/10.1007/s00894-012-1404-5

Haber-Pohlmeier, S., Abarca-Heidemann, K., Körschen, H. G., Dhiman, H. K., Heberle, J., Schwalbe, H., … Pohlmeier, a. (2007). Binding of Ca2+ to glutamic acid-rich polypeptides from the rod outer segment. *Biophysical Journal*, *92*(9), 3207–3214. https://doi.org/10.1529/biophysj.106.094847

Habibi, I., Chebil, A., Falfoul, Y., Allaman-Pillet, N., Kort, F., Schorderet, D. F., & El Matri, L. (2016). Identifying mutations in Tunisian families with retinal dystrophy. *Scientific Reports*, *6*(November), 37455. https://doi.org/10.1038/srep37455

Hack, I., Peichl, L., & Brandstätter, J. H. (1999). An alternative pathway for rod signals in the rodent retina: rod photoreceptors, cone bipolar cells, and the localization of glutamate receptors. *Proceedings of the National Academy of Sciences of the United States of America*, *96*(24), 14130–14135. https://doi.org/10.1073/pnas.96.24.14130

Hagins, W. A., Penn, R. D., & Yoshikami, S. (1970). Dark Current and Photocurrent in Retinal Rods. *Biophysical Journal*, *10*(5), 380–412. https://doi.org/10.1016/S0006-3495(70)86308-1

Hassan-Karimi, H., Jafarzadehpur, E., Blouri, B., Hashemi, H., Sadeghi, a Z., & Mirzajani, A. (2012). Frequency Domain Electroretinography in Retinitis Pigmentosa versus Normal Eyes. *J Ophthalmic Vis Res*, *7*(1), 34–38.

Haverkamp, S., Wässle, H., Duebel, J., Kuner, T., Augustine, G. J., Feng, G., & Euler, T. (2005). The Primordial, Blue-Cone Color System of the Mouse Retina. *Journal of Neuroscience*, *25*(22), 5438–5445. https://doi.org/10.1523/JNEUROSCI.1117-05.2005

Hayreh, S. S. (1962). The Ophthalmic Artery: III. Branches. *The British Journal of Ophthalmology*, *46*(4), 212–247. https://doi.org/10.1136/bjo.46.4.212

He, Y., Ruiz, M., & Karpen, J. W. (2000). Constraining the subunit order of rod cyclic nucleotide-gated channels reveals a diagonal arrangement of like subunits. *Proceedings of the National Academy of Sciences of the United States of America*, *97*(2), 895–900.

Heidelberger, R., Heinemann, C., Neher, E., & Matthews, G. (1994). Calcium

dependence of the rate of exocytosis in a synaptic terminal. *Nature*, *371*(6497), 513–515. https://doi.org/10.1038/371513a0

Hendry, F., & Jones, T. G. (1980). Haems and chlorophylls: comparison of function and formation. *Journal of Medical Genetics*, *17*(1), 1–14. https://doi.org/10.1136/jmg.17.1.1

Henneguy, L. F. (1898). Les rapports des cils vibratiles avec les centrosomes'. *Archives d'anatomie Microscopique*.

Hennig, A. K., Peng, G.-H. H., & Chen, S. (2013). Transcription Coactivators p300 and CBP Are Necessary for Photoreceptor-Specific Chromatin Organization and Gene Expression. *PLoS ONE*, *8*(7), e69721. https://doi.org/10.1371/journal.pone.0069721

Heynen, H., Wachtmeister, L., & van Norren, D. (1985). Origin of the oscillatory potentials in the primate retina. *Vision Research*, *25*(10), 1365–1373. https://doi.org/10.1016/0042-6989(85)90214-7

Hood, D. C., & Birch, D. G. (1993). Light adaptation of human rod receptors: the leading edge of the human a-wave and models of rod receptor activity. *Vision Research*, *33*(12), 1605–1618. https://doi.org/10.1016/0042-6989(93)90027-T

Hughes, T. E. (1997). Are there ionotropic glutamate receptors on the rod bipolar cell of the mouse retina? *Visual Neuroscience*, *14*(1), 103–109. https://doi.org/10.1017/S0952523800008804

Hull, S., Attanasio, M., Arno, G., Carss, K., Robson, A. G., Thompson, D. A., … Webster, A. R. (2017). Clinical Characterization of CNGB1 -Related Autosomal Recessive Retinitis Pigmentosa. *JAMA Ophthalmology*, *135*(2), 137. https://doi.org/10.1001/jamaophthalmol.2016.5213

Huttl, S., Michalakis, S., Seeliger, M. W., Luo, D.-G., Acar, N., Geiger, H., … Biel, M. (2005). Impaired Channel Targeting and Retinal Degeneration in Mice Lacking the Cyclic Nucleotide-Gated Channel Subunit CNGB1. *Journal of Neuroscience*, *25*(1), 130–138. https://doi.org/10.1523/JNEUROSCI.3764-04.2005

Ishioka, N., Isobe, T., Okuyama, T., Numata, Y., & Wada, H. (1980). A New Acidic Protein in Porcine Brain. *Biochimica et Biophysica Acta*, *625*, 281–290.

Isobe, T., Ishioka, N., Kadoya, T., & Okuyama, T. (1982). Isolation of micro glutamic acid-rich protein from bovine brain. *Biochemical and Biophysical Research Communications*, *105*(3), 997–1004. https://doi.org/10.1016/0006-291X(82)91069-5

Isobe, T., & Okuyama, T. (1985). Brain micro glutamic acid-rich protein is the C-terminal endpiece of the neurofilament 68-kDa protein as determined by the primary sequence. *FEBS Letters*, *182*(2), 389–392. https://doi.org/10.1016/0014-5793(85)80339-2

Israeli, E. (2013). FOXO3A directs a protective autophagy program in hematopoietic stem cells. *Israel Medical Association Journal*, *15*(5), 225. https://doi.org/10.1038/nature11895

Johnson, N. F. (1975). Phagocytosis in the normal and ischaemic retinal pigment epithelium of the rabbit. *Experimental Eye Research*, *20*(2), 97–107.

Kalloniatis, M., & Luu, C. (2007, June 5). Temporal Resolution. Retrieved July 1, 2018, from http://www.ncbi.nlm.nih.gov/pubmed/21413411

Kaupp, U. B., Niidome, T., Tanabe, T., Terada, S., Bönigk, W., Stühmer, W., … Hirose, T. (1989). Primary structure and functional expression from complementary DNA of the rod photoreceptor cyclic GMP-gated channel. *Nature*, *342*(6251), 762–766.

https://doi.org/10.1038/342762a0

Keeling, E., Lotery, A. J., Tumbarello, D. A., & Ratnayaka, J. A. (2018). Impaired Cargo Clearance in the Retinal Pigment Epithelium (RPE) Underlies Irreversible Blinding Diseases. *Cells*, *7*(2). https://doi.org/10.3390/cells7020016

Kevany, B. M., Palczewski, K., & Brian M. Kevany and Krzysztof Palczewsk. (2010). Phagocytosis of Retinal Rod and Cone Photoreceptors. *Physiology*, *25*(1), 8–15. https://doi.org/10.1152/physiol.00038.2009

Kiser, P. D., Golczak, M., Maeda, A., & Palczewski, K. (2013). Key enzymes of the retinoid (visual) cycle in vertebrate retina. *Biochem Biophys Acta*, *1821*(1), 137–151. https://doi.org/10.1016/j.bbalip.2011.03.005.Key

Kiser, P. D., Golczak, M., & Palczewski, K. (2014). Chemistry of the retinoid (visual) cycle. *Chemical Reviews*, *114*(1), 194–232. https://doi.org/10.1021/cr400107q

Kizhatil, K., Baker, S. A., Arshavsky, V. Y., & Bennett, V. (2009). Cyclic Nucleotide-Gated Channels Require Ankryin-G for Transport to the Sensory Cilium of Rod Photoreceptors. *Science*, *323*(5921), 1614–1617. https://doi.org/10.1126/science.1169789

Kizhatil, K., Sandhu, N. K., Peachey, N. S., & Bennett, V. (2008). Ankyrin-B is required for coordinated expression of beta-2-spectrin, the Na/K-ATPase and the Na/Ca exchanger in the inner segment of rod photoreceptors. https://doi.org/10.1016/j.exer.2008.09.022

Klenchin, V. A., Calvert, P. D., & Bownds, M. D. (1995). Inhibition of rhodopsin kinase by recoverin. Further evidence for a negative feedback system in phototransduction. *Journal of Biological Chemistry*, *270*(27), 16147–16152. https://doi.org/10.1074/jbc.270.27.16147

Koch, K.-W., Cook, N. J., & Kaupp, U. B. (1987). The cGMP-dependent Channel of Vertebrate Rod Photoreceptors Exists in Two Forms of Different cGMP Sensitivity and Pharmacological Behavior. *THE JOURNAL OF BIOLOGICAL CHEMISTRY* , *262*(30), 14415–14421.

Koch, S., Sothilingam, V., Garrido, M. G., Tanimoto, N., Becirovic, E., Koch, F., … Mu, R. (2012). Gene therapy restores vision and delays degeneration in the CNGB1 -/- mouse model of retinitis pigmentosa. *Human Molecular Genetics*, *21*(20), 4486–4496. https://doi.org/10.1093/hmg/dds290

Kondo, H., Qin, M., Mizota, A., Kondo, M., Hayashi, H., Hayashi, K., … Hayashi, K. (2004). A homozygosity-based search for mutations in patients with autosomal recessive retinitis pigmentosa, using microsatellite markers. *Investigative Ophthalmology & Visual Science*, *45*(12), 4433–4439. https://doi.org/10.1167/iovs.04-0544

Körschen, H. G., Beyermann, M., Müller, F., Heck, M., Vantler, M., Koch, K.-W. W., … Kaupp, U. B. (1999). Interaction of glutamic-acid-rich proteins with the cGMP signalling pathway in rod photoreceptors. *Nature*, *400*(6746), 761–766. https://doi.org/10.1038/23468

Körschen, H. G., Illing, M., Seifer, R., Sesti, F., Williams, A., Gotzes, S., … Molday, R. S. (1995). A 240 kDa protein represents the complete β subunit of the cyclic nucleotide-gated channel from rod photoreceptor. *Neuron*, *15*(3), 627–636. https://doi.org/10.1016/0896-6273(95)90151-5

Krajewski, J. L., Luetje, C. W., & Kramer, R. H. (2003). Tyrosine phosphorylation of rod

cyclic nucleotide-gated channels switches off Ca2+/calmodulin inhibition. *The Journal of Neuroscience : The Official Journal of the Society for Neuroscience*, *23*(31), 10100–10106.

Krämer, A., Green, J., Pollard, J., Tugendreich, S., & Tugendreich, S. (2014). Causal analysis approaches in Ingenuity Pathway Analysis. *Bioinformatics (Oxford, England)*, *30*(4), 523–530. https://doi.org/10.1093/bioinformatics/btt703

Križaj, D. (2012). Calcium stores in vertebrate photoreceptors. *Advances in Experimental Medicine and Biology*, *740*, 873–889. https://doi.org/10.1007/978-94-007-2888-2_39

Kulie, T., Groff, A., Redmer, J., Hounshell, J., & Schrager, S. (2009). Vitamin D: An Evidence-Based Review. *The Journal of the American Board of Family Medicine*, *22*(6), 698–706. https://doi.org/10.3122/jabfm.2009.06.090037

Kumar, A., Pandey, R. K., Miller, L. J., Singh, P. K., & Kanwar, M. (2013). Muller glia in retinal innate immunity: a perspective on their roles in endophthalmitis. *Critical Reviews in Immunology*, *33*(2), 119–135.

Kupersmith, M. J., Shakin, E., Siegel, I. M., & Lieberman, A. (1982). Visual system abnormalities in patients with Parkinson's disease. *Archives of Neurology*, *39*(5), 284–286.

Lamb, T. D., & Pugh, E. N. (1992). A quantitative account of the activation steps involved in phototransduction in amphibian photoreceptors. *The Journal of Physiology*, *449*, 719–758. https://doi.org/10.1113/jphysiol.1992.sp019111

Leng, N., Dawson, J. A., Thomson, J. A., Ruotti, V., Rissman, A. I., Smits, B. M. G., … Kendziorski, C. (2013). EBSeq: An empirical Bayes hierarchical model for inference in RNA-seq experiments. *Bioinformatics*, *29*(8), 1035–1043. https://doi.org/10.1093/bioinformatics/btt087

Leng, N., Li, Y., McIntosh, B. E., Nguyen, B. K., Duffin, B., Tian, S., … Kendziorski, C. (2015). EBSeq-HMM: A Bayesian approach for identifying gene-expression changes in ordered RNA-seq experiments. *Bioinformatics*, *31*(16), 2614–2622. https://doi.org/10.1093/bioinformatics/btv193

Lenhossek, M. (1898). Uber flimmerzellen. *Verhandl. Der Anat. Gesel*.

Li, B., & Dewey, C. N. (2011). RSEM: accurate transcript quantification from RNA-Seq data with or without a reference genome. *BMC Bioinformatics*, *12*(1), 323. https://doi.org/10.1186/1471-2105-12-323

Li, S., Mitchell, J., Briggs, D. J., Young, J. K., Long, S. S., Fuerst, P. G., & Barnes, S. (2016). Morphological Diversity of the Rod Spherule: A Study of Serially Reconstructed Electron Micrographs. https://doi.org/10.1371/journal.pone.0150024

Lieberman, I. (1956). Enzymatic Amination of Uridine Triphosphate To Cytidine Triphosphate*. *The Journal of Biological Chemistry*, *222*, 765–775.

Lingao, M. D., Ganesh, A., Karthikeyan, A. S., Zuhaibi, S. Al, Al-Hosni, A., Khayat, A. Al, … Levin, A. V. (2016). Macular cystoid spaces in patients with retinal dystrophy. *Ophthalmic Genet.*, *37*(4), 1–7. https://doi.org/10.3109/13816810.2015.1101775

Lioubinski, O., Alonso, M. T., Alvarez, Y., Vendrell, V., Garrosa, M., Murphy, P., & Schimmang, T. (2006). FGF signalling controls expression of vomeronasal receptors during embryogenesis. *Mechanisms of Development*, *123*(1), 17–23. https://doi.org/10.1016/j.mod.2005.10.004

Lisman, J., & Fain, G. (1995). Support for the equivalent light hypothesis for RP. *Nature Medicine*, *1*(12), 1254–1255.

Liu, G., Li, H., Liu, X., Xu, D., & Wang, F. (2016). Structural analysis of retinal photoreceptor ellipsoid zone and postreceptor retinal layer associated with visual acuity in patients with retinitis pigmentosa by ganglion cell analysis combined with OCT imaging. *Medicine (United States)*, *95*(52). https://doi.org/10.1097/MD.0000000000005785

Lo, W. K., & Bernstein, M. H. (1981). Daily patterns of the retinal pigment epithelium. Microperoxisomes and phagosomes. *Experimental Eye Research*, *32*(1), 1–10.

Lyubarsky, A. L., Daniele, L. L., & Pugh, E. N. (2004). From candelas to photoisomerizations in the mouse eye by rhodopsin bleaching in situ and the light-rearing dependence of the major components of the mouse ERG. *Vision Research*, *44*(28 SPEC.ISS.), 3235–3251. https://doi.org/10.1016/j.visres.2004.09.019

Macdonald, I. M., Naash, M. I., & Ayyagari, R. (2011). Retinal degenerations: genetics, mechanisms, and therapies. *Journal of Ophthalmology*, *2011*, 764873. https://doi.org/10.1155/2011/764873

Mactier, H., Bradnam, M. S., & Hamilton, R. (2013). Dark-adapted oscillatory potentials in preterm infants with and without retinopathy of prematurity. *Documenta Ophthalmologica*, *127*(1), 33–40. https://doi.org/10.1007/s10633-013-9373-2

Madden, T. L., Tatusov, R. L., & Zhang, J. (1996). Applications of network BLAST server. *Methods in Enzymology*, *266*, 131–141.

Maerker, T., van Wijk, E., Overlack, N., Kersten, F. F. J., Mcgee, J., Goldmann, T., … Wolfrum, U. (2008). A novel Usher protein network at the periciliary reloading point between molecular transport machineries in vertebrate photoreceptor cells. *Human Molecular Genetics*, *17*(1), 71–86. https://doi.org/10.1093/hmg/ddm285

Maranhao, B., Biswas, P., Gottsch, A. D. H., Navani, M., Naeem, M. A., Suk, J., … Ayyagari, R. (2015). Investigating the molecular basis of retinal degeneration in a familial cohort of pakistani decent by exome sequencing. *PLoS ONE*, *10*(9), e0136561. https://doi.org/10.1371/journal.pone.0136561

Marc, R. E., & Lam, D. M. (1981). Uptake of aspartic and glutamic acid by photoreceptors in goldfish retina. *Proc Natl Acad Sci U S A*, *78*(11), 7185–7189. https://doi.org/10.1073/pnas.78.11.7185

Maria, M., Ajmal, M., Azam, M., Waheed, N. K., Siddiqui, S. N., Mustafa, B., … Cremers, F. P. M. (2015). Homozygosity mapping and targeted sanger sequencing reveal genetic defects underlying inherited retinal disease in families from pakistan. *PLoS ONE*, *10*(3), e0119806. https://doi.org/10.1371/journal.pone.0119806

Marmor, M. F., Hock, P., Schechter, G., Pfefferbaum, A., Berger, P. A., & Maurice, R. (1988). Oscillatory potentials as a marker for dopaminergic disease. *Documenta Ophthalmologica. Advances in Ophthalmology*, *69*(3), 255–261. https://doi.org/10.1007/BF00154406

Marshall, J. (1971). The phagocytic nature of the retinal pigment epithelium. *Experimental Eye Research*, *11*(1), 143.

Massey, S. C. (1990). Cell Types Using Glutamate as a Neurotransmitter in the Vertebrate Retina. *Progress in Retinal Research*, *9*, 399–425.

Massof, R. W., Wu, L., Finkelstein, D., Perry, C., Starr, S. J., & Johnson, M. A. (1984). Properties of electroretinographic intensity-response functions in retinitis

pigmentosa. *Documenta Ophthalmologica*, *57*(3), 279–296. https://doi.org/10.1007/BF00143087

Matte, A., Tari, L. W., & Delbaere, L. T. J. (1998). How do kinases transfer phosphoryl groups? *Structure*, *6*(4), 413–419. https://doi.org/10.1016/S0969-2126(98)00043-4

Matthews, G. (1987). Single-channel recordings demonstrate that cGMP opens the light-sensitive ion channel of the rod photoreceptor. *Proceedings of the National Academy of Sciences of the United States of America*, *84*(1), 299–302. https://doi.org/10.1073/PNAS.84.1.299

McCabe, S. L., Pelosi, D. M., Tetreault, M., Miri, A., Nguitragool, W., Kovithvathanaphong, P., … Zimmerman, A. L. (2004). All-trans-retinal is a closed-state inhibitor of rod cyclic nucleotide-gated ion channels. *The Journal of General Physiology*, *123*(5), 521–531. https://doi.org/10.1085/jgp.200409011

Mcculloch, D. L., Marmor, M. F., Brigell, M. G., & Bach, M. (2015). ISCEV STANDARDS ISCEV Standard for full-field clinical electroretinography (2015 update). *Documenta Ophthalmologica*, *130*(1), 1–12. https://doi.org/10.1007/s10633-014-9473-7

Meighan, P. C., Meighan, S. E., Rich, E. D., Brown, R. L., & Varnum, M. D. (2012). Matrix metalloproteinase-9 and -2 enhance the ligand sensitivity of photoreceptor cyclic nucleotide-gated channels. *Channels*, *6*(3), 181–196. https://doi.org/10.4161/chan.20904

Meighan, S. E., Meighan, P. C., Rich, E. D., Brown, R. L., & Varnum, M. D. (2013). Cyclic nucleotide-gated channel subunit glycosylation regulates matrix metalloproteinase-dependent changes in channel gating. *Biochemistry*, *52*(46), 8352–8362. https://doi.org/10.1021/bi400824x

Melo Hanchuk, T. D., Papa, P. F., La Guardia, P. G., Vercesi, A. E., & Kobarg, J. (2015). Nek5 interacts with mitochondrial proteins and interferes negatively in mitochondrial mediated cell death and respiration. *Cellular Signalling*, *27*(6), 1168–1177. https://doi.org/10.1016/J.CELLSIG.2015.02.021

Michalakis, S., Koch, S., Sothilingam, V., Garrido, M. G., Tanimoto, N., Schulze, E., … Biel, M. (2014). Gene therapy restores vision and delays degeneration in the CNGB1(-/-) mouse model of retinitis pigmentosa. *Advances in Experimental Medicine and Biology*, *801*(20), 733–739. https://doi.org/10.1007/978-1-4614-3209-8_92

Michalakis, S., Reisert, J., Geiger, H., Wetzel, C., Zong, X., Bradley, J., … Biel, M. (2006). Loss of CNGB1 protein leads to olfactory dysfunction and subciliary cyclic nucleotide-gated channel trapping. *Journal of Biological Chemistry*, *281*(46), 35156–35166. https://doi.org/10.1074/jbc.M606409200

Michalakis, S., Schäferhoff, K., Spiwoks-Becker, I., Zabouri, N., Koch, S., Koch, F., … Haverkamp, S. (2013). Characterization of neurite outgrowth and ectopic synaptogenesis in response to photoreceptor dysfunction. *Cellular and Molecular Life Sciences*, *70*(10), 1831–1847. https://doi.org/10.1007/s00018-012-1230-z

Molday, L. L., Cook, N. J., Kaupp, U. B., & Molday, R. S. (1990). The cGMP-gated Cation Channel of Bovine Rod Photoreceptor Cells Is Associated with a 240-kDa Protein Exhibiting Immunochemical Cross-reactivity with Spectrin. *The Journal of Biological Chemistry*, *265*(30), 18690–18695.

Molokanova, E., Krajewski, J. L., Satpaev, D., Luetje, C. W., & Kramer, R. H. (2003).

Subunit contributions to phosphorylation-dependent modulation of bovine rod cyclic nucleotide-gated channels. *The Journal of Physiology*, *552*(Pt 2), 345–356. https://doi.org/10.1113/jphysiol.2003.047167

Moore, D. J., Onoufriadis, A., Shoemark, A., Simpson, M. A., Zur Lage, P. I., De Castro, S. C., … Mitchison, H. M. (2013). Mutations in ZMYND10, a gene essential for proper axonemal assembly of inner and outer dynein arms in humans and flies, cause primary ciliary dyskinesia. *American Journal of Human Genetics*, *93*(2), 346–356. https://doi.org/10.1016/j.ajhg.2013.07.009

Morgans, C. W. (2000). Neurotransmitter release at ribbon synapses in the retina. *Immunology and Cell Biology*, *78*(4), 442–446. https://doi.org/10.1046/j.1440-1711.2000.00923.x

Morgans, C. W., El Far, O., Berntson, a, Wässle, H., & Taylor, W. R. (1998). Calcium extrusion from mammalian photoreceptor terminals. *The Journal of Neuroscience : The Official Journal of the Society for Neuroscience*, *18*(7), 2467–2474. https://doi.org/10.1523/JNEUROSCI.18-07-02467.1998

Morgulis, A., Coulouris, G., Raytselis, Y., Madden, T. L., Agarwala, R., & Schäffer, A. A. (2008). Database indexing for production MegaBLAST searches. *Bioinformatics*, *24*(16), 1757–1764. https://doi.org/10.1093/bioinformatics/btn322

Morris, A. C., Forbes-Osborne, M. A., Pillai, L. S., & Fadool, J. M. (2011). Microarray Analysis of XOPS-mCFP Zebrafish Retina Identifies Genes Associated with Rod Photoreceptor Degeneration and Regeneration. *Investigative Opthalmology & Visual Science*, *52*(5), 2255. https://doi.org/10.1167/iovs.10-6022

Mou, H., & Cote, R. H. (2001). The Catalytic and GAF Domains of the Rod cGMP Phosphodiesterase (PDE6) Heterodimer Are Regulated by Distinct Regions of Its Inhibitory γ Subunit. *Journal of Biological Chemistry*, *276*(29), 27527–27534. https://doi.org/10.1074/jbc.M103316200

Nair, K. S., Hanson, S. M., Mendez, A., Gurevich, E. V., Kennedy, M. J., Shestopalov, V. I., … Slepak, V. Z. (2005). Light-dependent redistribution of arrestin in vertebrate rods is an energy-independent process governed by protein-protein interactions. *Neuron*, *46*(4), 555–567. https://doi.org/10.1016/j.neuron.2005.03.023

Nawy, S., & Jahr, C. E. (1991). cGMP-gated conductance in retinal bipolar cells is suppressed by the photoreceptor transmitter. *Neuron*, *7*(4), 677–683. https://doi.org/10.1016/0896-6273(91)90380-I

Nemet, I., Tian, G., & Imanishi, Y. (2014). Organization of cGMP sensing structures on the rod photoreceptor outer segment plasma membrane. *Channels (Austin, Tex.)*, *8*(6), 528–535. https://doi.org/10.4161/19336950.2014.973776

Nigg, E. A., & Stearns, T. (2011). The centrosome cycle: Centriole biogenesis, duplication and inherent asymmetries. *Nature Cell Biology*, *13*(10), 1154–1160. https://doi.org/10.1038/ncb2345

Nishiguchi, K. M., Tearle, R. G., Liu, Y. P., Oh, E. C., Miyake, N., Benaglio, P., … Rivolta, C. (2013). Whole genome sequencing in patients with retinitis pigmentosa reveals pathogenic DNA structural changes and NEK2 as a new disease gene. *Proceedings of the National Academy of Sciences of the United States of America*, *110*(40), 16139–16144. https://doi.org/10.1073/pnas.1308243110

Noel, J. P., Hamm, H. E., & Sigler, P. B. (1993). The 2.2 A crystal structure of transducin-alpha complexed with GTP gamma S. *Nature*, *366*(6456), 654–663.

https://doi.org/10.1038/366654a0
Nomata, Y., Watanabe, T., & Wada, H. (1983). Highly Acidic Proteins from Human Brain: Purification and Properties of Glu-50 Protein1. *J. Biochem*, *93*, 825–831.
Normann, R. A., & Perlman, I. (1979). The effects of background illumination on the photoresponses of red and green cones. *The Journal of Physiology*, *286*(1), 491–507. https://doi.org/10.1113/jphysiol.1979.sp012633
Oakley, B. (1977). Potassium and the photoreceptor-dependent pigment epithelial hyperpolarization. *The Journal of General Physiology*, *70*(4), 405–425.
Okawa, H., Sampath, A. P., Laughlin, S. B., & Fain, G. L. (2008). ATP Consumption by Mammalian Rod Photoreceptors in Darkness and in Light. *Current Biology*, *18*(24), 1917–1921. https://doi.org/10.1016/j.cub.2008.10.029
Palczewski, K., Kumasaka, T., Hori, T., Behnke, C. A., Motoshima, H., Fox, B. A., … Miyano, M. (2000). Crystal structure of rhodopsin: A G protein-coupled receptor. *Science (New York, N.Y.)*, *289*(5480), 739–745.
Paquet-Durand, F., Beck, S., Michalakis, S., Goldmann, T., Huber, G., Mühlfriedel, R., … Seeliger, M. W. (2011). A key role for cyclic nucleotide gated (CNG) channels in cGMP-related retinitis pigmentosa. *Human Molecular Genetics*, *20*(5), 941–947. https://doi.org/10.1093/hmg/ddq539
Pazour, G. J., & Witman, G. B. (2003). The vertebrate primary cilium is a sensory organelle. *Current Opinion in Cell Biology*, *15*(1), 105–110. https://doi.org/10.1016/S0955-0674(02)00012-1
Peachey, N. S., Alexander, K. R., & Fishman, G. A. (1989). The luminance-response function of the dark-adapted human electroretinogram. *Vision Research*, *29*(3), 263–270. https://doi.org/10.1016/0042-6989(89)90075-8
Pearring, J. N., Salinas, R. Y., Baker, S. A., & Arshavsky, V. Y. (2013). Protein sorting, targeting and trafficking in photoreceptor cells. *Progress in Retinal and Eye Research*, *36*, 24–51. https://doi.org/10.1016/j.preteyeres.2013.03.002
Penn, R. D., & Hagins, W. A. (1969). Signal transmission along retinal rods and the origin of the electroretinographic a-wave. *Nature*, *223*(5202), 201–204. https://doi.org/10.1038/223201a0
Pentia, D. C., Hosier, S., & Cote, R. H. (2006). The glutamic acid-rich protein-2 (GARP2) is a high affinity rod photoreceptor phosphodiesterase (PDE6)-binding protein that modulates its catalytic properties. *Journal of Biological Chemistry*, *281*(9), 5500–5505. https://doi.org/10.1074/jbc.M507488200
Perlman, I. (1983). Relationship between the amplitudes of the b wave and the a wave as a useful index for evaluating the electroretinogram. *British Journal of Ophthalmology*, *67*, 443–448.
Peters, K. R., Palade, G. E., Schneider, B. G., & Papermaster, D. S. (1983). Fine structure of a periciliary ridge complex of frog retinal rod cells revealed by ultrahigh resolution scanning electron microscopy. *Journal of Cell Biology*, *96*(1), 265–276. https://doi.org/10.1083/jcb.96.1.265
Petersen-Jones, S. M., Occelli, L. M., Winkler, P. A., Lee, W., Sparrow, J. R., Tsukikawa, M., … Tsang, S. H. (2018). Patients and animal models of CNGβ1-deficient retinitis pigmentosa support gene augmentation approach. *Journal of Clinical Investigation*, *128*(1), 190–206. https://doi.org/10.1172/JCI95161
Pettersen, E. F., Goddard, T. D., Huang, C. C., Couch, G. S., Greenblatt, D. M., Meng, E.

C., & Ferrin, T. E. (2004). UCSF Chimera - A visualization system for exploratory research and analysis. *Journal of Computational Chemistry*, *25*(13), 1605–1612. https://doi.org/10.1002/jcc.20084

Pirooznia, M., Nagarajan, V., & Deng, Y. (2007). GeneVenn - A web application for comparing gene lists using Venn diagrams. *Bioinformation*, *1*(10), 420–422. https://doi.org/10.6026/97320630001420

Poetsch, A., Molday, L. L., & Molday, R. S. (2001). The cGMP-gated Channel and Related Glutamic Acid-rich Proteins Interact with Peripherin-2 at the Rim Region of Rod Photoreceptor Disc Membranes. *Journal of Biological Chemistry*, *276*(51), 48009–48016. https://doi.org/10.1074/jbc.M108941200

Prosser, S. L., & Fry, A. M. (2015). Nek5: a new regulator of centrosome integrity. *Oncotarget*, *6*(28), 24594–24595. https://doi.org/10.18632/oncotarget.5139

Pugh, E. N., & Lamb, T. D. (1993). Amplification and kinetics of the activation steps in phototransduction. *BBA - Bioenergetics*, *1141*(2–3), 111–149. https://doi.org/10.1016/0005-2728(93)90038-H

Puller, C., Ivanova, E., Euler, T., Haverkamp, S., & Schubert, T. (2013). OFF bipolar cells express distinct types of dendritic glutamate receptors in the mouse retina. *Neuroscience*, *243*, 136–148. https://doi.org/10.1016/J.NEUROSCIENCE.2013.03.054

Rao, R., Buchsbaum, G., & Sterling, P. (1994). Rate of quantal transmitter release at the mammalian rod synapse. *Biophysical Journal*, *67*(1), 57–63. https://doi.org/10.1016/S0006-3495(94)80454-0

Raviola, E., & Dacheux, R. F. (1987). Excitatory dyad synapse in rabbit retina. *Proceedings of the National Academy of Sciences of the United States of America*, *84*(20), 7324–7328. https://doi.org/10.1073/pnas.84.20.7324

Raviola, E., & Gilula, N. B. (1973). Gap Junctions Between Photoreceptor Cells in the Vertebrate Retina. *Proceedings of the National Academy of Sciences*, *70*(6), 1677–1681.

Reiländer, H., Achilles, a, Friedel, U., Maul, G., Lottspeich, F., & Cook, N. J. (1992). Primary structure and functional expression of the Na/Ca,K-exchanger from bovine rod photoreceptors. *The EMBO Journal*, *11*(5), 1689–1695. https://doi.org/10.1002/J.1460-2075.1992.TB05219.X

Reiter, J. F., Blacque, O. E., & Leroux, M. R. (2012). The base of the cilium: Roles for transition fibres and the transition zone in ciliary formation, maintenance and compartmentalization. *EMBO Reports*, *13*(7), 608–618. https://doi.org/10.1038/embor.2012.73

Ritter, L. M., Khattree, N., Tam, B., Moritz, O. L., Schmitz, F., & Goldberg, A. F. X. (2011). In Situ Visualization of Protein Interactions in Sensory Neurons: Glutamic Acid-Rich Proteins (GARPs) Play Differential Roles for Photoreceptor Outer Segment Scaffolding. *Journal of Neuroscience*, *31*(31), 11231–11243. https://doi.org/10.1523/JNEUROSCI.2875-11.2011

Rosenbaum, J. L., & Witman, G. B. (2002). Intraflagellar transport. *Nature Reviews. Molecular Cell Biology*, *3*(11), 813–825. https://doi.org/10.1038/nrm952

Rosenbaum, T., Islas, L. D., Carlson, A. E., & Gordon, S. E. (2003). Dequalinium: a novel high-affinity blocker of CNGA1 channels. *The Journal of General Physiology*, *121*(1), 37–47. https://doi.org/10.1085/jgp.20028716

Roy, A., Kucukural, A., & Zhang, Y. (2010). I-TASSER: A unified platform for automated protein structure and function prediction. *Nature Protocols*, *5*(4), 725–738. https://doi.org/10.1038/nprot.2010.5

Sanders, T. E., Gay, A. J., & Newman, M. (1971). Hemorrhagic complications of drusen of the optic disk. *American Journal of Ophthalmology*, *71*(1 Pt 2), 204–217.

Saqib, M. A. N., Nikopoulos, K., Ullah, E., Sher Khan, F., Iqbal, J., Bibi, R., … Rivolta, C. (2015). Homozygosity mapping reveals novel and known mutations in Pakistani families with inherited retinal dystrophies. *Scientific Reports*, *5*(November 2014), 9965. https://doi.org/10.1038/srep09965

Sarfare, S., McKeown, A. S., Messinger, J., Rubin, G., Wei, H., Kraft, T. W., & Pittler, S. J. (2014). Overexpression of rod photoreceptor glutamic acid rich protein 2 (GARP2) increases gain and slows recovery in mouse retina. *Cell Communication and Signaling*, *12*(1), 67. https://doi.org/10.1186/s12964-014-0067-5

Sarthy, P. V., & Lam, D. M. K. (1978). Biochemical studies of isolated glial (muller) cells from the turtle retina. *Journal of Cell Biology*, *78*(3), 675–684. https://doi.org/10.1083/jcb.78.3.675

Saszik, S. M., Robson, J. G., & Frishman, L. J. (2002). The Scotopic Threshold Response of the Dark-Adapted Electroretinogram of the Mouse. *The Journal of Physiology*, *543*(3), 899–916. https://doi.org/10.1113/jphysiol.2002.019703

Schmidt, M., Giessl, A., Laufs, T., Hankeln, T., Wolfrum, U., & Burmester, T. (2003). How does the eye breathe? Evidence for neuroglobin-mediated oxygen supply in the mammalian retina. *The Journal of Biological Chemistry*, *278*(3), 1932–1935. https://doi.org/10.1074/jbc.M209909200

Schmucker, C., Seeliger, M., Humphries, P., Biel, M., & Schaeffel, F. (2005). Grating acuity at different luminances in wild-type mice and in mice lacking rod or cone function. *Investigative Ophthalmology and Visual Science*, *46*(1), 398–407. https://doi.org/10.1167/iovs.04-0959

Schneider, C. A., Rasband, W. S., & Eliceiri, K. W. (2012). NIH Image to ImageJ : 25 years of image HISTORICAL commentary NIH Image to ImageJ : 25 years of image analysis. *Nature Methods*, *9*(7), 671–675. https://doi.org/10.1038/nmeth.2089

Schön, C., Asteriti, S., Koch, S., Sothilingam, V., Garrido, M. G., Tanimoto, N., … Michalakis, S. (2015, March 15). Loss of HCN1 enhances disease progression in mouse models of CNG channel-linked retinitis pigmentosa and achromatopsia. https://doi.org/10.1093/hmg/ddv639

Schön, C., Paquet-Durand, F., & Michalakis, S. (2016). Cav1.4 L-type calcium channels contribute to calpain activation in degenerating photoreceptors of rd1 mice. *PLoS ONE*, *11*(6), e0156974. https://doi.org/10.1371/journal.pone.0156974

Schorderet, D. F., Bernasconi, M., Tiab, L., Favez, T., & Escher, P. (2014). IROme, a new high-throughput molecular tool for the diagnosis of inherited retinal dystrophies???A price comparison with sanger sequencing. *Advances in Experimental Medicine and Biology*, *801*, 171–176. https://doi.org/10.1007/978-1-4614-3209-8_22

Shammat, I. M., & Gordon, S. E. (1999). Stoichiometry and Arrangement of Subunits in Rod Cyclic Nucleotide–Gated Channels. *Neuron*, *23*(4), 809–819. https://doi.org/10.1016/S0896-6273(01)80038-6

Shiells, R. A., & Falk, G. (1990). Glutamate receptors of rod bipolar cells are linked to a

cyclic GMP cascade via a G-protein. *Proceedings of the Royal Society B: Biological Sciences*, *242*(1304), 91–94. https://doi.org/10.1098/rspb.1990.0109

Shlaer, S., Smith, E., & Chase, A. (1941). Visual Acuity and Illumination in Different Spectral Regions. *Journal of General Physiology*, *29*(5), 277–297.

Shuart, N. G., Haitin, Y., Camp, S. S., Black, K. D., & Zagotta, W. N. (2011). Molecular mechanism for 3:1 subunit stoichiometry of rod cyclic nucleotide-gated ion channels. *Nature Communications*, *2*(May), 457. https://doi.org/10.1038/ncomms1466

Simpson, D. A., Clark, G. R., Alexander, S., Silvestri, G., & Willoughby, C. E. (2011). Molecular diagnosis for heterogeneous genetic diseases with targeted high-throughput DNA sequencing applied to retinitis pigmentosa. *J Med Genet*, *48*(3), 145–151. https://doi.org/10.1136/jmg.2010.083568

Slep, K. C., Kercher, M. A., He, W., Cowan, C. W., Wensel, T. G., & Sigler, P. B. (2001). Structural determinants for regulation of phosphodiesterase by a G protein at 2.0 Å. *Nature*, *409*(6823), 1071–1077. https://doi.org/10.1038/35059138

Solomon, S. G., Lee, B. B., & Sun, H. (2006). Suppressive Surrounds and Contrast Gain in Magnocellular-Pathway Retinal Ganglion Cells of Macaque. *Journal of Neuroscience*, *26*(34), 8715–8726. https://doi.org/10.1523/JNEUROSCI.0821-06.2006

Solovei, I., Kreysing, M., Lanctôt, C., Kösem, S., Peichl, L., Cremer, T., … Joffe, B. (2009). Nuclear Architecture of Rod Photoreceptor Cells Adapts to Vision in Mammalian Evolution. *Cell*, *137*(2), 356–368. https://doi.org/10.1016/j.cell.2009.01.052

Sondek, J., Bohm, A., Lambright, D. G., Hamm, H. E., & Sigler, P. B. (1996). Crystal structure of a G-protein beta gamma dimer at 2.1A resolution. *Nature*, *379*(6563), 369–374. https://doi.org/10.1038/379369a0

Speros, P., & Price, J. (1981). Oscillatory potentials. History, techniques and potential use in the evaluation of disturbances of retinal circulation. *Survey of Ophthalmology*, *25*(4), 237–252. https://doi.org/10.1016/0039-6257(81)90093-X

States, D. J., & Gish, W. (1994). Combined use of sequence similarity and codon bias for coding region identification. *Journal of Computational Biology : A Journal of Computational Molecular Cell Biology*, *1*(1), 39–50. https://doi.org/10.1089/cmb.1994.1.39

Steinberg, R. H. (1974). Phagocytosis by pigment epithelium of human retinal cones. *Nature*, *252*(5481), 305–307.

Steinberg, R. H., Fisher, S. K., & Anderson, D. H. (1980). Disc morphogenesis in vertebrate photoreceptors. *Journal of Comparative Neurology*, *190*(3), 501–518. https://doi.org/10.1002/cne.901900307

Stern, J. H., Kaupp, U. B., & Macleish, P. R. (1986). Control of the light-regulated current in rod photoreceptors by cyclic GMP, calcium, and l-cis-diltiazem. *Proc. Natl. Acad. Sci. USA*, *83*, 1163–1167.

Sugimoto, Y., Yatsunami, K., Tsujimoto, M., Khorana, H. G., & Ichikawa, a. (1991). The amino acid sequence of a glutamic acid-rich protein from bovine retina as deduced from the cDNA sequence. *Proceedings of the National Academy of Sciences of the United States of America*, *88*(8), 3116–3119. https://doi.org/10.1073/pnas.88.8.3116

Sullivan, J. M., Prewitt, R. L., Josephs, J. A., Sacerdote, A., Molino, R., Solimano, N., & Ravalico, G. (1995). Attenuation of the microcirculation in young patients with high-output borderline hypertension. *Hypertension (Dallas, Tex. : 1979)*, *5*(6), 844–851. https://doi.org/10.1161/01.hyp.25.4.839

Surya, A., Foster, K. W., & Knox, B. E. (1995). Transducin activation by the bovine opsin apoprotein. *The Journal of Biological Chemistry*, *270*(10), 5024–5031. https://doi.org/10.1074/JBC.270.10.5024

Szmajda, B. A., Grünert, U., & Martin, P. R. (2008). Retinal ganglion cell inputs to the koniocellular pathway. *Journal of Comparative Neurology*, *510*(3), 251–268. https://doi.org/10.1002/cne.21783

Taniguchi, T., Tanaka, S., Ishii, A., Watanabe, M., Fujitani, N., Sugeo, A., … Konishi, H. (2013). A brain-specific Grb2-associated regulator of extracellular signal-regulated kinase (Erk)/mitogen-activated protein kinase (MAPK) (GAREM) subtype, GAREM2, contributes to neurite outgrowth of neuroblastoma cells by regulating erk signaling. *Journal of Biological Chemistry*, *288*(41), 29934–29942. https://doi.org/10.1074/jbc.M113.492520

Trifunović, D., Karali, M., Camposampiero, D., Ponzin, D., Banfi, S., & Marigo, V. (2008). A high-resolution RNA expression atlas of retinitis pigmentosa genes in human and mouse retinas. *Investigative Ophthalmology and Visual Science*, *49*(6), 2330–2336. https://doi.org/10.1167/iovs.07-1513

Trudeau, M. C., & Zagotta, W. N. (2002a). An intersubunit interaction regulates trafficking of rod cyclic nucleotide-gated channels and is disrupted in an inherited form of blindness. *Neuron*, *34*(2), 197–207. https://doi.org/10.1016/S0896-6273(02)00647-5

Trudeau, M. C., & Zagotta, W. N. (2002b). Mechanism of calcium/calmodulin inhibition of rod cyclic nucleotide-gated channels. *Proceedings of the National Academy of Sciences of the United States of America*, *99*(12), 8424–8429. https://doi.org/10.1073/pnas.122015999

Trudeau, M. C., & Zagotta, W. N. (2003). Calcium/calmodulin modulation of olfactory and rod cyclic nucleotide-gated ion channels. *Journal of Biological Chemistry*, *278*(21), 18705–18708. https://doi.org/10.1074/jbc.R300001200

Trudeau, M. C., & Zagotta, W. N. (2004). Dynamics of Ca2+-calmodulin-dependent inhibition of rod cyclic nucleotide-gated channels measured by patch-clamp fluorometry. *The Journal of General Physiology*, *124*(3), 211–223. https://doi.org/10.1085/jgp.200409101

Tsang, S. H. (2006). GAP-Independent Termination of Photoreceptor Light Response by Excess Subunit of the cGMP-Phosphodiesterase. *Journal of Neuroscience*, *26*(17), 4472–4480. https://doi.org/10.1523/JNEUROSCI.4775-05.2006

Tsang, S. H., Woodruff, M. L., Janisch, K. M., Cilluffo, M. C., Farber, D. B., & Fain, G. L. (2007). Removal of phosphorylation sites of gamma subunit of phosphodiesterase 6 alters rod light response. *The Journal of Physiology*, *579*(Pt 2), 303–312. https://doi.org/10.1113/jphysiol.2006.121772

Turgut, B. (2017). Past and Present Terminology for the Retinal and Choroidal Structures in Optical Coherence Tomography. *European Ophthalmic Review*, *11*(1), 59–61. https://doi.org/10.17925/EOR.2017.11.01.59

Ungerer, N., Mäcke, N., Broecker, J., Keller, S., Frings, S., & Möhrlen, F. (2011).

Distinct binding properties distinguish LQ-type calmodulin-binding domains in cyclic nucleotide-gated channels. *Biochemistry*, *50*(15), 3221–3228. https://doi.org/10.1021/bi200115m

Uversky, V. N. (2010). Seven lessons from one IDP structural analysis. *Structure*, *18*(9), 1069–1071. https://doi.org/10.1016/j.str.2010.08.003

Vaithianathan, T., & Matthews, G. (2014). Visualizing synaptic vesicle turnover and pool refilling driven by calcium nanodomains at presynaptic active zones of ribbon synapses. *Proceedings of the National Academy of Sciences*, *111*(23), 8655–8660. https://doi.org/10.1073/pnas.1323962111

van der Vos, K. E., Eliasson, P., Proikas-Cezanne, T., Vervoort, S. J., van Boxtel, R., Putker, M., … Coffer, P. J. (2012). Modulation of glutamine metabolism by the PI(3)K–PKB–FOXO network regulates autophagy. *Nature Cell Biology*, *14*(8), 829–837. https://doi.org/10.1038/ncb2536

Vaney, D. I. (1990). The mosaic of amacrine cells in the mammalian retina. *Progress in Retinal Research*, *9*, 49–100. https://doi.org/10.1016/0278-4327(90)90004-2

Wachtmeister, L. (1998). Oscillatory potentials in the retina: What do they reveal. *Progress in Retinal and Eye Research*, *17*(4), 485–521. https://doi.org/10.1016/S1350-9462(98)00006-8

Wald, G. (1968). Molecular basis of visual excitation. *Science, New Series*, *162*(3850), 230–239. https://doi.org/10.1126/science.162.3850.230

Wang, J.-S., & Kefalov, V. J. (2009). Report An Alternative Pathway Mediates the Mouse and Human Cone Visual Cycle. *Current Biology*, *19*, 1665–1669. https://doi.org/10.1016/j.cub.2009.07.054

Wang, T., & Chen, J. (2014). Induction of the unfolded protein response by constitutive g-protein signaling in rod photoreceptor cells. *Journal of Biological Chemistry*, *289*(42), 29310–29321. https://doi.org/10.1074/jbc.M114.595207

Wang, Z., & Storm, D. R. (2006). Extraction of DNA from mouse tails. *BioTechniques*, *41*(4), 410–412. https://doi.org/10.2144/000112255

Weber, K., & Geisler, N. (1983). Proteolysis of the neurofilament 68 kDa protein explains several previously described brain proteins of unique composition and high acidity. *FEBS Letters*, *164*(1), 129–131. https://doi.org/10.1016/0014-5793(83)80034-9

Weiler, R., & Kewitz, B. (1993). The marker for nitric oxide synthase, NADPH-diaphorase, co-localizes with GABA in horizontal cells and cells of the inner retina in the carp retina. *Neuroscience Letters*, *158*(2), 151–154. https://doi.org/10.1016/0304-3940(93)90251-F

Weitz, D., Ficek, N., Kremmer, E., Bauer, P. J., & Kaupp, U. B. (2002). Subunit stoichiometry of the CNG channel of rod photoreceptors. *Neuron*, *36*(5), 881–889. https://doi.org/10.1016/S0896-6273(02)01098-X

Wessling-Resnick, M., & Johnson, G. L. (1987). Allosteric behavior in transducin activation mediated by rhodopsin. Initial rate analysis of guanine nucleotide exchange. *Journal of Biological Chemistry*, *262*(8), 3697–3705.

White, R. D., & Neal, M. J. (1976). The uptake of l-glutamate by the retina. *Brain Research*, *111*(1), 79–93. https://doi.org/10.1016/0006-8993(76)91050-7

Winger, J. A., Derbyshire, E. R., Lamers, M. H., Marletta, M. A., & Kuriyan, J. (2008). The crystal structure of the catalytic domain of a eukaryotic guanylate cyclase. *BMC*

Structural Biology, *8*(1), 42. https://doi.org/10.1186/1472-6807-8-42

Winkler, B. S., & Riley, M. V. (1977). Na+-K+ and HCO3- ATPase activity in retina: dependence on calcium and sodium. *Investigative Ophthalmology and Visual Science*, *16*(12), 1151–1154.

Winkler, P. A., Ekenstedt, K. J., Occelli, L. M., Frattaroli, A. V., Bartoe, J. T., Venta, P. J., & Petersen-Jones, S. M. (2013). A large animal model for CNGB1 autosomal recessive retinitis pigmentosa. *PLoS ONE*, *8*(8), e72229. https://doi.org/10.1371/journal.pone.0072229

Wu, S. M. (1992). Feedback connections and operation of the outer plexiform layer of the retina. *Current Opinion in Neurobiology*, *2*(4), 462–468. https://doi.org/10.1016/0959-4388(92)90181-J

Wu, S., & Zhang, Y. (2007). LOMETS: A local meta-threading-server for protein structure prediction. *Nucleic Acids Research*, *35*(10), 3375–3382. https://doi.org/10.1093/nar/gkm251

Xu, Y., Guan, L., Shen, T., Zhang, J., Xiao, X., Jiang, H., … Zhang, Q. (2014). Mutations of 60 known causative genes in 157 families with retinitis pigmentosa based on exome sequencing. *Hum Genet*, *133*, 1255–1271. https://doi.org/10.1007/s00439-014-1460-2

Xue, Y., Shen, S. Q., Jui, J., Rupp, A. C., Byrne, L. C., Hattar, S., … Kefalov, V. J. (2015). CRALBP supports the mammalian retinal visual cycle and cone vision. *Journal of Clinical Investigation*, *125*(2), 727–738. https://doi.org/10.1172/JCI79651

Xue, Z., Xu, D., Wang, Y., & Zhang, Y. (2013). ThreaDom: extracting protein domain boundary information from multiple threading alignments. *Bioinformatics (Oxford, England)*, *29*(13), i247-56. https://doi.org/10.1093/bioinformatics/btt209

Yamashiro, S., Totsukawa, G., Yamakita, Y., Sasaki, Y., Madaule, P., Ishizaki, T., … Matsumura, F. (2003). Citron kinase, a Rho-dependent kinase, induces di-phosphorylation of regulatory light chain of myosin II. *Molecular Biology of the Cell*, *14*(5), 1745–1756. https://doi.org/10.1091/mbc.E02-07-0427

Yamashita, M., & Wässle, H. (1991). Responses of rod bipolar cells isolated from the rat retina to the glutamate agonist 2-amino-4-phosphonobutyric acid (APB). *The Journal of Neuroscience : The Official Journal of the Society for Neuroscience*, *11*(8), 2372–2382.

Yang, H., Shi, P., Zhang, Y. P., & Zhang, J. Z. (2005). Composition and evolution of the V2r vorneronasal receptor gene repertoire in mice and rats. *Genomics*, *86*(3), 306–315. https://doi.org/10.1016/j.ygeno.2005.05.012

Yang, J., Gao, J., Adamian, M., Wen, X.-H., Pawlyk, B., Zhang, L., … Li, T. (2005). The Ciliary Rootlet Maintains Long-Term Stability of Sensory Cilia. *Molecular and Cellular Biology*, *25*(10), 4129–4137. https://doi.org/10.1128/MCB.25.10.4129-4137.2005

Yang, J., Roy, A., & Zhang, Y. (2013). BioLiP: a semi-manually curated database for biologically relevant ligand–protein interactions. *Nucleic Acids Research*, *41*(Database Issue), D1096–D1103. https://doi.org/10.1093/nar/gks966

Yang, J., Yan, R., Roy, A., Xu, D., Poisson, J., & Zhang, Y. (2015). The I-TASSER Suite: protein structure and function prediction. *Nature Methods*, *12*(1), 7–8. https://doi.org/10.1038/nmeth.3213

Young, R. W. (1968). Passage of Newly Formed Protein through the Connecting Cilium of Retinal Rods in the Frog z. *J. ULTRASTRUCTURE RESEARCH*, *23*, 462–473.

Yücel, Y. H., Zhang, Q., Weinreb, R. N., Kaufman, P. L., & Gupta, N. (2003). Effects of retinal ganglion cell loss on magno-, parvo-, koniocellular pathways in the lateral geniculate nucleus and visual cortex in glaucoma. *Progress in Retinal and Eye Research*, *22*(4), 465–481. https://doi.org/10.1016/S1350-9462(03)00026-0

Zhan, X., Gimenez, L. E., Gurevich, V. V., & Spiller, B. W. (2011). Crystal structure of arrestin-3 reveals the basis of the difference in receptor binding between two non-visual subtypes. *Journal of Molecular Biology*, *406*(3), 467–478. https://doi.org/10.1016/j.jmb.2010.12.034

Zhang, J., & Madden, T. L. (1997). PowerBLAST: a new network BLAST application for interactive or automated sequence analysis and annotation. *Genome Research*, *7*(6), 649–656.

Zhang, J., Richmond, A. M., & Ogilvie, J. M. (2014). Inhibition of dopamine signaling suppresses cGMP accumulation in rd1 retinal organ cultures. *NeuroReport*, *25*(8), 1. https://doi.org/10.1097/WNR.0000000000000145

Zhang, Y. (2008). I-TASSER server for protein 3D structure prediction. *BMC Bioinformatics*, *9*(40). https://doi.org/10.1186/1471-2105-9-40

Zhang, Y., Molday, L. L., Molday, R. S., Sarfare, S. S., Woodruff, M. L., Fain, G. L., … Pittler, S. J. (2009). Knockout of GARPs and the beta-subunit of the rod cGMP-gated channel disrupts disk morphogenesis and rod outer segment structural integrity. *Journal of Cell Science*, *122*(Pt 8), 1192–1200. https://doi.org/10.1242/jcs.042531

Zhang, Y., Rubin, G. R., Fineberg, N., Huisingh, C., McGwin, G., Pittler, S. J., & Kraft, T. W. (2012). Age-related changes in Cngb1-X1 knockout mice: Prolonged cone survival. *Documenta Ophthalmologica*, *124*(3), 163–175. https://doi.org/10.1007/s10633-012-9317-2

Zhang, Z., Schwartz, S., Wagner, L., & Miller, W. (2000). A Greedy Algorithm for Aligning DNA Sequences. *Journal of Computational Biology*, *7*(1–2), 203–214. https://doi.org/10.1089/10665270050081478

Zhao, J., Brault, J. J., Schild, A., Cao, P., Sandri, M., Schiaffino, S., … Goldberg, A. L. (2007). FoxO3 Coordinately Activates Protein Degradation by the Autophagic/Lysosomal and Proteasomal Pathways in Atrophying Muscle Cells. *Cell Metabolism*, *6*(6), 472–483. https://doi.org/10.1016/j.cmet.2007.11.004

Zheng, J., Trudeau, M. C., & Zagotta, W. N. (2002). Rod cyclic nucleotide-gated channels have a stoichiometry of three CNGA1 subunits and one CNGB1 subunit. *Neuron*, *36*(5), 891–896. https://doi.org/10.1016/S0896-6273(02)01099-1

Zhong, H., Molday, L. L., Molday, R. S., & Yau, K.-W. (2002). The heteromeric cyclic nucleotide-gated channel adopts a 3A:1B stoichiometry. *Nature*, *420*(6912), 193–198. https://doi.org/10.1038/nature01201

APPENDIX A

INSTITUTIONAL ANIMAL CARE AND USE COMMITTEE APPROVAL

THE UNIVERSITY OF ALABAMA AT BIRMINGHAM
Institutional Animal Care and Use Committee (IACUC)

MEMORANDUM

DATE: 21-Dec-2015

TO: Pittler, Steven J

FROM:

Robert A. Kesterson, Ph.D., Chair

Institutional Animal Care and Use Committee (IACUC)

SUBJECT: **NOTICE OF APPROVAL**

The following application was approved by the University of Alabama at Birmingham Institutional Animal Care and Use Committee (IACUC) on 21-Dec-2015.

Protocol PI: Pittler, Steven J

Title: Analysis of Retina Rod Photoreceptor GARP and cGMP-Gated Cation Channel

Sponsor: National Eye Institute/NIH/DHHS

Animal Project Number (APN): IACUC-08381

This institution has an Animal Welfare Assurance on file with the Office of Laboratory Animal Welfare (OLAW), is registered as a Research Facility with the USDA, and is accredited by the Association for Assessment and Accreditation of Laboratory Animal Care International (AAALAC).

Institutional Animal Care and Use Committee (IACUC) | Mailing Address:
CH19 Suite 403 | CH19 Suite 403
933 19th Street South | 1530 3rd Ave S
(205) 934-7692 | Birmingham, AL 35294-0019
FAX (205) 934-1188 |

APPENDIX B

GENE MAP OF GARP2 OPEN READING FRAME

Odd numbered exons are labeled gray. The first and last nucleotides of the transcript are highlighted yellow. The line immediately above the DNA transcript is the protein transcript from start codon to termination codon. Mutations of the CNGB1 gene from patients with retinal disease corresponding to regions within the GARP2 coding region appear in larger green boldface font with the corresponding citation appearing in-line above the mutation.

```
     E1 5′ UTR                                                  E2
   1 ccagctacga gtggcagcaa gaaggcaatt cctggctggc ggttggcatc taagcaggca

1          M  L   G  W  V   Q  R  V   L  P  Q  P   P  G  T   P  R  K
  61 tcaggatgtt gggctgggtc cagagggtgc tgcctcagcc cccagggacc cctcggaaga

19   T  K  M  Q   E  E  E   E  V  E   P  E  P  E   M  E  A   E  V  E
 121 ccaagatgca ggaggaagag gaagtggaac cagagccaga gatggaggcg gaggtggaac
                                                      E3
39   P  E  P  N   P  E  E   A  E  T   E  S  E  S   M  P  P   E  E  S
 181 cagaaccgaa tcctgaggag gccgagacag agtccgagtc catgcccccc gaagagtcat
                                                     E4
59   F  K  E  E   E  V  A   V  A  D   P  S  P  Q   E  T  K   E  A  A
 241 tcaaggagga ggaagtggct gTggcagacc caagccctca ggagaccaag gaggctgccc
                                                                  E5
     RP phenotype – c.262C>T p.Q88* (Hull et al., 2017)
79   L  T  S  T   I  S  L   R  A  Q   G  A  E  I   S  E  M   N  S  P
 301 ttacttccac catatccctc cgggccCagg gcgctgagat ttctgaaatg aatagtccca

99   S  R  R  V   L  T  W   L  M  K   G  V  E  K   V  I  P   Q  P  V
 361 gccgcagggt actgacctgg ctcatgaagg gcgtagagaa ggtgatcccg caGcctgttc
                                 E6                                E7
119  H  S  I  T   E  D  P   A  Q  I   L  G  H  G   S  T  G   D  T  G
 421 acagcatcac ggaggacccg gctcagatcc tggggcatgg cagcactggg gacacagggt
                                                      E8
     RP phenotype - p.C139Afs*138 (Saqib et al., 2015)
139  C  T  D  E   P  N  E   A  L  E   A  Q  D  T   R  P  G   L  R  L
 481 gcacagatga acccaatgag gcccttgagg cccaagacac taggcctggg ctgcggctgc
                                                                    E9
     Macular cystoid spaces phenotype p.K175fs  (Lingao et al., 2016)
     RP phenotype c.522_523insC p.K175Pfs*3 (Petersen-Jones et al.,
2018)
159  L  L  W  L   E  Q  N   L  E  R   V  L  P  Q   P  P  K   S  S  E
 541 ttctgtggct ggagcagaat ctggaaagag tgcttcctca gcccccCaaa tcctctgagg
                                                        E10
179  V  W  R  D   E  P  A   V  A  T   G  A  A  S   D  P  A   P  P  G
 601 tctggagaga tgagcctgca gttgctacag gtgctgcctc agacccagcg cctccaggac

199  R  P  Q  E   M  G  P   K  L  Q   A  R  E  T   P  S  L   P  T  P
```

```
 661 gcccccagga aatggggccc aagctgcagg cccgggagac cccctccctg cccacaccca

     RP phenotype – c.664C>T p.Q222* (Hull et al., 2017)
219  I  P  L  Q   P  K  E   E  P  K   E  A  P  A   P  E  P   Q  P  G

 721 tccccctgca gcccaaggag gaacccaagg aggcaccagc tccagagccc cagcccggct
                                                          E11
239  S  Q  A  Q   T  S  S   L  P  P   T  R  D  P   A  R  L   V  A  W
 781 cccaggccca gacctcctcc ctgccaccaa ccagggaccc tgccaggctg gtggcatggg
     259
259  V  L  H  R   L  E  M   A  L  P   Q  P  V  L   H  G  K   I  G  E
 841 tcctgcacag gctggagatg gccttgccgc agccagtgct acatgggaaa ataggggaac
       E12                                     E12a
279  Q  E  P  D   S  P  G   I  C  D   V  Q  T  R   V  M  G   A  G  G
 901 aggagcctga ctcccctggg atatgtgatg tgcagaccag ggtgatggga gctggaggtc

299  L STOP 3'UTR
 961 tctgaaataa gggagaaggg aatctgggag agctcagatg gacacatgga tggaaggaaa

1021 gaaggatgcc ctgaagagaa gaccttcccg ggggaggtgg ccactgacac cccaccctat

1081 ttgaacagcg aacccctccc tctccacaca ctcccaggca ggacaagggg agccagagtc

1141 acctgcacca gccccagagc ctcccagacc agaacaaggg gaaggccagc catgggcagc

1201 ctgcaagatt taggctagac agcaggactt acccccagag ggctgtggaa aaggcccata

1261 gccgggcgtg gtggctcacg cctgtaatcc cagcactttg ggaggctgag gcaggaggat

1321 tgcttgagcc ccgaagttcg agaccaccgt gggcaacaca gtgagaccct gtctctaaaa

1381 aaccttttt aaattaataa attaaaaagc cccatggatg gaggactcag tattgagcat

1441 ctctttgaga ggacgcgtgc acagccccca gtgtggtacc tggcaccgtc agcacctcga

1501 caggatacag tttttcccag aagaggttct ccctaggcct ggccacactc tctccttcca

1561 aggcttgggg acaccaatga gcagcaacaa atgttttcat taacattaaa agagtgtaaa
                 Poly A Tail
1621 tgagcacatc aaaaaaaaaa aaaaaaaa
```

APPENDIX C

SEQUENCES OF QRT-PCR PRIMERS

Gene Symbol	Gene Name	Context Sequence	Group	Chr	Target Exons
18S	Eukaryotic 18S rRNA	N/A	Miscellaneous function	16	1
Abca8b	ATP-binding cassette, sub-family A (ABC1), member 8b	GCAATGAGAAGAACCACAGCTTTTC	Mitochondrial carrier protein	11	21
Adnp	activity-dependent neuroprotective protein	ACGAAAAATCAGGACTATCGGACAA	Other miscellaneous function protein	2	4
Apod	apolipoprotein D	GACGTGAAAAAGTATCTTGGAAGAT	Actin family cytoskeletal protein	16	3
Apol9b, Apol9a	apolipoprotein L 9b, apolipoprotein L 9a	CATCTGGGTCCTGTTAGAGAGCAGA	Actin family cytoskeletal protein	15	1
Arhgap20	Rho GTPase activating protein 20	GAGCACCAGAGACAGCCATTCTGCC	G-protein modulator	9	1
Arhgap5	Rho GTPase activating protein 5	TTATTGAAGACACAGGATTATGTAC	G-protein modulator	12	2
Arid5b	AT rich interactive domain 5B (MRF1-like)	CTACTTGGGTTTCAAACAGATTAAC	Transcription cofactor	10	4
Atp7b	ATPase, Cu++ transporting, β polypeptide	AGAGGCCAGTCGGAAAATCTTATCT	Apolipoprotein	8	2
BC018473	cDNA sequence BC018473	GCCATGTCAACCTCGAAAAAGAGAT	Miscellaneous function	11	3
Birc7	baculoviral IAP repeat-containing 7 (livin)	CCACTCCCTCAGCTCCTGCCCATGG	Miscellaneous function	2	4
Cacna1e	calcium channel, voltage-dependent, R type, α 1E subunit	TTCTGGCCTGAGTGGTCGGAGTGGA	Sugar transporter	1	42
Capn11	calpain 11	ATCTTCCACTTTCAGCTTTGGCAGT	Cadherin	17	4
Car6	carbonic anhydrase 6	CTTTGTCCAAGGCCCAGGTGGTGAC	Dehydratase	4	5
Chat	choline acetyltransferase	ACCAGCCAGGTGCCCACGACCATGG	Acetyltransferase	14	14
Chrm2	cholinergic receptor, muscarinic 2, cardiac	AAGACTTTTAAGCACCTCCTTATGT	G-protein coupled receptor	6	14
Cit	citron	CCTCCCGCAGCAGCCCCAACAAGCG	Ligand-gated ion channel	5	46
Clvs1	clavesin 1	ACAAGACAAGAAAACGGATTTTCCT	Other cytoskeletal proteins	4	4
Cngb1	cyclic nucleotide gated channel β 1	GAGGTCCAGGCCCTGCCACCAGAGG	Receptor	8	3
Cnp	2',3'-cyclic nucleotide 3' phosphodiesterase	ACGCCCAGCAGGAGGTGGTGAAGAG	Phosphodiesterase	11	3
Cntn5	contactin 5	TTCCTTCATATTCAGGTGGGAAAAT	Kinase modulator	9	20
Crebbp	CREB binding protein	CAGGTTTCTCAAGGGATGAATTCAT	Transcription cofactor	16	9
Crygb	crystallin, gamma B	CATCCCCCAACACTCTGGCACTTAC	Structural protein	1	2
Cryge	crystallin, gamma E	CAACACCAGCCATGGGGAAGATCAC	Structural protein	1	1
Diap2	diaphanous homolog 2 (Drosophila)	GGTGTTGTGATGAGCACGGTGAAAA	Nuclease	X	19
Fa2h	fatty acid 2-hydroxylase	GCGGACCCGCAGGATCCCACAGAGA	Hydroxylase	8	1
Foxo3	forkhead box O3	GGGCAAAGCAGACCCTCAAACTGAC	Other transcription factor	10	3

Gabbr2	gamma-aminobutyric acid (GABA) B receptor, 2	TCAAGAACCGGAACCAAAAGCTGAT	G-protein coupled receptor	4	10
Gal3st1	galactose-3-O-sulfotransferase 1	TCCCAACATGGCCTTCACGACCTCA	Transferase	11	1
Garem	GRB2 associated, regulator of MAPK1	CAAATCTGAAGCTGTCAGGGAAGAA	Miscellaneous function	18	4
Gatad2b	GATA zinc finger domain containing 2B	GTGCTAGACGGAGTGAGCCAGACCG	Miscellaneous function	3	2
Glg1	golgi apparatus protein 1	CTGCCAACAGGCGCTTCAGACACTG	Other signaling molecule	8	8
Gpr17	G protein-coupled receptor 17	GCTCACAGGAGAGCCCAGTCCCCTT	G-protein coupled receptor	18	50
Grifin	galectin-related inter-fiber protein	GGGAGAGCCCTTTGAGATGGAGGTG	Other signaling molecule	5	3
Gucy1a2	guanylate cyclase 1, soluble, α 2	AGCAATTCAGATGCGGATAGGCATT	Cyclase	9	2
Hba-a2, Hba-a1	hemoglobin α, adult chain 2,hemoglobin α, adult chain 1	AATGCTGCAGGCCACCTCGATGACC	Other cytoskeletal proteins	11	3
Hcn4	hyperpolarization-activated, cyclic nucleotide-gated K+ 4	CCATCAATGGCATGGTGAATAACTC	Cation transporter	9	3
Hfe2	hemochromatosis type 2 (juvenile) (human homolog)	TTTGATGTTTCAGTCTCCGGTGACC	Miscellaneous function	3	6
Hivep3	human immunodeficiency virus type I enhancer binding protein 3	CGAAGGAGGGTACAAATCAAACGAA	Zinc finger transcription factor	4	3
Igfals	insulin-like growth factor binding protein, acid labile subunit	AAGGAGGGGAGGTGCTCAGCAGCAC	Select regulatory molecule	17	22
Irs2	insulin receptor substrate 2	GTCGTGAAAGAGTGAAGCGCTACCA	Other miscellaneous function protein	8	1
Itgb8	integrin β 8	CGGACTGGGCCAAAGTGAACACAAT	Receptor	12	1
Klf5	Kruppel-like factor 5	N/A	Zinc finger transcription factor	14	1
Klf9	Kruppel-like factor 9	ACAGAGTGCATACAGGTGAACGGCC	Zinc finger transcription factor	19	1
Klk6	kallikrein related-peptidase 6	GATTCCTGTCAGGGTGATTCTGGAG	Serine protease	7	6
Lgsn	lengsin, lens protein with glutamine synthetase domain	CCGAATACTGATCCCACCCGGTACA	Synthetase	1	3
Lim2	lens intrinsic membrane protein 2	CGAGAGCATCGCATATTGGAATGCC	Other receptor	7	2
Lmln	leishmanolysin-like (metallopeptidase M8 family)	CACCTCCAGCAATGCAGGGTCTGCC	Cam family adhesion molecule	16	5
Lrch3	leucine-rich repeats and calponin homology (CH) domain containing 3	GGTGTACCCCAGGAGCAATTGTGCT	Miscellaneous function	16	20
Mag	myelin-associated glycoprotein	N/A	Kinase modulator	7	5
Map3k13	mitogen-activated protein kinase kinase kinase 13	GCCCCTTCAGAAGAGTGGCGATGAC	Ligand-gated ion channel	16	1
Mbp	myelin basic protein	AGAACATTGTGACACCTCGAACACC	Myelin protein	18	5

Mobp	myelin-associated oligodendrocytic basic protein	CCTGCCAGAAGACTAGATTGAGGAG	G-protein modulator	9	2
Mog	myelin oligodendrocyte glycoprotein	TGCAGCTATGCAGGACAATTCAGAG	Myelin protein	17	1
Myb	myeloblastosis oncogene	TGCCAATTATCTGCCCAACCGGACA	Other transcription factor	10	3
Myl2	myosin, light polypeptide 2, regulatory, cardiac, slow	N/A	Chaperonin	5	4
Nebl	nebulette	ACCTGGGATCATTGTTGCACCTGTC	Actin family cytoskeletal protein	2	3
Nek5	NIMA (never in mitosis gene a)-related expressed kinase 5	TGTGGCCCAGAAGCAGAGGGTTTCT	Ligand-gated ion channel	8	15
Nkx6-2	NK6 homeobox 2	AGTGAAGGTGTGGTTCCAGAATCGG	Homeobox transcription factor	7	2
Nptxr	neuronal pentraxin receptor	AGCGCATCGAGCAGGAGCTCCCAGC	Receptor	15	1
Nr2c2	nuclear receptor subfamily 2, group C, member 2	GAAGATACTTACAGATTGGCCAGGA	Nuclear hormone receptor	6	13
Nrip1	nuclear receptor interacting protein 1	CACAGGAGTTGGGCCAGAGAGAGCA	Transcription cofactor	16	N/A
Ntsr2	neurotensin receptor 2	CGCCCAGGTTCTCAGAGCCATCGTG	G-protein coupled receptor	12	2
Olig2	oligodendrocyte transcription factor 2	N/A	Basic helix-loop-helix transcription factor	16	1
Opalin	oligodendrocytic myelin paranodal and inner loop protein	TGCCAAAGCCACAGACTGTGGTCCC	Miscellaneous function	19	3
N/A	N/A	GACTTGCAGAAGAGTTTCTCCACTG	Miscellaneous function	4	4
Pcdh17	protocadherin 17	ATAATTCAGACAGACAATTTTCCCG	Phosphatase modulator	14	2
Pcdha6	protocadherin α 6	CATTGCTCAAGACCCCGGCAGCCCA	Phosphatase modulator	18	1
Pde3a	phosphodiesterase 3A, cGMP inhibited	GCCACGAGGATCCCAGTCAGGAACC	Phosphodiesterase	6	2
Pdpr	pyruvate dehydrogenase phosphatase regulatory subunit	ATACACAGCCCTCAATCTGATTGGC	Dehydrogenase	8	14
Peg3	paternally expressed 3	AAAGCTGCTCTCGCTGGGAGTCCAG	Miscellaneous function	7	7
Ptch1	patched homolog 1	CCAGGCTGAGAATCCCAGCAGCAGA	Other receptor	13	17
Rec8	REC8 meiotic recombination protein	CCTTTTGATATTCCTCAGATTCGAC	Miscellaneous function	14	6
Rho	rhodopsin	TCATGTTGAACAAGCAGTTCCGGAA	G-protein coupled receptor	6	4
Rims1	regulating synaptic membrane exocytosis 1	CGTCGCCTATTAGTTCGCATCCTGT	G-protein modulator	1	7
Slc22a6	solute carrier family 22 (organic anion transporter), member 6	CACAATGATTCGGCAGACGGGCCTG	Other transfer/carrier protein	19	8
Slurp1	secreted Ly6/Plaur domain containing 1	ACAGTGGAAGCAGCGTTCCCCTTCA	Miscellaneous function	15	2
Spen	SPEN homolog, transcriptional regulator (Drosophila)	TTTGGAGAAATTGTGGACATTGACA	Transcription cofactor	4	5

Stx1b	syntaxin 1B	TGTAGATGCCCCGACCCTCTTGCTG	Snare protein	7	N/A
Sugct	succinyl-CoA glutarate-CoA transferase	GCCGCCCGCAGTCAGATTGTGACAG	Dehydratase	13	1
Syngap1	synaptic Ras GTPase activating protein 1 homolog (rat)	ATGCTGGATGAGGATGAGATACACC	G-protein modulator	17	2
Tenm4	teneurin transmembrane protein 4	TCCTCCTTCCCATACTCAGTTTGAC	Other receptor	7	6
Tnks2	tankyrase, TRF1-interacting ankyrin-related ADP-ribose polymerase 2	GATGTTATTTCATGGGTCTCCTTTT	Nucleotidyltransferase	19	22
Trpm6	transient receptor potential cation channel, subfamily M, member 6	TAAAGCAGCACACCCTTCTCTCGAG	Other transporter	19	13
Ugt1a6b	UDP glucuronosyltransferase 1 family, pol-ypeptide A6B	CCCCCTGATGGGTCCTCTAAGAGAG	Glycosyltransferase	1	5
Ush2a	Usher syndrome 2A (autosomal recessive, mild)	TGCTCAAAGATGGTGCATTTTGCTA	Other kinase	1	19
Usp53	ubiquitin specific peptidase 53	GGGTGAAGAAAACATGGGATGTGGA	Miscellaneous function	3	N/A
Vmn2r29	vomeronasal 2, receptor 29	CATACCAGTGGAAGAAGTCCTTTTC	Miscellaneous function	7	N/A
Trpc2	transient receptor potential cation channel, subfamily C, member 2, pseudogene	GCCCATCGGGACCTTTACCAACCCC	Other transporter	7	15
Xrn1	5'-3' exoribonuclease 1	GAGAAGAGAAAACCGAAGGGTCAGG	Nuclease	9	10
Zfp429	zinc finger protein 429	TAAATGGATGTTGTCATGGCTGACC	Zinc finger transcription factor	13	18
Zfp804b	zinc finger protein 804B	ACAGTCTGAATGTGTTTCTGGAAAT	Miscellaneous function	5	1
Zkscan2	zinc finger with KRAB and SCAN domains 2	CGAAAGCAGGTCAGTAGCCCTCTGC	Zinc finger transcription factor	7	1
Zmynd10	zinc finger, MYND domain containing 10	ACCATGGGAAGATCCCAACGCTGGT	Miscellaneous function	9	2
Hist1h2bc	histone cluster 1, H2bc	GCCGTGCGCCTGCTGCTGCCCGGGG	Histone	13	4
Cdkl5	cyclin-dependent kinase-like 5	ACCCCAGCCTGGAGAACAGCTCCCT	Ligand-gated ion channel	X	11

APPENDIX D

NEXT GENERATION SEQUENCING RESULTS: DIFFERENTIALLY EXPRESSED GENES FOR GARP2-KO, *Cngb1*-X1, AND *Cngb1*-X26 VERSUS WILDTYPE

Differentially Expressed Genes Unique to GARP2-KO (406)

Gene Symbol	Gene Name	GARP2-KO Fold Change
1110008P14Rik	RIKEN cDNA 1110008P14	2.49
1700001O22Rik	RIKEN cDNA 1700001O22	2.70
1700020L24Rik	RIKEN cDNA 1700020L24	2.83
1700071M16Rik	RIKEN cDNA 1700071M16	-4.12
2010001A14Rik	RIKEN cDNA 2010001A14	2.60
2510003B16Rik	RIKEN cDNA 2510003B16	8.57
2810428I15Rik	RIKEN cDNA 2810428I15	2.73
4933409K07Rik	RIKEN cDNA 4933409K07	-2.98
5031434O11Rik	RIKEN cDNA 5031434O11	4.44
5330417C22Rik	RIKEN cDNA 5330417C22	-2.66
5430419D17Rik	RIKEN cDNA 5430419D17	-7.60
5830418P13Rik	RIKEN cDNA 5830418P13	4.46
A730008H23Rik	RIKEN cDNA A730008H23	-39.18
A730063M14Rik	RIKEN cDNA A730063M14	-2.73
AA465934	expressed sequence AA465934	16.35
Abca6	ATP binding cassette subfamily A member 6	3.03
Abhd11os	abhydrolase domain containing 11, opposite strand	-2.77
Abhd14a	abhydrolase domain containing 14A	3.03
Abhd14b	abhydrolase domain containing 14B	-2.38
Abhd2	abhydrolase domain containing 2	2.27
Acbd4	acyl-CoA binding domain containing 4	-2.29
Acpp	acid phosphatase, prostate	2.70
Acsbg1	acyl-CoA synthetase bubblegum family member 1	-10.33
Actg2	actin, gamma 2, smooth muscle, enteric	-8.71
Adgrf2	adhesion G protein-coupled receptor F2	-2.30
Adgrl2	adhesion G protein-coupled receptor L2	-2.23
Adgrl3	adhesion G protein-coupled receptor L3	-56.24
Adh6a	alcohol dehydrogenase 6A (class V)	-3.68
Adh7	alcohol dehydrogenase 7 (class IV), mu or sigma polypeptide	8.16
AF251705	CD300C molecule 2(Cd300c2)	-2.95
Aff2	AF4/FMR2 family member 2	-7.90
Ago3	argonaute 3, RISC catalytic component	-3.65
Alkbh8	alkB homolog 8, tRNA methyltransferase	-3.55
Alms1-ps2	alstrom syndrome protein 1	2.86
Alox15	arachidonate 15-lipoxygenase	-2.56
Ammecr1	alport syndrome, mental retardation, midface hypoplasia and elliptocytosis chromosomal region gene 1	-2.99
Anapc13	anaphase promoting complex subunit 13	2.26
Ankrd12	ankyrin repeat domain 12	-2.25
Ankrd26	ankyrin repeat domain 26	-2.75
Ankrd34c	ankyrin repeat domain 34C	-5.34
Ano3	anoctamin 3	-2.32
Ap2s1	adaptor related protein complex 2 sigma 1 subunit	2.28

Apoc1	apolipoprotein C1	3.00
Apol9b	apolipoprotein L 9b	4.74
Arfgef3	ARFGEF family member 3	-4.66
Arg1	arginase 1	2.26
Arhgap15	tubulointerstitial nephritis antigen like 1	-3.19
Arhgdib	rho GTPase activating protein 15	2.80
Arl5b	rho GDP dissociation inhibitor β	-2.48
Armc2	ADP ribosylation factor like GTPase 5B	2.63
Atad2b	armadillo repeat containing 2	-2.38
Atxn7	ATPase family, AAA domain containing 2B	-2.24
B3galt2	ataxin 7	-2.35
B9d1	β-1,3-galactosyltransferase 2	3.44
Baiap2l2	BAI1 associated protein 2 like 2	10.67
BC005561	B9 domain containing 1	3.43
Best3	bestrophin 3	-6.67
Bfsp2	beaded filament structural protein 2	-6.99
Bod1l	biorientation of chromosomes in cell division 1 like 1	-2.29
Bola2	bolA family member 2	2.81
Btbd7	BTB domain containing 7	-3.23
C030023E24Rik	RIKEN cDNA C030023E24	-2.60
C030037D09Rik	RIKEN cDNA C030037D09	-8.80
C130083M11Rik	RIKEN cDNA C130083M11	-5.17
C1qtnf4	C1q and TNF related 4	2.74
C3	complement C3	2.39
Cacna2d3	calcium voltage-gated channel auxiliary subunit α2delta 3	-2.96
Cacnb4	calcium voltage-gated channel auxiliary subunit β 4	-2.23
Calcrl	calcitonin receptor like receptor	-2.65
Cbl	cbl proto-oncogene	-4.33
Ccdc124	coiled-coil domain containing 124	2.37
Ccdc88b	coiled-coil domain containing 88B	2.26
Ccdc88c	coiled-coil domain containing 88C	-2.38
Ccl21b	C-C motif chemokine 21b	-65.52
Ccnd2	cyclin D2	-2.32
Ccnt2	cyclin T2	-2.41
Cdc34	cell division cycle 34	2.22
Cdc42ep5	CDC42 effector protein 5	2.26
Cdcp1	CUB domain containing protein 1	-2.99
Cdh10	cadherin 10	-2.60
Cdh12	cadherin 12	-2.76
Cdh6	cadherin 6	-5.30
Cep170	centrosomal protein 170	-2.23
Cep350	centrosomal protein 350	-2.56
Ces1e	carboxylesterase 1E	3.13
Chit1	chitinase 1	2.36
Clcn5	chloride voltage-gated channel 5	-4.64

Clec2g	C-type lectin domain family 2 member G	-4.19
Clec3b	C-type lectin domain family 3 member B	4.36
Cmtm5	CKLF like MARVEL transmembrane domain containing 5	3.17
Col24a1	collagen type XXIV α 1 chain	3.64
Col6a3	collagen type VI α 3 chain	-2.38
Col6a4	collagen type VI α 4 pseudogene 1	-35.95
Cox8b	cytochrome c oxidase subunit 8B, pseudogene	2.23
Cpeb3	cytoplasmic polyadenylation element binding protein 3	-2.27
Cyp4a12a	cytochrome P450 4A12A	3.04
Cyp4a12b	cytochrome P450 family 4, subfamily A, polypeptide 12B	2.23
Cyp4x1	cytochrome P450 family 4 subfamily X member 1	-7.46
D330041H03Rik	RIKEN cDNA D330041H03	5.48
Dcc	DCC netrin 1 receptor	-2.41
Dennd4c	DENN domain containing 4C	-2.20
Dgkb	diacylglycerol kinase β	-2.58
Dio2	iodothyronine deiodinase 2	-2.40
Dnah7b	dynein, axonemal, heavy chain 7B	-2.76
Dpy19l4	dpy-19 like 4	-2.54
Dsg3	desmoglein 3	-2.60
Dusp4	dual specificity phosphatase 4	-2.24
Duxbl1	double homeobox B-like 1	-33.17
Duxbl2	double homeobox B-like 2	-3.66
Duxbl3	double homeobox B-like 3	-3.66
Dynlrb2	dynein light chain roadblock-type 2	5.50
Dynlt1c	dynein light chain Tctex-type 1C	2.54
Edil3	EGF like repeats and discoidin domains 3	-2.24
Elobl	elongin B-like	-6.60
Enho	energy homeostasis associated	2.46
Enox1	ecto-NOX disulfide-thiol exchanger 1	-3.50
Epha3	EPH receptor A3	-3.31
Epm2aip1	EPM2A interacting protein 1	-2.85
Erbb3	erb-b2 receptor tyrosine kinase 3	-2.69
Ern1	endoplasmic reticulum to nucleus signaling 1	-2.72
Ero1lb	endoplasmic reticulum oxidoreductase 1 β	-2.41
Etnppl	ethanolamine-phosphate phospho-lyase	-4.19
Etohi1	zinc finger protein 971	-2.77
Etv1	ETS variant 1	-2.38
Etv4	ETS variant 4	2.62
Exosc5	exosome component 5	2.56
F420014N23Rik	RIKEN cDNA F420014N23	-3.46
Fam129a	family with sequence similarity 129, member A	-2.65
Fam135b	family with sequence similarity 135, member B	-4.11
Fam205a2	family with sequence similarity 205, member A2	-3.76
Fam25c	family with sequence similarity 25, member C	4.85
Fam32a	family with sequence similarity 32, member A	2.20

Fam84a	family with sequence similarity 84, member A	-2.37
Fat4	FAT atypical cadherin 4	-2.27
Fem1c	fem-1 homolog C	-2.64
Fetub	fetuin B	3.46
Fhit	fragile histidine triad	3.37
Flywch2	FLYWCH family member 2	2.47
Foxn3	forkhead box N3	-3.50
Frmpd4	FERM and PDZ domain containing 4	-2.66
Frrs1l	ferric chelate reductase 1 like	-6.47
Fxyd1	FXYD domain containing ion transport regulator 1	2.26
Fxyd2	FXYD domain containing ion transport regulator 2	3.69
Fxyd7	FXYD domain containing ion transport regulator 7	2.47
G2e3	G2/M-phase specific E3 ubiquitin protein ligase	-2.68
Galnt15	polypeptide N-acetylgalactosaminyltransferase 15	-3.40
Gbp2b	guanylate binding protein 2b	516.46
Gdf1	growth differentiation factor 1	2.68
Gfap	glial fibrillary acidic protein	2.96
Gja5	gap junction protein α 5	-18.81
Glra1	glycine receptor α 1	-5.60
Glra3	glycine receptor α 3	-5.54
Gm10406	α7-takusan	4.89
Gm10857	predicted gene 10857	-17.31
Gm12250	predicted gene 12250	8.57
Gm14305	predicted gene 14305	-2.79
Gm14308	predicted gene 14308	3.25
Gm14326	predicted gene 14326	-2.47
Gm14430	predicted gene 14430	3.25
Gm14431	predicted gene 14431	-3.96
Gm14434	novel KRAB box and zinc finger, C2H2 type domain containing protein	3.25
Gm14440	predicted gene 14440	-2.86
Gm15706	predicted gene 15706	2.44
Gm16982	predicted gene 16982	-4.93
Gm20139	predicted gene 20139	-2.93
Gm2897	uncharacterized protein	3.17
Gm3414	putative uncharacterized protein ENSP00000382790 homolog	-3.50
Gm3500	α 10-takusan	16.56
Gm3558	predicted gene, ENSMUSG00000063277	5.78
Gm3636	uncharacterized protein	4.49
Gm37013	protocadherin (Fragment)	-24.51
Gm4724	predicted gene 4724	3.25
Gm5617	uncharacterized protein C11orf71 homolog	2.72
Gm5796	uncharacterized protein	3.69
Gm8580	predicted gene 8580	16.78
Gm94	uncharacterized protein C5orf46 homolog	4.87
Gng13	G protein subunit gamma 13	2.28

Gp2	glycoprotein 2	2.53
Gpr135	G protein-coupled receptor 135	-2.79
Gpr165	G protein-coupled receptor 165	-6.51
Gpr26	G protein-coupled receptor 26	-3.67
Gprin3	G protein-regulated inducer of neurite outgrowth 3	-27.12
Gramd1b	GRAM domain containing 1B	-2.24
Gramd2	GRAM domain containing 2A	-2.96
Grin2c	glutamate ionotropic receptor NMDA type subunit 2C	2.64
Gsta1	glutathione S-transferase α 1	2.50
Gstp3	glutathione S-transferase pi 3	-3.52
Hba-a2	hemoglobin α, adult chain 2	2.30
Hdac4	histone deacetylase 4	-2.78
Hectd2	HECT domain E3 ubiquitin protein ligase 2	-2.82
Hgf	hepatocyte growth factor	-8.45
Hmbox1	SOS Ras/Rac guanine nucleotide exchange factor 1	-2.72
Hook1	hook microtubule tethering protein 1	-2.27
Hspb2	heat shock protein family B (small) member 2	2.88
Htr2a	5-hydroxytryptamine receptor 2A	-19.74
Ict1	mitochondrial ribosomal protein L58	2.25
Ifi27l2a	interferon α-inducible protein 27-like protein 2A	3.48
Ifi44	interferon induced protein 44	11.70
Ifi44l	interferon induced protein 44 like	40.11
Il3ra	interleukin 3 receptor subunit α	3.28
Impad1	inositol monophosphatase domain containing 1	-2.54
Ipo7	importin 7	-2.23
Iqcf1	IQ motif containing F1	19.16
Kcna3	potassium voltage-gated channel subfamily A member 3	-6.28
Kcnj6	potassium voltage-gated channel subfamily J member 6	-3.65
Kif13b	kinesin family member 13B	-2.55
Klf12	Kruppel like factor 12	-2.28
Klf7	Kruppel like factor 7	-7.97
Klhl11	kelch like family member 11	-3.77
Klhl15	kelch like family member 15	-4.69
Klhl24	kelch like family member 24	-2.24
Klhl28	kelch like family member 28	-5.54
Klhl3	kelch like family member 3	-3.23
Lacc1	laccase domain containing 1	-2.40
Larp4b	la ribonucleoprotein domain family member 4B	-4.63
Lcor	ligand dependent nuclear receptor corepressor	-4.08
Lhx1	LIM homeobox 1	2.49
Lipg	lipase G, endothelial type	-4.90
Lmbrd2	LMBR1 domain containing 2	-2.84
Lncppara	long noncoding RNA near Ppara	-3.18
Lnpep	leucyl and cystinyl aminopeptidase	3.26
Lrch2	leucine rich repeats and calponin homology domain containing 2	-2.83

Lrch4	leucine rich repeats and calponin homology domain containing 4	-4.48
Lrit3	leucine rich repeat, Ig-like and transmembrane domains 3	-2.98
Lrp1b	LDL receptor related protein 1B	-3.89
Lrrc8c	leucine rich repeat containing 8 VRAC subunit C	-2.88
Mcoln3	mucolipin 3	-10.82
Megf9	multiple EGF like domains 9	-2.91
Metrn	meteorin, glial cell differentiation regulator	2.43
Mgat5	mannosyl (α-1,6-)-glycoprotein β-1,6-N-acetyl-glucosaminyltransferase	-2.94
Mib1	mindbomb E3 ubiquitin protein ligase 1	-3.04
Mns1	meiosis specific nuclear structural 1	-8.36
Mob1a	MOB kinase activator 1A	-3.47
Mob1b	MOB kinase activator 1B	-3.46
Mroh6	maestro heat like repeat family member 6	-3.14
Mrpl23	mitochondrial ribosomal protein L23	2.21
Mrpl54	mitochondrial ribosomal protein L54	2.27
Mt1	metallothionein 1I, pseudogene	2.58
Mtr	metallothionein 1L, pseudogene	-3.09
Muc13	mucin 13, cell surface associated	3.61
Myt1l	myelin transcription factor 1 like	-2.22
N4bp2	NEDD4 binding protein 2	-4.51
Naa25	N(α)-acetyltransferase 25, NatB auxiliary subunit	-2.27
Nat8f6	N-acetyltransferase 8 (GCN5-related) family member 6	26.58
Nav3	neuron navigator 3	-3.22
Nbeal1	neurobeachin like 1	-3.88
Ncam2	neural cell adhesion molecule 2	-3.19
Ncapg2	non-SMC condensin II complex subunit G2	-2.70
Ndnf	neuron derived neurotrophic factor	-2.40
Ndufa13	NADH:ubiquinone oxidoreductase subunit A13	2.19
Ndufb7	NADH:ubiquinone oxidoreductase subunit B7	2.34
Nhs	NHS actin remodeling regulator	-4.07
Nos1ap	nitric oxide synthase 1 adaptor protein	-3.16
Npm3-ps1	nucleophosmin/nucleoplasmin 3	6.81
Nr4a3	nuclear receptor subfamily 4 group A member 3	-2.89
Nrtn	neurturin	2.55
Nupr1l	nuclear protein 2, transcriptional regulator	3.06
Nwd1	NACHT and WD repeat domain containing 1	-3.59
Nyap2	neuronal tyrosine-phosphorylated phosphoinositide-3-kinase adaptor 2	-5.24
Oas1a	2'-5'-oligoadenylate synthase 1A	3.65
Oas3	2'-5'-oligoadenylate synthetase 3	2.67
Olfml2a	olfactomedin like 2A	-3.32
Oxld1	oxidoreductase like domain containing 1	2.79
P2rx2	purinergic receptor P2X 2	2.49
Pax3	paired box 3	-21.19
Pcdh7	protocadherin 7	-2.41
Pcdha6	protocadherin α 6	-27.52

Pcdhb12	protocadherin β 12	-2.45
Pcdhb13	protocadherin β 13	-2.62
Pck1	phosphoenolpyruvate carboxykinase 1	26.14
Pde10a	phosphodiesterase 10A	-2.29
Pds5a	PDS5 cohesin associated factor A	-3.35
Pifo	primary cilia formation	3.98
Pigr	polymeric immunoglobulin receptor	2.48
Pih1d1	PIH1 domain containing 1	2.20
Pisd-ps2	phosphatidylserine decarboxylase	-2.46
Plag1	PLAG1 zinc finger	-3.33
Plvap	plasmalemma vesicle associated protein	2.47
Pop5	POP5 homolog, ribonuclease P/MRP subunit	2.18
Pou2f2	POU class 2 homeobox 2	-5.21
Ppdpf	pancreatic progenitor cell differentiation and proliferation factor	2.47
Ppp1r12a	protein phosphatase 1 regulatory subunit 12A	-2.43
Ppp1r12b	protein phosphatase 1 regulatory subunit 12B	-4.04
Ppp1r14a	protein phosphatase 1 regulatory inhibitor subunit 14A	5.44
Prdm10	PR/SET domain 10	-3.20
Prex2	phosphatidylinositol-3,4,5-trisphosphate dependent Rac exchange factor 2	-2.38
Prkaa2	protein kinase AMP-activated catalytic subunit α 2	-2.30
Prox1	prospero homeobox 1	-2.49
Prrc2c	proline rich coiled-coil 2C	-2.33
Ptpn4	protein tyrosine phosphatase, non-receptor type 4	-2.85
Ptprg	protein tyrosine phosphatase, receptor type G	-2.46
Rab17	RAB17, member RAS oncogene family	2.83
Ramp3	receptor activity modifying protein 3	2.18
Ranbp2	RAN binding protein 2	-2.33
Rapgef5	Rap guanine nucleotide exchange factor 5	-3.53
Rcor1	REST corepressor 1	-3.21
Rest	RE1 silencing transcription factor	-3.07
Rgs4	regulator of G protein signaling 4	-2.20
Rhoc	ras homolog family member C	2.16
Rims3	ras homolog family member C	-3.02
Rnd2	rho family GTPase 2	2.62
Rnpc3	RNA binding region (RNP1, RRM) containing 3	-3.10
Robo1	roundabout guidance receptor 1	-2.24
Rpl31-ps12	ribosomal protein L31, pseudogene 1 2	2.90
Rpp21	ribonuclease P/MRP subunit p21	2.31
Rps15	ribosomal protein S15	2.53
S100pbp	S100P binding protein	-3.01
Sap25	Sin3A associated protein 25	2.38
Saysd1	SAYSVFN motif domain containing 1	2.38
Scai	suppressor of cancer cell invasion	-2.47
Scarb2	scavenger receptor class B member 2	-2.20
Scn1a	sodium voltage-gated channel α subunit 1	-2.30

Serpina3n	serine protease inhibitor A3N	3.16
Sh3bgrl3	SH3 domain binding glutamate rich protein like 3	2.27
Shprh	SNF2 histone linker PHD RING helicase	-2.45
Slc22a18	solute carrier family 22 member 18	2.35
Slc24a4	solute carrier family 24 member 4	-2.92
Slc26a2	solute carrier family 26 member 2	-2.66
Slc35a3	solute carrier family 35 member A3	-2.48
Slc4a11	solute carrier family 4 member 11	2.36
Slc5a7	solute carrier family 5 member 7	-2.34
Slc6a5	solute carrier family 6 member 5	-5.22
Slc9a7	solute carrier family 6 member 2	-3.07
Slfn8	schlafen 8	-12.31
Slit1	slit guidance ligand 1	-2.47
Slitrk3	slit guidance ligand 3	-2.62
Smtnl1	smoothelin like 1	14.51
Snord15b	small nucleolar RNA, C/D box 15B	-7.78
Sntb1	syntrophin β 1	-3.29
Sntb2	syntrophin β 2	-2.34
Snx29	sorting nexin 29	-2.79
Spata9	spermatogenesis associated 9	5.85
Sphkap	SPHK1 interactor, AKAP domain containing	-2.30
Spin4	spindlin family member 4	-3.57
Spp1	secreted phosphoprotein 1	-2.41
Spred2	CXXC finger protein 1	-2.50
Ssh1	slingshot protein phosphatase 1	-2.40
Stard10	StAR related lipid transfer domain containing 10	2.44
Stard4	StAR related lipid transfer domain containing 4	-2.35
Ston1	stonin 1	-3.26
Strn	striatin	-3.56
Sult1b1	sulfotransferase family 1B member 1	8.57
Sv2c	synaptic vesicle glycoprotein 2C	-3.22
Tarbp1	TAR RNA binding protein 1	-2.69
Tbc1d4	TBC1 domain family member 4	-2.35
Tbc1d9	TBC1 domain family member 9	-2.34
Tbl1x	transducin β like 1 X-linked	-2.87
Tbx20	T-box 20	-2.52
Tcaf1	TRPM8 channel associated factor 1	-2.30
Tdg	thymine DNA glycosylase	-2.26
Tectb	tectorin β	-7.46
Tenm1	teneurin transmembrane protein 1	-5.30
Tet1	tet methylcytosine dioxygenase 1	-2.64
Timm13	translocase of inner mitochondrial membrane 13	2.30
Tjp1	tight junction protein 1	-2.32
Tmem132d	transmembrane protein 132D	-3.19
Tmem178b	transmembrane protein 178B	-4.95

Tmem205	transmembrane protein 205	2.24
Tmem245	transmembrane protein 245	-2.52
Tmem254b	Transmembrane protein 254b	-2.64
Tmtc3	transmembrane and tetratricopeptide repeat containing 3	-2.23
Tnni1	troponin I1, slow skeletal type	3.18
Tnpo1	transportin 1	-2.97
Tnr	tenascin R	-4.08
Tpgs1	tubulin polyglutamylase complex subunit 1	2.20
Trank1	tetratricopeptide repeat and ankyrin repeat containing 1	-2.21
Trappc2l	trafficking protein particle complex 2 like	2.20
Trub2	TruB pseudouridine synthase family member 2	2.18
Ttc14	tetratricopeptide repeat domain 14	-2.29
Ttc36	tetratricopeptide repeat domain 36	3.20
Ttc9b	tetratricopeptide repeat domain 9B	2.48
Ttr	transthyretin	2.39
Uba6	ubiquitin like modifier activating enzyme 6	-2.59
Ube3a	ubiquitin protein ligase E3A	-2.43
Ugt1a6a	UDP-glucuronosyltransferase 1-6	-2.45
Uprt	uracil phosphoribosyltransferase homolog	-13.41
Uqcr11	ubiquinol-cytochrome c reductase, complex III subunit XI	2.46
Uqcrq	ubiquinol-cytochrome c reductase complex III subunit VII	2.20
Urah	urate (hydroxyiso-) hydrolase, pseudogene	2.36
Vcan	versican	-2.72
Wdfy1	WD repeat and FYVE domain containing 1	2.62
Wdfy2	WD repeat and FYVE domain containing 2	-4.81
Xaf1	XIAP associated factor 1	7.36
Xkr7	XK related 7	-3.52
Xpnpep3	X-prolyl aminopeptidase 3	-2.88
Xpo4	exportin 4	-2.97
Yod1	YOD1 deubiquitinase	-3.74
Zan	zonadhesin (gene/pseudogene)	-2.57
Zbed6	zinc finger BED-type containing 6	-7.89
Zbp1	Z-DNA binding protein 1	3.37
Zbtb8os	zinc finger and BTB domain containing 8 opposite strand	2.33
Zc3h12c	zinc finger CCCH-type containing 12C	-2.72
Zfp109	zinc finger protein 109	-3.57
Zfp169	zinc finger protein 169	-2.61
Zfp433	zinc finger protein 433	-2.56
Zfp536	zinc finger protein 536	-2.77
Zfp618	zinc finger protein 618	-4.35
Zfp771	zinc finger protein 771	2.32
Zfp81	zinc finger protein 81	-2.70
Zfp868	putative uncharacterized protein	2.25
Zfp966	zinc finger protein 966	-3.96
Zfp973	zinc finger protein 973	-2.90

Zfp991	zinc finger protein 991	-2.65
Zhx3	zinc fingers and homeoboxes 3	-2.61
Zkscan16	zinc finger protein 483	-5.76
Zkscan7	zinc finger with KRAB and SCAN domains 7	-3.43

Differentially Expressed Genes Unique to *Cngb1*-X1 (262)

Gene Symbol	Gene Name	*Cngb1*-X1 Fold Change
1190007I07Rik	RIKEN cDNA 1190007I07	2.35
1300017J02Rik	RIKEN cDNA 1300017J02	-11.01
1500015O10Rik	RIKEN cDNA 1500015O10	-2.39
2010315B03Rik	RIKEN cDNA 2010315B03	-2.92
2310002L09Rik	RIKEN cDNA 2310002L09	-11.01
2610528A11Rik	RIKEN cDNA 2610528A11	-2.06
4930480K23Rik	RIKEN cDNA 4930480K23	2.70
4930481A15Rik	RIKEN cDNA 4930481A15	-2.54
4930525G20Rik	RIKEN cDNA 4930525G20	2.62
4933429O19Rik	RIKEN cDNA 4933429O19	-2.97
A930005H10Rik	RIKEN cDNA A930005H10	1.97
AA467197	expressed sequence AA467197	-1.91
Abhd1	abhydrolase domain containing 1	3.73
Acta2	actin, α 2, smooth muscle, aorta	-2.31
Adamdec1	ADAM like decysin 1	-23.00
Aebp1	AE binding protein 1	-1.82
Agtr1a	angiotensin II receptor type 1	4.12
Ajuba	ajuba LIM protein	-1.83
Alas2	5'-aminolevulinate synthase 2	-2.53
Aldh1a2	aldehyde dehydrogenase 1 family member A2	-5.17
Ankrd11	ankyrin repeat domain 11	1.78
Ankrd35	ankyrin repeat domain 35	1.84
Arhgap31	Rho GTPase activating protein 31	1.86
Asap3	ArfGAP with SH3 domain, ankyrin repeat and PH domain 3	1.88
Aspa	aspartoacylase	-3.33
Atp13a5	ATPase 13A5	-5.52
Atxn2l	ataxin 2 like	1.81
Bbs7	Bardet-Biedl syndrome 7	-1.82
Bcl9l	B cell CLL/lymphoma 9 like	2.01
Bcor	BCL6 corepressor	1.80
Bglap3	osteocalcin-related protein	3.96
Bnc1	basonuclin 1	-2.14
Bst1	bone marrow stromal cell antigen 1	6.41
C1ql3	complement C1q like 3	1.82
C1qtnf5	C1q and TNF related 5	-1.84
C2	complement C2	-2.00
Cacna1a	calcium voltage-gated channel subunit α1 A	1.78
Cacng7	calcium voltage-gated channel auxiliary subunit gamma 7	2.05
Capns2	calpain small subunit 2	-2.29
Car3	carbonic anhydrase 3	-1.79
Casz1	castor zinc finger 1	1.94
Cetn4	centrin-4	-2.17

Cfap58	cilia and flagella associated protein 58	3.22
Cfap69	cilia and flagella associated protein 69	2.01
Clcn6	chloride voltage-gated channel 6	2.04
Cldn19	claudin 19	-1.95
Cldn5	claudin 5	-1.95
Clic6	chloride intracellular channel 6	-1.99
Cntf	ciliary neurotrophic factor	-2.25
Col26a1	collagen type XXVI α 1 chain	3.32
Col8a2	collagen type VIII α 2 chain	-2.58
Cox7a2l	cytochrome c oxidase subunit 7A2 like	-1.95
Cryaa	crystallin α A	-2.40
Cryab	crystallin α B	-2.20
Cryba1	crystallin β A1	-2.27
Cryba2	crystallin β A2	-2.55
Cryba4	crystallin β A4	-3.37
Crybb1	crystallin β B1	-2.83
Crygs	crystallin gamma S	-3.28
Ctsl	cathepsin L	-2.75
Dapl1	death associated protein like 1	-1.84
Dbhos	dopamine β hydroxylase, opposite strand	-3.01
Dct	dopachrome tautomerase	-2.18
Dera	deoxyribose-phosphate aldolase	-2.09
Dhdh	dihydrodiol dehydrogenase	2.24
Diap3	protein diaphanous homolog 3	2.07
Dlg5	discs large MAGUK scaffold protein 5	1.91
Dnaic2	dynein intermediate chain 2, axonemal	2.02
Dnase2b	deoxyribonuclease 2 β	-3.93
Dot1l	DOT1 like histone lysine methyltransferase	1.83
Dyx1c1	dynein axonemal assembly factor 4	2.37
E030030I06Rik	RIKEN cDNA E030030I06	10.54
Ebf3	early B cell factor 3	1.94
Efcab12	EF-hand calcium binding domain 12	2.42
Egfl7	EGF like domain multiple 7	-2.05
Egr4	early growth response 4	3.42
Eif2s3y	eukaryotic translation initiation factor 2 subunit 3, Y-linked	-150.15
Eif4ebp1	eukaryotic translation initiation factor 4E binding protein 1	-1.88
Entpd4	ectonucleoside triphosphate diphosphohydrolase 4	-1.76
Epha8	EPH receptor A8	-1.87
Ephb2	EPH receptor B2	-2.06
Ermn	ermin	-1.80
Eva1c	eva-1 homolog C	-2.20
Exoc4	exocyst complex component 4	1.91
F3	coagulation factor III, tissue factor	-1.94
Fabp5	fatty acid binding protein 5	-2.80
Fam180a	family with sequence similarity 180 member A	-32.43

Fam20a	FAM20A, golgi associated secretory pathway pseudokinase	-2.69
Fam217b	family with sequence similarity 217 member B	2.16
Fcrls	Fc receptor-like S, scavenger receptor	-3.47
Fezf1	FEZ family zinc finger 1	3.40
Fmod	fibromodulin	-1.86
Fos	Fos proto-oncogene, AP-1 transcription factor subunit	2.67
Gatm	glycine amidinotransferase	-3.02
Gbp5	guanylate binding protein 5	4.63
Gcat	glycine C-acetyltransferase	-1.96
Gjc3	gap junction protein gamma 3	-6.24
Gltscr1	BRD4 interacting chromatin remodeling complex associated protein	1.90
Glycam1	glycosylation dependent cell adhesion molecule 1 (pseudogene)	4.19
Gm10037	uncharacterized protein	29.86
Gm10052	predicted pseudogene 10052	2.62
Gm15421	predicted gene 15421	-3.95
Gm4858	uncharacterized protein	12.44
Gm5148	predicted gene, EG381438	-1.81
Gm6277	predicted gene 6277	3.30
Gm6548	predicted gene 6548	-1.85
Gm6756	predicted gene 6756	11.66
Gm7367	predicted pseudogene 7367	-1.80
Gm9895	predicted gene 9895	-6.37
Gnaz	G protein subunit α z	1.93
Gpnmb	glycoprotein nmb	-2.01
Gpr137b	G protein-coupled receptor 137B	-2.75
Gpr143	G protein-coupled receptor 143	-2.52
Gpr37l1	G protein-coupled receptor 37 like 1	-3.25
Gpr50	G protein-coupled receptor 50	-9.07
Grik3	glutamate ionotropic receptor kainate type subunit 3	2.05
H2-Q9	H-2 class I histocompatibility antigen, Q9 α chain (Fragment)	29.46
Hao2	hydroxyacid oxidase 2	7.71
Hbb-b1	hemoglobin subunit β-1	-3.94
Hbb-b2	hemoglobin subunit β-2	-3.87
Hbb-bt	hemoglobin, β adult t chain	-3.87
Hebp1	heme binding protein 1	-2.80
Hist1h4i	histone cluster 1 H4 family member i	-2.32
Hist2h2aa2	histone H2A type 2-A	42.64
Ifi47	GTP-binding protein	-2.48
Il18r1	interleukin 18 receptor 1	3.73
Ism2	isthmin 2	-2.24
Jph2	junctophilin 2	-2.35
Kat6b	lysine acetyltransferase 6B	1.89
Kcnc3	potassium voltage-gated channel subfamily C member 3	1.96
Kdm5d	lysine demethylase 5D	-103.03
Kdm6a	lysine demethylase 6A	1.87

Kdr	kinase insert domain receptor	1.87
Krt76	keratin 76	4.43
L1cam	L1 cell adhesion molecule	1.91
L3mbtl4	L3MBTL4, histone methyl-lysine binding protein	3.16
Lctl	lactase like	-3.83
Lgals3	galectin 3	-1.91
Lmod1	leiomodin 1	-2.23
Lrrc71	leucine rich repeat containing 71	-5.83
Mamld1	mastermind like domain containing 1	2.33
Matn4	matrilin 4	-4.76
Mbd5	methyl-CpG binding domain protein 5	2.03
Mef2d	myocyte enhancer factor 2D	2.19
Mfap4	microfibril associated protein 4	-1.78
Mfi2	melanotransferrin	3.21
Mfsd4	major facilitator superfamily domain containing 4A	1.93
Mgp	matrix Gla protein	-1.97
Mgst1	microsomal glutathione S-transferase 1	-2.01
Mip	major intrinsic protein of lens fiber	-2.17
Mir6236	microRNA 6236	-4.05
Mlana	melan-A	-1.92
Mlph	melanophilin	-1.89
Mt2	metallothionein 2A	-1.94
Muc5ac	mucin 5AC, oligomeric mucus/gel-forming	3.33
Myl9	myosin light chain 9	-2.34
Nbl1	neuroblastoma 1, DAN family BMP antagonist	-1.81
Ndst3	N-deacetylase and N-sulfotransferase 3	2.01
Nop10	NOP10 ribonucleoprotein	-1.81
Npc1	NPC intracellular cholesterol transporter 1	1.83
Npr1	natriuretic peptide receptor 1	-2.37
Npy2r	neuropeptide Y receptor Y2	20.24
Nr4a1	nuclear receptor subfamily 4 group A member 1	2.47
Ntm	neurotrimin	2.25
Nup62-il4i1	Gm21948	24.14
Olfml3	olfactomedin like 3	-3.93
Oscar	osteoclast associated, immunoglobulin-like receptor	6.43
Osr2	odd-skipped related transciption factor 2	1.91
Papln	papilin, proteoglycan like sulfated glycoprotein	2.83
Pappa2	pappalysin 2	2.06
Pcdhgb1	protocadherin gamma subfamily B, 1	1.99
Pdlim2	PDZ and LIM domain 2	-2.53
Penk	proenkephalin	-1.92
Phlda3	pleckstrin homology like domain family A member 3	-1.84
Piwil2	piwi like RNA-mediated gene silencing 2	-3.60
Pltp	phospholipid transfer protein	-2.21
Plxna4	plexin A4	2.08

Pmel	premelanosome protein	-1.98
Pnmal1	PNMA family member 8A	2.02
Pnp	purine nucleoside phosphorylase	-2.28
Pon1	paraoxonase 1	-2.16
Ppargc1b	PPARG coactivator 1 β	1.87
Pqlc3	PQ loop repeat containing 3	-2.96
Prg4	proteoglycan 4	-4.42
Psmb5	proteasome subunit β 5	-1.91
Pstpip2	proline-serine-threonine phosphatase interacting protein 2	2.39
Ptgds	prostaglandin D2 synthase	-1.98
Ptprt	protein tyrosine phosphatase, receptor type T	1.97
Pxdc1	PX domain containing 1	-2.20
Rapsn	receptor associated protein of the synapse	-2.40
Rassf2	Ras association domain family member 2	-2.18
Rb1	RB transcriptional corepressor 1	1.86
Rgs6	regulator of G protein signaling 6	2.01
Rhbdf2	rhomboid 5 homolog 2	2.10
Rimbp2	RIMS binding protein 2	2.08
Rpl22l1	ribosomal protein L22 like 1	-1.95
Rpl37rt	ribosomal protein L37, retrotransposed	-1.90
Rpl39	ribosomal protein L39	-2.29
Rplp1	ribosomal protein lateral stalk subunit P1	-1.95
Rprl3	ribonuclease P RNA-like 3	91.69
Rps14	ribosomal protein S14	-1.87
Rps27l	ribosomal protein S27 like	-1.90
Rps9	ribosomal protein S9	-1.78
Rwdd4a	RWD domain containing 4	1.88
S100a7a	S100 calcium binding protein A7A	2.97
S100b	S100 calcium binding protein B	-1.99
Samd15	sterile α motif domain containing 15	2.83
Sapcd1	suppressor APC domain containing 1	-2.10
Satb2	SATB homeobox 2	2.78
Scn4a	sodium voltage-gated channel α subunit 4	1.98
Scnn1a	sodium channel epithelial 1 α subunit	2.33
Sdhaf4	succinate dehydrogenase complex assembly factor 4	-1.91
Selenbp1	selenium binding protein 1	-2.63
Serpinb3a	MCG129038	2.07
Serpind1	serpin family D member 1	-10.51
Serpine3	serpin family E member 3	-7.56
Sgcg	sarcoglycan gamma	30.85
Sh2d2a	SH2 domain containing 2A	112.30
Shank1	SH3 and multiple ankyrin repeat domains 1	2.67
Shisa7	shisa family member 7	1.91
Sik2	salt inducible kinase 2	3.05
Slc13a3	solute carrier family 13 member 3	-2.00

Slc13a4	solute carrier family 13 member 4	-1.99
Slc38a8	solute carrier family 38 member 8	-2.54
Smco4	single-pass membrane protein with coiled-coil domains 4	-2.90
Spef2	sperm flagellar 2	3.05
Spink5	serine peptidase inhibitor, Kazal type 5	2.18
Srgap1	SLIT-ROBO Rho GTPase activating protein 1	1.85
St8sia2	ST8 α-N-acetyl-neuraminide α-2,8-sialyltransferase 2	1.88
Stac	SH3 and cysteine rich domain	-2.27
Synpo2	synaptopodin 2	1.91
Syt6	synaptotagmin 6	2.08
Tagln	transgelin	-2.31
Tenm2	teneurin transmembrane protein 2	1.87
Tepp	testis, prostate and placenta expressed	8.06
Tfap2b	transcription factor AP-2 β	1.80
Thbd	thrombomodulin	-2.50
Tmed1	transmembrane p24 trafficking protein 1	-1.79
Tmem132b	transmembrane protein 132B	1.88
Tmem254c	transmembrane protein 254c	-3.05
Tmem45a	transmembrane protein 45A	-3.85
Tmod4	tropomodulin 4	3.01
Tox2	TOX high mobility group box family member 2	1.88
Tpm3	tropomyosin 3	-1.79
Tspan10	tetraspanin 10	-1.83
Tspan2	tetraspanin 2	-3.44
Tspo	translocator protein	-2.45
Tst	thiosulfate sulfurtransferase	-1.85
Ttc21a	tetratricopeptide repeat domain 21A	2.53
Ttc27	tetratricopeptide repeat domain 27	-2.08
Uap1l1	UDP-N-acetylglucosamine pyrophosphorylase 1 like 1	-1.91
Unc5c	unc-5 netrin receptor C	1.93
Wif1	WNT inhibitory factor 1	-2.40
Wnt10a	Wnt family member 10A	-2.02
Wnt6	Wnt family member 6	-2.71
Xlr4c	putative uncharacterized protein	-2.23
Zfp319	zinc finger protein 319	1.91
Zfp39	zinc finger protein 39	2.22
Zfp462	zinc finger protein 462	1.79
Zfp488	zinc finger protein 488	2.84
Zfp609	zinc finger protein 609	1.80
Zmiz1	zinc finger MIZ-type containing 1	1.93

Differentially Expressed Genes Unique to *Cngb1*-X26 (448)

Gene Symbol	Gene Name	*Cngb1*-X26 Fold Change
1700003M07Rik	RIKEN cDNA 1700003M07	7.32
1700113A16Rik	RIKEN cDNA 1700113A16	1.72
2310034O05Rik	RIKEN cDNA 2310034O05	-2.58
2700069I18Rik	RIKEN cDNA 2700069I18	-5.00
2810032G03Rik	RIKEN cDNA 2810032G03	2.83
3010001F23Rik	RIKEN cDNA 3010001F23	-3.17
6430411K18Rik	RIKEN cDNA 6430411K18	3.00
9430037G07Rik	RIKEN cDNA 9430037G07	6.84
9530091C08Rik	RIKEN cDNA 9530091C08	2.65
9630028B13Rik	RIKEN cDNA 9630028B13	-3.51
A2m	α-2-macroglobulin	3.35
A730006G06Rik	RIKEN cDNA A730006G06	-8.17
A930004D18Rik	MCG147224	-2.19
A930016O22Rik	RIKEN cDNA A930016O22	2.44
Abcc1	ATP binding cassette subfamily C member 1	1.85
Ache	acetylcholinesterase (Cartwright blood group)	1.76
Acsm1	acyl-CoA synthetase medium chain family member 1	1.73
Adam32	ADAM metallopeptidase domain 32	2.93
Adamts3	ADAM metallopeptidase with thrombospondin type 1 motif 3	2.07
Adamts4	ADAM metallopeptidase with thrombospondin type 1 motif 4	-2.34
Adcy4	adenylate cyclase 4	3.51
Adgrg5	adhesion G protein-coupled receptor G5	29.30
Adipoq	adiponectin, C1Q and collagen domain containing	13.05
Adra2c	adrenoceptor α 2C	-1.99
Adtrp	androgen dependent TFPI regulating protein	-1.90
Agrn	agrin	2.68
AI847159	expressed sequence AI847159	-1.92
Akap5	A-kinase anchoring protein 5	3.56
Akr1b8	aldose reductase-related protein 2	2.88
Aldh1a7	aldehyde dehydrogenase, cytosolic 1 retinal dehydrogenase 2	-2.16
Amer2	APC membrane recruitment protein 2	1.70
Angptl4	angiopoietin like 4	-2.57
Angptl7	angiopoietin like 7	3.68
Ankrd29	ankyrin repeat domain 29	1.75
Ano1	anoctamin 1	2.60
Ano7	anoctamin 7	3.07
Ano9	anoctamin 9	2.41
Aox1	aldehyde oxidase 1	2.94
Arhgap40	Rho GTPase activating protein 40	2.06
Arl4d	ADP ribosylation factor like GTPase 4D	-1.85
Arl6	ADP ribosylation factor like GTPase 6	2.24
Arntl2	aryl hydrocarbon receptor nuclear translocator like 2	2.19

Arsi	arylsulfatase family member I	-2.70
Art1	ADP-ribosyltransferase 1	6.49
Asf1b	anti-silencing function 1B histone chaperone	2.93
Aspn	asporin	3.24
Ass1	argininosuccinate synthase 1	-2.97
Atp13a3	ATPase 13A3	1.77
Atp1a2	ATPase Na+/K+ transporting subunit α 2	-1.88
Atp6v1c1	ATPase H+ transporting V1 subunit C1	-1.68
B230312C02Rik	RIKEN cDNA B230312C02	6.72
Bad	BCL2 associated agonist of cell death	-1.87
Baz2a	bromodomain adjacent to zinc finger domain 2A	1.85
Bbc3	BCL2 binding component 3	2.13
Bcl3	B cell CLL/lymphoma 3	3.86
Bmf	Bcl2 modifying factor	1.90
Bst2	bone marrow stromal cell antigen 2	2.70
C130046K22Rik	RIKEN cDNA C130046K22	-4.27
C1qa	complement C1q A chain	1.74
C1qc	complement C1q C chain	1.93
C1qtnf1	C1q and TNF related 1	2.11
C1ra	complement C1r-A subcomponent	1.97
C1s2	complement component 1, s subcomponent 2	14.08
C4b	complement C4B (Chido blood group)	3.27
Cabp4	calcium binding protein 4	-1.66
Cabp5	calcium binding protein 5	-1.74
Cadm4	cell adhesion molecule 4	-1.68
Cadps2	calcium dependent secretion activator 2	3.77
Calca	calcitonin related polypeptide α	3.86
Cartpt	CART prepropeptide	-1.74
Casq1	calsequestrin 1	1.78
Cbln3	cerebellin 3 precursor	3.12
Cbr2	carbonyl reductase [NADPH] 2	1.97
Ccdc24	coiled-coil domain containing 24	-3.58
Ccdc3	coiled-coil domain containing 3	2.30
Ccno	cyclin O	4.54
Cd276	CD276 molecule	1.72
Cd47	CD47 molecule	2.15
Cdk5rap1	CDK5 regulatory subunit associated protein 1	1.81
Cdr2	cerebellar degeneration related protein 2	-1.95
Ceacam1	carcinoembryonic antigen related cell adhesion molecule 1	1.82
Cebpzos	CEBPZ opposite strand	-2.02
Cenpa	centromere protein A	-2.13
Cep85	centrosomal protein 85	-1.76
Cercam	cerebral endothelial cell adhesion molecule	2.34
Cfap20	cilia and flagella associated protein 20	-1.69
Chad	chondroadherin	5.74

Chd7	chromodomain helicase DNA binding protein 7	2.05
Chrnb4	cholinergic receptor nicotinic β 4 subunit	3.26
Ckmt2	creatine kinase, mitochondrial 2	4.22
Clec2d	C-type lectin domain family 2 member D	2.03
Clec7a	C-type lectin domain containing 7A	3.46
Clrn1	clarin 1	2.18
Cnfn	cornifelin	3.61
Col14a1	collagen type XIV α 1 chain	2.81
Col15a1	collagen type XV α 1 chain	2.54
Col1a1	collagen type I α 1 chain	3.36
Col1a2	collagen type I α 2 chain	2.59
Col20a1	collagen type XX α 1 chain	-1.78
Col3a1	collagen type III α 1 chain	3.31
Col5a3	collagen type V α 3 chain	3.39
Col9a2	collagen type IX α 2 chain	-2.01
Cpq	carboxypeptidase Q	-1.78
Crym	crystallin mu	1.76
Csf2ra	colony stimulating factor 2 receptor α subunit	1.78
Cthrc1	collagen triple helix repeat containing 1	-8.87
Ctss	cathepsin S	1.72
Cutal	CutA divalent cation tolerance homolog-like	-1.85
Cyb561	cytochrome b561	-2.00
Cyp1a2	cytochrome P450 family 1 subfamily A member 2	-20.36
Cyp2a4	cytochrome P450 2A4	-23.65
Cyp3a44	cytochrome P450, CYP3A	-19.97
Cyth4	cytohesin 4	2.17
D17H6S56E-5	DNA segment, Chr 17, human D6S56E 5	2.09
D1Ertd622e	UNC119-binding protein C5orf30 homolog	-1.66
D2hgdh	D-2-hydroxyglutarate dehydrogenase	2.49
D430019H16Rik	MCG1155	1.82
D630045J12Rik	RIKEN cDNA D630045J12	1.70
Ddx60	DExD/H-box helicase 60	2.02
Defb2	defensin β 4A	-22.29
Dixdc1	DIX domain containing 1	1.72
Dleu7	deleted in lymphocytic leukemia, 7	-11.20
Dnttip2	deoxynucleotidyltransferase terminal interacting protein 2	2.40
Dok7	docking protein 7	4.88
Dpep1	dipeptidase 1	3.33
Dpt	dermatopontin	3.94
Dusp15	dual specificity phosphatase 15	-2.02
Dynlt1b	dynein light chain Tctex-type 1B	1.74
E2f2	E2F transcription factor 2	-2.35
E2f6	E2F transcription factor 6	2.87
Ecm1	extracellular matrix protein 1	1.86
Efnb3	ephrin B3	-1.73

Eif4g3	eukaryotic translation initiation factor 4 gamma 3	1.67
Elk3	ELK3, ETS transcription factor	1.76
Enpp1	ectonucleotide pyrophosphatase/phosphodiesterase 1	-2.09
Epas1	endothelial PAS domain protein 1	1.68
Eppk1	epiplakin 1	2.21
Epyc	epiphycan	13.32
Erdr1	uncharacterized protein	1.84
Esrrb	estrogen related receptor β	-2.15
Fabp4	fatty acid binding protein 4	1.96
Fabp7	fatty acid binding protein 7	-10.35
Faim	Fas apoptotic inhibitory molecule	-2.45
Fam46b	family with sequence similarity 46 member B	2.06
Fbxo24	F-box protein 24	2.30
Fbxw21	F-box and WD-40 domain protein 21	10.42
Fcer1g	Fc fragment of IgE receptor Ig	2.58
Fcgr3	Fc fragment of IgG receptor IIIa	2.32
Fgd5	FYVE, RhoGEF and PH domain containing 5	2.36
Fgf2	fibroblast growth factor 2	7.68
Fgr	FGR proto-oncogene, Src family tyrosine kinase	12.24
Fhad1	forkhead associated phosphopeptide binding domain 1	2.13
Fitm1	fat storage inducing transmembrane protein 1	3.81
Flnc	filamin C	2.22
Flt4	fms related tyrosine kinase 4	2.25
Foxe3	forkhead box E3	-3.86
Foxj1	forkhead box J1	-2.45
Foxn1	forkhead box N1	6.19
Frat2	FRAT2, WNT signaling pathway regulator	-1.75
Frem2	FRAS1 related extracellular matrix protein 2	-1.83
Fscn2	fascin actin-bundling protein 2, retinal	-2.86
Fyco1	FYVE and coiled-coil domain containing 1	1.99
Fzd6	frizzled class receptor 6	-1.76
Gadd45b	growth arrest and DNA damage inducible β	3.73
Gas7	growth arrest specific 7	-1.69
Gfy	golgi associated olfactory signaling regulator	3.54
Gja8	gap junction protein α 8	-3.18
Glo1	glyoxalase I	2.11
Gm11961	predicted gene 11961	-3.02
Gm12191	predicted gene 12191	-1.74
Gm14827	predicted gene 14827	2.00
Gm21992	predicted gene 21992	27.46
Gm28042	phospholipase A2	-2.45
Gm3435	predicted gene 3435	2.98
Gm5424	MCG15755	-1.69
Gm5478	uncharacterized protein	2.45
Gm7120	transmembrane protein 267	2.19

Gm7616	predicted gene 7616	-4.08
Gm9573	uncharacterized protein	2.20
Gnb3	G protein subunit β 3	2.46
Gngt1	G protein subunit gamma transducin 1	-2.17
Gpr152	G protein-coupled receptor 152	-1.72
Grin2d	glutamate ionotropic receptor NMDA type subunit 2D	-1.80
Gsto1	glutathione S-transferase omega 1	2.09
Gtf2a1	general transcription factor IIA subunit 1	1.71
H2-Q7	H-2 class I histocompatibility antigen, Q7 α chain	3.51
Hcls1	hematopoietic cell-specific Lyn substrate 1	-2.57
Hcrtr1	hypocretin receptor 1	2.29
Hdac9	histone deacetylase 9	-1.70
Hist1h1c	histone cluster 1 H1 family member c	-1.78
Hist1h2bc	histone cluster 1 H2B family member c	1.72
Hist1h2bg	histone cluster 1 H2B family member g	5.89
Hmgcs2	3-hydroxy-3-methylglutaryl-CoA synthase 2	-2.18
Hpdl	4-hydroxyphenylpyruvate dioxygenase like	-2.98
Hrg	histidine rich glycoprotein	-20.36
Hspb7	heat shock protein family B (small) member 7	2.67
Htra2	HtrA serine peptidase 2	-1.70
Htra3	HtrA serine peptidase 3	-1.95
Ifitm3	interferon induced transmembrane protein 3	1.68
Ift57	intraflagellar transport 57	1.82
Igfbp7	insulin like growth factor binding protein 7	-1.94
Igfn1	immunoglobulin-like and fibronectin type III domain containing 1	1.72
Igsf10	immunoglobulin superfamily member 10	2.49
Igsf9	immunoglobulin superfamily member 9	-2.01
Irf9	interferon regulatory factor 9	1.72
Itgb1bp2	integrin subunit β 1 binding protein 2	2.74
Itgb2	integrin subunit β 2	3.04
Itih5	inter-α-trypsin inhibitor heavy chain family member 5	2.20
Kcng4	potassium voltage-gated channel modifier subfamily G member 4	2.91
Kcnh6	potassium voltage-gated channel subfamily H member 6	1.82
Kcnj14	potassium voltage-gated channel subfamily J member 14	-2.70
Kcns1	potassium voltage-gated channel modifier subfamily S member 1	5.48
Kctd19	potassium channel tetramerization domain containing 19	-5.06
Kif14	kinesin family member 14	2.90
Kif1b	kinesin family member 1B	1.81
Kif27	kinesin family member 27	-3.86
Klf10	Kruppel like factor 10	1.84
Klhl31	kelch like family member 31	3.65
Kprp	keratinocyte proline rich protein	3.90
Krt4	keratin 4	2.36
Krt7	keratin 7	1.67
Krt90	keratin 90	4.44

Lalba	lactalbumin α	8.77
Laptm5	lysosomal protein transmembrane 5	1.99
Lbh	limb bud and heart development	-1.65
Lce3a	late cornified envelope 3A	3.65
Lcn2	lipocalin 2	2.89
Ldb3	LIM domain binding 3	3.18
Ldlrap1	low density lipoprotein receptor adaptor protein 1	-1.72
Lif	LIF, interleukin 6 family cytokine	4.04
Lin28a	lin-28 homolog A	3.34
Lin7b	lin-7 homolog B, crumbs cell polarity complex component	3.20
Lix1	limb and CNS expressed 1	-1.93
Lonrf1	LON peptidase N-terminal domain and ring finger 1	2.01
Lrrc17	leucine rich repeat containing 17	6.59
Lrrc66	leucine rich repeat containing 66	2.15
Ltbp2	latent transforming growth factor β binding protein 2	-2.06
Ly86	lymphocyte antigen 86	2.22
Map3k6	mitogen-activated protein kinase kinase kinase 6	2.59
Marveld3	MARVEL domain containing 3	1.75
Mef2c	myocyte enhancer factor 2C	-2.27
Mfap5	microfibril associated protein 5	2.35
Mfsd2a	major facilitator superfamily domain containing 2A	-2.14
Miat	myocardial infarction associated transcript (non-protein coding)	1.75
Mid1	midline 1	1.80
Mir124a-1hg	Mir124-1 host gene (non-protein coding)	1.73
Mknk1	MAP kinase interacting serine/threonine kinase 1	1.96
Mlf1	myeloid leukemia factor 1	2.30
Mmp17	matrix metallopeptidase 17	-1.83
Mmp2	matrix metallopeptidase 2	2.34
Mob3c	MOB kinase activator 3C	3.55
Mphosph9	M-phase phosphoprotein 9	1.83
Mrc1	mannose receptor C-type 1	2.99
Mtcl1	microtubule crosslinking factor 1	1.87
Muc6	mucin 6, oligomeric mucus/gel-forming	5.27
Mybpc1	myosin binding protein C, slow type	3.17
Mybpc2	myosin binding protein C, fast type	2.49
Mybphl	myosin binding protein H like	3.15
Myh1	myosin heavy chain 1	4.86
Myh15	myosin heavy chain 15	2.24
Myh2	myosin heavy chain 2	4.20
Myh8	myosin heavy chain 8	7.31
Myl1	myosin light chain 1	3.68
Mylk4	myosin light chain kinase family member 4	3.73
Myo18b	myosin XVIIIB	2.31
Myot	myotilin	3.03
Nanos2	nanos C2HC-type zinc finger 2	7.22

Neb	nebulin	2.64
Nlrc5	NLR family CARD domain containing 5	3.69
Notch1	notch 1	2.18
Npff	neuropeptide FF-amide peptide precursor	1.92
Npl	N-acetylneuraminate pyruvate lyase	-1.92
Npvf	neuropeptide VF precursor	-15.99
Nrap	nebulin related anchoring protein	2.56
Nrl	neural retina leucine zipper	-1.83
Nsun4	NOP2/Sun RNA methyltransferase family member 4	1.77
Nt5e	5'-nucleotidase ecto	-1.95
Nudt6	nudix hydrolase 6	2.46
Nxnl1	nucleoredoxin like 1	-2.29
Obscn	obscurin, cytoskeletal calmodulin and titin-interacting RhoGEF	1.97
Olfr1372-ps1	olfactory receptor 1372, pseudogene 1	3.16
Optc	opticin	-1.91
Osbpl6	oxysterol binding protein like 6	2.08
Osmr	oncostatin M receptor	2.42
Oxtr	oxytocin receptor	-2.32
P3h3	prolyl 3-hydroxylase 3	1.73
Parp14	poly(ADP-ribose) polymerase family member 14	2.07
Parp4	poly(ADP-ribose) polymerase family member 4	1.86
Pcdha7	protocadherin α 7	-2.07
Pcdhb15	protocadherin β 15	2.99
Pcmtd2	protein-L-isoaspartate (D-aspartate) O-methyltransferase domain containing 2	-1.77
Pcolce	procollagen C-endopeptidase enhancer	2.21
Pcp2	Purkinje cell protein 2	-1.76
Pcp4l1	Purkinje cell protein 4 like 1	2.39
Pcsk2	proprotein convertase subtilisin/kexin type 2	1.72
Pdc	phosducin	-2.69
Pde6b	phosphodiesterase 6B	-1.92
Pde6d	phosphodiesterase 6D	-1.96
Pde6g	phosphodiesterase 6G	-1.72
Pdia5	protein disulfide isomerase family A member 5	-2.73
Per2	period circadian regulator 2	1.98
Perm1	PPARGC1 and ESRR induced regulator, muscle 1	1.83
Phactr3	phosphatase and actin regulator 3	-1.75
Phf21b	PHD finger protein 21B	1.78
Pkig	cAMP-dependent protein kinase inhibitor gamma	1.96
Plac9b	placenta specific 9b	-2.74
Pld4	phospholipase D family member 4	2.62
Pld5	phospholipase D family member 5	-2.58
Plec	plectin	1.73
Plekha4	pleckstrin homology domain containing A4	1.91
Plekhb1	pleckstrin homology domain containing B1	2.05

Plekhg4	pleckstrin homology and RhoGEF domain containing G4	-2.47
Pmvk	phosphomevalonate kinase	1.83
Postn	periostin	2.03
Ppap2c	phospholipid phosphatase 2	-1.72
Ppm1n	protein phosphatase, Mg2+/Mn2+ dependent 1N (putative)	-2.06
Ppp1r3b	protein phosphatase 1 regulatory subunit 3B	-2.68
Ppp1r3c	protein phosphatase 1 regulatory subunit 3C	-1.67
Ppt1	palmitoyl-protein thioesterase 1	-1.64
Prag1	PEAK1 related kinase activating pseudokinase 1	2.53
Prph	peripherin	3.65
Prph2	peripherin 2	-1.73
Prps1	phosphoribosyl pyrophosphate synthetase 1	-2.35
Ptpn20	protein tyrosine phosphatase, non-receptor type 20	4.35
Ptprr	protein tyrosine phosphatase, receptor type R	-1.89
Pyhin1	pyrin and HIN domain family member 1	3.26
R3hcc1l	R3H domain and coiled-coil containing 1 like	1.97
Rab15	RAB15, member RAS oncogene family	-1.95
Rabgef1	RAB guanine nucleotide exchange factor 1	-2.09
Rasal2	RAS protein activator like 2	1.87
Rasgef1a	RasGEF domain family member 1A	2.00
Rasl11a	RAS like family 11 member A	-2.93
Rbm17	RNA binding motif protein 17	2.16
Rbm3	RNA binding motif protein 3	1.90
Rcn2	reticulocalbin 2	-1.72
Rdh10	retinol dehydrogenase 10	-1.70
Rdh12	retinol dehydrogenase 12	-1.84
Rdh7	retinol dehydrogenase 7	-22.29
Retn	resistin	2.83
Rgr	retinal G protein coupled receptor	-1.80
Rgs16	regulator of G protein signaling 16	-1.75
Rgs20	regulator of G protein signaling 20	-1.77
Rgs9bp	regulator of G protein signaling 9 binding protein	-1.75
Rhbdl2	rhomboid like 2	3.90
Rhebl1	RHEB like 1	1.89
Rho	rhodopsin	-2.04
Rlbp1	retinaldehyde binding protein 1	-1.74
Rnf123	ring finger protein 123	-1.92
Rock2	Rho associated coiled-coil containing protein kinase 2	1.82
Rpl30	ribosomal protein L30	-2.00
Rsc1a1	regulator of solute carriers 1	1.76
Rspo2	R-spondin 2	-2.50
Runx1	runt related transcription factor 1	2.09
Ryr1	ryanodine receptor 1	2.35
Samd11	sterile α motif domain containing 11	1.72
Samd4	sterile α motif domain containing 4A	2.04

Samd7	sterile α motif domain containing 7	2.60
Sbno2	strawberry notch homolog 2	1.84
Scube1	signal peptide, CUB domain and EGF like domain containing 1	3.12
Sdc2	syndecan 2	-6.45
Sebox	SEBOX homeobox	-1.84
Sema4c	semaphorin 4C	-1.91
Sema7a	semaphorin 7A (John Milton Hagen blood group)	-2.46
Serpina3g	serine protease inhibitor A3G	-2.50
Serping1	serpin family G member 1	2.28
Setd1b	SET domain containing 1B	1.73
Sfrp2	secreted frizzled related protein 2	5.84
Sfxn2	sideroflexin 2	1.81
Sh2d1a	SH2 domain containing 1A	-7.48
Slc25a20	solute carrier family 25 member 20	-1.75
Slc25a37	solute carrier family 25 member 37	2.50
Slc37a2	solute carrier family 37 member 2	2.72
Slc38a6	solute carrier family 38 member 6	2.08
Slc43a3	solute carrier family 43 member 3	2.36
Slc6a2	solute carrier family 6 member 2	7.81
Slco4a1	solute carrier organic anion transporter family member 4A1	1.69
Sln	sarcolipin	5.85
Smim15	small integral membrane protein 15	-1.68
Smim17	small integral membrane protein 17	-2.50
Snhg15	small nucleolar RNA host gene 15	2.87
Snx31	sorting nexin 31	-9.20
Sostdc1	sclerostin domain containing 1	-2.17
Spata6	spermatogenesis associated 6	2.35
Spc25	SPC25, NDC80 kinetochore complex component	-2.35
Spsb2	splA/ryanodine receptor domain and SOCS box containing 2	1.88
Srl	sarcalumenin	3.00
Srpk3	SRSF protein kinase 3	2.17
Srrm4	serine/arginine repetitive matrix 4	1.81
St6galnac5	ST6 N-acetylgalactosaminide α-2,6-sialyltransferase 5	2.93
Stab2	stabilin 2	-2.86
Stk32c	serine/threonine kinase 32C	-1.71
Stox1	storkhead box 1	-3.01
Sult3a1	sulfotransferase family 3A, member 1	-22.29
Sult5a1	amine sulfotransferase	3.70
Susd3	sushi domain containing 3	-1.88
Synb	syncytin b	40.88
Syne3	spectrin repeat containing nuclear envelope family member 3	-1.74
Sypl2	synaptophysin like 2	4.03
Tagln3	transgelin 3	-1.64
Tbx15	T-box 15	2.47
Tgm2	transglutaminase 2	-1.68

Thbs1	thrombospondin 1	1.95
Tirap	TIR domain containing adaptor protein	1.90
Tm7sf2	transmembrane 7 superfamily member 2	-1.82
Tmeff1	transmembrane protein with EGF like and two follistatin like domains 1	-2.22
Tmem100	transmembrane protein 100	3.28
Tmem107	transmembrane protein 107	-1.78
Tmem120b	transmembrane protein 120B	2.85
Tmem150c	transmembrane protein 150C	1.88
Tmem218	transmembrane protein 218	-1.78
Tmem229b	transmembrane protein 229B	-1.79
Tmod1	tropomodulin 1	1.72
Tnfaip3	TNF α induced protein 3	-3.04
Tnfrsf8	TNF receptor superfamily member 8	6.33
Tnnt1	troponin T1, slow skeletal type	1.94
Traf3ip3	TRAF3 interacting protein 3	-1.84
Trdn	triadin	2.29
Trhde	thyrotropin releasing hormone degrading enzyme	-2.07
Trim43b	tripartite motif containing 43B	10.55
Trim43c	tripartite motif-containing protein 43C	12.00
Trim72	tripartite motif containing 72	2.71
Tsc22d3	TSC22 domain family member 3	-1.85
Ttc39aos1	Ttc39a opposite strand RNA 1	2.14
Ttn	titin	2.40
Ttyh2	tweety family member 2	2.45
Tyro3	TYRO3 protein tyrosine kinase	2.22
Tyrobp	TYRO protein tyrosine kinase binding protein	2.06
Ubxn7	UBX domain protein 7	1.67
Ufsp1	UFM1 specific peptidase 1 (inactive)	2.43
Upb1	β-ureidopropionase 1	2.83
Uvssa	UV stimulated scaffold protein A	1.95
Vax2os	ventral anterior homeobox 2, opposite strand	-2.06
Vip	vasoactive intestinal peptide	-2.35
Vwc2	von Willebrand factor C domain containing 2	-2.03
Vwf	von Willebrand factor	1.92
Wdr31	WD repeat domain 31	-1.80
Wdr60	WD repeat domain 60	-1.68
Wdr95	WD40 repeat domain 95	3.03
Wnt7a	Wnt family member 7A	-2.83
Wnt9b	Wnt family member 9B	-5.19
Wwox	WW domain containing oxidoreductase	2.14
Wwtr1	WW domain containing transcription regulator 1	1.92
Xiap	X-linked inhibitor of apoptosis	-2.01
Xirp2	xin actin binding repeat containing 2	2.25
Xrcc6bp1	ATP23 metallopeptidase and ATP synthase assembly factor homolog	-2.72
Zbtb7c	zinc finger and BTB domain containing 7C	2.26

Zfp605	zinc finger protein 605	1.85

Commonly Differentially Expressed Genes: GARP2-KO and *Cngb1*-X1 (176)

Gene Symbol	Gene Name	GARP2-KO Fold Change	*Cngb1*-X1 Fold Change
1810009A15Rik	RIKEN cDNA 1810009A15	2.90	-2.20
4930402H24Rik	RIKEN cDNA 4930402H24	-2.88	1.96
4930503L19Rik	RIKEN cDNA 4930503L19	-3.43	2.68
6430562O15Rik	RIKEN cDNA 6430562O15	-44.08	10.37
8030462N17Rik	RIKEN cDNA 8030462N17	-2.48	1.84
9430065F17Rik	RIKEN cDNA 9430065F17	-13.72	19.15
9930021J03Rik	RIKEN cDNA 9930021J03	-2.22	1.83
Abca8b	ATP-binding cassette sub-family A member 8-B	-3.09	2.14
Actn3	actinin α 3 (gene/pseudogene)	2.86	-2.14
Adat2	adenosine deaminase, tRNA specific 2	2.67	-2.74
Adnp	activity dependent neuroprotector homeobox	-4.50	3.45
Ago2	argonaute 2, RISC catalytic component	-3.87	2.43
Alg10b	ALG10B, α-1,2-glucosyltransferase	-3.23	1.95
Apod	apolipoprotein D	2.97	-5.24
Apol9a	Apol9a protein	10.08	-2.85
Arhgap20	Rho GTPase activating protein 20	-3.18	2.14
Arhgap5	Rho GTPase activating protein 5	-3.95	1.99
Arid5b	AT-rich interaction domain 5B	-3.82	2.08
Asb11	ankyrin repeat and SOCS box containing 11	4.55	-2.71
Atp7b	ATPase copper transporting β	-4.75	3.08
BC018473	cDNA sequence BC018473	19.47	-16.43
Bcas1	breast carcinoma amplified sequence 1	2.59	-1.96
Bfsp1	beaded filament structural protein 1	2.66	-3.54
Birc7	baculoviral IAP repeat containing 7	22.58	-6.75
Cacna1e	calcium voltage-gated channel subunit α1 E	-6.22	3.55
Capn11	calpain 11	-8.01	5.54
Car6	Carbonic anhydrase 6	5.36	-4.67
Ccdc171	coiled-coil domain containing 171	-3.55	3.09
Ccdc186	coiled-coil domain containing 186	-4.71	2.49
Ccdc39	coiled-coil domain containing 39	-2.38	2.89
Ccnt1	cyclin T1	-4.48	2.50
Cdkl5	cyclin dependent kinase like 5	-3.45	4.08
Cep295	centrosomal protein 295	-2.43	2.35
Cers6	ceramide synthase 6	-4.71	2.32
Ces1d	Carboxylesterase 1D	2.19	-2.39
Chat	choline O-acetyltransferase	-2.67	2.09
Chrm2	cholinergic receptor muscarinic 2	-8.98	5.61
Chst5	carbohydrate sulfotransferase 5	2.50	-2.65
Cit	citron rho-interacting serine/threonine kinase	-4.95	3.56
Cldn11	claudin 11	5.00	-15.40

Clvs1	clavesin 1	-3.12	2.56
Cnksr2	connector enhancer of kinase suppressor of Ras 2	-2.73	2.13
Cnp	2',3'-cyclic nucleotide 3' phosphodiesterase	2.91	-2.87
Cntn5	contactin 5	-7.69	4.55
Crebbp	CREB binding protein	-2.75	2.47
Crybb2	crystallin β B2	2.43	-2.91
Crybb3	crystallin β B3	2.46	-2.92
Crygb	crystallin gamma B	5.01	-4.20
Crygc	crystallin gamma C	3.94	-4.30
Crygd	crystallin gamma D	3.92	-3.87
Cryge	Gamma-crystallin E	11.61	-3.87
Ddi2	DNA damage inducible 1 homolog 2	-2.60	2.23
Diap2	Protein diaphanous homolog 2	-2.44	2.21
Elfn2	extracellular leucine rich repeat and fibronectin type III domain containing 2	-2.49	2.04
Etfb	electron transfer flavoprotein β subunit	2.19	-1.98
Fa2h	fatty acid 2-hydroxylase	7.91	-6.10
Fam171b	family with sequence similarity 171 member B	-3.19	2.36
Fam8a1	family with sequence similarity 8 member A1	-3.23	2.14
Fktn	fukutin	-3.82	2.35
Flrt1	fibronectin leucine rich transmembrane protein 1	-2.78	2.19
Foxo3	forkhead box O3	-3.58	2.19
Gabbr2	gamma-aminobutyric acid type B receptor subunit 2	-2.59	2.57
Gal3st1	galactose-3-O-sulfotransferase 1	3.34	-2.23
Garem	GRB2 associated regulator of MAPK1 subtype 1	-2.77	2.20
Gatad2b	GATA zinc finger domain containing 2B	-5.42	3.37
Gjc2	gap junction protein gamma 2	3.65	-2.74
Glg1	golgi glycoprotein 1	-2.94	2.10
Gpr137b-ps	G protein-coupled receptor 137B, pseudogene	-4.06	4.31
Gpr17	G protein-coupled receptor 17	5.74	-12.79
Grifin	galectin-related inter-fiber protein	2.20	-2.80
Gucy1a2	guanylate cyclase 1 soluble subunit α 2	-3.82	2.27
Hapln2	hyaluronan and proteoglycan link protein 2	4.96	-14.00
Hba-a1	Hemoglobin subunit α	2.22	-4.69
Hcn4	hyperpolarization activated cyclic nucleotide gated potassium channel 4	-2.63	2.55
Heg1	heart development protein with EGF like domains 1	-3.26	2.66
Hemk1	HemK methyltransferase family member 1	2.86	-1.82
Hfe2	hemojuvelin BMP co-receptor	3.61	-2.99
Hist1h2bk	histone cluster 1 H2B family member k	56.67	-198.42
Hivep3	human immunodeficiency virus type I enhancer binding protein 3	-3.83	4.35
Hspb1	heat shock protein family B (small) member 1	2.24	-1.82
Igfals	insulin like growth factor binding protein acid labile subunit	3.63	-5.59
Ikzf4	IKAROS family zinc finger 4	-2.65	2.91
Irs2	insulin receptor substrate 2	-3.42	2.52

Isg15	ISG15 ubiquitin-like modifier	3.78	-2.35
Itgb8	integrin subunit β 8	-5.84	2.30
Klf5	Kruppel like factor 5	-2.57	1.96
Klf9	Kruppel like factor 9	-2.36	2.00
Klhl30	kelch like family member 30	4.57	-9.28
Klhl34	kelch like family member 34	-4.90	3.22
Klk6	kallikrein related peptidase 6	4.61	-9.40
Lactbl1	lactamase β like 1	-3.25	1.92
Lenep	lens epithelial protein	4.50	-3.31
Lgsn	lengsin, lens protein with glutamine synthetase domain	7.97	-3.02
Lim2	lens intrinsic membrane protein 2	2.61	-3.59
Lmln	leishmanolysin like peptidase	-2.72	2.26
Lrch3	leucine rich repeats and calponin homology domain containing 3	-2.39	1.83
Lrrc8b	leucine rich repeat containing 8 VRAC subunit B	-2.82	2.12
Lypd2	LY6/PLAUR domain containing 2	2.61	-2.03
Lyst	lysosomal trafficking regulator	-3.28	1.95
Mag	myelin associated glycoprotein	6.23	-17.01
Map3k13	mitogen-activated protein kinase kinase kinase 13	-2.52	2.19
Mbp	myelin basic protein	4.95	-5.48
Mobp	myelin-associated oligodendrocyte basic protein	5.07	-8.79
Mog	myelin oligodendrocyte glycoprotein	6.37	-11.28
Myb	MYB proto-oncogene, transcription factor	-2.94	3.00
Myl2	myosin light chain 2	11.22	-4.64
Nebl	nebulette	-5.12	2.01
Necab1	N-terminal EF-hand calcium binding protein 1	-2.56	2.00
Nek5	NIMA related kinase 5	-22.37	20.24
Nkx6-2	NK6 homeobox 2	13.12	-4.21
Nptxr	neuronal pentraxin receptor	-2.37	2.64
Nr2c2	nuclear receptor subfamily 2 group C member 2	-5.03	2.58
Nr3c2	nuclear receptor subfamily 3 group C member 2	-3.24	2.22
Nrip1	nuclear receptor interacting protein 1	-5.05	2.98
Ntsr2	neurotensin receptor 2	12.63	-6.68
Olig2	oligodendrocyte transcription factor 2	7.46	-7.41
Opalin	oligodendrocytic myelin paranodal and inner loop protein	8.66	-7.55
Osr1	odd-skipped related transciption factor 1	4.35	-7.90
Pakap	paralemmin A kinase anchor protein	-51.21	37.25
Pcdh17	protocadherin 17	-3.16	2.07
Pcdha6	protocadherin α 6	-3.03	2.66
Pcdhac2	protocadherin α subfamily C, 2	-2.28	2.17
Pde3a	phosphodiesterase 3A	-4.20	2.58
Pdpr	pyruvate dehydrogenase phosphatase regulatory subunit	-5.56	3.13
Peg3	paternally expressed 3	-4.77	2.35
Plbd1	phospholipase B domain containing 1	2.85	-2.48
Plxnb3	plexin B3	4.74	-7.42

Ppp1r14b	protein phosphatase 1 regulatory inhibitor subunit 14B	2.23	-1.99
Prr18	proline rich 18	3.53	-5.25
Ptch1	patched 1	-3.99	1.95
Rassf8	Ras association domain family member 8	-3.44	2.43
Rec8	REC8 meiotic recombination protein	-16.35	30.05
Rgs7bp	regulator of G protein signaling 7 binding protein	-2.37	1.85
Rims1	regulating synaptic membrane exocytosis 1	-3.01	2.24
Rplp2-ps1	ribosomal protein, large, P2	3.79	-3.61
Rsbn1	round spermatid basic protein 1	-3.04	1.84
Sdk2	sidekick cell adhesion molecule 2	-3.69	2.91
Shank2	SH3 and multiple ankyrin repeat domains 2	-3.91	3.08
Slc16a8	solute carrier family 16 member 8	2.20	-2.24
Slc22a6	solute carrier family 22 member 6	5.66	-59.15
Slc25a36	solute carrier family 25 member 36	-2.57	1.89
Slc2a4	solute carrier family 2 member 4	2.43	-2.22
Slc36a4	solute carrier family 36 member 4	-5.02	2.62
Slurp1	secreted LY6/PLAUR domain containing 1	2.22	-1.96
Spen	spen family transcriptional repressor	-2.37	2.16
Stx1b	syntaxin 1B	-2.99	2.34
Sugct	succinyl-CoA:glutarate-CoA transferase	-16.27	17.49
Supt20	Transcription factor SPT20 homolog	-2.77	2.10
Syn3	synapsin III	-2.39	2.11
Syngap1	synaptic Ras GTPase activating protein 1	-2.30	2.40
Tenm4	teneurin transmembrane protein 4	-3.09	2.01
Tmem160	transmembrane protein 160	2.61	-1.81
Tmem256	transmembrane protein 256	2.26	-2.06
Tmem88b	transmembrane protein 88B	3.93	-5.59
Tnks	tankyrase	-5.30	2.45
Trip11	thyroid hormone receptor interactor 11	-3.72	2.22
Trpm6	transient receptor potential cation channel subfamily M member 6	-2.70	2.50
Tsen54	tRNA splicing endonuclease subunit 54	2.56	-2.55
Ugt1a6b	UDP-glucuronosyltransferase	2.64	-2.30
Ush2a	usherin	-2.60	1.90
Usp34	ubiquitin specific peptidase 34	-2.63	1.84
Usp53	ubiquitin specific peptidase 53	-4.38	3.08
Vmn2r29	Vomeronasal 2, receptor 29	-6.04	5.81
Vps13c	vacuolar protein sorting 13 homolog C	-3.98	2.05
Wasf3	WAS protein family member 3	-2.43	1.99
Wwc2	WW and C2 domain containing 2	-2.44	1.92
Xntrpc	Xndc1-transient receptor potential cation channel, sub-family C, member 2 readthrough	-19.29	44.09
Xrn1	5'-3' exoribonuclease 1	-6.05	3.72
Zbtb38	zinc finger and BTB domain containing 38	-4.93	3.50
Zfp236	Zinc finger protein 236	-2.54	1.92
Zfp429	Regulator of sex-limitation 2	-80.16	80.04

Zfp738	Zinc finger protein 738	-3.46	2.77
Zfp804a	zinc finger protein 804A	-2.64	2.01
Zfp804b	Zinc finger protein 804B	-9.02	4.21
Zkscan2	zinc finger with KRAB and SCAN domains 2	-3.64	2.35
Zmynd10	zinc finger MYND-type containing 10	5.16	-2.92

Commonly Differentially Expressed Genes: GARP2-KO and *Cngb1*-X26 (93)

Gene Symbol	Gene Name	GARP2-KO Fold Change	*Cngb1*-X26 Fold Change
0610010B08Rik	RIKEN cDNA 0610010B08	-4.88	2.31
1700029J07Rik	RIKEN cDNA 1700029J07	-2.63	2.10
2010107G23Rik	RIKEN cDNA 2010107G23	2.37	-1.87
A930031H19Rik	RIKEN cDNA A930031H19	-52.06	210.68
Abcc9	ATP binding cassette subfamily C member 9	-3.40	3.42
Actc1	actin, α, cardiac muscle 1	2.90	2.64
Actn2	actinin α 2	2.71	2.05
Adgrf5	adhesion G protein-coupled receptor F5	-3.77	2.76
AI429214	expressed sequence AI429214	2.97	-3.84
Aldob	aldolase, fructose-bisphosphate B	3.89	-2.63
Alox5	arachidonate 5-lipoxygenase	3.82	-3.33
Ambp	α-1-microglobulin/bikunin precursor	28.94	-39.72
Anxa8	annexin A8	-2.88	2.54
Apoa4	apolipoprotein A4	33.13	-12.74
Apoc3	apolipoprotein C3	16.42	-8.04
Apof	apolipoprotein F	20.56	-12.29
Atp2a1	ATPase sarcoplasmic/endoplasmic reticulum Ca2+ trans-porting 1	2.47	2.42
Atp6v0c-ps2	ATPase, H+ transporting, lysosomal 16kDa, V0 subunit c	-94.80	142.17
AW046200	expressed sequence AW046200	-4.89	7.81
B3gnt3	UDP-GlcNAc:βGal β-1,3-N-acetylglucosaminyltransferase 3	-6.29	4.29
B3gnt7	UDP-GlcNAc:βGal β-1,3-N-acetylglucosaminyltransferase 7	7.96	-3.50
BC002163	NADH dehydrogenase Fe-S protein 5 pseudogene	8.86	-3.39
Casc1	cancer susceptibility 1	3.67	-3.51
Ccbe1	collagen and calcium binding EGF domains 1	-3.34	3.05
Cfd	complement factor D	20.56	3.65
Ckm	creatine kinase, M-type	3.13	2.17
Cml2	probable N-acetyltransferase CML2	9.15	-6.87
Cox6a2	cytochrome c oxidase subunit 6A2	5.22	2.02
Csmd2	CUB and Sushi multiple domains 2	-2.42	2.15
Cyp2a12	cytochrome P450 2A12	23.35	-31.97
Cyp2c29	cytochrome P450 2C29	21.95	-30.04
Cyp2d26	cytochrome P450 2D26	19.16	-26.16
D4Ertd617e	DNA segment, Chr 4, ERATO Doi 617, expressed	-21.61	47.00
Ddr2	discoidin domain receptor tyrosine kinase 2	-2.89	2.61
Des	desmin	2.34	2.64
Drd4	dopamine receptor D4	2.24	1.89
Edn3	endothelin 3	-2.83	2.00
Extl1	exostosin like glycosyltransferase 1	-2.65	2.87
Gas5	growth arrest specific 5 (non-protein coding)	-2.45	2.04
Glb1l3	galactosidase β 1 like 3	-2.70	-6.84

Gm10409	predicted gene 10409	13.85	-2.51
Gm2083	major urinary protein LOC100048885	22.07	-30.19
Gpsm3	G protein signaling modulator 3	3.00	-1.99
H19	H19, imprinted maternally expressed transcript (non-protein coding)	2.47	2.54
H2-T24	histocompatibility 2, T region locus 24	-3.86	3.24
Hbb-bs	hemoglobin, β adult s chain	240.47	-4.44
Hdc	histidine decarboxylase	-3.64	-2.83
Heatr5a	HEAT repeat containing 5A	-3.74	1.81
Hyi	hydroxypyruvate isomerase (putative)	3.17	-2.05
Ifi203	interferon-activable protein 203	4.77	-3.09
Ifi204	interferon-activable protein 204	-7.54	11.26
Kng1	kininogen 1	18.98	-57.14
LOC100861615	α takusan-like	79.13	-2.88
Lum	lumican	-2.95	3.02
Macrod1	MACRO domain containing 1	2.57	-1.68
Mb	myoglobin	4.40	2.66
Mcm6	minichromosome maintenance complex component 6	-3.11	3.34
Mef2b	myocyte enhancer factor 2B	3.57	-3.63
Mettl7b	methyltransferase like 7B	20.56	-28.10
Myh3	myosin heavy chain 3	3.22	3.61
Mylpf	myosin light chain, phosphorylatable, fast skeletal muscle	2.97	2.63
Myoz1	myozenin 1	3.69	2.25
Ndufs5	NADH:ubiquinone oxidoreductase subunit S5	-3.86	4.58
Nnat	neuronatin	2.19	-1.98
Ocel1	occludin/ELL domain containing 1	4.22	-2.17
Pah	phenylalanine hydroxylase	19.16	-11.44
Pcdhgb8	uncharacterized protein	2.48	-2.14
Pde6c	phosphodiesterase 6C	-4.35	3.75
Peg10	paternally expressed 10	-2.85	2.20
Pi16	peptidase inhibitor 16	3.16	3.10
Pla2g2f	phospholipase A2 group IIF	3.82	-2.07
Plg	plasminogen	6.39	-26.68
R3hdml	R3H domain containing like	3.73	-3.01
Rab7b	RAB7B, member RAS oncogene family	-2.28	2.63
Rgs5	regulator of G protein signaling 5	-5.36	2.14
Rpl3l	ribosomal protein L3 like	4.35	3.10
Rtkn2	rhotekin 2	15.90	-7.87
Serinc2	serine incorporator 2	-3.07	4.79
Serpina1d	α-1-antitrypsin 1-4	23.36	-13.25
Serpina3m	serine protease inhibitor A3M	32.65	-44.86
Serpinc1	serpin family C member 1	13.87	-5.60
Sla2	Src like adaptor 2	3.97	-3.05
Slc25a18	solute carrier family 25 member 18	4.41	-2.42
Slc27a2	solute carrier family 27 member 2	4.76	-6.10

Slc30a2	solute carrier family 30 member 2	4.84	-7.20
Slco1b2	solute carrier organic anion transporter family member 1B2	28.94	-11.12
Tnnt3	troponin T3, fast skeletal type	3.33	2.56
Trem2	triggering receptor expressed on myeloid cells 2	2.95	2.08
Trpc1	transient receptor potential cation channel subfamily C member 1	-2.50	-2.45
Uhmk1	U2AF homology motif kinase 1	-2.82	-2.15
Wdr63	WD repeat domain 63	3.02	-3.87
Xlr3a	X-linked lymphocyte-regulated protein 3A	5.82	-3.39
Xlr3b	X-linked lymphocyte-regulated protein 3B	3.16	-1.86

Commonly Differentially Expressed Genes: *Cngb1*-X26 and *Cngb1*-X1 (143)

Gene Symbol	Gene Name	*Cngb1*-X26 Fold Change	*Cngb1*-X1 Fold Change
1700119H24Rik	RIKEN cDNA 1700119H24	-7.11	-2.97
2900057B20Rik	RIKEN cDNA 2900057B20	29.54	11.89
3110070M22Rik	RIKEN cDNA 3110070M22	3.65	2.87
5330413P13Rik	RIKEN cDNA 5530413P13	2.42	2.50
5730507C01Rik	RIKEN cDNA 5730507C01	4.05	5.39
6530402F18Rik	RIKEN cDNA 6530402F18	2.01	1.91
9330159M07Rik	RIKEN cDNA 9330159M07	16.14	6.55
Acoxl	acyl-CoA oxidase like	7.99	4.97
Adam7	ADAM metallopeptidase domain 7	2.42	-2.83
Agtpbp1	ATP/GTP binding protein 1	2.86	2.20
Ahr	aryl hydrocarbon receptor	2.24	1.96
Antxr2	anthrax toxin receptor 2	5.89	3.81
Apbb1ip	amyloid β precursor protein binding family B member 1 interacting protein	4.22	4.43
Apold1	apolipoprotein L domain containing 1	2.39	2.33
Atf3	activating transcription factor 3	4.62	2.54
Atf7	activating transcription factor 7	2.01	1.81
Atp5e	ATP synthase F1 subunit epsilon	1.75	-2.40
Aurka	aurora kinase A	-2.17	-2.26
BC051142	cDNA sequence BC051142	4.06	3.40
Bcl6	B cell CLL/lymphoma 6	2.12	1.91
Bmp6	bone morphogenetic protein 6	-2.58	-2.06
Bmp7	bone morphogenetic protein 7	-1.72	-1.82
Bok	BOK, BCL2 family apoptosis regulator	-2.16	-2.29
Btc	βcellulin	2.25	2.20
C1qb	complement C1q B chain	1.82	-2.17
Ccl28	C-C motif chemokine ligand 28	17.77	7.49
Cdsn	corneodesmosin	4.51	3.13
Cebpd	CCAAT enhancer binding protein delta	4.46	3.51
Cfi	complement factor I	9.21	3.70
Cngb1	cyclic nucleotide gated channel β 1	-2.25	-12.55
Crygn	crystallin gamma N	-1.90	-2.22
Cryzl2	crystallin zeta like 2	3.15	2.62
Ctxn1	cortexin 1	2.09	2.53
Cyp2a5	cytochrome P450 2A5	2.32	2.03
Cyp2f2	cytochrome P450 2F2	2.12	2.43
Dcbld2	discoidin, CUB and LCCL domain containing 2	1.71	1.82
Ddx3y	DEAD-box helicase 3, Y-linked	-1.86	-524.36
E130310I04Rik	RIKEN cDNA E130310I04	-6.07	-1.95
Edn2	endothelin 2	19.52	8.10
Egr1	early growth response 1	1.91	4.59
Eif4e3	eukaryotic translation initiation factor 4E family member 3	4.39	1.97

Enpp3	ectonucleotide pyrophosphatase/phosphodiesterase 3	1.80	2.06
Fam3c	family with sequence similarity 3 member C	-2.84	-1.81
Fam78b	family with sequence similarity 78 member B	2.37	1.89
Fosb	FosB proto-oncogene, AP-1 transcription factor subunit	3.32	2.81
Frmpd1	FERM and PDZ domain containing 1	1.86	1.98
Gabrp	gamma-aminobutyric acid type A receptor pi subunit	4.73	4.33
Gbp6	guanylate binding protein family member 6	2.29	2.02
Ggt1	gamma-glutamyltransferase 1	-2.41	-2.23
Gja3	gap junction protein α 3	-2.02	-2.11
Gm12992	predicted gene 12992	2.68	2.36
Gm4792	predicted gene, EG215472	1.81	1.97
Gm5512	predicted gene 5512	3.27	2.85
Greb1	growth regulating estrogen receptor binding 1	2.30	2.12
Guca1a	guanylate cyclase activator 1A	-2.28	-2.03
Guca1b	guanylate cyclase activator 1B	-3.43	-2.29
H2-Q4	histocompatibility 2, Q region locus 4	2.21	2.06
H2-Q6	class Ib MHC antigen Qa-2	-24.17	-19.81
H2-Q8	H-2 class I histocompatibility antigen, Q8 α chain	62.63	33.17
Heatr5b	HEAT repeat containing 5B	1.77	2.29
Hes5	hes family bHLH transcription factor 5	-2.72	-2.19
Hist2h3c1	histone cluster 2, H3c1	83.20	45.47
Id3	inhibitor of DNA binding 3, HLH protein	-2.35	-2.38
Igsf11	immunoglobulin superfamily member 11	2.48	1.95
Impg2	interphotoreceptor matrix proteoglycan 2	4.96	4.62
Ins2	insulin-2	-6.78	-6.64
Ipo5	importin 5	2.65	2.02
Islr	immunoglobulin superfamily containing leucine rich repeat	-1.69	-1.97
Itga4	integrin subunit α 4	2.26	1.85
Itih2	inter-α-trypsin inhibitor heavy chain 2	-3.28	-14.30
Jak3	Janus kinase 3	1.94	1.85
Klhl29	kelch like family member 29	3.60	2.97
Klk10	kallikrein related peptidase 10	3.00	4.99
Krt17	keratin 17	2.91	3.67
Lars2	leucyl-tRNA synthetase 2, mitochondrial	-1.83	-3.92
Limch1	LIM and calponin homology domains 1	1.80	1.80
Lrfn2	leucine rich repeat and fibronectin type III domain containing 2	2.39	2.60
Lrrc2	leucine rich repeat containing 2	7.85	4.50
Map1b	microtubule associated protein 1B	1.81	1.91
Matn3	matrilin 3	-3.39	-2.95
Mctp1	multiple C2 and transmembrane domain containing 1	10.03	4.99
Mkrn2os	MKRN2 opposite strand	2.95	2.37
Mpeg1	macrophage expressed 1	2.03	2.12
Muc4	mucin 4, cell surface associated	2.29	1.94
Muc5b	mucin 5B, oligomeric mucus/gel-forming	3.38	6.20
Myh7b	myosin heavy chain 7B	-2.84	-2.84

Myo10	myosin X	2.68	1.81
Myo1g	myosin IG	5.38	3.34
Myo5b	myosin VB	2.52	1.91
Myo7a	myosin VIIA	1.79	2.05
Nav1	neuron navigator 1	2.90	1.93
Ncoa6	nuclear receptor coactivator 6	1.82	2.25
Npy4r	neuropeptide Y receptor Y4	18.95	25.45
Padi4	peptidyl arginine deiminase 4	-3.22	-3.03
Pbxip1	PBX homeobox interacting protein 1	2.54	2.31
Pcdh15	protocadherin related 15	1.87	2.19
Pcdhb20	protocadherin β 20	1.88	1.86
Pdlim3	PDZ and LIM domain 3	3.93	2.93
Pdzph1	MCG20355	-5.93	-2.84
Phgdh	phosphoglycerate dehydrogenase	-1.66	-1.92
Plekhf2	pleckstrin homology and FYVE domain containing 2	-2.26	-1.86
Plxna2	plexin A2	1.74	1.87
Polr2a	RNA polymerase II subunit A	1.75	1.92
Prtg	protogenin	8.71	3.87
Ptgis	prostaglandin I2 synthase	-2.07	-2.03
Rab37	RAB37, member RAS oncogene family	-3.33	-2.78
Rfx2	regulatory factor X2	5.10	2.92
Rgs22	regulator of G protein signaling 22	7.80	7.87
Rgs9	regulator of G protein signaling 9	1.75	1.89
Rmrp	RNA component of mitochondrial RNA processing endoribonu-clease	-2.16	-3.07
Rn45s	45S pre-ribosomal RNA	-2.03	-2.97
Rnf144b	ring finger protein 144B	3.08	1.93
Rpe65	RPE65, retinoid isomerohydrolase	-1.75	-2.28
Rpph1	ribonuclease P RNA component H1	-2.84	-3.59
Scn8a	sodium voltage-gated channel α subunit 8	2.07	1.84
Sec22c	SEC22 homolog C, vesicle trafficking protein	3.43	2.91
Serpine1	serpin family E member 1	-2.14	-2.91
Slc16a1	solute carrier family 16 member 1	-1.80	-1.88
Slc6a13	solute carrier family 6 member 13	-2.46	-1.95
Snapc3	small nuclear RNA activating complex polypeptide 3	-2.26	-1.88
Socs3	suppressor of cytokine signaling 3	6.11	2.05
Sox1	SRY-box 1	-2.22	-2.53
Spon2	spondin 2	-1.71	-2.24
Sprr1a	small proline rich protein 1A	3.70	8.12
Stat3	signal transducer and activator of transcription 3	3.37	2.17
Stk32a	serine/threonine kinase 32A	2.03	2.79
Tbc1d30	TBC1 domain family member 30	2.37	2.02
Tceanc2	transcription elongation factor A N-terminal and central domain containing 2	9.91	5.17
Tgfbr3l	transforming growth factor β receptor 3 like	2.70	2.86
Tmem261	distal membrane arm assembly complex 1	-1.80	-2.10

Tmem37	transmembrane protein 37	-2.46	-2.23
Tnfrsf11b	TNF receptor superfamily member 11b	-3.19	-2.95
Tnnt2	troponin T2, cardiac type	15.11	5.80
Ttc28	tetratricopeptide repeat domain 28	2.24	2.32
Ubap1l	ubiquitin associated protein 1 like	2.29	2.33
Uty	ubiquitously transcribed tetratricopeptide repeat containing, Y-linked	-2.40	-217.89
Vsig10l	V-set and immunoglobulin domain containing 10 like	2.51	2.11
Wfdc5	WAP four-disulfide core domain 5	33.16	39.48
Wfikkn2	WAP, follistatin/kazal, immunoglobulin, kunitz and netrin domain containing 2	-2.05	-2.75
Wnt3a	Wnt family member 3A	-2.08	-2.35
Xist	X inactive specific transcript (non-protein coding)	2.10	3.26
Xylb	xylulokinase	2.31	2.01
Zfyve28	zinc finger FYVE-type containing 28	2.29	1.88

Commonly Differentially Expressed Genes: GARP2-KO, *Cngb1*-X1, and *Cngb1*-X26 (111)

Gene Symbol	Gene Names	GARP2-KO Fold Change	*Cngb1*-X26 Fold Change	*Cngb1*-X1 Fold Change
1700030C10Rik	RIKEN cDNA 1700030C10	-10.72	12.81	40.33
2410018L13Rik	RIKEN cDNA 2410018L13	-4.31	4.81	8.12
2610507I01Rik	RIKEN cDNA 2610507I01	-4.08	3.54	5.61
4833420G17Rik	RIKEN cDNA 4833420G17	-3.42	3.29	2.45
A930013F10Rik	RIKEN cDNA A930013F10	-4.34	2.29	3.10
Acaa1b	3-ketoacyl-CoA thiolase B, peroxisomal	5.03	-3.63	-2.56
Acta1	actin, α 1, skeletal muscle	2.88	2.48	-1.85
Ahcy	adenosylhomocysteinase	-2.67	2.86	3.01
Ahrr	aryl-hydrocarbon receptor repressor	-2.51	3.58	2.89
Ahsg	α 2-HS glycoprotein	315.30	-38.66	-5.77
Akr1c6	estradiol 17 β-dehydrogenase 5	17.76	-24.23	-19.86
Alb	albumin	764.85	-101.37	-6.44
Ankrd52	ankyrin repeat domain 52	-2.19	1.74	2.00
Apcs	amyloid P component, serum	21.95	-30.04	-24.57
Apoa1	apolipoprotein A1	77.28	-23.83	-6.33
Apoa2	apolipoprotein A2	4.78	-2.72	-7.05
Apoa5	apolipoprotein A5	30.33	-41.65	-14.32
Apob	apolipoprotein B	133.71	-30.09	-7.43
Apoh	apolipoprotein H	9.71	-3.71	-4.15
Bhmt	βine--homocysteine S-methyltransferase	9.65	-7.65	-5.19
C330024D21Rik	RIKEN cDNA C330024D21	-8.43	9.60	7.15
Cep250	centrosomal protein 250	-2.44	2.24	2.34
Ces1c	carboxylesterase 1C	64.96	-89.64	-6.22
Clca3b	chloride channel accessory 3B	-2.73	2.20	2.62
Cps1	carbamoyl-phosphate synthase 1	3.43	-2.53	-5.72
Cryga	crystallin gamma A	11.20	3.05	-2.78
Crygf	gamma-crystallin F	5.81	4.29	-3.47
Cyp24a1	cytochrome P450 family 24 subfamily A member 1	5.57	-3.89	-2.70
Cyp2e1	cytochrome P450 family 2 subfamily E member 1	33.82	-2.80	-3.94
Cyp2j13	cytochrome P450, family 2, subfamily j, polypeptide 13	6.25	-5.40	-5.82
Cyp3a11	cytochrome P450 3A11	30.48	-40.25	-3.97
Cyp3a41a	cytochrome P450 3A41	15.17	-45.60	-7.26
Dbx2	developing brain homeobox 2	5.73	-3.65	-3.78
Dvl3	dishevelled segment polarity protein 3	-2.41	1.74	2.43
Eps8	epidermal growth factor receptor pathway substrate 8	-2.42	1.78	2.09
Fabp1	fatty acid binding protein 1	47.10	-28.38	-3.95
Fga	fibrinogen α chain	75.04	-45.31	-7.03
Fgb	fibrinogen β chain	70.84	-27.37	-8.61
Fgg	fibrinogen gamma chain	61.07	-23.58	-7.42
Gbp8	guanylate binding protein 8	5.44	-5.37	-7.63

Gc	GC, vitamin D binding protein	122.53	-47.42	-4.84
Gjb1	gap junction protein β 1	7.56	-3.10	-8.19
Glp2r	glucagon like peptide 2 receptor	-3.04	2.85	2.57
Gm4737	predicted gene 4737	6.53	-5.46	-4.32
Gm6793	EG627828 protein	-7.44	5.13	7.71
Gm7334	predicted gene 7334	-141.82	126.59	47.01
Gm7609	predicted pseudogene 7609	6.48	-2.83	-3.78
Gm8615	predicted pseudogene 8615	9.30	-8.36	-2.98
Gm9855	predicted pseudogene 9855	-2.42	2.49	2.86
Gprc5a	G protein-coupled receptor class C group 5 member A	-5.30	7.01	5.04
Gsta2	glutathione S-transferase α 2	2.31	-1.70	-2.19
Gstk1	glutathione S-transferase kappa 1	2.33	-1.94	-1.95
Gzmm	granzyme M	2.95	-2.26	-1.93
H60c	histocompatibility antigen 60c	-32.13	20.01	27.92
Hmox1	heme oxygenase 1	2.72	1.88	-2.75
Hp	haptoglobin	21.82	-3.80	-5.13
Hpd	4-hydroxyphenylpyruvate dioxygenase	41.51	-57.14	-4.39
Hpx	hemopexin	8.82	-4.27	-2.62
Ifi202b	interferon-activable protein 202	2.21	-1.80	-1.78
Igfbp2	insulin like growth factor binding protein 2	2.66	-1.78	-2.02
Itih4	inter-α-trypsin inhibitor heavy chain family member 4	36.22	-9.69	-5.09
Kcnk15	potassium two pore domain channel subfamily K member 15	20.56	-12.29	-23.00
Kmt2a	lysine methyltransferase 2A	-2.43	2.30	2.08
Kmt2e	lysine methyltransferase 2E	-2.46	1.73	2.28
Krt16	keratin 16	-2.65	5.85	2.93
Krt75	keratin 75	-6.33	7.00	10.33
Mat1a	methionine adenosyltransferase 1A	24.09	-20.33	-3.67
Med12	mediator complex subunit 12	-2.24	1.76	2.10
Msx1	msh homeobox 1	3.20	-6.22	-3.09
Mt3	metallothionein 3	3.46	-1.83	-1.93
Mug1	murinoglobulin-1	18.51	-37.69	-8.91
Mup9	major urinary protein 9	47.50	-18.32	-53.32
Myh13	myosin heavy chain 13	32.72	4.26	-2.28
Myh4	myosin heavy chain 4	2.79	2.65	-2.14
Nog	noggin	3.85	-2.77	-4.35
Nov	nephroblastoma overexpressed	3.48	-3.30	-4.57
Oaz1-ps	ornithine decarboxylase antizyme 1, pseudo-gene	2.51	-2.38	-1.87
Olig1	oligodendrocyte transcription factor 1	9.72	-1.93	-13.72
Pbp2	phosphatidylethanolamine-binding protein 2	-70.42	118.82	92.74
Pcdhb9	protocadherin β 9	-2.73	2.42	2.18
Pgam2	phosphoglycerate mutase 2	2.86	1.77	-1.95
Piezo2	piezo type mechanosensitive ion channel com-ponent 2	-9.01	5.57	6.21

Pitx3	paired like homeodomain 3	3.10	-3.40	-2.27
Plcb4	phospholipase C β 4	-3.35	2.07	2.94
Plp1	proteolipid protein 1	4.54	-1.74	-10.23
Prss56	serine protease 56	2.64	-3.56	-3.73
Pttg1	pituitary tumor-transforming 1	-6.42	6.63	8.08
Pzp	PZP, α-2-macroglobulin like	29.27	-38.21	-4.31
Rbp1	retinol binding protein 1	2.54	-1.80	-2.13
Rbp4	retinol binding protein 4	5.77	-2.93	-2.49
Rdh5	retinol dehydrogenase 5	2.63	-2.10	-2.05
Rnaseh2c	ribonuclease H2 subunit C	2.46	-2.33	-2.07
Serpina1a	α-1-antitrypsin 1-1	68.85	-95.02	-6.98
Serpina1b	α-1-antitrypsin 1-2	14.88	-69.23	-4.20
Serpina1c	α-1-antitrypsin 1-3	59.80	-15.76	-4.04
Serpina3k	serine protease inhibitor A3K	160.72	-62.23	-6.59
Sfrp5	secreted frizzled related protein 5	3.34	-2.41	-2.86
Slc24a2	solute carrier family 24 member 2	-3.12	2.13	2.61
Slc26a7	solute carrier family 26 member 7	-4.04	4.35	3.39
Sned1	sushi, nidogen and EGF like domains 1	-9.06	2.92	3.77
Spink7	serine peptidase inhibitor, Kazal type 7 (putative)	8.40	-5.30	-8.31
St6galnac2	ST6 N-acetylgalactosaminide α-2,6-sialyltransferase 2	-2.76	1.94	3.30
Syt15	synaptotagmin 15	-5.56	3.73	4.01
Tcap	titin-cap	4.22	3.83	-2.02
Tfcp2l1	transcription factor CP2 like 1	-3.12	3.33	3.50
Tmem26	transmembrane protein 26	-3.02	10.65	10.57
Tnnc2	troponin C2, fast skeletal type	4.05	1.79	-2.18
Tnni2	troponin I2, fast skeletal type	3.25	2.28	-1.89
Tusc1	tumor suppressor candidate 1	3.06	-3.19	-2.53
Ugt8a	2-hydroxyacylsphingosine 1-β-galactosyltransferase	3.99	-2.21	-10.69
Uox	urate oxidase (pseudogene)	19.16	-11.44	-21.43